WT-1601

Operation HARDTACK (U)

April - October 1958

Program 32

HIGH ALTITUDE MEASUREMENTS (U)

Issuance Date: April 30, 1962

SANDIA CORPORATION
ALBUQUERQUE, NEW MEXICO

Attachment 9

[redacted]

[redacted]

ACKNOWLEDGEMENTS

We wish especially to thank the following people and organizations for their sincere interest and help in the Doorknob program:

Posthumously, the late [redacted] of LRL, whose support and enthusiasm for an instrumented high-altitude test kept us moving toward a goal which in the pre-Sputnik age was considered by many a fanciful pipe dream.

[redacted], [redacted], and [redacted] of RAND Corporation, for most helpful data and suggestions relating to the neutron, radiofrequency attenuation, and optical measurements.

[redacted] Meyerott of Lockheed Missiles Division, [redacted] of [redacted] and Associates, and [redacted], then of NRL, now at the University of Rochester, for stimulating ideas on early burst phenomena.

[redacted] and [redacted] of LRL, and [redacted] of RAND Corporation, for calculated data on X-ray ouputs from the warheads used on Teak and Orange.

[redacted] and [redacted] of LRL, for calculations of neutron output from the warheads.

[redacted] and other J-10 personnel at LASL, for data especially relating to cloud rise and optical phenomena, and [redacted] and T-Division at LASL for several key calculations, including the X-ray output calculation by [redacted].

[redacted], [redacted], [redacted], and [redacted] of J-11, LASL, for help with the radiochemical sampling project. [redacted] and [redacted] of LRL, for their cooperation in the early planning of this project.

Commander [redacted] of TG 7.3, for the excellent job he did in recovering twelve of the fifteen instrumented nose cones which Sandia fired on Teak and Orange.

[redacted]

Major [redacted] of WADC, for extreme patience in development phases of the Sandia high-altitude wind project and for this cooperation in gathering radar data from the chaff-rocket firings.

[redacted] and others of CWL, for their counting of neutron-activated specimens which provide the bulk of presently available neutron data from Teak and Orange shots.

[redacted] and Maj. [redacted] of LASL, for help and hardware for nuclear radiation measurements.

Sandia Salton Sea field test personnel, Allegany Ballistics Laboratory, TG 7.3, Thiokol Chemical Corporation, Grand Central Rocket Company, and Army Ballistic Missile Agency, for their essential and outstanding contributions to the success of Program 32.

Very special thanks are due [redacted] Office of Advance Planning of the Albuquerque Operations Office, AEC, for steering us through many hazardous administrative mazes, and to [redacted], Manager of ALO, for his strong support from the start of work on the program in August 1956.

We appreciate the vital efforts put forth by numerous persons in the Division of Military Application of the AEC under Brig. General [redacted] The support of Sandia management, esspecially the late [redacted], President, [redacted] Vice President, [redacted] former Director of Field Testing, and [redacted] former Director of Research, had a strong and direct effect on the program. The success of Program 32 is in a real sense due to their decisions.

Thanks are also due to [redacted], Commander, Task Group 7.1, [redacted] Commander, Task Unit 7.1.4, and his scientific adviser, [redacted]

The following Sandia Corporation employees made significant contributions to the success of the Doorknob program. Each individual is listed only once under the project to which he contributed most. However, in many cases individuals contributed to more than one project. Asterisks (*) indicate overseas service during the operation.

[redacted] DATA

Operation Hardtack - Program 32

SWR-1501

HIGH ALTITUDE MEASUREMENTS [U]

T. B. Cook, Jr., Scientific Adviser

M. L. Kramm, Program Director

Contributing Authors:

J. R. Banister
J. A. Beyeler
Frank Biggs
C. D. Broyles
W. J. Byatt
T. B. Cook, Jr.
J. L. Dossey
H. M. Dumas
R. L. Eno
C. T. Force
D. E. Henry
R. A. Jeffrey
M. L. Kramm
T. P. Krein
C. R. Mehl
M. A. Palmer
J. M. Proud, Jr.
J. W. Reed
C. G. Scott
L. B. Smith
H. A. Wente

Edited by G. R. Miller

Sandia Corporation
Albuquerque, New Mexico
March 1962

This document contains information affecting the National Defense of the United States within the meaning of the Espionage Laws, Title 18, U.S.C., Sections 793 and 794. Its transmission or the revelation of its contents in any manner to an unauthorized person is prohibited by law.

[redacted] DATA

This document contains restricted data as defined in the Atomic Energy Act of 1954. Its transmittal or the disclosure of its contents in any manner to an unauthorized person is prohibited.

[redacted]

[redacted]

Project 32.1 - Warhead

[redacted], Project Officer
[redacted] (Project Officer during early planning)

[redacted]

Project 32.2 - Transducers

[redacted] Project Officer

[redacted]

Project 32.3 - RF Attenuation Studies

[redacted] Project Officer

[redacted]

Project 32.4 - RF Telemetering System

[redacted] Project Officer

[redacted]

Project 32.5 - Rad-Chem Sampling and High-Altitude Wind Measurements

[redacted] Project Officer

[redacted]

[redacted]

[redacted]

Project 32.5 (Continued)

[redacted]

Project 32.6 - Instrument and Rad-Chem Rocket Systems

*T. P. Krein, Project Officer
*V. G. Redmond, (original Project Officer)

[redacted]

Project 32.8 - Optical Measurements

[redacted], Project Officer

[redacted]

Project 34.4 - Microbarograph

* [redacted], Project Officer
* [redacted]

Operational Support Personnel

[redacted]

(Report Coordinator for planning phase)

* [redacted]
* [redacted] (LRR and WT Report Editor)
[redacted]

[redacted]

[redacted]

ABSTRACT

Data from Teak and Orange shots of Operation Hardtack are reported in the following spheres of interest: X-ray, total thermal radiation, gamma-ray dose and dose rate, neutron flux, radio-frequency attenuation, burst-produced pressure at ground level, an attempt to gather radiochemical samples, optical phenomena as seen from ground level, winds at burst altitude, and other topics pertinent to gathering and interpreting data on the above phenomena.

Emphasis in Sandia Corporation's Program 32 is on measurement of these phenomena by rocket-borne instrumentation packages except where noted in the report.

[redacted]

[redacted]

[redacted]

PREFACE

This report presents results obtained from high altitude measurements made on Teak and Orange shots of Operation Hardtack on July 31 and August 11, 1958, respectively, Johnston Island time. (The dates in continental United States were, therefore, August 1 and August 12, respectively.) Originally scheduled and set up for launch from Bikini during April, the two Redstone-borne warheads with launching equipment and associated instrumentation were moved to Johnston Island because of the international situation and concern over the possibility of retinal burns on the eyes of islanders within line of site of the Bikini-launched bursts. Teak shot was burst at an altitude of approximately 252,000 feet, Orange at approximately 142,000 feet.

The reader will note departure from conventional report format in chapter treatment in that each is a separate entity with author or authors shown in the Table of Contents. References are listed at the end of each chapter which, together with illustrations, may be considered separately from others in the report.

All chapters of this report were completed by early Spring 1961, with the exception of Chapters 7 and 9. These were delayed until completion of an experimental program to determine rocket trajectories.

[redacted]

[redacted]

CONTENTS

[redacted]

[redacted]

CHAPTER 2 (Cont)

ILLUSTRATIONS

[redacted]

[redacted]

DNA (b)(3)

[redacted]

11

[redacted]

CHAPTER 3 (Cont)

ILLUSTRATIONS

TABLES

[redacted]

CHAPTER 5 (Cont)

ILLUSTRATIONS

TABLES

[redacted]

CHAPTER 7 (Cont)

ILLUSTRATIONS

[redacted]

CHAPTER 7 (Cont)

ILLUSTRATIONS

TABLES

[redacted]

[redacted]

[redacted]

ILLUSTRATIONS

TABLES

[redacted]

[redacted]

[redacted]

[redacted]

CHAPTER 11 (Cont)

ILLUSTRATIONS

TABLES

[redacted]

[redacted]

Chapter 1

INTRODUCTION AND SUMMARY OF PROGRAM

1.1 SCIENTIFIC OBJECTIVES AND RESULTS

On August 17, 1956, Sandia Laboratory received a request from the AEC to make recommendations for tests at very high altitudes. At that time major interest centered around the detectability of bursts above 100,000 feet. Long-range detection of such bursts could not be guaranteed and detection ranges of U. S. intelligence equipment for such bursts had to be reasonably well determined before the United States could seriously consider a test-ban agreement and an appropriate monitoring system for enforcing such a ban. In the spring of 1956 while Operation Redwing was under way, efforts were made to add a missile-carried burst to the end of the Redwing program. Because of operational problems such a burst was not accomplished, but Sandia Laboratory, as well as many other agencies, had put much thought into consideration of desirable experiments which should be performed on any high-altitude test. Thus Sandia answered AEC's request by submitting In October 1956 a proposal for a high-altitude test program. This proposal suggested that two shots be fired: [redacted] at 250,000 feet altitude and [redacted] at 100,000 feet. Teak and Orange shots of Hardtack bear considerable similarity to the program outlined in Sandia's proposal.

DNA

1.1.1 Technical Objectives

The principal objectives of such a test were stated in the October 1956 proposal, viz., to provide data on:

(1) United States detection and intelligence capabilities;
(2) Unexpected phenomena;
(3) Feasibility of very high altitude proving grounds; and
(4) Weapons effects at high altitudes, in particular as they affect
    (a) design criteria for decreasing the vulnerability of U. S. ballistic warheads;

[redacted]

[redacted]

(b) design of U. S. ballistic missile defense systems and optimum warheads for use in these systems; and

(c) verification of the Sumlamp concept* and design of optimum warhead for this application.

The objectives stated above were used by Sandia throughout all stages of planning and implementation of the program described in this report. Sandia Laboratory's program as carried out on Hardtack has contributed toward all the objectives given above in spite of the extremely short time for instrument development, theoretical calculations, and hardware procurement, and in spite of difficulties generated by the April 9, 1958, decision that caused Teak and Orange shots to be moved from Bikini to Johnston Island.

1.1.2 Summary of Technical Data

A summary of instrumentation is given in Figs. 1.1 and 1.2 and in Tables 1.1, 1.2, and 1.3.

Brief summary statements on major technical aspects of the program follow:

[redacted]

*The use of multimegaton air-defense weapon bursts above the atmosphere to produce lethal prompt nuclear radiation doses over areas many tens of miles in diameter at bomber altitudes.

[redacted]

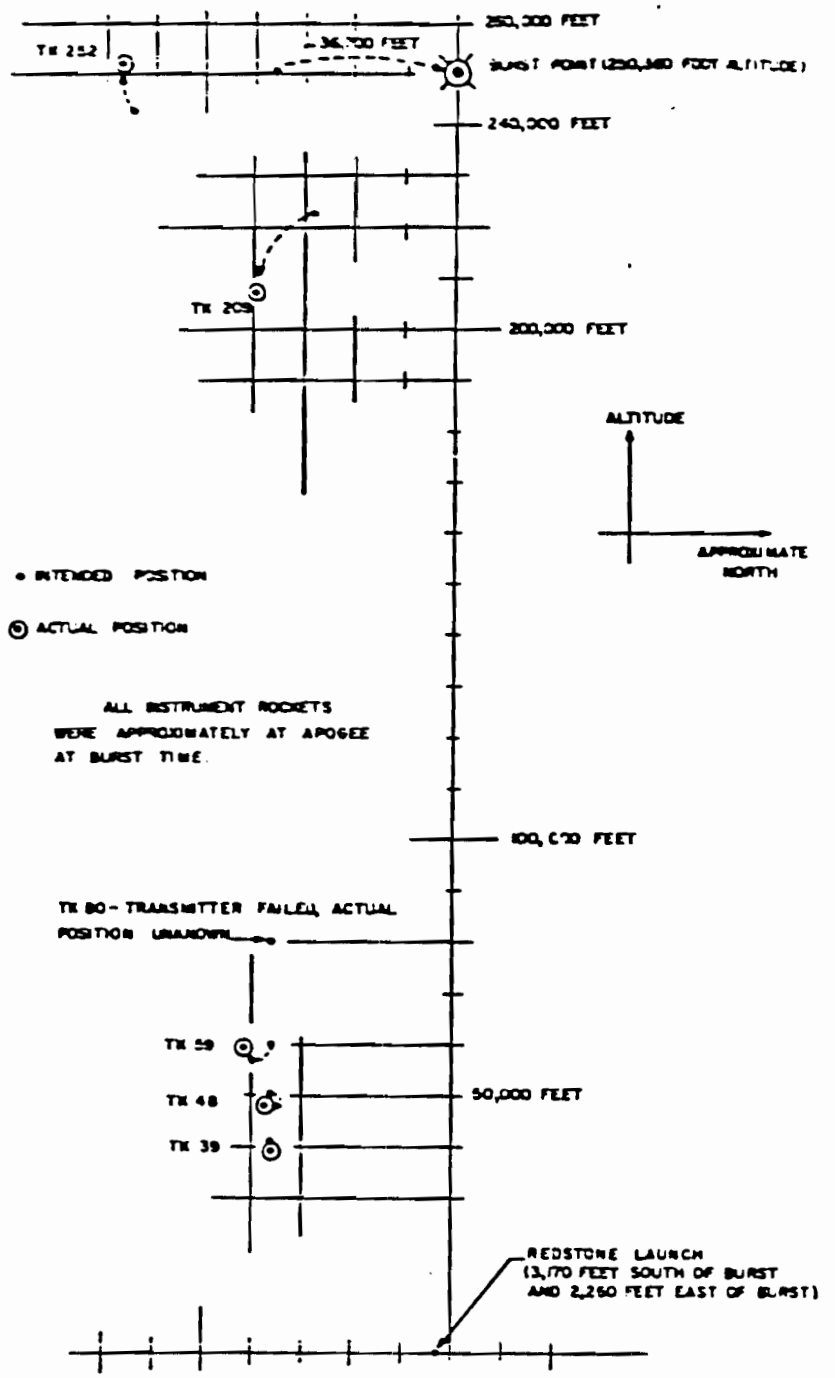

Fig. 1.1--Instrument location at time zero, Teak shot.

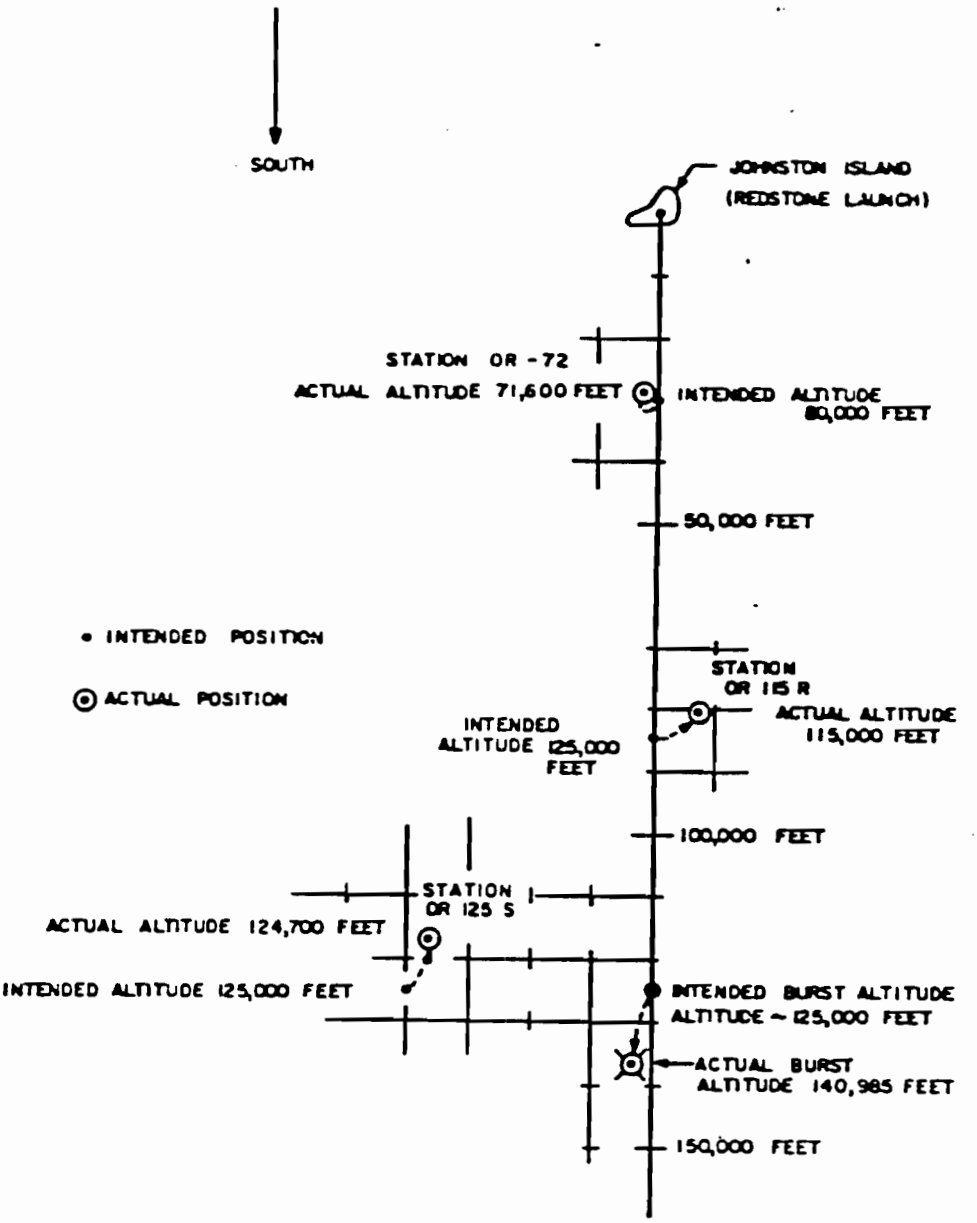

Fig. 1.2--Projection on ground plane of Orange instrument array.

TABLE 1.1--TEAK AND ORANGE ROCKET POSITIONS

Burst-Time Positions Relative to Redstone Launch Point				Instrument Rocket Positions Relative to Burst				
Teak				**Teak**				
Station designation	Altitude (ft)	South (ft)	West (ft)	Station designation	Altitude (ft)	South (ft)	West (ft)	Slant range (ft)
Burst	250,360	-3,170	2,260	39	-211,760	36,100	3,700	214,800
39	38,600	32,900	6,000	48	-202,360	37,100	2,400	205,700
48	48,000	33,900	4,700	59	-190,960	41,700	3,800	195,500
59	59,400	38,500	6,100	80	--	--	--	--
80	RF failed	No data	--	209	41,600	39,400	12,700	58,700
209	208,700	36,300	15,000	252	+1,640	66,500	16,900	68,600
252	252,000	63,300	19,200					
Orange				**Orange**				
Burst	140,985	136,775	3,060	72	-69,400	-107,600	-600	128,100
72	71,600	29,200	2,500	115R	-26,000	-56,200	-10,300	62,700
115R	115,000	80,600	-7,200	125S	-16,300	-19,600	+33,500	42,100
125S	124,700	117,200	36,600					

DNA 3

TABLE 1.2--DATA FROM TEAK

	Chapter No.	Other measurements	Rocket station number				
			252	192	52	48	32
[redacted]							
Technical photography	11	X					
Rocket positions measured	9	X^2	X	X	X	X	X
Rocket-borne instruments recovered	5	X^3	X	X	X		X

X - Significant data gathered and analyzed.

X^1 - Significant data from three Hi-Lo rockets in addition to data from instrument carriers.

X^2 - Position of one Hi-Lo rocket was measured in addition to the positions of the instrument carriers.

X^3 - The two radiochemical sampler rockets were recovered even though they malfunctioned early in their flight.

TABLE 1.3--DATA FROM ORANGE

	Chapter No.	Other measurements	Rocket station number		
			[redacted]	[redacted]	[redacted]
Rocket positions measured	9	X[3]	X	X	X
Rocket-borne instruments recovered	5	X[4]		X	X

X - Significant data gathered and analyzed.

X[1] - Significant data from three Hi-Lo rockets in addition to data from instrument carriers.

X[2] - Instruments carried on the Redstone missile.

X[3] - Positions of the Redstone missile and one Hi-Lo rocket were measured in addition to the positions of the instrument carriers.

X[4] - All four radiochemical samplers were recovered.

[redacted]

Page 32 is deleted.

Weapon Diagnostics. A high-resolution, 4-kilomegacycle telemetry system was incorporated in the Redstone payload for the purpose of transmitting data [redacted] Data were obtained which prove the usefulness of this technique on rocket-delivered nuclear tests in the upper atmosphere.

Optical Measurements. Useful data were obtained on Teak, but cloud cover negated the Orange experiment. Data on optical phenomena produced by Teak and Orange are adequate only to demonstrate the complexity of these phenomena and the very strong need for much heavier investment in these programs on any future test. Data obtained on Teak suffer from the fact that instruments were looking toward the intended burst point which was missed by over 6 miles.

Warhead. Teak and Orange used the first nuclear warheads to be nuclear-detonated from a missile. Warhead functioning was successfully monitored and accomplished; no outstanding problems were encountered. Safety was of extreme importance in this unprecedented test and was successfully handled without incident.

With reference to the first objective, it is now clearly understood that bursts such as Teak and Orange cannot be hidden. They were seen for 1000 miles, detected around the world by EM signals and radars, showed unique magnetograms at magnetic observatories around the world, produced radiofrequency transmission difficulties throughout the Pacific Ocean area, and in general were more detectable than nearly any other nuclear event that can be specified. The Sandia microbarograph project (34.4) successfully gathered data on acoustic disturbances from stations on Johnston Island, French Frigate Shoals, and Oahu. Prior to these shots, there was doubt by some groups that any detectable acoustic signal would be present at the earth's surface. Data on decay of acoustic signal strength with horizontal distance and data on expected asymmetry of acoustic signal strength were not as complete as would have been the case had Teak been fired from Bikini. This is because of lack of suitable land masses around Johnston Island for microbarograph stations.

Many phenomena were observed which fall into the unexpected category. In this connection it is appropriate to pay tribute to the late Dr. Mark Mills of Lawrence Radiation Laboratory whose enthusiastic interest in the "unexpected" had a strong influence on Sandia's program for the Teak and Orange shots.

[redacted]

Optical measurements described in Chapter 11 were made primarily to record unexpected optical phenomena. Indeed, when the six 100-frame-per-second cameras with running times of 2.5 minutes and 45-degree fields of view were included in Program 32, there were no predictions that interesting optical phenomena would occur at such a late time and over such a large part of the sky. However, it is now obvious that spectacular, scientifically interesting, and possibly militarily significant optical phenomena were present [redacted]

DNA (b)(1)

Written descriptions of what various people saw are the sole existing permanent record of many of the peculiar phenomena which took place, and for this reason such descriptions are included in the appendix to this report. A considerable fraction of optical coverage on Teak was lost because of the approximately 35-kilofoot displacement of the actual burst from intended burst zero; cloud cover on Orange caused many data to be lost. However, optical data which were obtained are of much interest.

In addition to the spectacular and unexpected optical display,* many unexpected phenomena occurred in radiofrequency propagation, acoustic signals, rise and spread of bomb debris, thermal radiation on the ground, gamma-ray output from the warhead, thermal neutron output from the warhead, and many others. Nearly every Sandia project gathered some "unexpected" data the potential significance of which, in many instances, is not clear. It is obvious, certainly, that Teak and Orange uncovered more problems than they answered.

As to the third objective, the feasibility of telemetering certain informative diagnostic data on device performance has been demonstrated (see Chapter 9). It is self-evident that testing in the upper atmosphere is feasible and, even further, the experience gained on Teak and Orange show that it is feasible to carry out proof tests of warheads in space as well as in the high atmosphere. Space tests will, initially at least, lack the advantages of detailed optical coverage and recoverable instrumentation.

Much was learned pertinent to radiochemical sampling of bursts such as Teak and Orange. In view of the many estimates of a debris radius for Teak of 1000 feet, it was surprising to some to learn that within 10 seconds after burst

*For an excellent unclassified article on the optical display in Hawaii, see "Photographs of the High Altitude Nuclear Explosion 'Teak'," Journal of Geophysical Research, Vol. 65, No. 2, February 1960, p. 545.

[redacted]

[redacted]

the debris was spread over a radius [redacted] Rate of rise of the debris was measured from Edgerton, Germeshausen and Grier (EG&G) photographs [redacted] These data indicate that radiochemical samplings by rocket penetration are not nearly as difficult as was believed before Teak, when many estimates gave the debris a 1000-foot radius and a rise velocity of over 10,000 feet per second.

Based on early estimates of a very small debris radius and possibly 200- to 400-knot expected winds at Teak burst altitude, a system was developed for ejecting chaff at up to 300,000 feet altitude to obtain wind data at and above Teak burst altitude. These winds would allow radiochemical sampling rockets to be aimed to intercept the moving debris. After experience with Teak, it is apparent, because of the tremendous debris volume, that a wind correction is not needed in order to intercept the cloud. However, the 15 pre-Teak firings of high-altitude chaff rockets gathered data of much scientific interest per se, and these observations, together with those which followed, are summarized in a report by L. B. Smith.[1]

On Orange shot the radiochemical sampling rockets and associated instrumentation worked with almost 100-percent success, and there is little doubt that a sample would have been obtained had the rockets intercepted the rapidly moving debris (see Chapter 5). Interception would probably have taken place had the burst point not been about 3 miles higher than planned.

Recovery of missile-carried instrumentation from the open ocean has been demonstrated to be a reliable and practical means for gathering data on high-altitude tests (see Chapter 5). Of the 15 nose cones for which recovery was attempted, 12 were successfully retrieved. During initial planning for the Teak and Orange shots, chances for such a recovery record were believed to be nearly impossible. Limitations of telemetry from instrumented structures in the air at burst time are reasonably well established (see Chapters 7 and 9).

Optical data from ground stations appear to offer much diagnostic evidence, and air-borne measurements of neutron, gamma-ray, and X-ray yields of high-altitude bursts can now be attempted with high likelihood of success (see Chapters 2, 3, and 4). Thus it seems feasible to test many aspects of improven warheads at high altitudes where fallout of radioactivity is negligible. It is interesting to note that Teak and Orange shots were actually fired on the scheduled days. This has seldom been accomplished with megaton-yield devices.

[redacted]

[redacted]

Data from Teak and Orange indicate much more clearly the advantages and disadvantages of testing devices at high altitudes as compared to atmospheric or underground testing. It is clear that lack of detectability is not one of the "advantages."

DNA (b)(1)

Chapters 2, 3, 4, 7, and 11 discuss measurements relating to the fourth objective. Displacement of the burst point relative to Program 32 instrument carriers caused serious degradation in quality of X-ray data. [redacted]

Improper angular orientation between burst and total thermal detectors at Teak Stations 252 and 209, together with a narrow field of view (about 15 degrees) over which thermal detectors approximate black-body absorbers, complicated analysis of these data. Much time and postcalibration have allowed significant results to be extracted.

DNA (b)(1)

[redacted] Film badges were used on all lower stations, and data from these, together with total dose data from other stations, are given in Chapter 4. Gamma-ray dose-rate records from the logarithmic detectors at the lower altitude stations gave excellent time-dependent data. In view of the complexity of gamma-ray dose calculations in such an extremely inhomogeneous propagation medium and for such highly uncertain source characteristics, these

[redacted]

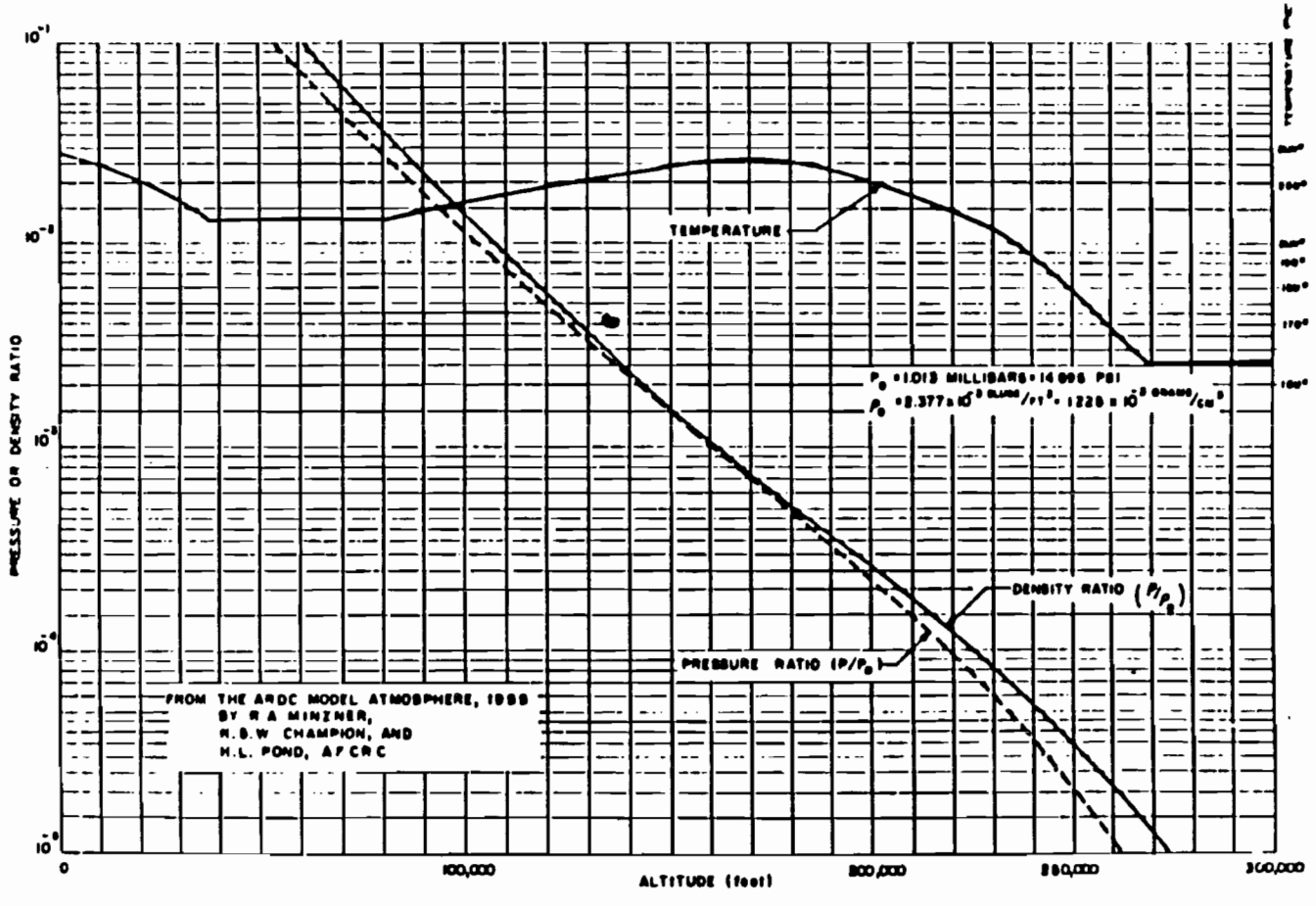

Fig. 1.3--ARDC Model Atmosphere, 1959.

[redacted]

data are extremely useful in the proof of a calculational model to produce reasonably accurate predictions. Gamma-ray dose-rate data were lost at the two high stations because of the low gamma-ray level caused by burst position error [redacted] The combination of both these effects, plus possibly the rapid rise of fission products debris, caused the dose rate to be below detectability at the time telemetered data began to be recorded after burst. On Orange, dose-rate data were gathered at Station OR-80, and total gamma-ray dose data were gathered at Stations OR-80 and OR-125S (see Chapter 4).

Microbarograph data are adequate to allow estimates to be made of blast parameters at any point in the atmosphere beneath burst altitude with sufficient accuracy for most practical problems. Blast phenomena are noticeable at aircraft altitudes for a burst such as Teak [redacted]

Radio-frequency attenuation data gathered by Project 32.3 are given in Chapter 7. Many data are available and every attempt has been made to include all pertinent facts necessary for analysis of the data to suit particular needs. These data have been analyzed by many groups and analyses are not repeated here.

A one-week meeting was held in early 1960 which emphasized the need to make a vigorous attempt to determine the position of Sandia's Hi-Lo rockets with as much accuracy as possible.[2] Work on rocket positioning was funded by DASA.* This included eight sea level firings of Deacon-Arrow rockets which were as nearly as possible like those used on Johnston Island. Numerous statistical data on the variability of impulse for these motors were also examined, as were the specific Johnston Island records. Johnston Island time-of-flight data, coupled with understanding gained by intensive analysis of rocket performance, have given considerable improvement in knowledge of the location of the rockets during the Teak and Orange bursts. Their altitude history in particular is now known with good confidence. This is the most critical aspect of their flight trajectory from the standpoint of attenuation of radiofrequency transmissions. It is unfortunate that the time allowed for execution of this project was insufficient to permit procurement of tracking facilities on Johnston Island for these Hi-Lo rockets. However, much was learned which warrants predictions of radiofrequency blackout times to a greater degree of accuracy than pre-Teak

*Order No. HT Hi-Lo Nr. 1, dated July 12, 1960.

[redacted]

[redacted]

estimates; [redacted] In view of the critical need for radiofrequency attenuation data in design of communications and anti-ICBM defense systems, and because of the short time available, the high degree to which the data satisfy technical objectives is particularly complimentary to all who were engaged in this project.

1.1.3 Conclusions

In summary, Program 32 met its technical objectives to an extent greater than it was reasonable to expect. The program gathered over 75 percent of the information desired. Degradation of scientific data because of the displaced burst points on both Teak and Orange appears as the most disappointing feature of the tests. In looking for changes in the program which would be made if similar tests were being designed, it is clear that much better long-time and wide-angle optical coverage should be included, and the world-wide scientific community should be alerted. Recoverable instrumentation proved very practical and would receive more emphasis in future test designs of shots similar to Teak and Orange.

1.2 SUMMARY OF EXPERIMENTAL PROGRAMS

1.2.1 Development of Techniques for Teak Shot

The original intent of Program 32 was to measure neutron, X-ray, total thermal, and gamma-ray emission from a megaton-range nuclear device burst at an altitude of 250,000 feet. Additional measurements were incorporated in the program as techniques became available for attempting them. These were sampling of radioactive debris, optical coverage of the burst, and measurement of radio-frequency attenuation and refraction caused by ionization of the atmosphere. Techniques designed to accomplish the mission of the program and specific measurements involved are discussed in the following paragraphs. Positions of the Redstone and Sandia's rocket-launching stations can be seen from photographs in Figs. 1.4 and 1.5.

Stations for measuring neutron, gamma-ray, X-ray, and total thermal emissions were placed at specified locations (see Figs. 1.1 and 1.2) by one- and two-stage rocket-propelled instrument carriers. The propulsion units were modified LaCrosse solid-propellant motors. Auxiliary hardware was designed

[redacted]

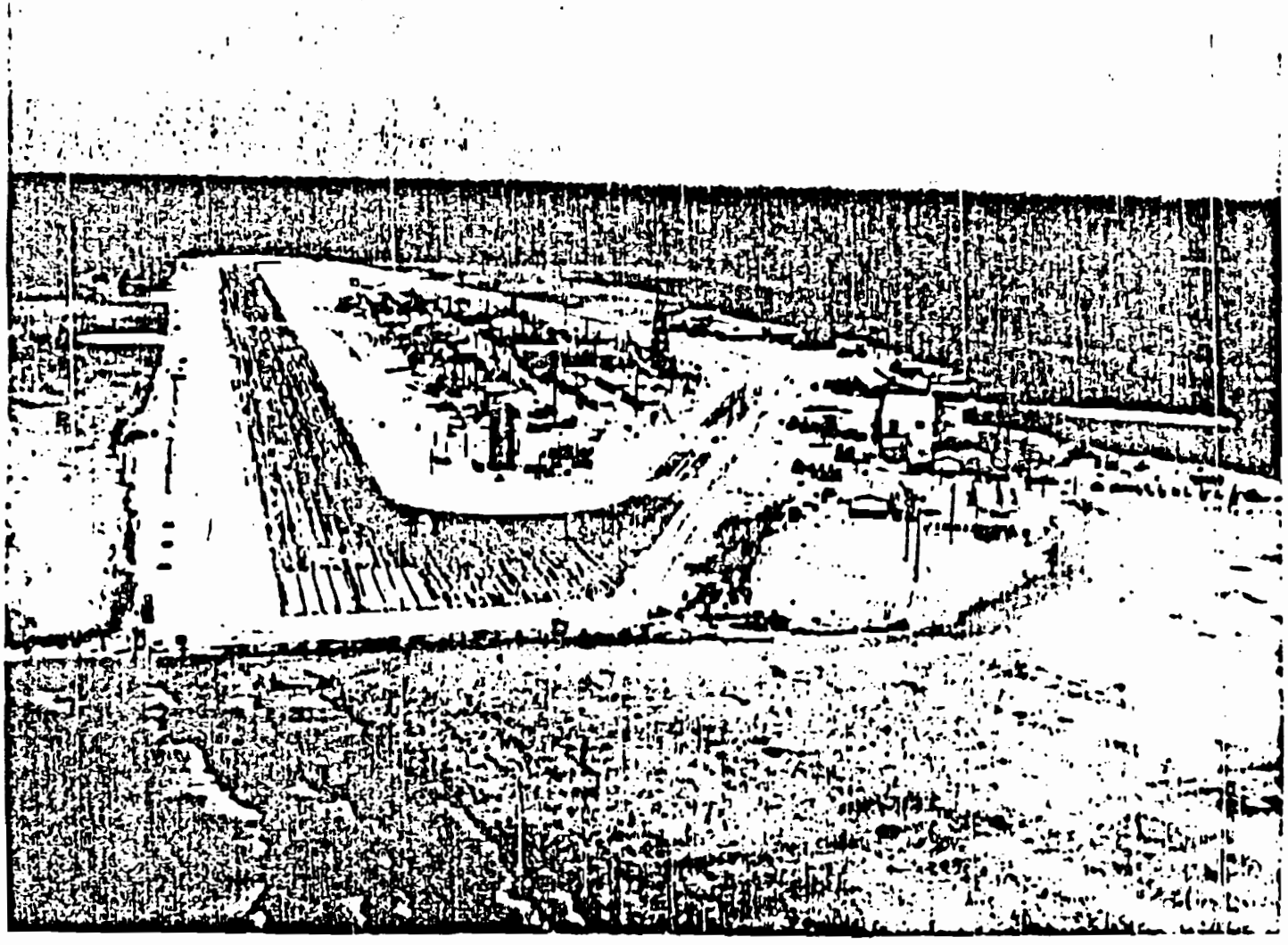

Fig. 1.4--Helicopter view from east of Johnston Island.

[redacted]

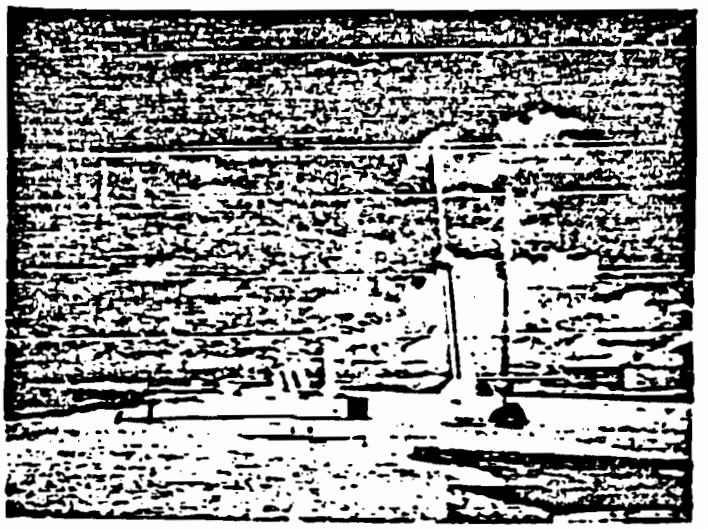

Fig. 1.5a—View to west of Sandia Hi-Lo rockets on launchers on southern edge of Johnston.

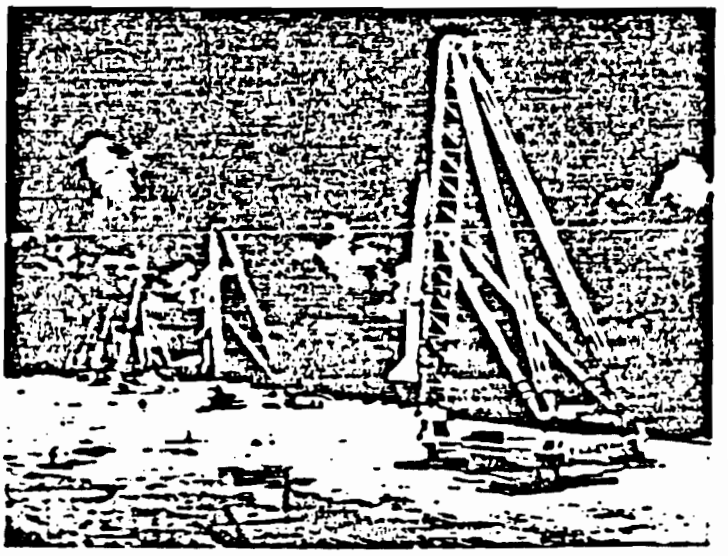

Fig. 1.5b--View to east of Sandia instrument carriers on launchers on southern edge of Johnston.

[redacted]

[redacted]

specifically for these tests. The carriers were unguided, rail-launched ballistic rockets, with variations of weight and drag for altitude control (see Chapter 8).

Each carrier had a 226- to 235-mc band telemetering system aboard equipped with from four to eight subcarriers. The FM-FM receiving and recording station was located near the launch site on Johnston Island (see Chapter 9). All six carriers contained transducers for measuring neutron and gamma-ray fluxes. The neutron transducer consisted of activation foils counted by a scintillometer circuit during the fall time of the nose. Gamma-ray dose rates were measured by scintillometers and total dose by silver-activated phosphor-glass and film.

In addition, the two rocket stations nearest the burst attempted measurement of X-ray and total thermal inputs. Both transducers utilized ballistic calorimeters containing resistance wires connected in a four-arm bridge. Total thermal radiation was absorbed by a polished aluminum cone mounted inside a truncated cone. X-rays were filtered by aluminum and beryllium filters. These six carriers also contained film packs for measuring gamma-ray dose. Noses were designed for parachute retardation and for recovery from the ocean.

The Redstone carried two 4-kmc diagnostic systems for measuring high explosive transit time and early alpha of the primary bomb. This system and the warhead fuzing system were monitored by 226-mc telemetry equipment.

All six instrument carriers and the Redstone were tracked by two MIDOT (radio interferometer positioning system) stations for postshot determination of the position of transducers relative to the burst. The transmitters aboard each carrier served as beacons for MIDOT to follow.

Two radiochemical sampling noses were to be carried through the Teak debris by two stages of the modified LaCrosse motors. These were to have sampled, sealed, and lowered to the water a collection of the burst residue for laboratory analysis.

A system for measuring wind velocity at 250,000 feet altitude was designed to permit adjustment of the rad-chem sampler trajectories to increase the likelihood of sending the sampler through the densest debris. This measurement was made by utilization of 5-cm chaff, carried to altitude on a Deacon-Arrow II rocket, ejected, and tracked by MSQ radar.

[redacted]

[redacted]

Radio-frequency attenuation measurements were attempted by the employment of 225-mc and 1500-mc transmitters, carried aloft on two-stage rockets, and the recording of received signal strength at two separate locations.

Optical instrumentation included high-speed and longer time photography through three different narrow-band filters, a high-resolution spectral record, location of burst position by plate cameras located at each MIDOT station, and black and white and color documentary photography.

Warheads used on the high-altitude shots were modified, installed, checked out, and armed by Program 32 personnel.

1.2.2 Teak Conclusions

All equipment used on the Teak experiment operated as designed with the following exceptions:

(1) The two rad-chem samplers appeared to suffer structural damage at the time of second-stage burning, became unstable, and fell back to the reef near Johnston Island. Many of the parts were recovered by skin diving, and the type of failure, if not the primary cause, was deduced.

(2) Two Viper II-Arrow II transmitter-carrying rockets failed at first-stage burnout and fell back on the western part of Johnston Island. These were to have been above the burst at burst time, and their failure thereby resulted in no data on radiofrequency attenuation through the "fireball" region. A subsequent test firing verified this failure, although the assembly was flown successfully in one pre-Teak test firing. Three of the transmitter-carrying rockets produced good data.

(3) The displaced burst point was outside the beam of the antenna receiving the 4-kmc diagnostic signal and no information was received for this reason. The signal, though weak, was seen at the receiving station, and operation of the system was verified by 200-mc monitor telemetry.

(4) Two of the instrument carriers, those planned for the 50,000- and 80,000-foot stations (TK-48 and TK-80), were not recovered. Radio-frequency signals indicated that the TK-48 chute operated satisfactorily, but the length of time consumed in searching for other nose cones and pods may have permitted this nose to fill with water and sink. The RF signal from TK-80 indicated failure of either the TM transmitter or the rocket shortly after launch.

[redacted]

[redacted]

The displaced burst caused the stations to be substantial distances outside the intended areas of interest, but much of the desired data was recovered from the records and from the four recovered noses. Some optical data were also lost because of burst-point displacement.

1.2.3 Orange Measurements

After the Teak shot it was determined that Sandia would participate in the Orange shot to a greater extent than was originally planned. No attenuation measurements nor instrument carriers were originally scheduled for Orange. Instrumentation used on the test was as follows:

(1) Four rad-chem samplers.
(2) Three instrument carriers (see Fig. 1.2 for location).
(3) Eight Deacon-Arrow II RF attenuation rockets.
(4) MIDOT tracking of the three instrument carriers, two of the RF attenuation rockets, and the Redstone.
(5) The 4-kmc diagnostic measurement.
(6) Photo coverage as on Teak in addition to documentary coverage from French Frigate Shoals.
(7) Warhead preparation and monitoring.

DNA (b)(1)

1.2.4 Orange Conclusions

(1) Four samplers were recovered, [redacted]

The fact that the burst point was 16,000 feet higher than was planned is possibly the reason that Sandia samplers missed the debris.

(2) Telemetered data from the three instrument carriers appear to be satisfactory. The station 40,000 feet north of the burst (OR-115R) was not recovered.

(3) Only seven RF attenuation rockets were fired. The three 225-mc systems recorded good data.

(4) MIDOT tracking was good.

(5) The 4-kmc diagnostic measurement gave transit time and early alpha.

(6) Photo coverage was lost because of cloud cover.

(7) The warhead operated as expected.

[redacted]

[redacted]

REFERENCES

1. Smith, L. B., Monthly Observations of Winds Between 100,000 and 300,000 Feet, SC-4[illegible](RR), Sandia Corporation, September 1960.

2. Report on Nuclear Interference, TR 60-3, IDA ARPA, The Pentagon, Washington 25, D. C., August 1960.

[redacted]

[redacted]

Chapter 2

X-RAY AND THERMAL RADIATION

2.1 THEORY AND ANALYSIS

2.1.1 Introduction

X-ray measurements were made on the Teak event and thermal measurements were made on both the Teak and Orange events.

The rocket-borne stations, TX-252 and TX-209, were planned to be 30,000 feet from Teak air zero with Station TX-252 in a direction perpendicular to the Redstone axis and Station TX-209 in a direction parallel to the Redstone axis as shown in Fig. 1.1. As it turned out, at zero time Station TX-252 was at an altitude of 252,000 feet and at a radial distance of 68,600 feet from air zero, Station TX-209 was at an altitude of 208,700 feet and at a radial distance of 58,800 feet from air zero. The instrument rocket of Station TX-252 was exposed side-on to the detonation as planned; however, the rocket station, TX-209, was not exposed exactly nose-on as planned but tilted about 55 degrees from planned orientation with an uncertainty of about 5 degrees.

Air zero of the Orange event was at an altitude of 140,985 feet. The rocket-borne station, OR-125S, located at an altitude of 124,700 feet and at a radial distance of 42,100 feet, carried thermal detectors. The station was in a direction perpendicular to the Redstone axis and the instrument rocket was exposed to the detonation with a side-on attitude.

The instruments are described in Section 2.2; however, designations will be given here to the X-ray detectors to clarify references to them. Each X-ray instrument consists of a pair of calorimeters each shielded by a different X-ray filter. A calorimeter and the thin filter are designated detector A, and calorimeter and thick filter are designated detector B. The filters of these detectors are designated filters A and B, respectively. Subscripts going from 1 to 6 are used to indicate the angular position of the detector on the rocket.

In a sea level atmosphere, 10-kev X-rays are attenuated to one-half intensity in about 1 meter, whereas in a 250,000-foot atmosphere a half-thickness is

[redacted]

[redacted]

about 30,000 meters. In either case the half-thickness is roughly proportional to the third power of the photon energy. Hence, at peak altitude, X-rays penetrate to an extent sufficient to have a direct effect on materials exposed many thousands of feet from the burst point. This effect is expected to be quite severe for an intense beam of soft X-rays, since it becomes absorbed in a surface thickness of a few microns is most dense materials. Thus X-ray damage potential has produced much interest in the X-ray yield of nuclear warheads. There are certainly situations where the X-ray yield of a device would have a strong influence on its effectiveness as an anti-ICBM warhead.

DNA (b)(1)

[redacted]

After emission from the case, the X-rays propagate to the measuring stations with consequent absorption in the intervening air as well as absorption in the detector filters. Energy E of X-rays reaching the unit area of the calorimeter surface is

$$E = \cos\beta \int_{v=0}^{v=\infty} \Psi(v)\, e^{-\left[\mu_1(v)\int_0^R \rho_1(r)dr + \left(\mu_2(v)\rho_2 x_2 + \mu_3(v)\rho_3 x_3\right)\sec\beta\right]} dv , \quad (2.1)$$

[redacted]

Pages 48 and 49 are deleted.

[redacted]

where $\bar{\tau}(\nu)d\nu$ is X-ray energy in a frequency increment $d\nu$ about ν; n is a number used here to accommodate discrepant standards for air density-height profile; R is radial distance from air zero to the station; ρ_1 is air density which is a function of altitude; μ_2, ρ_2, and x_2 are the mass absorption coefficient, density, and thickness of the beryllium part of the filter; and μ_3, ρ_3, and x_3 are the same parameters for the aluminum part of the filter. The orientation β of the detector takes into account the effect of the projected area of the detector aperture as well as the effective filter thickness on E. Orientation β is defined as magnitude of the angle between the beam of X-rays and the normal to the surface of the most directly exposed detector.

[redacted]

b(3)
DOE

[redacted]

Page 51 is deleted.

[redacted]

2.1.2 Predictions

These numbers are now calculated to show what X-ray energy would be expected to reach the stations under the geometric situation which actually existed at zero time which, of course, is quite different from the planned geometry because

[redacted]

of the failure of the Redstone to program into its planned trajectory and failure of the instrument rocket of Station [redacted]-209 to reach its planned altitude of about 220,000 feet.

[redacted]

b(3)
Doe

DNA
(b)(1)

[redacted]

2.1.3 Analysis of Data

Angular orientation β for Teak Station 252 was determined to be 10 degrees, where the ratio R_1 (see previous section for definition) obtained from Table 2.1 and the curves of Fig. 2.7 are used.

In Eq. 1 the number m appears as a parameter for air density. Figures 2.11 and 2.12 show the ratio R_2 versus effective case temperature for different values of the parameter m and with β = 10 degrees and β = 50 degrees, respectively. Figure 2.13 shows transmittance from air zero to the calorimeter of each detector versus m for the effective case temperature indicated by Figs. 2.11 and 2.12 when R_2 from the data of Table 2.1 is used.

[redacted]

b(3) DNA

DNA (b)(1)

[redacted]

Pages 55 through 65 are deleted.

TABLE 2.1--X-RAY DATA

Task Station 252

Instrument designation	Instrument number	Ohms/°F	ΔR (ohms)	ΔR_b (ohms)	Av. ΔR (ohms)	ΔT (°F)	Heat capacity (cal/°F)	Total energy (cal)	Corrected total (cal)
A_1	2109								
A_2	2106								
A_3	2100								
A_4	2076								
A_5	2092								
A_6	2089								
B_1	2096								
B_2	2068								
B_3	2104								
B_4	2097								
B_5	2098								
B_6	2069								
Task Station 209									
A_1	2103								
A_2	2122								
B_1	2072								
B_2	2074								

[redacted]

[redacted]

Accuracy of the telemetry system is estimated to be better than 5 percent. Heat capacity of the detectors is known to about 3 percent, and the relative locations of the stations with respect to air zero are known, from MIDOT,* to about 1 percent. [redacted]

The ratio R_2 from which the effective temperature is calculated is less dependent on errors in location and in absorption. This ratio is given by:

$$R_2 = \frac{e^{-(\mu_1\rho_1x_1+\mu_2\rho_2x_2+\mu_3\rho_3x_3)}}{e^{-(\mu_1\rho_1x_1+\mu_2\rho_2x_2)}} = e^{-\mu_3\rho_3x_3} .$$

The error in R_2 for 1-percent error in μ_3 is less than 0.5 percent. A 1-percent error in distance gives an insignificant error in ratio R_1.

Combining the errors for telemetry, for heat capacity of two detectors, and for the attenuation coefficients, gives a 6.6-percent error in case-temperature measurements; the errors in telemetry, heat capacity, distance, and attenuation coefficients, give a 6.7-percent error for X-ray yield measurements.

[redacted]

*Multiple Interference Determination of Trajectory, see Chapter 9.

[redacted]

[redacted]

TABLE 2.2--THERMAL DATA

Teak Station 252

Instrument designation	Instrument number	ΔR (ohms)	Ohms/°F	ΔT (°F)	Cal/°F	Total energy (cal)
z_1	6468	[redacted]				
z_2	6472					
z_3	6469					
z_4	6450					
z_5	6485					
z_6	6520					
z_7	6470					
z_8	6443					
		Teak Station 209				
z_1	6526	[redacted]				
z_2	6464					
		Orange Station 1255				
z_1	6479	[redacted]				
z_2	6521					
z_3	6488					
z_4	6487					
z_5	6441					
z_6	6522					
z_7	6442					
z_8	6481					

b(3)
DOE

DNF
(b)(3)

[redacted]

64

[redacted]

[redacted]

[redacted]

b(3) DOE

DNA (b)(3)

2.2 INSTRUMENTATION

2.2.1 Design Criteria

Most of the design requirements for transducers used in the measurement of energy appearing as X-ray or thermal radiation were exacted by the operating environment.

b(3) DOE

[redacted] limited space in the instrument nose cones of the carrier vehicles dictated that these instruments operate in an unpressurized midsection and also that transmission

DNA (b)(3)

[redacted]

Page 70 is deleted.

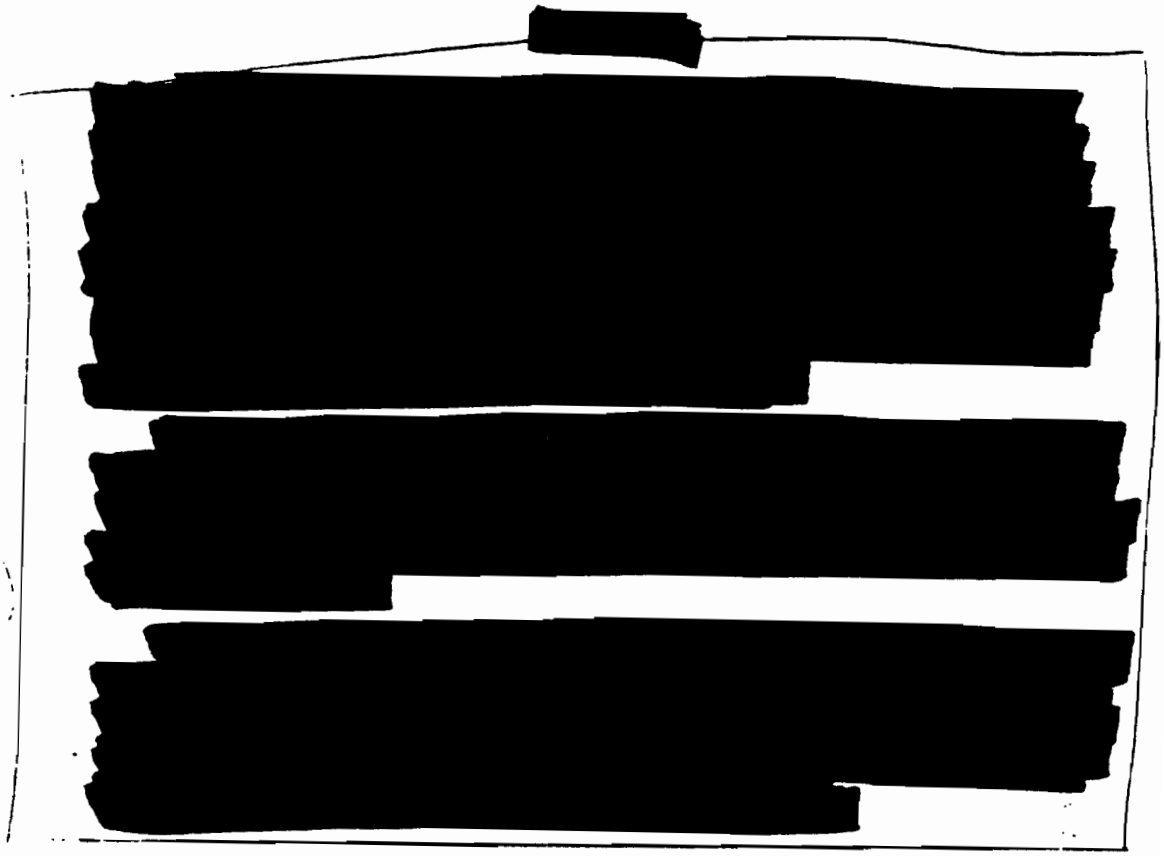

2.2.2 Instrument Description, Calibration, and Response

Both X-ray and total thermal instruments were designed to operate as ballistic calorimeters; upon absorbing a large pulse of radiant energy in a short time interval, the instruments reach thermal equilibrium some time later. The amount of energy absorbed by such a calorimeter is directly proportional to the product of the resulting temperature rise times its thermal mass.

Each X-ray transducer consisted of a pair of these calorimeters mounted behind appropriate filter windows as shown in Fig. 2.16. These filters served three equally important purposes:

(1) They rejected radiation of longer wavelength than desired;

(2) They attenuated incident X-ray energy in such a manner as to prevent vaporization of the calorimeter surface and a consequent loss of energy;

(3) They yielded information on the spectral distribution of X-ray energy from which the effective radiating temperature could be obtained.

[redacted]

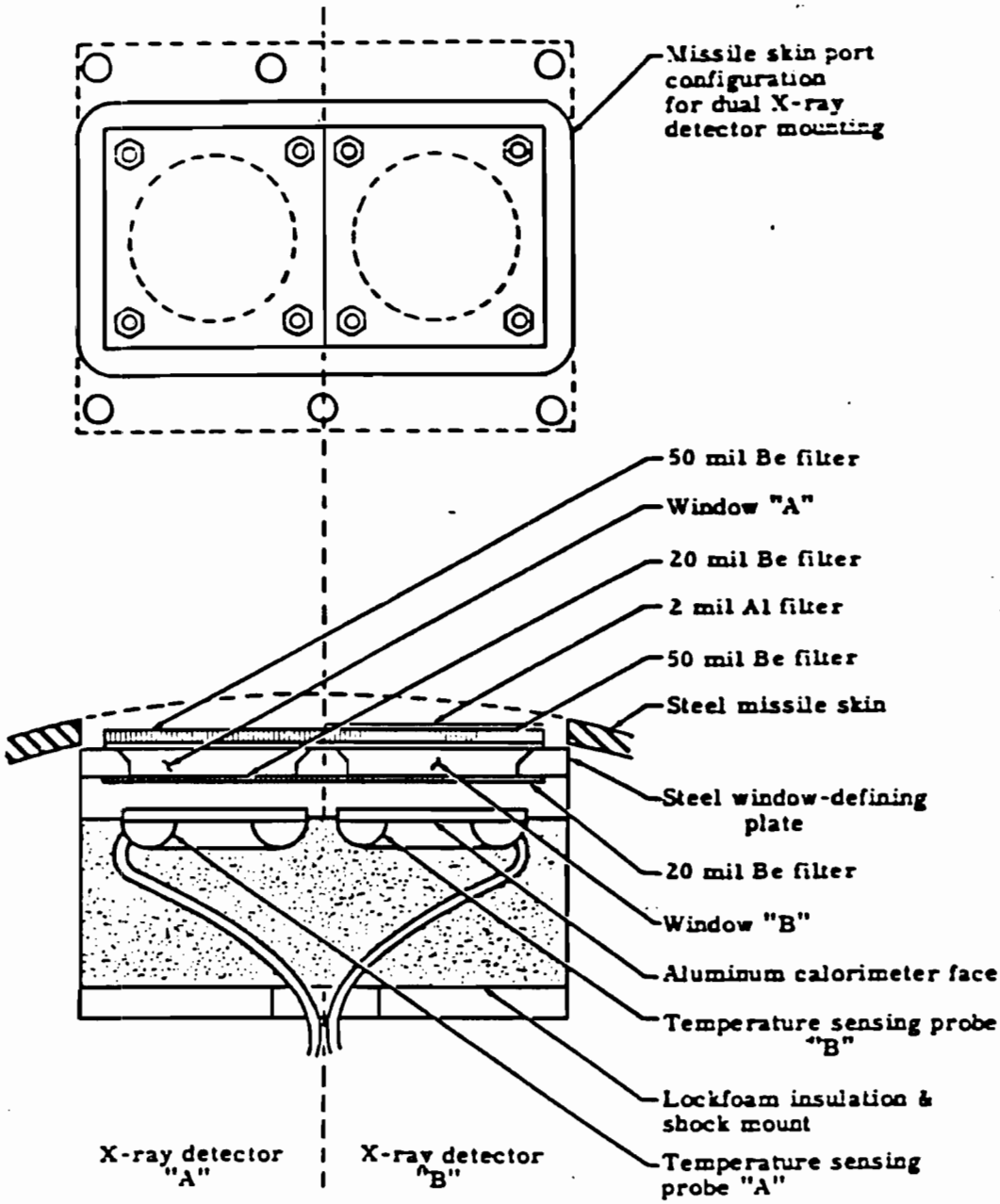

Fig. 2.16--X-ray transducer.

The X-ray calorimeters consisted of aluminum discs in which temperature-sensing elements of nickel wire were embedded. These were mounted in foamed plastic for thermal insulation and shock resistance. The heat capacity of each calorimeter was around 0.5 cal/degree Centigrade and was known to within 3 percent from laboratory calculation. These calorimeters required about 12 seconds to reach thermal equilibrium.

Figure 2.17 represents a sectional view of the thermal radiation calorimeter. Since these instruments were subjected to high intensities of X-ray energy, as well as all radiant energy of longer wavelengths, the absorbing surfaces were necessarily more elaborate than in the case of X-rays. The cone in the Fig. 2.17 is of spun, polished aluminum. The outer shell is also of spun aluminum, but processed to a dull black surface. These were both soldered to a copper base containing an embedded temperature-sensing element.

Upon entering the port, thermal energy reflected by the polished aluminum cone is preferentially absorbed by the blackened side walls. Nonreflecting wavelengths and X-rays are absorbed at the point of incidence. The high-temperature gradients produced in the absorbing surfaces promote heat transfer into the body of the metal, resulting in rapid surface cooling. This, in conjunction with the geometry of the cavity, minimizes heat losses by radiation and surface vaporization. The thermal radiation calorimeters were designed for a heat capacity of around 20 cal/degree Centigrade, and the heat capacity of each was measured to an accuracy of about 5 percent.

Prior to the operation, both types of transducers were exposed to neutron and gamma dosages exceeding those experienced from the nuclear burst. No detectable temperature increase or other change in characteristics was noted.

Calibration sheets on each of the temperature-sensing elements were furnished by the manufacturer. Resistance-versus-temperature checks which were performed after the elements were embedded in the calorimeters failed to show any discrepancies from the original calibration.

The most exacting measurements performed in the calibration of both types of transducers were the measurements of their thermal mass or heat capacity. These were determined separately for each calorimeter in its final mounted position.

[redacted]

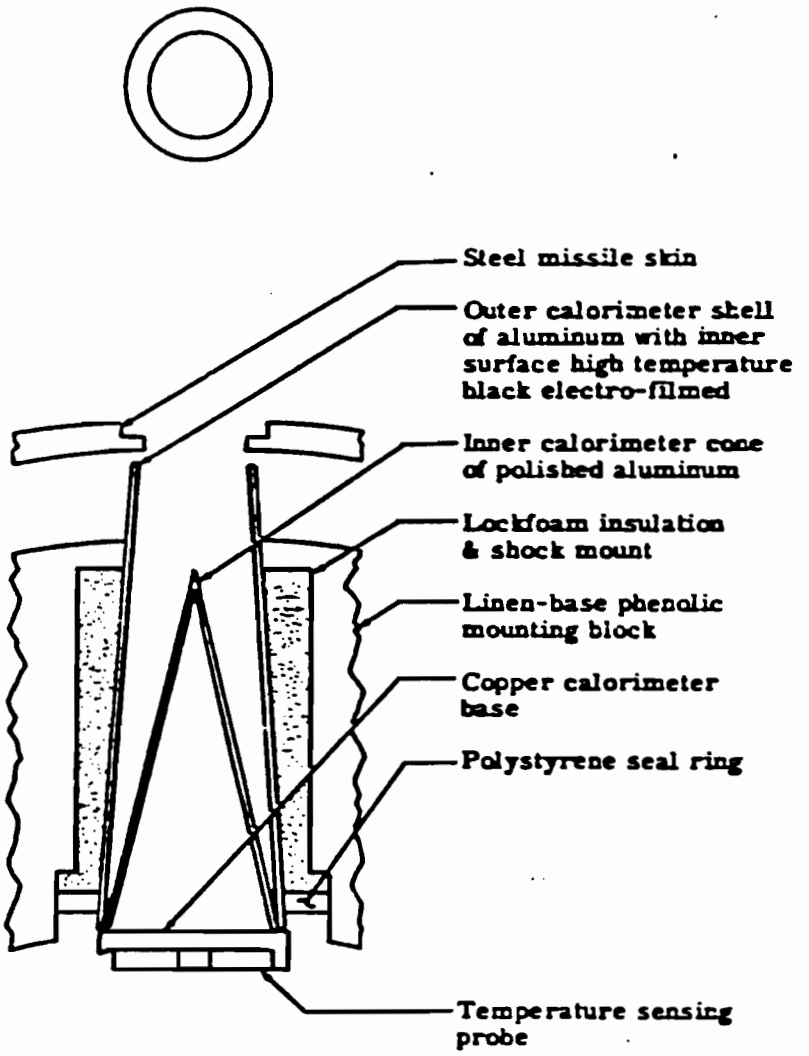

Fig. 2.17--Sectional view of thermal radiation calorimeter.

[redacted]

Standard water calorimetry methods were sufficiently accurate (± 5 percent) for the larger thermal radiation instruments, but this method was ruled out for the X-ray instruments because of the need for greater accuracy in these measurements. The heat capacity of these calorimeters was measured to within 3 percent by simultaneously employing the embedded sensing elements as electrical heaters and thermometers, recording temperature rise versus time as a function of energy input. Upon reaching steady-state conditions, the time rate of energy input equals the product of heat capacity times the time rate of temperature increase. Actually, heat losses became significant about 2 minutes after reaching the steady-state conditions, so that values recorded after this time were never used for deriving heat capacity.

The two upper instrument rockets carried X-ray and thermal transducers of the types shown in Figs. 2.16 and 2.17 with the exception of a change in X-ray filters on the lower rocket, as previously noted in Section 2.1.2, due to lower predicted X-ray intensities at this position.

Since these instruments were mounted in the carrier midsections and the carriers were spin stabilized, a problem was immediately evident. Examination of the planned positions of these two rockets at burst time reveals the difficulties more clearly. In the case of the uppermost carrier (Station TK-252, Fig. 1.1), the transducers had to face radially outward from the midsection and see equally well around the midsection circumference. Six dual X-ray transducers and eight thermal radiation calorimeters accomplished this satisfactorily, as discussed previously in Section 2.1.1. Since a limited number of telemetering subchannels were available, a total of 20 calorimeter outputs had to be monitored by three subchannels. This was accomplished by employing readout circuits of the type shown in Fig. 2.18. This circuit consisted of a simple Wheatstone bridge which monitored the temperature of six calorimeters and supplied four voltage calibration steps each second by subcommutation; eight calorimeters were monitored by the same circuit by sacrificing two of the calibration steps. The fixed bridge resistors and calibration resistors used were notably insensitive to temperature. It was necessary to have the "read" position separated by ground positions, as shown in the illustration, to prevent overdriving the subchannel during the "make-before-break" intervals of the subcommutating cycle.

Instruments in the second rocket (Station TK-209, Fig. 1.1) had to face upward along the rocket axis and had to be located about 8 inches outside the

[redacted]

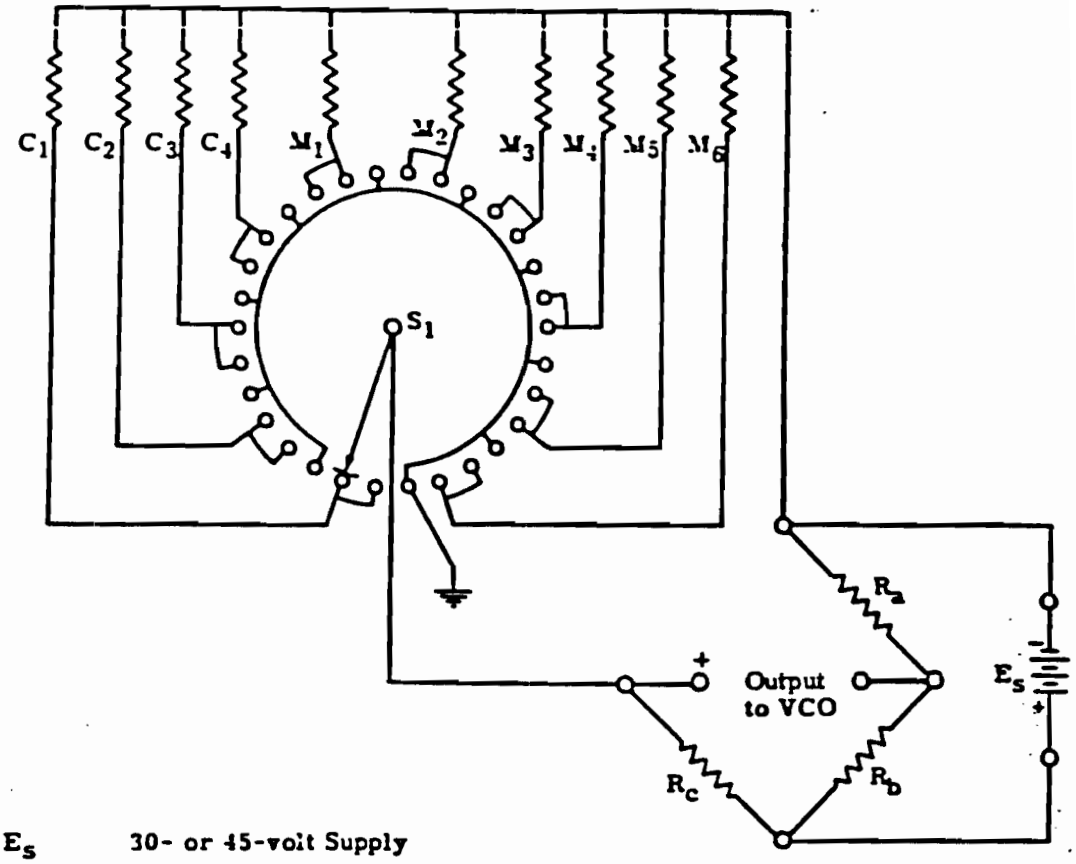

E_s 30- or 45-volt Supply

$R_{a,b,c}$ - Fixed 20,000 Ω Precision Resistors

C_1 - }
C_2 - } Fixed Calibrate Precision
C_3 - } Resistors
C_4 - }

M(1-6) - Wire Wound Temperature Sensing Probes, 20,000 Ω at 77° F

S_1 - Commutating Switch, Make-Before-Break; Approximately 1RPS

Calibrate - Measure Circuit for X-Ray & Total Thermal Detectors

Fig. 2.13--Readout circuit.

midsection skin in order to view the burst properly. This was accomplished by projecting the transducers out on doors which, when closed, formed arcs of the midsection circumference. Two such doors were used directly opposite each other on a circumference and each projected one set of transducers. Thus the Station TK-209 rocket used a total of six calorimeters and required only one readout circuit and one telemetering subchannel. A second subchannel was used for backup, since it was available.

The instrument ports of the Station TK-252 rocket were kept covered and the projecting doors of the Station 209 rocket were kept closed by tight spring-steel belts. The belts were released at predetermined altitudes by means of squib-fired retaining bolts.

2.2.3 Operational Problems

Two problems concerning these instruments were revealed in Tonopah test firings involving one of each type of carrier vehicle. In the case of the 252,000-foot rocket, it was noted that the temperature of the thermal radiation calorimeters rose approximately 40 degrees Centigrade above ambient upon ignition of the second stage. An examination of the geometry involved showed that upon assembly of the vehicle a portion of the second-stage igniter protruded into the instrumented midsection and was free to radiate heat into the base of these calorimeters. The instrumented Teak flights showed that corrective measures taken to eliminate radiation heating helped only slightly. It must be assumed that this trouble arose from another cause. Evidence of hot igniter gases leaking into the midsection compartment of a rad-chem sampler recovered from the Teak shot has caused some speculation that this could have caused the trouble in the instrumented midsections.

In the Tonopah test of the 209,000-foot rocket, it was found that, in assembling the vehicle for firing, the instrument doors were used as access ports to facilitate the making of mechanical couplings. It has been established that one or more lead wires were severed because of this situation, but the difficulty was eliminated by placing the lead wire connectors inside a protective aluminum box.

[redacted]

2.2.4 Data

Resistance versus time of the exposed X-ray detectors of Station TK-252 is shown in Figs. 2.19 through 2.22. [redacted]

Resistance versus time of detectors A_1 and B_1 of Station TK-209 is shown in Figs. 2.23 and 2.24. The energy recieved by each detector is given in Table 2.1. One door seems to have been partially in the nose cone shadow.

Resistance versus time of the Station TK-252 Z_1 detector is shown in Fig. 2.25. The rise in temperature prior to zero is discussed in Section 2.2.3. Table 2.2 gives the energy received by each thermal detector.

Resistance versus time of Station TK-209 Z_1 is shown in Fig. 2.26. The energy received by each of the thermal detectors of Station 209 is given in Table 2.2.

The resistance versus time for thermal detector Z_4 of Orange Station 125S is shown in Fig. 2.27. The energy received by each thermal detector at Orange Station 125S is given in Table 2.2.

The instrument arrangement and the energy received by each detector (both X-ray and thermal) for Teak Station 252 and Orange Station 125S are shown in Fig. 2.15.

2.2.5 Summary of Instrument Performance

The large error in burst-point positioning considerably exceeded allowances made for positioning errors in the design of these instruments;

[redacted]

Pages 79 through 87 are deleted.

[redacted]

consequently, the degree of accuracy of data collected by the instruments suffered to a great extent, and no useful X-ray data were obtained from Test Station 209 as noted in the previous section. Under these circumstances the ballistic calorimeter system probably functioned more satisfactorily than would have any of the other systems under consideration for the measurement of X-ray and total thermal energy.

Heat leakage into the calorimeter compartment after second-stage firing was unfortunate. This heating effect was most evident in sidesections where the instruments were designed to look radially outward, which lends support to the theory that the heat came from an internal source rather than from skin heating, since these were better insulated against skin heating than were the transducers mounted on the projecting doors. The instruments performed quite satisfactorily from an evaluation standpoint. This technique should prove useful in future tests of this nature. Also, no heating occurred before second-stage firing in the higher density air.

REFERENCES

1. Minzer, R. A., Champion, K. S. W., and Pond, H. L., The AFCC Model Atmosphere, Air Force Cambridge Research Center, Washington, D. C., 1959.
2. Victoreen, John A., The Calculation of X-Ray Mass Absorption Coefficients, J. Appl. Phys., Vol. 20, 1949, pp. 1141-1147.
3. Henke, B. L., White, R., and Lundberg, B., Semi-empirical Determination of Mass Absorption Coefficients for the 5 to 50 Angstrom X-Ray Region, J. Appl. Phys., Vol. 28, 1947, pp. 98-105.
4. Grodstein, G. W., X-Ray Attenuation Coefficients from 10 kev to 100 Mev, NBS Circular 583, National Bureau of Standards, April 30, 1957.
5. Bethe, H. A., Some Phenomena in High Altitude Explosions, LA-2184, Los Alamos Scientific Laboratory, December 11, 1957.
6. [redacted]

DNA (1)(3)

[redacted]

84

[redacted]

Chapter 3
NEUTRONS

3.1 THEORY AND ANALYSES

3.1.1 Introduction

The objectives of this project were twofold. The first of these was measurement of neutron spectrum from the warhead. Such measurements have previously been made of high-energy neutrons. At sea level, where measurement must be made at a distance from the detonation, interpretation of low-energy data in terms of weapon output is nearly impossible because of the complicated neutron transport through air to the detectors. On Teak, neutron detectors at Stations 252 and 209 directly measured the case spectrum since, with the low air density at this altitude, essentially no scattering occurred out to the detectors. Station 252 was located at 90 degrees to the warhead axis and Station 209 at an angle of 45 degrees, so that an estimate of the variation in output with angle can be made. These measurements are compared with calculated values of the output.

The second objective was to measure neutron flux at such positions that data from neutrons which had passed through considerable amounts of air could be compared with transport calculations. Only data from one Teak rocket is of value to this comparison and its value is questionable, since the data were gathered in a direction which did not receive an unshielded view of the output neutrons. Fortunately, one good set of data was obtained for comparison from the Orange event.

3.1.2 Discussion of Teak Experiment

Good data were obtained from the two highest rockets, Stations 209 and 252 (Fig. 1.1) which define the neutron spectrum from the warhead. In the original plan, at burst time one of these rockets was to be on the warhead axis and the other was to be perpendicular to the axis. A combination of placement and orientation errors resulted in positions at angles of 45 and

[redacted]

[redacted]

90 degrees from this axis. One of the Redstone pods, instrumented by Project 8.6[1] and which carried neutron detectors, was located at an angle[2*] less than 15 degrees from the Redstone axis. Thus the neutron output was measured at three different angles from the Redstone axis.

Neutron data obtained from all Sandia rockets are given in Table. 3.1. Angular dependence of the neutron output from the burst is shown graphically in Fig. 3.1; these values were obtained by R^2 extrapolation of the data to the source. Corresponding quantities calculated by Bing and Lessler[3] are included in this illustration for comparison. An independent calculation by Walter Goad[4] gives the spectrum averaged over all directions but does not give the angular dependence. These averages are also included in Fig. 3.1. Accuracy of these calculations has been estimated to be a factor of 2.

[redacted]

An uncertainty difficult to evaluate obtains when a comparison is made between calculated and measured neutron flux. The absolute calibration of the activation sample-measuring system is not well-known. Furthermore, this absolute calibration depends on the neutron spectrum, since activation cross sections are not ideal step functions with energy. This calibration error is perhaps 25 percent.

DNA (b)(3)

*Letter cited states that final neutron data of Project 8.6 is unchanged from ITR-1652. Angle of pod to Redstone axis is stated to be less than 15 degrees (ABMA calculations yield value of 13.5 degrees and MSQ tracking data give 1.3 degrees).

[redacted]

Pages 91, 92, and 93 are deleted.

[redacted]

Low-altitude rockets, Teak Stations 35 through 60, were so placed that calculations of neutron transport[5,6] could be experimentally checked. Unfortunately, data obtained at these positions were seriously degraded [redacted] Because of this low flux, the only activation samples which had sufficient activity at recovery to yield flux values were the sulfur and gold samples at Station 59. Of these two measurements only the sulfur sample offers a check on the transport calculations.

[redacted]

TABLE 3.2--COMPARISON OF CALCULATED AND MEASURED FLUX AT TK-59

[redacted]

[redacted]

DNA (b)(3)

[redacted]

3.1.3 Discussion of Orange Experiment

Data from Orange Station 72 provide a good check on neutron transport calculations.[6,7] Station 125S data are good; however, this rocket was too close to the burst to allow a critical check of the calculations (see Fig. 1.2).

Station 72 was located at an angle of 30 degrees to the weapon axis, and thus was away from the shadow region so troublesome to interpretation of Teak results. Based on weapon output measured on Teak, transport calculations were made of flux at both of these Orange stations. Accuracy of calculations is estimated to be a factor of 2 for Station 72. At Station 125S the calculational error is estimated to be 10 percent for zirconium, increasing to a factor of 2 in the plutonium flux. Calculated values are compared in Table 3.3.

TABLE 3.3--COMPARISON OF CALCULATED AND MEASURED FLUX ON ORANGE

[redacted]

3.1.4 Summary

Data obtained on Teak for the warhead output at 90 degrees to the axis agree with calculated values within stated calculational accuracy. Measured

[redacted]

[redacted]

values show that variation with angle, at least between 30 and -5 degrees, is about as calculated.

Orange data substantiate transport calculations through the atmosphere to about the estimated accuracy of the calculations.

3.2 INSTRUMENTATION

3.2.1 Design Criteria

Instrumentation design was influenced by space and weight limitations imposed by the instrument carrier. In selecting systems and components, preference was given to those which were simple and compact.

Time-of-flight techniques were considered for measuring the neutron energy spectrum at the two highest Teak stations, 209 and 252 (Fig. 1.1); however, such a system would have required a record-playback memory device because of both early-time radiofrequency blackout and frequency-response limitations of the telemetry system. This would have resulted in a very complex system for development within the limitations imposed by the instrument carrier and time scales. At the lower Teak stations, 39 through 60, neutron transport would have complicated time dependence of the flux energies to an extent that spectral determination from a time-of-flight measurement would have been practically impossible. For these reasons it was decided that a modified form of the conventional threshold-detector technique should be used.

This system in principle has two major advantages over a time-of-flight system, namely: (a) activation samples themselves act as a memory device in that their activity decreases slowly with time so that counting may continue during the entire time of the rocket's descent, and (b) activation sample measurements give an energy spectrum independent of the time dependence of neutron flux. Disadvantages of activation techniques will be apparent in the following sections.

3.2.2 Instrument Description and Calibration

Conventional threshold activation samples, i.e., zirconium, sulfur, uranium 238, neptunium 237, and plutonium 239, were used. Beta rather than gamma activity of the sulfur and fission foil samples was counted, since it was expected that gamma background from the detonation would interfere with

[redacted]

[redacted]

sample counting. Despite the high beta-to-gamma sensitivity ratio of the detector, [redacted] sample counting was, therefore, continued after the parachute-suspended nose cone dropped out of the region of high gamma flux until impact with the ocean.

Two views of the neutron-detector assembly are shown in Figs. 3.2 and 3.3. The detector consisted of a photomultiplier tube having a terphenyl activated-plastic scintillator, 0.030 inch thick by 1 inch in diameter, an integrated counting-rate amplifier to drive a subcarrier oscillator, and a wheel to hold the activation samples. The samples were stepped past the scintillator by a Geneva step mechanism driven by a small electric motor. The sample wheel, except for an access hole for the photomultiplier and wheel-drive shaft, was surrounded by 2 centimeters of powdered boron 10 in a 1/32-inch-thick steel container.

In addition to the activation samples, a blank (background) position was included in the wheel. To extend the range of neutron flux which might be detected, each sample was counted on different sensitivity ranges of the detector on alternate revolutions of the wheel. Samples were calibrated by exposing the entire detector assembly to the flux from the Godiva II and Cockroft-Walton facilities at Los Alamos. Nominal calibration data for a fission foil are given in Fig. 3.4.

Figure 3.5 shows two views of an instrument nose cone with location of major components indicated. Additional sulfur samples on all stations and fission foils in a boron 10 canister on the two highest stations of both Teak and Orange were included for laboratory counting. These were located on the shelf immediately below the neutron detector but are not visible in the illustration.

3.2.3 Data and Instrument Performance

Results of neutron data obtained from Teak and Orange are summarized in Table 3.1. Four of six instrument nose cones on Teak and two out of three on Orange were recovered, permitting laboratory evaluation of the activation foils. The recovered fission and zirconium foils were counted at Johnston Island; the sulfur samples were flown to Eniwetok. Laboratory analysis of these recovered samples was performed by Project 2.-. All samples from Teak Stations 20, and

[redacted]

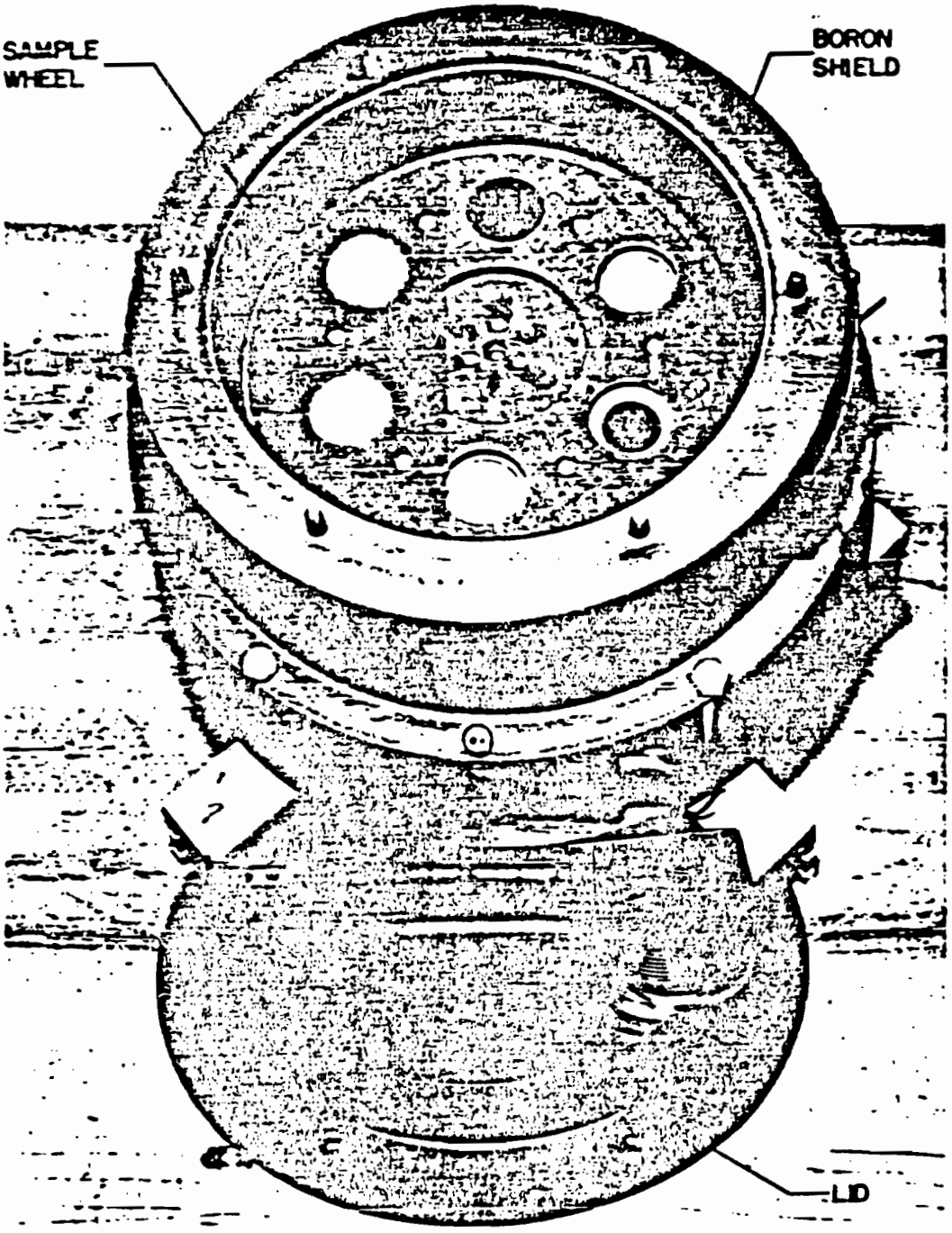

Fig. 3.2--Neutron detector, top view.

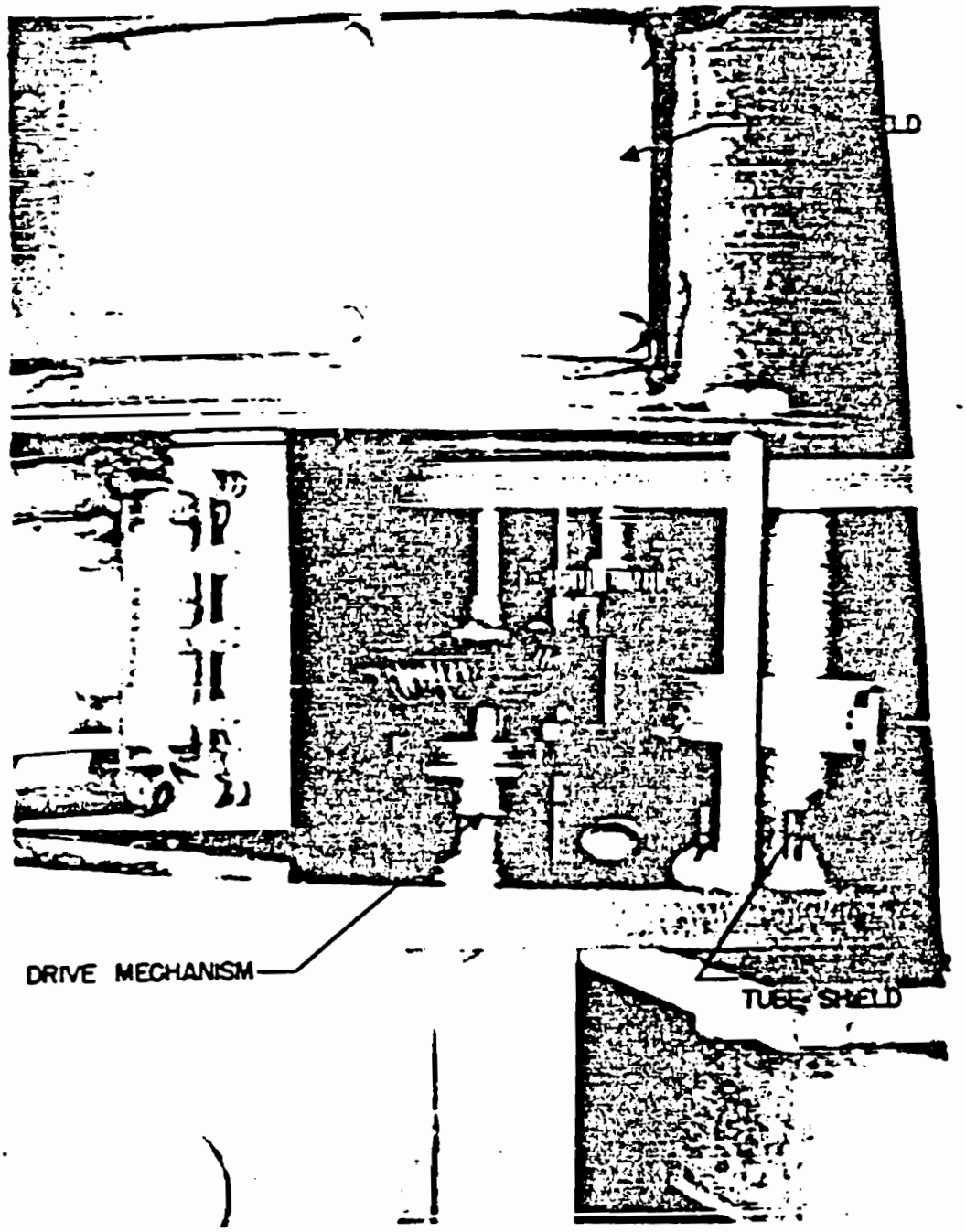

Fig. 3.3--Neutron detector, side view.

[redacted]

Fig. 3.4--Calibration of neptunium foil #336, 0.404 g.

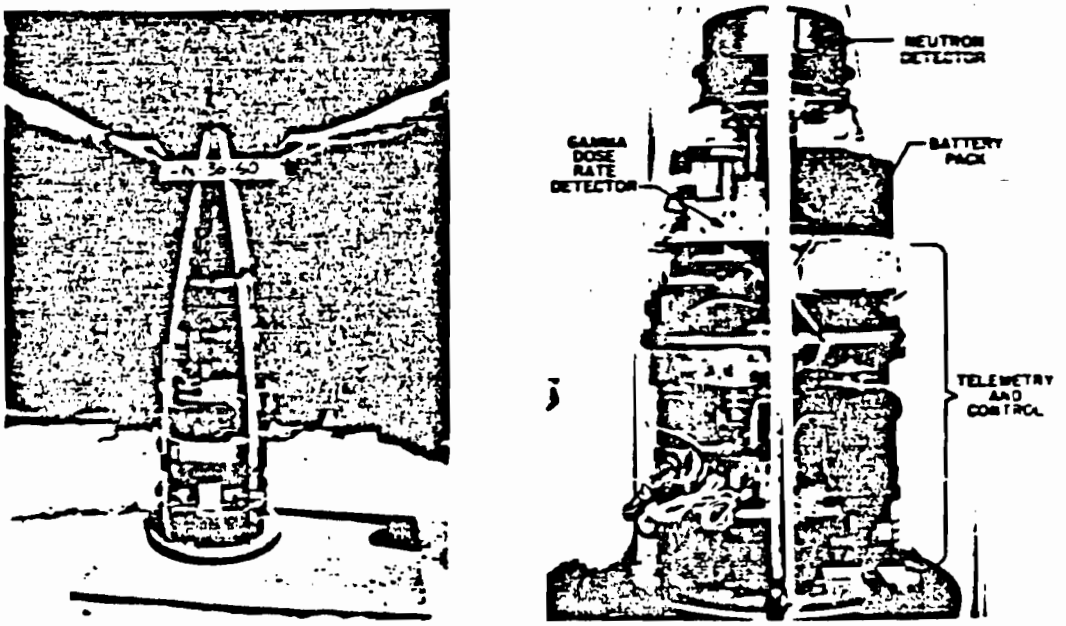

Fig. 3.5--Fully instrumented nose cone with skin removed.

[redacted]

[redacted]

252 and Orange Stations 72 and 135 were sufficiently active to yield good data. Those from Teak Stations 39 and 59, with the exception of sulfur from Station 59, had decayed to near background levels. Thermal neutron data were obtained from gold and cobalt samples which were flown to Sandia for evaluation.

Telemetered records showed that all neutron detectors functioned mechanically (i.e., the sample wheel was turning) until impact. There was an electrical malfunction on Station 39 during the entire time of fall; also, Station 60 data were lost because its transmitter went off the air at 4 seconds after launch. Station 252 operated properly until 175 seconds after burst at which time there was an electrical malfunction. The background was still sufficiently high to mask foil activity during the time Station 252 was functioning. All other detectors functioned until impact. Background count masked sulfur data on the Teak stations and all data on the three Orange stations. Telemetered data were obtained from fission foils at Teak Stations 48, 59, and 209. For reasons given in Section 3.2.4, the uncertainty in values given in telemetered data is at least a factor of 3.

3.2.4 Conclusions and Recommendations

Background caused more difficulty than was anticipated in the evaluation of telemetered data. There is evidence that an appreciable portion of this interference activity came from materials outside the detector itself.

When instruments at Godiva II were calibrated, access to the exposed detectors was not allowed until approximately 20 minutes after burst because of radiation hazard in the vicinity of the machine. Since all instrument nose cones impacted less than 20 minutes after burst, it was necessary to extrapolate the calibration curves backward in time. As a result of different induced background activities at calibration and in the actual event, the slopes of the observed decay curves differed in the two cases. The flux as read from the data would, therefore, depend upon the time at which it was read out. This caused the uncertainty cited in Section 3.2.3. The numbers given in Table 3.1 represent the average of telemetered data read out at 200 seconds and 1000 seconds after burst.

Because of the high probability of recovery of instrument packages from the ocean, laboratory counting of recovered activation samples is probably the simplest and certainly the most accurate technique for measurement of neutron

[redacted]

[redacted]

flux spectra from bursts similar to Teak or Orange. Small rockets and sample packages could be used.

The feasibility of telemetering neutron-flux data has been established. This might be desirable for bursts at locations where recovery of samples would be unlikely, at regions of low flux where sample activity decay might preclude the possibility of obtaining data after recovery, or as a backup measure for unrecovered samples.

Accuracy of telemetered data could be improved considerably by the following means:

(a) Use of a nose cone designed primarily for neutron measurements and having low-activation materials throughout;

(b) Selection of threshold detectors with half-lives of the order of a few minutes and thresholds at energy levels of interest (if these can be found); this would increase the sample-activity-to-background ratio and also aid in isolation of desired activity from recorded data;

(c) Use of separate pulse-height channels for each type sample to discriminate against unwanted activities.

[redacted]

*Based on work performed by W. H. Buckalew, Sandia Corporation.

DNA (6)(3)

[redacted]

[redacted]

REFERENCES

1. Annis, M., et al., Vulnerability of Missile Structures to Nuclear Detonations, ITR-1652, Part 1, Allied Research Associates, Boston, March 13, 1959.

2. Letter, Mr. Chinn, WADC, Wright-Patterson Air Force Base, Ohio, to C. R. Mehl, Sandia Corporation, dated December 10, 1959.

DNA (b)(3)

3. [redacted]

4. Goad, Walter B., and Allen, Lew Jr., Vulnerability of Nuclear Weapons to Neutrons from a Nuclear Explosion, LA-2246, Los Alamos Scientific Laboratory, October 3, 1958.

5. Latter, Albert and Latter, Richard, Remarks on the Sunlamp Proposal, TRC-RM-1831, RAND Corporation, Santa Monica, California, December 1956.

6. Mehl, Clarence R., unpublished work on Sunlamp calculation for a 250,000-foot burst, Sandia Corporation, Albuquerque, New Mexico.

7. Burnett, William D., unpublished work on a Monte Carlo neutron flux calculation for the geometry of Orange shot, Sandia Corporation, Albuquerque, New Mexico.

8. Zipprich, L. J., Radiation Effects Testing at the Los Alamos Godiva II Facility, SCR-76, Sandia Corporation, April 1959.

[redacted]

[redacted]

Chapter 4

GAMMA RAYS

4.1 THEORY AND ANALYSIS

4.1.1 Introduction

It is the purpose of this section to compare experimental data on gamma-ray intensity versus time with a calculational model of fission-product attenuation and time decay. Table 4.1 outlines the principal variables which enter the model and gives the sources of data on the variables.

TABLE 4.1--VARIABLES AND DATA SOURCES

Variables	Assumptions
Spatial distribution of gamma-ray activity	Point source with a rate of rise approximately that observed
Energy distribution of fission-product gamma rays	Mott Water Boiler Spectrum, Phys. Rev., 86, 753 (1952), and LA-1620,[1] Fig. 5.3, p. 87
Attenuation and buildup of photons of various energy	LA-1620,[1] Fig. 7.10, p. 117
Time dependence of fission-product gamma-radiation source	LA-1620,[1] Fig. 5.2, p. 86

On the left are the quantities which we must know to solve the problem. On the right are assumptions regarding the nature of the variables. LA-1620 provides the basis for these assumptions, but modifications have been made and are discussed in this chapter.

An adjustment was made in the attenuation and buildup curves of LA-1620. That an adjustment was necessary was observed and pointed out by J. Marcum of RAND Corporation and is based on considerations of the conversion between photon buildup and energy buildup. Table 4.2 shows the results.

[redacted]

[redacted]

TABLE 4.2--NORMALIZED FISSION-PRODUCT GAMMA-RAY ENERGY VERSUS RANGE IN AIR

Source \ Range (gm/cm^2)	0	10	20	40	60
LA-1620	1.00	0.846	0.687	0.361	0.160
Adjusted	1.00	0.848	0.696	0.394	0.200
Source \ Range (gm/cm^2)	**100**	**120**	**140**	**160**	**180**
LA-1620	0.0575	0.0225	0.0099	4.18×10^{-3}	1.88×10^{-3}
Adjusted	0.0573	0.0481	0.0251	0.0126	6.33×10^{-3}

Since a point-source geometry is used, geometrical $1/r^2$ divergence of energy must be inserted. The distance between the source and the instrument carriers can be found as a function of time. A cloud-rise rate [redacted] was used for Teak and [redacted] for Orange, as determined from preliminary photographic data. The rocket trajectory is accurately known for most instruments flown by Sandia (see Chapter 9).

Results presented below are based on calculations which proceeded as follows. First, the spatial distribution of gamma-ray intensity at zero time was found from Table 4.2, [redacted] The time dependence of the spherical spreading term was then found by computing the time-dependent distance between the rocket and the fission-product debris as explained above. This distance was then converted into an appropriate number of gm/cm^2 of air by using the ARDC model atmosphere.[2] The assumption that the inhomogeneous atmosphere can be treated in this way is implicit here and is legitimate according to Monte Carlo calculations done by Marcum. Finally, the time decay of the intensity of the source was treated according to Fig. 5.2 of LA-1620.[1]

[redacted]

[redacted]

4.1.2 Results

Results of calculations outlined above are presented in a series of graphs and in Table 4.3. Figures 4.1 through 4.5 give comparisons of computed values and Teak measurements. Figures 4.6 through 4.8 are similar displays for the Orange event. Table 4.3 summarizes the results.

TABLE 4.3--SUMMARY OF GAMMA-RAY DATA FROM TEAK AND ORANGE

Station	Integrated dose (roentgens) Experiment*	Calculated
TK-252	[redacted]	[redacted]
TK-209	[redacted]	[redacted]
TK-59	[redacted]	[redacted]
TK-48	[redacted]	[redacted]
TK-39	[redacted]	[redacted]
OR-125S	[redacted]	[redacted]
OR-115R	[redacted]	[redacted]
OR-72	[redacted]	[redacted]

DNA (b)(3)

*Under the experimental values, F stands for film badge; G means the reading was obtained with a glass dosimeter; T means a dose obtained by integration of telemetered dose-rate-versus-time data on all Teak stations and OR-72. On Orange Stations 115R and 125S, data with T designations come from telemetry recordings of total gamma-dose transducers. All calculated total doses are time integrated.

[redacted]

Pages 107 through 114 are deleted.

[redacted]

4.1.3 Discussion

Preshot calculations similar to those presented here were made at Sandia Laboratory.[3] The differences between the present effort and preshot work are as follows:

(a) Accurate, rather than predicted, rocket trajectories were used, together with accurate positioning of the warhead at zero time.

(b) Cloud-rise rates were inserted on the basis of observations; in ITR-1601 they were neglected.

(c) No effort was made in this analysis to include the effects of gamma rays produced by neutrons captured in nitrogen. This is a defect in the present treatment. However, the large mass of material in the Redstone missile between the warhead and the earth prevented a good fraction of the neutrons which otherwise would have escaped in that direction from so doing. Monte Carlo calculations by C. R. Mehl[4] of Sandia indicate that the frequency of (n, γ) reaction is somewhat lower than had been estimated.[3] Further, the (n, γ) source is extended in space. For these reasons, it is felt that (n, γ) contributions were not significant, and no indication of this component is found in the data.

There is more information available from the model. From Table 4.2 one can find a quantity proportional to the energy deposited per unit path length in the atmosphere. This is done in a straightforward way by converting the number of gm/cm^2 of air traversed to an equivalent height in the atmosphere. This results in the integral curve shown in Fig. 4.9.

Actually, the intensity is given by

$$I(r) = I_o B_r \frac{e^{-\mu r}}{4\pi r^2}$$

and Fig. 4.9 is, as indicated, a plot of $4\pi r^2 I(r)/I_o$ versus r. The derivative of this function is also plotted in Fig. 4.9. This curve is, together with the integral curve, a measure of energy deposition per unit path length in the atmosphere. The maximum of the derivative in Fig. 4.9 occurs at about 21 to 23 km above the earth's surface. This is in rough agreement with more sophisticated calculations of the height of maximum energy deposition. LASL results[5]

[redacted] Page 116 is deleted

give 25 km above the earth as the place of energy deposition for fission-product gamma rays.

[redacted]

flux. Estimates of such intensity, together with the inclusion of prompt gamma radiation, indicate that the net effect would be to increase measured fission-product gamma doses by only a few percent at most. There exists the possibility that film badges and glass dosimeters are themselves sensitive to neutron radiation. Experiments performed by J. A. Beyeler of Sandia* indicate, however, that under a flux of > 3.5×10^{13} neutrons/cm^2 [redacted] from the Godiva reactor at LASL, no effect on either the glass or film packs can be detected. [redacted]

4.1.4 Conclusions

The assumed model has been compared with measured dose rates and doses for the Teak and Orange events. [redacted]

*See Section 4.2 of this report.

[redacted]

According to E. York,[7] it is possible that most of the additional energy is concentrated in relatively low-energy gamma rays. Because the experiments mentioned above are not completely analyzed,[8] the point will be pursued no further beyond mentioning that there is a possibility that the discrepancy between the model of this report and the experiment can be explained when analysis is complete.

4.2 INSTRUMENTATION

4.2.1 Design Criteria

The gamma dose is caused by both fission-product decay and neutron capture by nitrogen in the atmosphere. At some stations the fission-product contribution was expected to predominate after several seconds. Extrapolating this fission-product contribution backward in time and subtracting it from the total would then give the dose arising from capture of neutrons by nitrogen.

In order to follow the gamma-dose rate for a time sufficient to accomplish this, a detector capable of covering several orders of magnitude was required.

4.2.2 Instrument Description and Calibration

The gamma-dose-rate-versus-time instrument for the four lower Teak stations and Orange Station 72 consisted of an RCA 6199 photomultiplier tube with a

[redacted]

terphenyl-activated plastic scintillator. The current to the photomultiplier divider was controlled through a 12A4. The scintillators were 1 inch in diameter, with thicknesses of 0.250 inch for Station TX-39, and 0.050 inch for Stations TX-48, TX-59, and TX-60. (See Figs. 1.1 and 1.2 for station locations.) Action of the circuit (Fig. 4.10) is such that the current through the 12A4 is maximum with no excitation of the photocathode. The 12A4 current decreases with increasing signal.[9] Voltage developed across a resistor in the plate circuit of the 12A4 is used to drive a subcarrier oscillator.

A plot of the ratio of output voltage to no-signal voltage versus light-energy input is linear on log-log paper over four orders of magnitude in energy input.

The DASA cobalt 60 source at Sandia was used to calibrate these instruments. Typical calibration data are shown in Fig. 4.11. The plotted points correspond to data obtained from the cobalt 60 source. Extrapolation to higher dose rates is justified by the fact that the instrument is linear to $V/V_o = 0.32$ when excited with a calibrated pulsed-light source.

At the two highest stations on both Teak and Orange the dose rate was expected to be high enough for selenium photovoltaic cells to monitor the light produced in a sodium iodide crystal. Transducers for these stations were 1-inch cubes of sodium iodide with a photovoltaic cell optically coupled to each face with silicone fluid. The assembly was hermetically sealed in a thin aluminum case by the Harshaw Chemical Company of Cleveland. The series voltage generated by the photovoltaic cells was used to drive a subcarrier oscillator directly. These units were calibrated with a kilocurie cobalt 60 source at Sandia Laboratory. Typical calibration data are shown in Fig. 4.12.

Total gamma-dose transducers were included in the nose cones at Stations 209 and 252 on Teak and 125R and 115S on Orange. These transducers consisted of glass, which darkens under gamma radiation (Corning #9762), placed between a tungsten light source and a selenium photocell. The decrease in photocell output is then a measure of the gamma dose seen by the by the glass. Calibration was accomplished by insertion of glass which had been exposed to known amounts of cobalt 60 radiation. Nominal calibration data are shown in Fig. 4.13.

In addition to telemetered instrumentation, passive elements, including film badges and chemical dye dosimeters, were installed for evaluation after

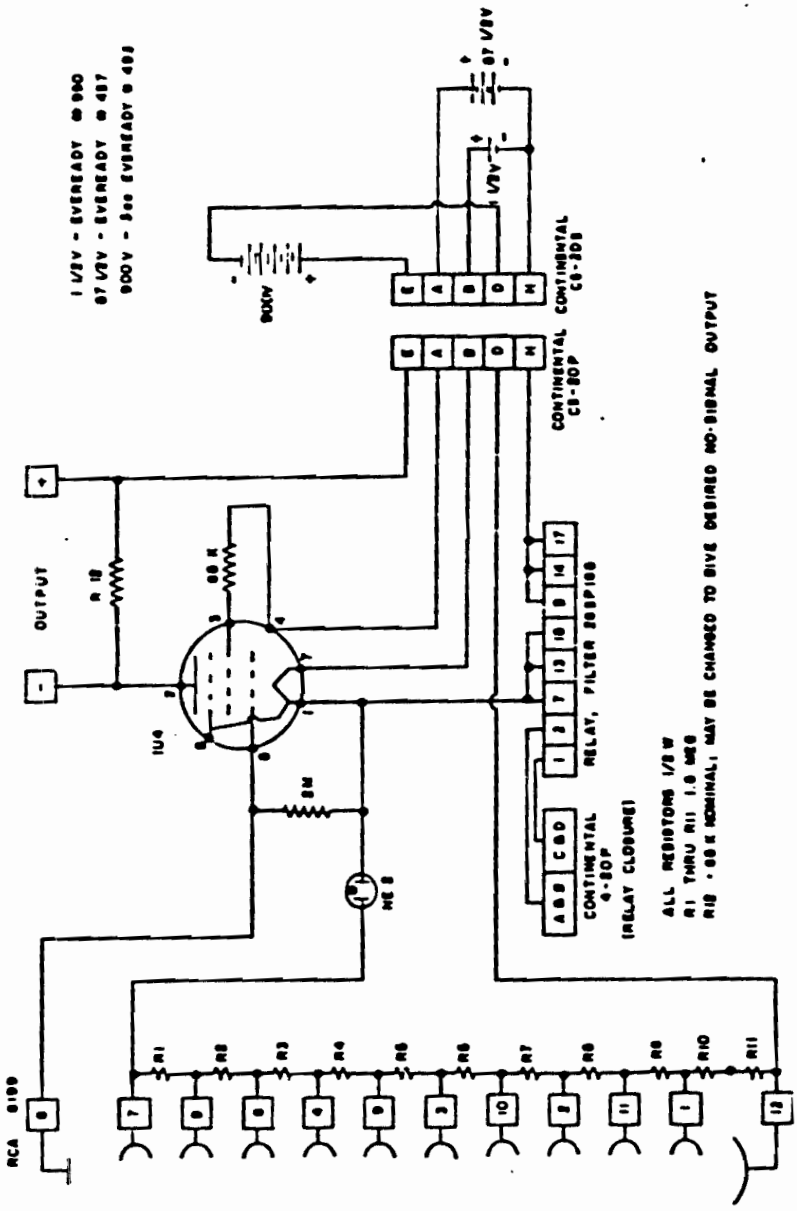

Fig. 4.10--Circuit diagram of low-altitude gamma-dose-rate instrument.

Fig. 4.11--Calibration of low-altitude gamma-dose-rate, Gauge No. 100.

[redacted]

Fig. 4.12--Calibration of high-altitude gamma-dose-rate, Gauge No. y971.

Pages 122+123 are deleted.

DNFI (b)(3)

117

nose-cone recovery. Provision was also made to evaluate the gamma glass dosimeters in the laboratory.

4.2.3 Data and Instrument Performance

Gamma-dose-rate-versus-time data were recorded from Stations 39, 48, and 59 on Teak and Station 72 on Orange. A typical record (Station TK-59) is shown in Fig. 4.14. The cyclic dips in the record are produced by varying shielding of the detector which is caused by nose-cone rotation. The curves shown in Fig. 4.15 are plotted by taking readings at the maximum points of these cycles. No data are available from Teak Station 60.

Total gamma doses received at each station as measured by the various types of detectors are summarized in Table 4.4. The total dose as seen by dose-rate-versus-time instruments was obtained by graphical integration to a point where the rate had decreased to 0.01 percent or less of its original value.

The gamma-dose-rate instruments recovered from Teak and Orange, and a spare which had not been flown, were recalibrated on the same cobalt 60 source used for preshot calibration. There were no significant differences in the two sets of calibrations after correction for the interim decay of the source strength.

Slight indications were noted on the recording channel allocated to the total gamma dose transducers at Teak Stations 209 and 252, but these were so close to noise level as to be unreliable. The lower detection threshold of these units was in excess of 20,000 roentgens. Results from the total gamma transducers at Orange Stations 115R and 125S are given in Table. 4.4. A zero-level shift occurred in these two telemetering channels; therefore, the integrated dose was read out as of the time of the postshot calibration sequence when a zero-level reference was available.

Film badges used were unshielded triple packs of DuPont emulsions 502, 834, and 1290, and packs of unshielded Eastman double-coated emulsion 548-0. The approximate upper limits of measurement for these emulsions are 20, 1000, 10,000, and 38,000 roentgens, respectively. Glass dosimeters were Corning #9762. Locations of the various components are shown in Fig. 3.5.

Pages 125 and 126 are deleted.

[redacted]

4.2.4 Conclusions and Recommendations

Information was obtained from each type of detector exposed except chemical dye dosimeters which suffered age deterioration, and gamma-dose-rate instruments at the two high stations on each shot which were apparently below their detection thresholds when radio propagation was resumed after several tens of seconds.

[redacted]

Most film emulsions show a marked increase in sensitivity to gamma rays of low energies (less than about 0.15 Mev), while the sensitivity of many organic fluors decreases in this region. One would, therefore, expect bare film badges to indicate considerably higher doses if an appreciable portion of the incident gamma were in the lower end of the spectrum.

[redacted]

REFERENCES

1. Malik, J. S., Summary of Information on Gamma Radiation from Atomic Weapons, LA-1620, Los Alamos Scientific Laboratory, January 1954.
2. Minzer, R. A., Champion, K. S. W., and Pond, H. L., The ARDC Model Atmosphere, Air Force Cambridge Research Center, 1959.
3. Cook, T. B., et al., High Altitude Measurements, HIR-1601, Sandia Corporation, January 1959.
4. Private communication from C. R. Mehl, Sandia Corporation.
5. LASL-DIR 1436, Monthly Program Status, Los Alamos Scientific Laboratory, March 1959.

[redacted]

6. Private communication from Capt. E. Hippoli, AFSWC, Kirtland Air Force Base, New Mexico.

7. Private communication from P. Fischer, Lockheed Missiles and Space Division, Palo Alto, California.

8. Verbal communication from E. York, Boeing Aircraft Corp., Seattle, Washington, in a conference at Kirtland Air Force Base, October 1959.

9. Brown, P., and Carp, G., Gamma Rate versus Time, Operation Castle, ITR-913, Signal Corps Engineering Laboratories, Ft. Monmouth, New Jersey, May 1954.

[redacted]

Chapter 5

RADIOCHEMICAL SAMPLING

5.1 SAMPLER DESIGN

5.1.1 Introduction

[redacted] It was decided, therefore, to attempt to obtain a debris sample from Teak for radiochemical analysis as a yield check. Additionally, if future tests are forced to high altitudes by political pressures, sampling technique development will have been started.

Los Alamos Scientific Laboratory (J-11 Division) indicated interest also in obtaining a sample from the rhodium labeled Orange shot. Sandia agreed to attempt to obtain a sample, provided spare rocket motors were left over from a successful first Teak shot. Later there was widespread interest in obtaining a sample from Orange; plans for the shot were expanded to include three sampler rockets on Orange at the expense of losing the complete repeat capability on Teak.

These developments, together with LASL calculations on the debris behavior of Teak shot, necessitated revisions of the sampling program. The final plan allocated two sampler rockets to Teak and four to Orange, with one spare sampler for a second Teak shot. One Teak sampler was to be at apogee above the burst at zero time; the second was to rise from beneath the burst to pass through burst point twenty seconds after time zero. The sampler placed above the burst was intended to sample debris carried upward by an immediate large-scale flow. A calculation by LASL (J-10 and T-5 Divisions) indicated that such a flow would occur. The second was a "hedge" in case debris behavior was similar to that for sea level detonations.

Such early sampling was necessary, not only because of cloud rise uncertainties, but also because winds at burst altitude can be high and unpredictable. A wind survey was conducted before the test to determine necessary wind corrections. Data on winds near Teak altitude are given in Section 5.3.

[redacted]

[redacted]

Early sampling of Orange shot did not seem feasible, since the debris cloud was expected to be fairly dense, and because of rocket limitations sampling at burst altitude would have been difficult at the planned range. It was decided to sample the cloud 35,000 feet above the burst point. Sampler rockets were to pass through this elevation above the burst at 40, 80, 90, and 120 seconds after burst time.

5.1.2 Debris Characteristics at 250,000 Feet

Before exploring sampler designs, certain aspects resulting from the detonation of the device should be examined. Of particular interest are debris cloud diameter, cloud rise, and particle size. In considering these effects in conjunction with sampler design, calculation results are summarized. SC-4172(TR) gives a more complete analysis.[1]

Ambient conditions at various altitudes were considered. By this is meant the values of pressure, density, and temperature assigned to the various elevations.

Cloud Diameter. Several authors have already considered burst effects at the 250,000-foot elevation.[2,3] Their treatments of the possible diameter achieved by debris from the burst are incomplete, since they consider debris behavior only until it has mixed with a mass of air equal to that of the bomb itself. This corresponds to radius of about 1000 feet from the burst point at 250,000 feet.

Their treatments overlook the momentum associated with device expansion. It is true that the kinetic energy which the expansion represents is rapidly dissipated as the material contacts the surrounding air. The momentum, however, is conserved. A study of the consequences of this momentum conservation is carried out in the above-mentioned report by the author. The result is a prediction of a spherical layer (termed "shell") of material expanding from the burst point. This shell is made up of the bomb debris and the air which was originally between the shell surface and the burst point. Analytic expressions may be written for this shell velocity, for the time required to achieve a particular radius, and for the kinetic energy remaining in the directed motion of the shell particles. These are:

[redacted]

[redacted]

$$v = \frac{4.55 \times 10^6}{1 + \left(\frac{r}{1000}\right)^3} \qquad \text{Velocity in ft/sec} \qquad (5.1)$$

$$t = \frac{1}{4.55 \times 10^6} \left[r + 250 \left(\frac{r}{1000}\right)^4 \right] \qquad \text{Time in seconds} \qquad (5.2)$$

$$KE = \frac{1}{\left[1 + \left(\frac{r}{1000}\right)^3\right]} \qquad \text{Kinetic energy in ergs} \qquad (5.3)$$

where r is the shell radius in feet.

The expanding shell was expected to maintain its identity until the speed of sound within the shell was about that of the directed shell motion. Since the radiation loss was high, the late shell temperature was expected to be about 10^4 degrees Kelvin. This corresponds to a sound speed of 10,000 feet per second. At a radius of 7500 feet the shell should lose its inward integrity, and debris, together with encompassed air, was expected to start filling the void within the shell. This turbulent phenomenon was expected to accomplish dispersion of the debris fragments throughout a volume having a radius nearly that which was initially obtained. An eventual hydrodynamic expansion of the heated air was expected. When these processes were completed the debris was expected to be situated in a sphere having a radius of about 15,000 feet. The debris cloud was expected, of course, to become even larger as the hot gas bubble lofted.

Cloud Rise. The possible initial debris cloud diameter achieved has been examined, since it is an important parameter in estimating the effectiveness of the sampling program. The second parameter, also of importance, is whether the debris rises with the heated air after the burst. By approximate arguments it can be shown that, for a given gas-bubble size and a given temperature ratio between the gas of the bubble and ambient, the same rise behavior can be expected. Such an argument does not take account of atmosphere

[redacted]

[redacted]

structure considerations, but it is none the less a useful "toe-hold" for applying scaling. Such scaling can be accomplished, once a rather arbitrary diameter to the hot bubble is assigned. For the 250,000-foot test a diameter [redacted] was taken. This dimension seemed physically reasonable, since it corresponds to the outermost range at which the temperature of the high-altitude fireball compares with that of the sea level fireball (6000 degrees Kelvin).

At 250,000 feet it was further assumed that the expected cloud rise would be the same as that for a sea level fireball of the same diameter. Using the curves given in TM 23-200,[4] the cloud rise can be predicted. This procedure predicts an eventual cloud rise [redacted] in a time of about 8 minutes. The initial rise velocity was expected to be about [redacted]

The previous cloud rise discussion could be termed conventional, since the prediction is based on sea level experience. A LASL (J-10, T-5 Divisions) calculation indicates that buoyant lofting of debris should not occur, but, instead, hydrodynamic forces should accomplish a much more rapid elevation. Physically, this effect should occur, since the pressure gradient is suddenly increased manyfold by heating, whereas the density is unchanged. LASL's calculation indicates that about 2 seconds after the burst the debris should achieve an upward velocity of [redacted]

Particle size. The last important parameter which needs to be considered for a sampler design is possible particle size. Momentum analysis has suggested an early cloud diameter so large that the debris from the device is widely dispersed. Since this dispersion is achieved while the gas is hot, it seems unlikely that significant particulation should occur. On the other hand, should the initial debris cloud be small until it is cooled, as suggested by the other analysis, considerable particulation, such as is experienced in lower elevation air bursts, could be expected. From the uncertainty of particle size, it is apparent that the filtering arrangement should be able to sample a large range of particle sizes down to molecules.

5.1.3 Filter Design for 250,000 Feet Altitude

Figure 5.1 depicts the impactor geometry. The air flow is deviated by the impactor vanes, while particles, by virtue of their larger inertia,

[redacted]

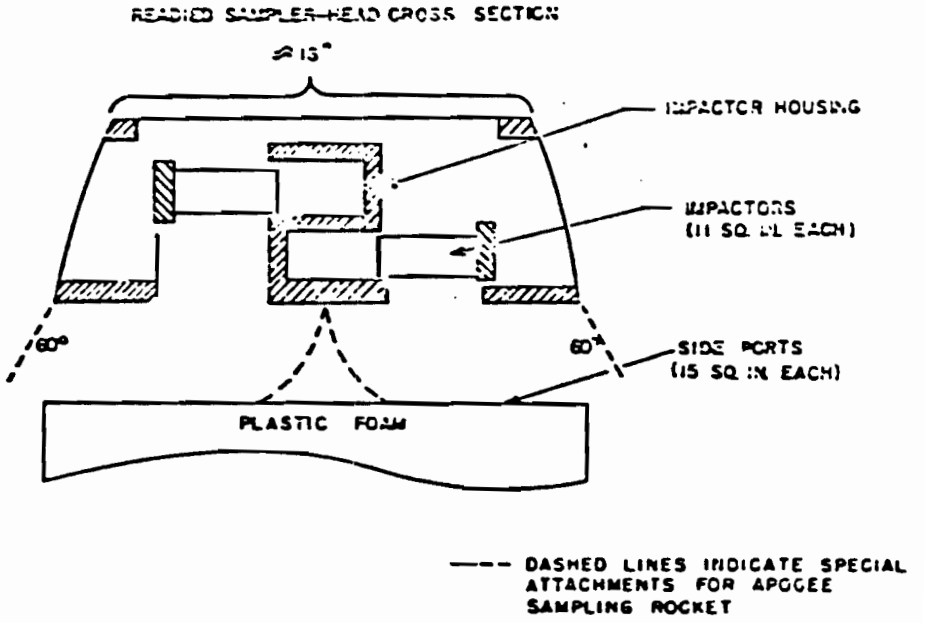

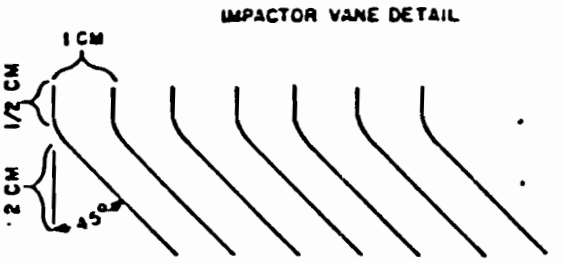

Fig. 5.1--Schematic diagram of impact sampler.

travel through this deviated air to be collected on the vanes. To insure collection, the vanes are coated with a grease. For molecules, the impactor collects by diffusion to the vanes.

Physical Laws. Before considering details of impactor performance, the physical laws covering the forces on particles, diffusion phenomena, and flow behavior must be examined. At 250,000 feet, instead of having a viscous flow slowing particles as at sea level, slowing is a bombardment process, since the particle diameter is small compared with the mean free path of the gas molecules.[5] The relation is

$$F = -1.35 \times \frac{4\pi}{3} \times \bar{v}\rho a^2 V , \tag{5.4}$$

where F is force, $\bar{v}$ is average thermal velocity of molecules, ρ is air density, a is particle radius, and V is the relative velocity of the particle.

The diffusion process is well enough known that detailed discussion is unnecessary. Computing the flow through the filter requires two steps. First, stagnation conditions in front of the sampler are calculated from sampler speed and air parameters. This may be easily accomplished by the use of NACA-TN-1428.[6] Once conditions in front of the sampler are known, the mass-flow rate through the impactor may be computed, since the side ports are at about side-on pressure. The flow through the impactor may be considered the flow between plates.[5]

The expression for the mass flow through the impactor per unit length (Q_m) is

$$Q_m = \frac{1}{12} \frac{W^3}{(RT)\eta L} \left(\bar{P} + 6\frac{\xi}{W}\right)(P_1 - P_2) , \tag{5.5}$$

where R is unit mass gas constant, T is the absolute temperature, W is the plate separation, η is viscosity, L is plate length, $\bar{P}$ is average pressure, ξ is the slip coefficient, and $(P_1 - P_2)$ is the pressure drop across the system.

The above relation is valid for viscous flow when flow velocity does not exceed acoustic. The flow through the impactor is considered isothermal,

since diffusion arguments show that the gas rapidly acquires the wall temperature. Furthermore, there is not enough gas flowing through the impactor to appreciably heat it. For the lowest elevations (220,000 feet), flow velocity, according to Eq. 5.5, would exceed acoustic. In this case the relation is still used but, instead of using the total pressure difference, a condition of acoustic flow velocity as it leaves the impactor has been applied.

Calculation of Impactor Performance. By use of the laws just discussed, impactor performance for a variety of conditions has been calculated. In these calculations, certain ranges of performance become apparent. First, for very small particles down to the diameter of molecules, the collection is effected through diffusion which, in nearly all cases, collects all debris carried by air flowing through the impactor. Next, for the range of particle sizes above molecular, impaction becomes important and, in most cases, a 100-percent impaction efficiency is achieved for diameters above 5×10^{-3} micron. There exists between these cases a transition range where collection is effected partly by impaction and partly by diffusion. Finally, for still larger particles of the order of above 10^{-2} micron, a third process becomes important. This process, which has been termed "gathering," results from particles penetrating the stagnation region in front of the impactor and striking the impactor or crossing streamlines leading to the impactor. Figure 5.2 shows the range of these various phenomena at 250,000 feet, where the sampler rocket velocity is 2000 ft/sec and ambient conditions are assumed. In addition to efficiencies for the various phenomena, a curve representing overall performance is also shown.

Impactor performance at 220,000 and 280,000 feet have also been examined in order to evaluate the variation of efficiency with altitude and speed.* Overall performance curves are presented in Fig. 5.3. Further, to examine the effect of the ambient temperature, overall performance has been calculated on the assumption that the temperature is 1000 degrees above ambient at 250,000 feet, while the pressure is ambient. The curve representing this overall performance is also shown in Fig. 5.3. Finally, in order to examine the effect of the constituents of the gas, it has been assumed that the air

*These calculations are based on a rocket apogee of 315,000 feet. The actual expected height was about 295,000 feet.

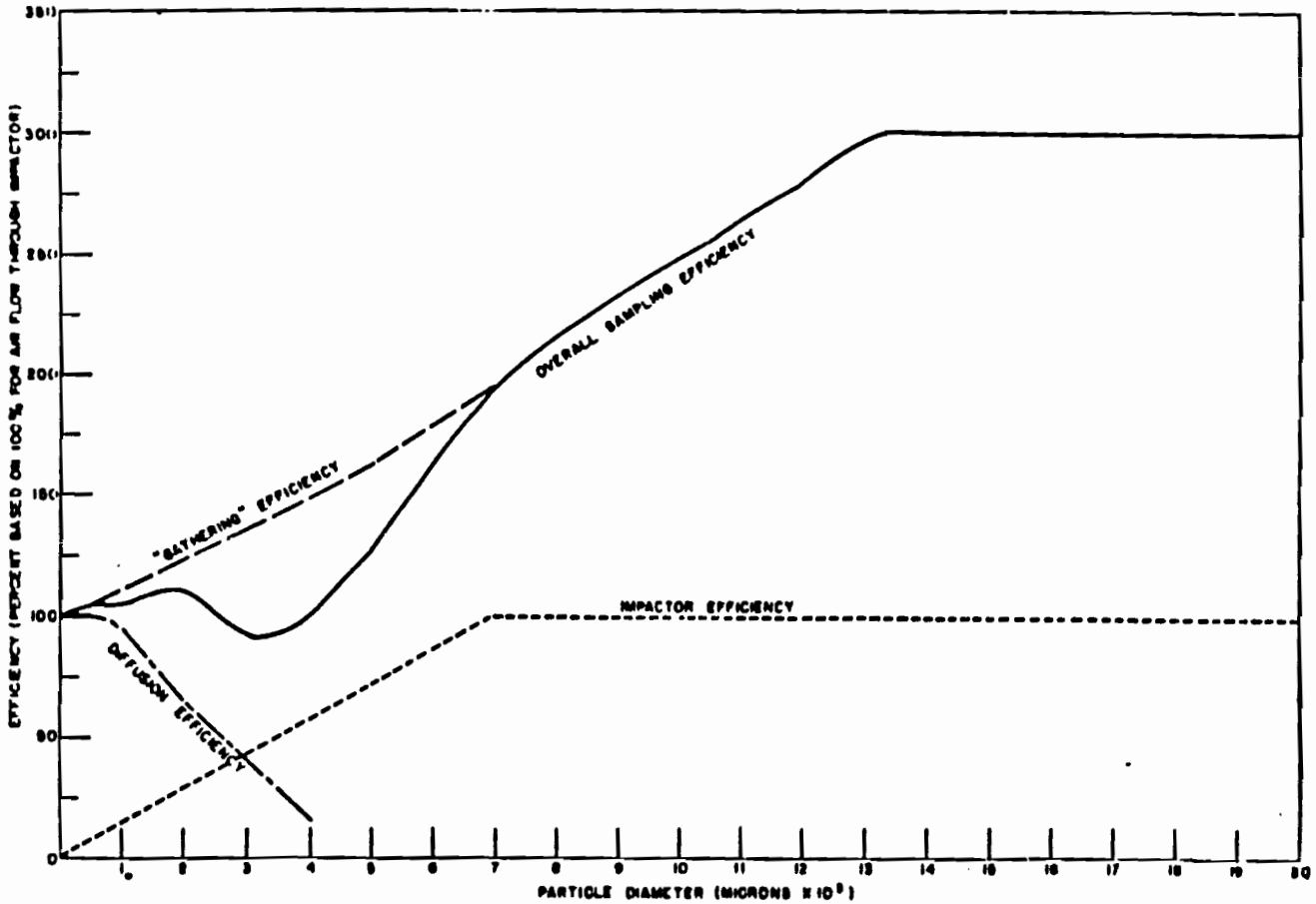

Fig. 5.2--Collection efficiency of the impactor for ambient conditions at 250,000 feet showing phenomena roles. Spherical particles are assumed to have a specific gravity of five.

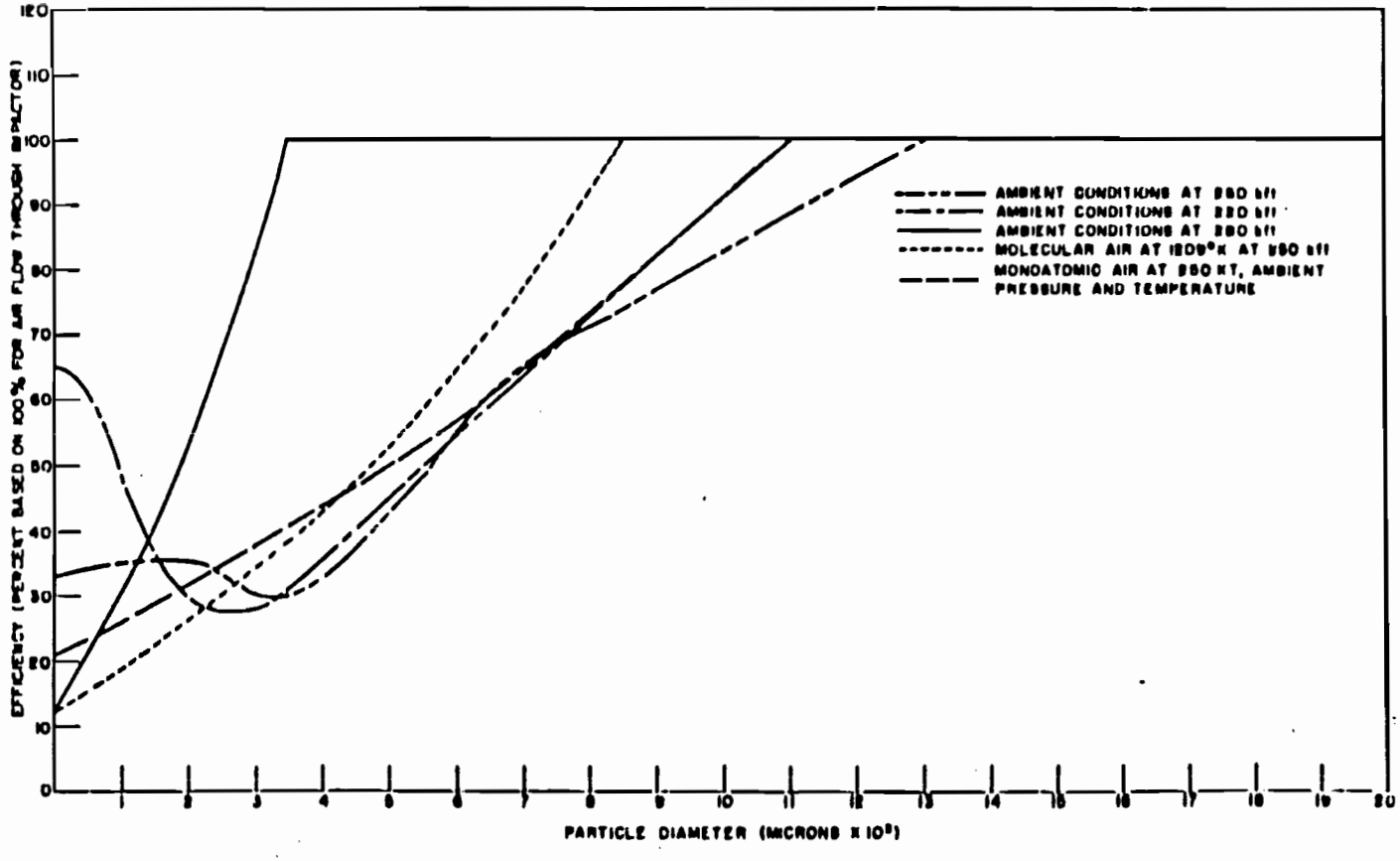

Fig. 5.3--Collection efficiencies of the impactor for various altitudes and conditions. Spherical particles are assumed to have a specific gravity of five. Efficiencies are based on the flow in the free stream through the normal impactor area.

[redacted]

is atomic rather than molecular, and calculations which assume ambient pressure and temperature at 250,000 feet have been repeated. Again the overall performance curve is presented in Fig. 5.3, which is based on 100-percent efficiency, provided all debris swept out by an area of the impactor were collected. Under all circumstances the collection is substantially the same for particles having diameters larger than 15×10^{-3} micron. Below this value there is some variation because of speed and air conditions. At low densities, the impaction and diffusion overlap in effectiveness to allow collection of all debris passing through the impactor. On the other hand, less air flows through the impactors under these conditions. At higher ambient densities, the flow through the impactor is large, but impaction and diffusion are less effective. On the whole, the impactor performance is markedly insensitive to conditions under which it samples.

The above considerations were based on a sampler rocket passing upward through the debris. Should the LASL debris-rise calculation be correct, the sampler rocket would never overtake the debris cloud, since the upward speed of this cloud exceeds that of the rocket by a factor of 2.5.

Since the LASL calculation seemed reasonable, a sampler rocket equipped with deflectors on the side ports was positioned to be at apogee above the burst at zero time. Performance of this arrangement could not be predicted with accuracy. It was believed probable that debris would be molecular because of the rapid expansion accompanying the rise. In this case collection would be accomplished by diffusion. About half the debris of the diverted flow would be collected on the impactor plates. The remainder would diffuse to internal channel walls before reaching the impactor plates.

Sampler Effectiveness. In determining expected impactor performance under various conditions, maximum sample size must be considered. Debris is assumed to be uniformly distributed in a sphere which has a radius of 15,000 feet. It is further assumed that the debris is of sufficient particle size to insure 100-percent collection. If the sampler rocket travels on a sphere diameter, a volume of $2\pi A$ would be swept out by the impactor, where r is cloud radius and A is impactor area. [redacted]

[redacted]

[redacted]

It was apparent that if the sampler rocket struck the cloud volume, an adequate sample would be obtained. (The estimated CEP for the rocket was 5000 feet.) In fact, samples could be so large as to require hot recovery techniques.

Thus far, sampler size based on conventional cloud-rise assumptions has been considered. A smaller sample would be obtained by the apogee rocket if the abrupt hydrodynamic debris rise occurred, since the cloud diameter would be larger (about 40,000 feet), and the sampler less effective. [redacted]

5.1.4 Debris Characteristics at 125,000 Feet

A device identical to that planned for the Teak 250,000-foot burst was planned for detonation at 125,000 feet. Since it was planned to label the debris from this weapon, LASL (J-11) requested that Sandia also obtain a sample from the lower Orange burst. Teak burst actually occurred at 252,000 feet and Orange at 141,000 feet.

Burst Phenomenology for 125,000 Feet Altitude. A different sampling technique was used for the lower Orange shot, since it did not seem feasible to sample a hot, relatively dense cloud. Furthermore, rockets used in sampling could be deviated from the vertical only by a limited amount. Therefore, it was determined to launch the sampler rocket at an angle which would allow sampling of the debris cloud at an elevation of 160,000 feet, or 35,000 feet above planned burst point.

Details of debris behavior in the burst vicinity were of less concern than the eventual cloud-debris diameter and the rise behavior. This was fortunate, since the burst at 125,000 feet had received less intense theoretical consideration than its higher companion shot.[3] It is known that energy radiated from the weapon is deposited relatively close, so it was expected that the eventual hydrodynamic behavior should be closer to that at sea level than for Teak shot.

[redacted]

At the same time, it was thought that sufficient energy might be lost through radiation in the first thermal pulse that a reduced yield should be used. Therefore, an effective yield of 2 mt was assumed and Sachs' scaling was used to estimate the bubble size. By this method, supplemented by approximate scaling of rise for identical cloud size and temperature ratios, cloud diameter and rise were estimated. It was assumed that the cloud diameter corresponded to the diameter of the fireball; the cloud-rise curves of TM 23-200 were used.[4] Results of this analysis indicated that an eventual cloud rise of about 120,000 feet could be expected. The cloud center should achieve an altitude of 160,000 feet at 80 seconds after burst, while the fireball top should arrive at 160,000 feet in about 25 seconds. Accordingly, the rockets were sent through a point above the burst, corrected laterally for winds at 40, 60, 90, and 120 seconds after zero. The first three samplers were to penetrate the cloud at 160,000 feet altitude and the 120-second sampler was to penetrate at 170,000 feet. The first sampler was expected to strike the cloud, but it was also intended as a hedge in the event of more rapid cloud rise than predicted. The expected cloud diameter was of the order of 50,000 feet.

Debris particle size was again of concern. With the wide dispersion implied by the scaling, it was believed probable that the debris would be molecular. On the other hand, particulate is often collected after air bursts in instances where dispersion should have been great. Either possibility was expected.

5.1.5 Filter Design for 125,000 Feet Altitude

A check calculation of Teak-type impactor performance indicated that this type instrument would be unsatisfactory for Orange, since high air density, together with the acoustic limitation of flow speed prevented its effective operation. Furthermore, diffusion is less significant at high air densities.

Fine screen, 200-mesh made of stainless steel, which can use the impaction phenomenon to collect debris was available. Analysis of the effectiveness of this type screen impactor was less thorough than for the impactor used on Teak. An analysis of sampling efficiency at ambient conditions for an elevation of 160,000 feet with a vehicle speed of 1560 ft/sec appeared sufficient. This vehicle speed corresponds to Mach 1.5. Such a limited

analysis range seemed justified, since the sampling was to be accomplished at substantially this altitude, and temperature effects were expected to be small. Furthermore, the percentage flow through the screen proved quite insensitive to Mach number. To compute the flow through the filter, an acoustically restricted flow through the holes of the screen was assumed. This yields about the same flow rate as does a friction analysis, and was accepted as being somewhat simpler and more physically realistic. The relation associating the mass flow per unit area (Q_m) and reservoir condition is

$$Q_m = \sqrt{\frac{2\gamma}{\gamma - 1} p_o \rho_o \left(\frac{p}{p_o}\right)^{2/\gamma} \left[1 - \left(\frac{p}{p_o}\right)^{\gamma-1/\gamma}\right]} \qquad (5.6)$$

Here p_o and ρ_o are reservoir pressure and density, while γ is the ratio of specific heats. The ratio p/p_o has a value of 0.52 for acoustical limiting.

Use of this equation, together with the values of stagnation conditions in front of the sampler rocket, indicates that the flow through the filter unit area is about 40 percent of the flow per unit area of the free stream. Impaction of particulate on screen wires proves very effective. Also, diffusion becomes effective well before the cutoff of impaction efficiency. Accordingly, of the material which flows through the screen, 66 percent is collected while the remainder passes through the openings. (This is pessimistic for debris molecules.) Gathering is still significant. It takes a particle with a diameter of 5×10^{-2} micron to penetrate the stagnation layer, here assumed to be 25 cm thick; therefore, the gathering effect causes variation of the overall efficiency for a large particle-diameter range. The overall performance of the screen impactor is presented in Fig. 5.4.

The screen has favorable characteristics for impaction collection but suffers from one weakness: the screen wire is rapidly heated by the flowing air. A rough computation demonstrates that it should reach ambient stagnation temperature in a few seconds at the 125,000 foot elevation. Therefore, late sampling at a higher elevation was found to be necessary. As a precautionary measure the screen was mounted on the front of the impactor arrangement, as backup in case of screen failure, and to collect fragments of grease which, on overheating, would flake off the screen.

[redacted]

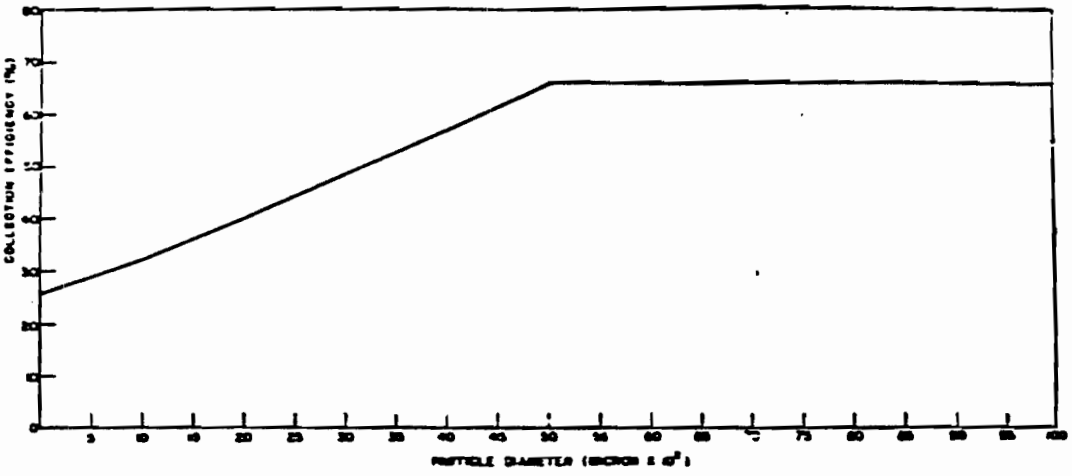

Fig. 5.4--Collection efficiency of 200-mesh screen at ambient conditions for 160,000 feet. Spherical particles are assumed to have a specific gravity of five. Efficiency is based on flow in the free stream through the normal screen area.

Sample Size. Maximum sample size may be computed by use of the same equations are were used for Teak. It will be recalled that the radius of the Orange cloud was expected to be [redacted] If the debris should be gaseous rather than larger than 1/2 micron, only about 40 percent of this amount would be collected. In either case, it was apparent that if the sampler struck the cloud an adequate sample would be collected.

5.1.6 Results and Analysis

No samples were obtained on either Teak or Orange shots. On Teak shot a number of measures, including lighter rocket fins, had been employed to achieve greater than design altitudes. Apparently these fins failed during or after second-stage burning, and the samplers fell within a mile of the launcher. Ironically, had they flown successfully, they probably would not have had a chance to sample, since detonation was about 35,000 feet north of the intended position.

[redacted]

[redacted]

Teak. The behavior of the Teak shot debris has been documented by Edgerton, Germeshausen, and Grier photography, while the very early behavior was recorded by a streak camera operated by LASL. [redacted]

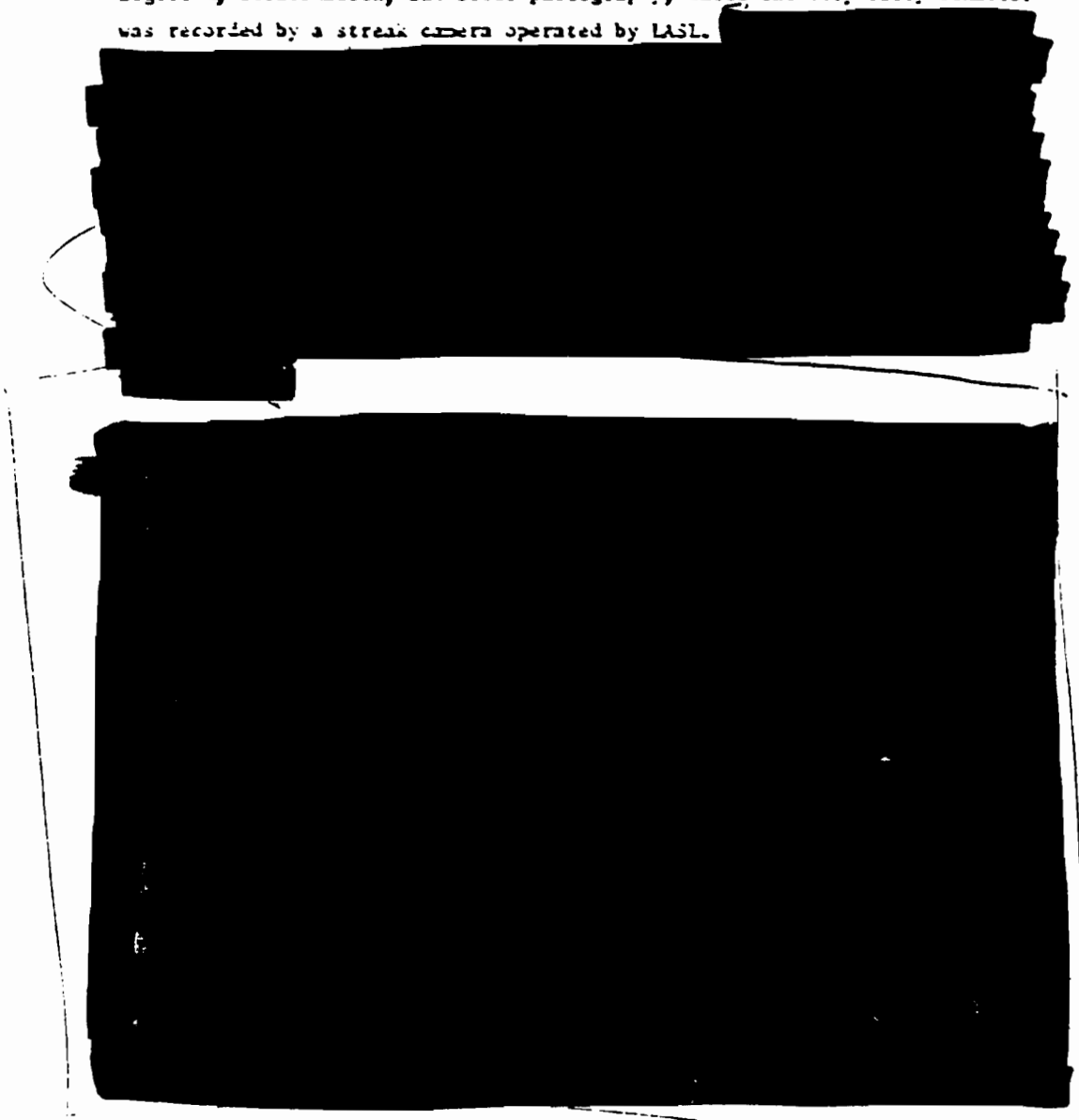

Fig. 5.5--Comparison of observed and predicted early Teak debris expansion.

DNA (b)(3)

[redacted]

[redacted]

Orange. Although no sample was obtained, the four Orange samplers performed satisfactorily. Impact points were close to those predicted, assurance that the intended trajectories were achieved. The rockets used on this shot were equipped with heavier fins than those used on Teak. The first sampler rocket (40 seconds) did show an activity suggesting a sample of [redacted] but a careful analysis by J-11 of LASL yielded no debris. Undoubtedly the activity observed in the field was neutron-induced.

It now appears that burst was 16,000 feet above the intended altitude as well as 11,000 feet beyond the intended range and that the debris rose more rapidly than was predicted. The situation is demonstrated graphically in Fig. 5.6. The observed behavior was obtained from EG&G photographs taken by cameras pointed specifically at the request of LASL (J-10 Division). It is evident that all sampler rockets passed well below the debris, although the first rocket skirted the lower edge of the fireball.

[redacted]

5.1.7 Discussion and Conclusions

No samples were obtained on either Teak or Orange. On Teak the vehicles failed because lighter fins were used than on the trial shots in an effort to achieve higher altitudes. On Orange shot the hardware performed perfectly but the sampler rockets passed below the debris cloud. The debris was missed because it rose more rapidly than was expected and because the detonation point was considerably above the expected burst altitude.

[redacted]

Page 145 is deleted.

[redacted]

An interesting question is whether an Orange sample would have been obtained if the burst had been at the intended position. If the rise rate of debris had been the observed rate, no sample would have been obtained. The first sampler would have passed below the lower edge of the debris even if it had passed through the fireball center. The debris rise rate would, of course, have been less had the burst been at intended altitude. However, it is still questionable whether the earliest sampler would have intercepted the debris; certainly all later samplers would have passed below it. In retrospect, if less dependence had been placed on prediction, positive results probably would have been obtained, because the sampler array would have been deployed to allow for a wider spectrum of debris rise rates rather than having been concentrated on obtaining a late cool sample.

While the rise-rate prediction method was unsuccessful, the estimate of the Teak debris-expansion behavior is more satisfying. There is detailed agreement in the early expansion, and even ultimate size, before considerable elevation, is about what was expected (30,000 feet diameter at 4 seconds).

In both Teak and Orange the debris appeared to be selectively elevated with respect to the fireball and it actually emerged above this ball of surrounding heated air. Certainly the debris was different in its hydrodynamic behavior from that of the heated air. Such a preference would be expected if debris presence somehow heated the surrounding air above that of the remaining fireball. It may be that the presence of debris enhances deactivation and molecular recombination, since local beta-particle heating seems implausible because of the long mean free path, particularly at the Teak altitude.

In conclusion, it is pointed out that although a sample was not obtained, the sample vehicle system was proven out. Should sampling under these shot conditions be attempted again there would be an excellent chance of success, since more is known now about debris rise rate and cloud shape. The task will not be small, however, as either a very early sample of the hot debris cloud must be obtained or the difficult target of the expanding torus must be pierced.

[redacted]

5.2 EQUIPMENT AND RECOVERY PROCEDURES

5.2.1 Introduction

The sampling elements which were to have been carried to Teak burst altitude are housed in nose cones having the same external configurations as those carrying instrumentation and are propelled by the same type rocket motors. Unfortunately, both rad-chem rockets on Teak went unstable at the approximate time of second-stage burnout, broke up, and fell into the sea about one mile from the launchers. The four sampler rockets fired on Orange flew their planned trajectories and were recovered. They did not, however, contain samples.

In operation, just before the rocket enters the radioactive cloud, the wind screen (the forward 24 inches of the nose cone) and two side-vent ports are ejected, exposing the sampling elements to the debris. At apogee the sampling elements are enclosed in a watertight compartment, and an RF homing beacon and a flashing light are actuated. During descent the nose cone separates from the second-stage rocket motor and a parachute is deployed to lower the nose cone to the sea. A search-and-recovery operation is then initiated for the sampler nose cones as well as for the instrumentation nose cones.

5.2.2 Sampler Nose Cone

The external configuration of the sampler nose cones is identical to that of the instrumentation nose cones (Fig. 5.7) and consists of a 24-inch wind screen, a 25 1/2-inch main body, and a 5-inch aft parachute ring. The wind screen is automatically ejected in flight to expose the filter just before the rocket enters the radioactive cloud. The parachute ring contains the parachute which is packed in a doughnut-shaped container, two dye-marker containers, and the flight-programming junction box. The main body contains two filters, a filter container having two separate watertight compartments, sampler-actuating mechanisms, a beacon transmitter antenna, a flashing light, two ejectable vent ports, a dye-marker container, and a watertight compartment containing the remainder of the beacon and flashing light components (Fig. 5.8).

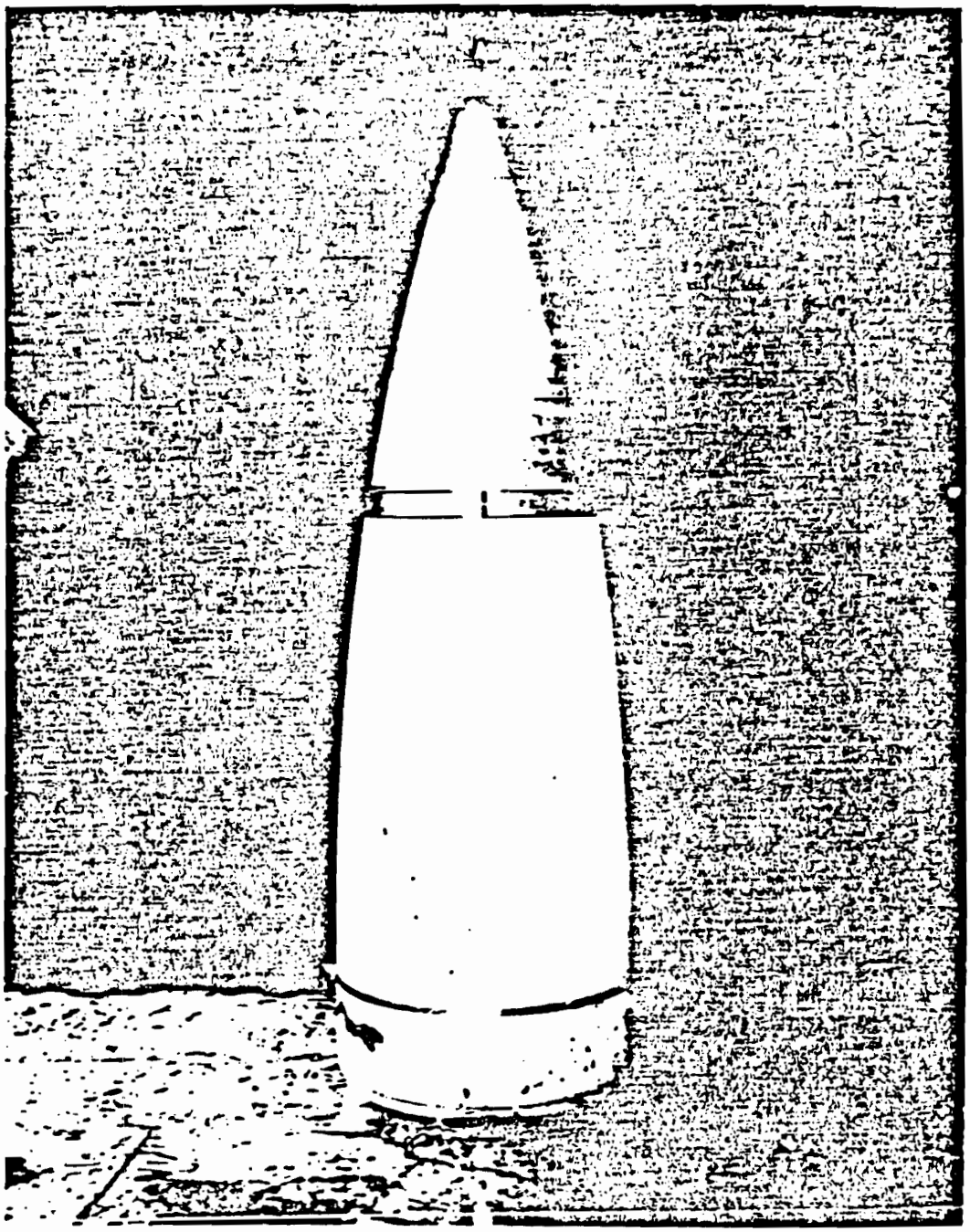

Fig. 5.7--External configuration of sampler nose cone.

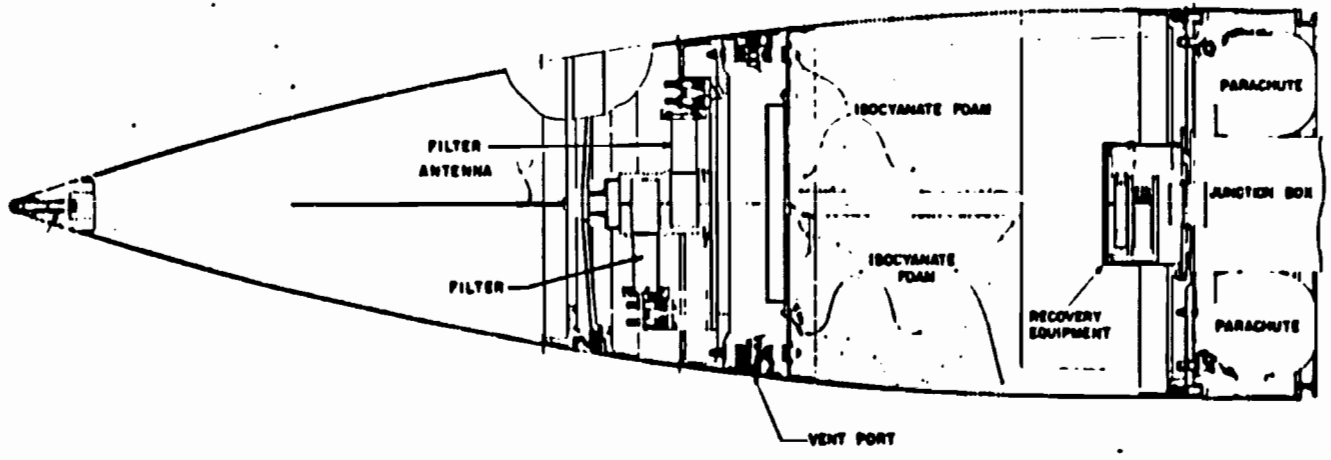

Fig. 5.8--Rad-chem sampler assembly.

[redacted]

Filter. The filter assembly is shown in Fig. 5.9. When the squib-actuated restraining bolts are blown out, the spring-loaded samplers are shoved toward the rocket axis into the center compartment. A watertight seal is maintained by a silicon-rubber "O" ring on the inside face of the sampler end plate.

Dye Marker. One dye-marker container is located in the vent passage just below the sampler container; two more are located on the bottom side of the base plate. The marker compound consists of equal parts by weight of polyethylene glycol (carbowax) and fluorescein disodium salt. Fluorescein is added to the melted carbowax and this mixture is poured into the containers. (Water soluble carbowax dissolves slowly in salt water. These containers continue to meter dye for 24 hours.)

Flashing Light. Since recovery of the nose cones from the ocean was scheduled to be made at night, the flashing light was added to aid recovery. This is a 30-volt, 30-watt bulb, potted in plastic and mounted on top of the sampler container. Its battery supply and flasher circuit are located in a watertight box on the top side of the base plate. The light flashes once each second and lasts for 35 hours.

RF Homing Beacon. Primary aids to recovery are UHF beacon transmitters in the 266.5-mc to 294.5-mc frequency range. Specifications of the beacon are:

Size	3 x 1-5/8 x 7/8 inches
Weight	7 ounces
Power Supply	two 33-volt, 3-amp/hour mercury batteries
Peak Power	1 watt
Average Power	100 milliwatts
Audio	1000 cps
Life	40 hours

Operation of the beacon is based on AM reception. However, during the approximately 100-microsecond period of each audio cycle that the beacon is transmitting, the carrier will shift 150 to 1500 kc. A shift of at least 150 kc is necessary, since the direction-finding equipment used in conjunction with the beacon is crystal-controlled and tunable in 100-kc steps. It was determined that the additional weight, cost, and time required to develop a crystal-controlled beacon was not warranted. When used with the airborne

[redacted]

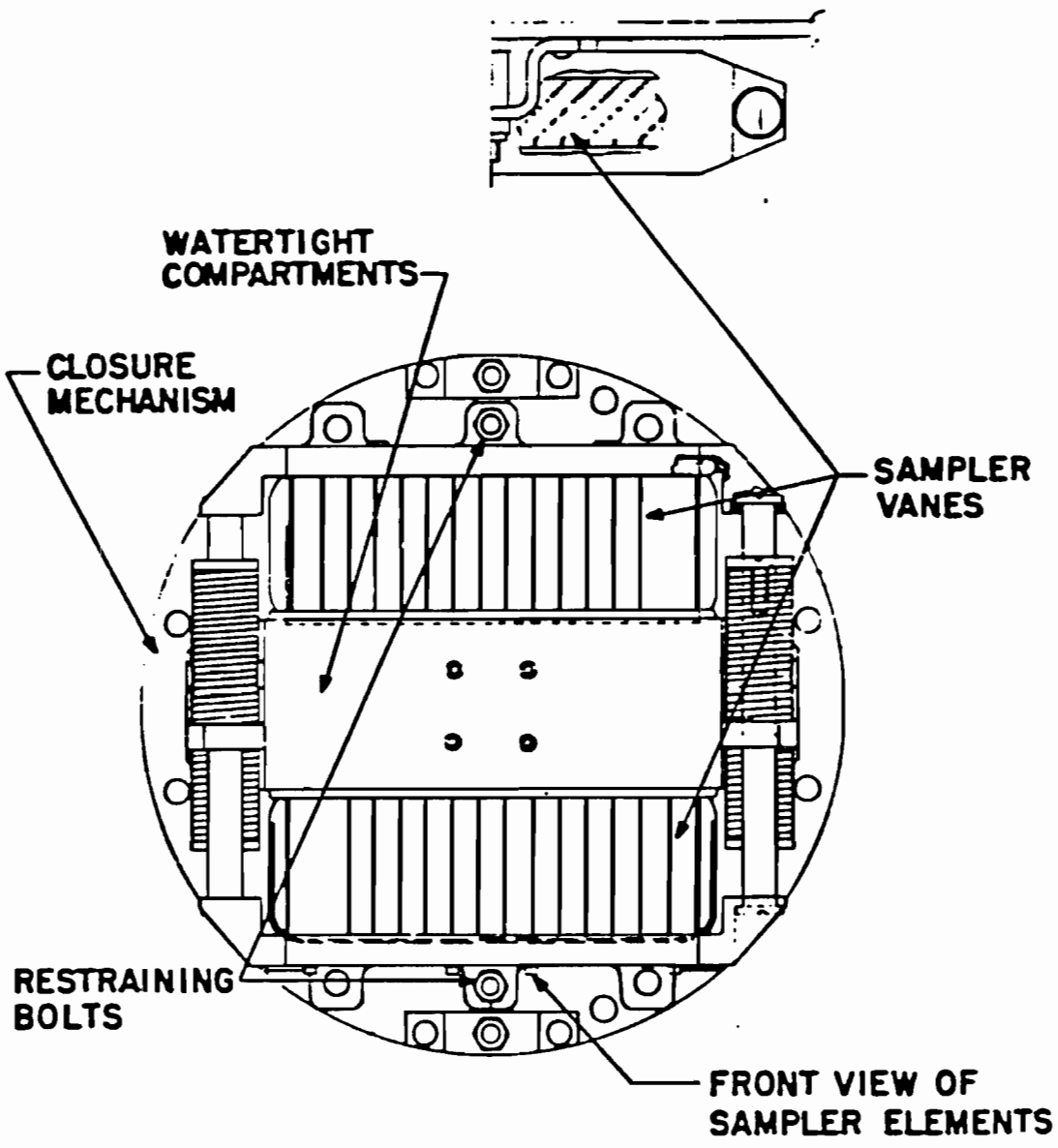

Fig. 5.9--Filter and plate assembly.

AN/ARC-7 receiver, the effective D.F range of the beacon is 15 miles; with the shipboard URD-4 receiver, the range is 3 miles. Beacon and battery are located in the base-plate compartment with the flashing-light battery and circuitry; the antenna is mounted on top of the sampler container. The beacon circuit is shown in Fig. 5.10.

Isocyanate Foam. Isocyanate foam, rather than watertight compartments, was used for buoyance because of the relative ease of fabrication and because structural damage that would rupture watertight compartments will not materially affect the foam.

5.2.3 Flight Sequence

All nose cone functions, which are controlled by an electrical timer located in the midsection between the second-stage rocket and the nose cone, are actuated by explosive squibs.

The first nose cone function is ejection of the wind screen and side-vent ports just before entry into the radioactive cloud. The vent ports are blown out radially by squibs acting against pistons attached to the inside face of the ports. The wind screen is held in place by a four-section split ring. The sections are first assembled in pairs. One section of each pair has a cylinder block containing a squib permanently attached to one end. The other section has a piston on one end which fits into the cylinder block attached to the first section; the piston is locked to the block by a shear pin. These two pairs are then fitted around the nose cone-wind screen junction and are bolted together. When the squibs are detonated, the lock pins shear, and the split rings are thrown from the nose cone with considerable force. A compressed spring then tilts up one side of the wind screen which is separated by the centrifugal force of the rocket's spin (3 rps) about its own axis.

At the time of sampler-door closure, which occurs at flight apogee, the RF homing beacon and flashing light are turned on. This is done by squib-actuated switches in the watertight compartment on the base plate.

At approximately 150,000 feet, the nose cone separates from the second-stage rocket in much the same manner as the wind screen leaves the nose cone. A static line is connected to the front end of the rocket motor; it deploys

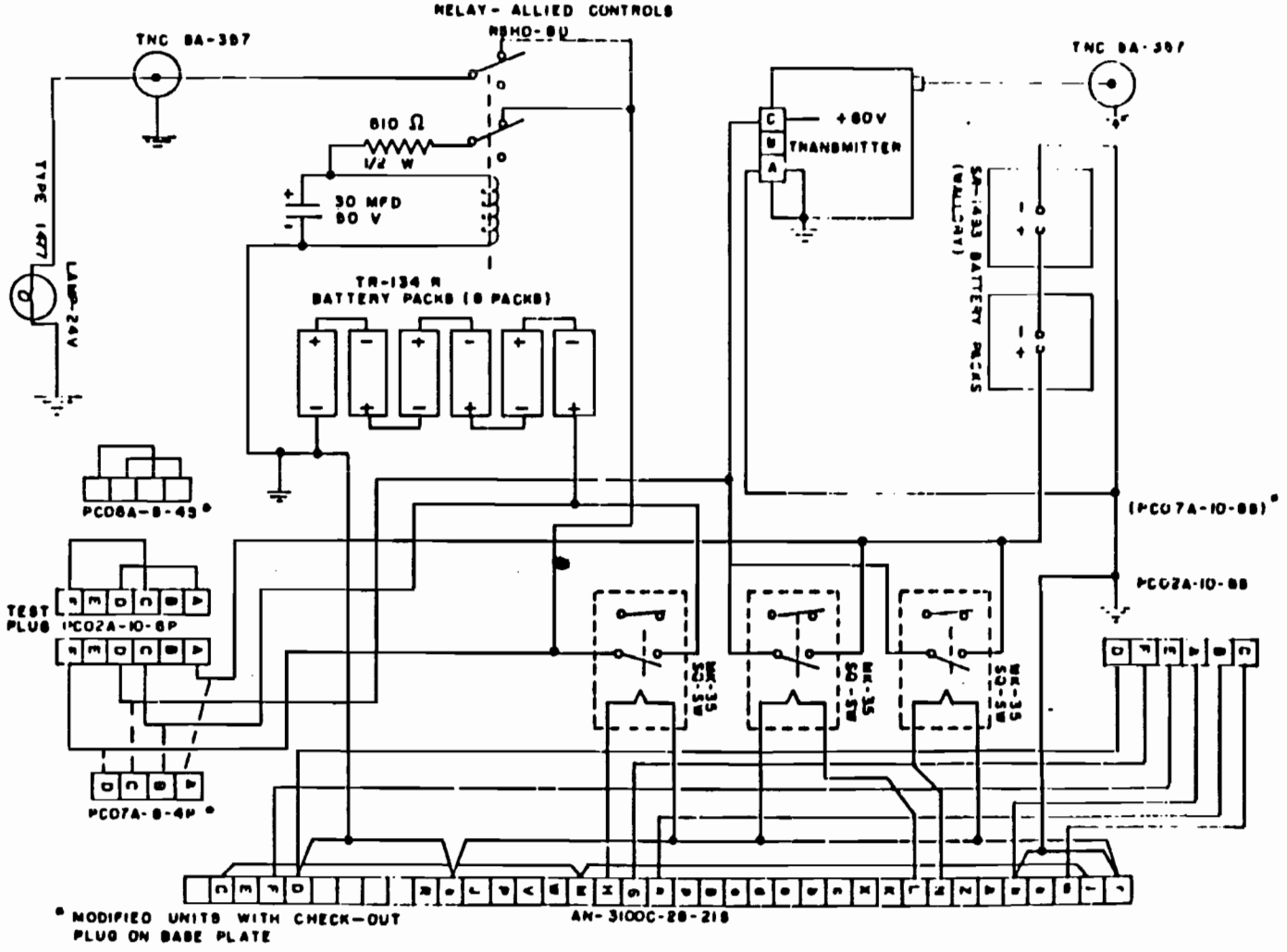

Fig. 5.10--Visual and RF beacon circuit diagram.

the parachute when the two units are well separated. Descent time from this altitude is approximately 25 minutes.

5.2.4 Recovery Planning

After both Teak and Orang shots, it was planned that the Naval Task Group (TG-7.3) would conduct recovery operations for the sampler and instrumentation nose cones and the WADC (Project 8.6) pod.

For Teak, the units to be employed were the destroyer escort Lansing, the salvage tug Safeguard, and two P2V aircraft. H-hour stations for the Lansing and Safeguard were to be on a bearing of 080 degrees from Johnston Island at a distance of 20 and 25 nautical miles, respectively. At H hour both ships were to depart for the impact area. The Lansing was to begin monitoring the telemetering frequencies of the instrumentation cones with URD/4 direction-finding gear for the dual purpose of obtaining time to impact and relative bearing at impact. During this same time interval the Lansing's air-search radar was to obtain as many fixes as possible on the descending objects.

The recovery controller in the Combat Information Center (CIC) aboard the Lansing was to use this information in conjunction with predicted times and positions of impact to give initial search directions to the P2V aircraft which were to take off from Johnston at H + 30 minutes. The Lansing CIC was to maintain a continuous radar track on the P2V, marking its position at such times as it reported being over a recovery object in the water. An order of priority for search and recovery was set in the following order: (1) WADC pod, (2) samplers, and (3) instrumentation nose cones.

Initial air search for a given unit was to cover thoroughly the probable impact areas. If the search was unsuccessful, it was to be switched to an object in the same or lower priority category. The aircraft were to drop flares on sighted objects to enable ships' personnel to recover them. The Lansing was scheduled to retrieve the WADC pod and the instrumentation nose cones; samplers were to be picked up by the Safeguard. It was considered necessary to use the Safeguard for sampler recovery, since possible radiation levels as high as 50 r/hr at one meter were expected, and the 1300-pound lead-lined pigs which were to house the radioactive samplers could not be handled safely on a destroyer having limited deck space and handling

[redacted]

equipment. The beacon used can be received by the P2V on ARC/27-ASA 25 homing gear up to a range of 15 miles, URD/4 homing gear used by the Lansing to a range of 3 miles, and by both the Lansing and Safeguard on the Sandia portable D/F sets to the same range.

The Lansing was scheduled to return the pod to Johnston by LCM no later than E + 10 hours, regardless of the number of instrumentation cones still in the water. The Safeguard was to return to Johnston as soon as all samplers were aboard. If any objects had not been recovered by daylight the P2V, aided by helicopters from the Boxer, was to make a systematic search of the impact area for dye-marker slicks. Objects found by this method were to be picked up by helicopters at the discretion of the Recovery Operations Officer. Sandia was to have one representative in the Lansing CIC, and a D/F set operator-advisor to the recovery party aboard both the Lansing and the Safeguard. There were to be rad-safe monitors aboard both ships.

For Orange the recovery plan was essentially the same as for Teak, with the following exceptions: (1) the floating dry-dock, the Belle Grove, was scheduled to search for the 72,000-foot instrumentation nose cone which was programmed to impact 27 miles north of the main impact area; (2) the portable D/F set on the Lansing was to be transferred to the Belle Grove; and (3) if all objects were not recovered by daylight, the WADC pod was to be transferred from the Lansing to Johnston Island by helicopter rather than by ship, thus saving the Lansing from making the 64-mile round trip to Johnston.

5.2.5 Results of Teak and Orange Recovery Operations

On Teak, as previously stated, the sampler rockets apparently broke up shortly after second-stage burnout. Both nose cones were recovered from the water within one mile of the launcher. Examination of the debris shows that no flight functions had occurred. Both wind-screen split rings, and possibly the wind screens themselves, failed before impact. Further discussion of these failures will be found in Section 8.1.4. With these exceptions, the nose cones appeared to have been intact on impact.

Four the the six instrumentation nose cones were recovered, and all but Station 39 were monitored by URD/4 until impact. The P2V found nose cones from Stations 59 and 39 by means of the homing beacon and marked them with

[redacted]

[redacted]

flares. Transmission from the 39,000-foot unit was too weak for the P2V to do more than indicate its general location. After off-loading the pod, the Lansing homed in on and recovered 39 and 59. Dye markers from Stations [illegible] and [illegible] were spotted by the P2V shortly after dawn; both of these were recovered by helicopters and returned to the Lansing.

A thorough daylight search was made for units which were at 60,000- and 40,000-foot apogee attitudes, but with no success. The P2V crew stated that it was impossible for a unit which was emitting dye-marker compound still to have been within the search area.

The beacons on all cones recovered were operating properly, but the cones floated approximately 30 degrees to the water surface, thereby causing the antenna pattern to be distorted and the antenna itself to be inundated about 70 percent of the time.

On Orange the recovery went much as planned. Nose cones of Stations 72 and 125S were tracked by CED/4 to impact, and radar fixes obtained on both of these units indicated impact within two miles of the predicted.

The P2V searched for the WADC pod for 20 minutes without success, then spotted a sampler light. Within the next 40 minutes the aircraft identified by beacon frequency, found, and marked all four samplers. One beacon was weak and provided homing for only two miles; the others operated properly, however, and provided homing to 15 miles.

The Lansing and the P2V then continued to search for the WADC pod until the Safeguard arrived at the impact area at H + 5 hours. At that time the beacon and light on one unit had failed, and a light had failed on another. The P2V dropped flares on three samplers, but by the time the Safeguard had recoverd two, the beacon on the third failed. Recovery was delayed until daylight, at which time both remaining units were promptly found by dye marker and recovered.

While searching for the pod during darkness, the P2V found Station 125S by means of the beacon. The unit was picked up by the Safeguard as it returned to Johnston. The parachute on Station 115R apparently did not operate; this unit was never found. The portable D/F gear aboard the Belle Grove failed, which prevented search for the Station 72 nose cone; however, it was spotted shortly after dawn and recovered by helicopter within two miles of its predicted impact.

[redacted]

[redacted]

Of the fifteen rocket cases which were objects of search, twelve were recovered. This recovery in open ocean was more successful than the most optimistic predictions indicated at the time the program was planned. Such success in recovery allows expansion of instrumentation techniques which can be used on future operations of this nature. It also proves the feasibility of rad-chem sampling, provided means are found to guarantee penetration of the radioactive debris by the sampler.

5.3 WINDS BETWEEN 100,000 and 300,000 FEET ALTITUDE

5.3.1 Introduction

The ability to obtain a cloud sample from either Teak or Orange was dependent upon the sampling instrumentation within the carrier and the capability of the rocket to hit the debris. This capability of penetration, in turn, was dependent upon the accuracy of the Redstone in positioning the device at its predetermined position, the accuracy of the sampling rocket in hitting its target, and the ability to prognosticate the cloud's coordinates with time after burst. The latter ability requires accurate information on size, rate of rise, and lateral movement of the cloud with winds. Initial planning for Teak event called for penetration of the debris at burst plus 40 seconds and burst plus 80 seconds. These times, resulting from original estimates of the cloud size, were based on qualitative extrapolation from low-level burst data [redacted]

discussed in Section 5.1, indicated rescheduling of the samples so that one rocket would be over the burst at zero time and the second rocket would pass through the burst area at zero plus 20 seconds. The first rocket would be approximately 40,000 feet above anticipated burst. The change in timing obviated the need for a wind forecast on Teak, since the 20-second interval between burst and penetration would reduce the wind influence on the cloud to a negligible value.

Although initial justification for a high-altitude wind-measuring system was to determine the movement of the radioactive cloud from Teak, the wind program at Teak altitude was continued for the following reasons:

[redacted]

1. Wind information would be required in postshot analysis of the trajectories of the instrument carrier rockets.

2. Wind information would be helpful in postshot analysis of acoustic signals received at ground stations, in the longer time movements of cloud drift, and in the behavior of possible unexpected phenomena at altitude.

3. The development of a capability for obtaining wind data at these altitudes and for accumulating at least a limited climatology based on actual observations for possible future high-altitude tests, particularly in the Pacific area, is needed.

4. The very scarcity of information available reveals the need for observations at high altitudes, particularly in equatorial regions, to be used in basic research and in the design and operation of manned and unmanned vehicles at these heights.

5. The requirement for wind information at Orange-shot altitudes and above is obvious.

To estimate the effect of wind errors on cloud movement, and thus the wind influence on successful penetration, computations of the probability of hitting a solid circular cloud were made. It was assumed that the cloud would move with the speed of the wind, that a large torus would not form rapidly after the burst with below-minimum density of debris in the center, and that vector errors in hitting the cloud would be randomly distributed and could be represented by a normal bivariate distribution, where the sum of errors in each orthogonal direction are equal, i.e., a circular distribution. In polar coordinates ρ and θ, with standard deviation σ of these errors, the probability of penetration is:

$$P = \frac{1}{\pi\sigma^2} \int_0^{2\pi} \int_0^{R} e^{-\frac{\rho^2}{\sigma^2}} \rho \, d\rho \, d\theta \qquad (5.7)$$

Integration, after substitution of total error variance,

$$\sigma^2 = \sigma_w^2 t^2 + \sigma_{Red}^2 + \sigma_D^2 ,$$

where individual terms represent, respectively, wind uncertainties, Redstone trajectory errors, and Doorknob sampler trajectory errors, gives the result:

$$P = 1 - e^{-\frac{R^2}{\sigma_w^2 t^2 + \sigma_{Red}^2 + \sigma_D^2}} . \qquad (5.8)$$

Here R is cloud radius and t is time between launch and penetration.

Deflection errors, all at the one standard deviation level, were estimated to be 2 mils for the Redstone missile, 46 mils for Teak, and 62 mils for Orange rockets. The Redstone value was furnished by the Army Ballistic Missile Agency, Huntsville, Alabama. In no-wind conditions, the Doorknob samplers were estimated to have a 15-mil error. Addition of the 24-hour August variation vector for Johnston Island increased this no-wind value to the 46 and 62 mils indicated. Resulting probabilities, when these estimates are used, are provided by Figs. 5.11 and 5.12.

The curves in Fig. 5.11 show the negligible effect of the wind on the cloud, since even a large wind error produces a small change in probability of penetration at early times. Only as revealed in curve c, showing an 80-second-after-burst penetration, would there by any appreciable improvement in probability by an accurate wind forecast. The curves in Fig. 5.12 pertain to the Orange event and are based on a cloud rise rate extrapolated from TM 23-200 and cloud size qualitatively estimated by modified Sachs scaling from sea level.[4] [redacted] Section 5.1 gives a more detailed explanation of these estimates. The slopes of all curves in Fig. 5.12, except that which refers to the 40-seconds-after-burst penetration, reveal that a significant improvement can be obtained by a wind forecast of good accuracy.

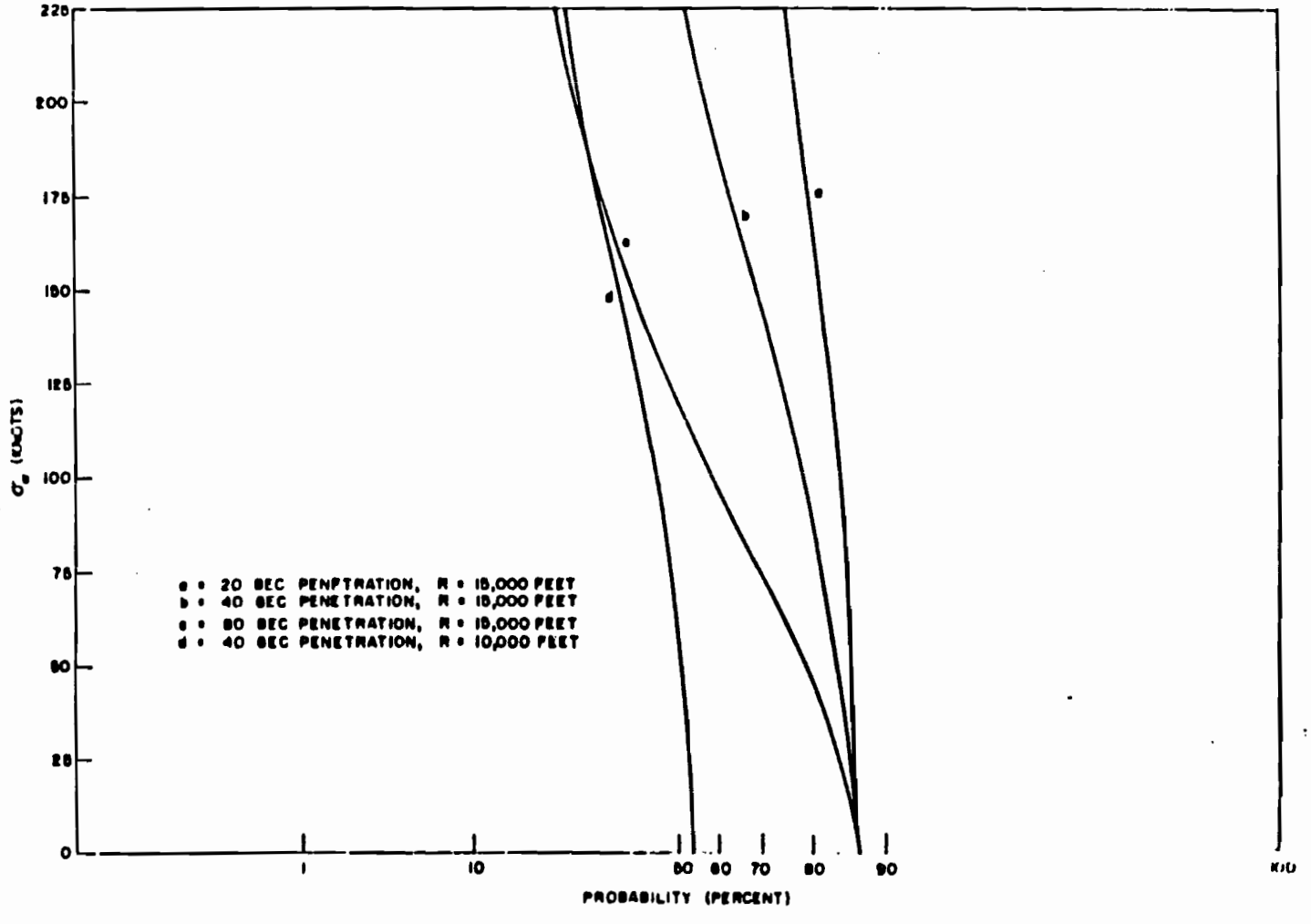

Fig. 5.11--Probability of cloud penetration on Teak shot.

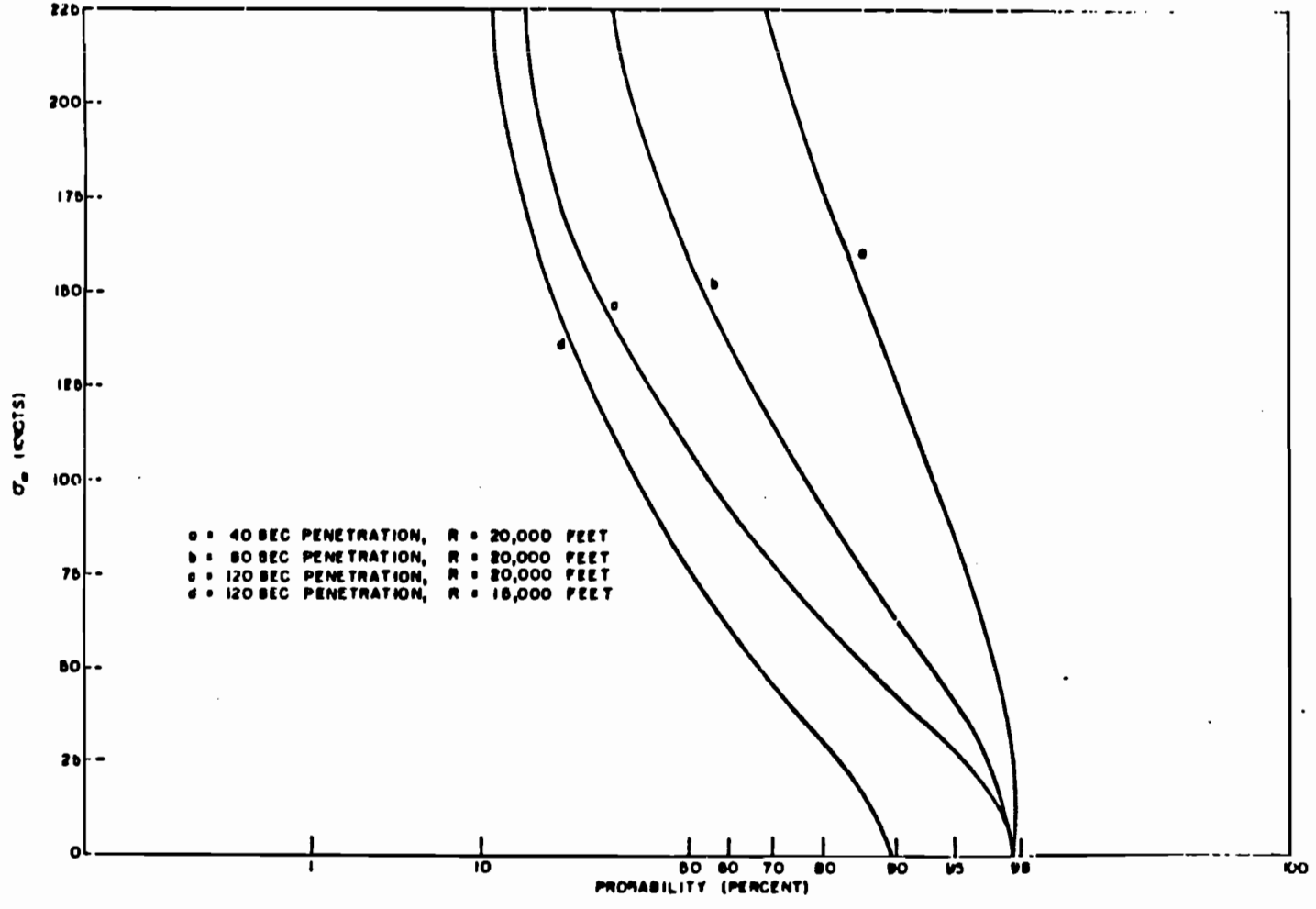

Fig. 5.12--Probability of cloud penetration on Orange shot.

[redacted]

5.3.2 Instrumentation

Measurement of winds at desired altitudes required design of a completely new system, since reliable instrumentation for this purpose was unavailable. Because of low fall rate, good radar reflecting qualities, and an excellent history as an atmospheric tracer, chaff or window was considered the best available target, although, for precision measurements, its high dispersive qualities are a disadvantage. A Deacon booster and Arrow II sustainer proved the most suitable delivery vehicle in terms of low cost, availability, and reliability. Experiments were conducted with the Viper as a substitute for the Deacon and with the Loki-Dart as a complete unit. Results of such experimentation were inconclusive within the limited development time.

The assembled unit on the launcher is shown in Fig. 5.13. In Fig. 5.14, close-ups of the nose section are shown. System specifications are provided in Fig. 5.15, while a more detailed description of the entire system is furnished by Force.[7]

The nose consisted of four sections: a forward nose cone, a cylinder housing chaff, a battery-timer cylinder, and a nose adapter. The last provided the link between the nose section and the Arrow. Three bundles of chaff comprised a customary load. Each bundle contained approximately 2×5^{10} individual aluminum-coated plastic strips, 2 inches in length, corresponding to one-half wavelength of the S-band frequency radar. Average width and thickness per dipole were 15 and 0.73 mils, respectively; total weight per load was 0.9 pound. The three bundles provide a cross-sectional area upon initial dispersion of approximately 8000 square feet.

Fall rate with altitude of these particles is depicted in Fig. 5.16. Here a best fit to a parabola was made by the method of least squares. Total data points used were 760, observed at altitudes between 100,000 and 300,000 feet. (These were predominantly between 130,000 and 160,000 and 210,000 and 250,000 feet.) Observations from Tonopah, Nevada, White Sands Missile Range, and the Marshall Islands, made during the summer months from May through August, were utilized. Vertical lines represent mean and standard deviations of distributions over 10,000-foot layers. Number of data points per layer are shown.

[redacted]

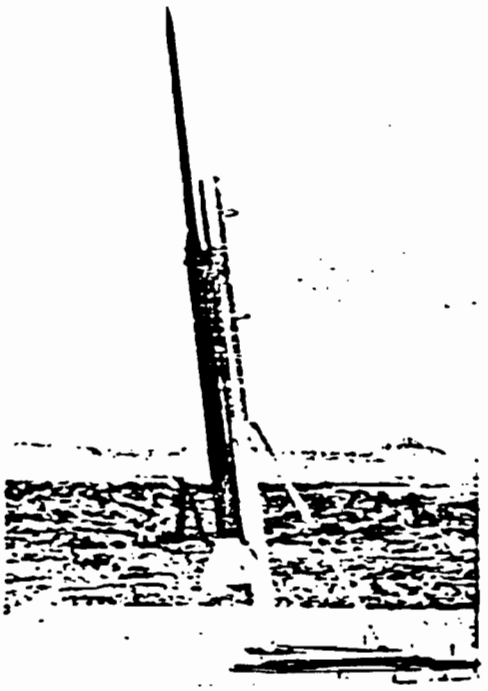

Fig. 5.13--Photo of system on launcher.

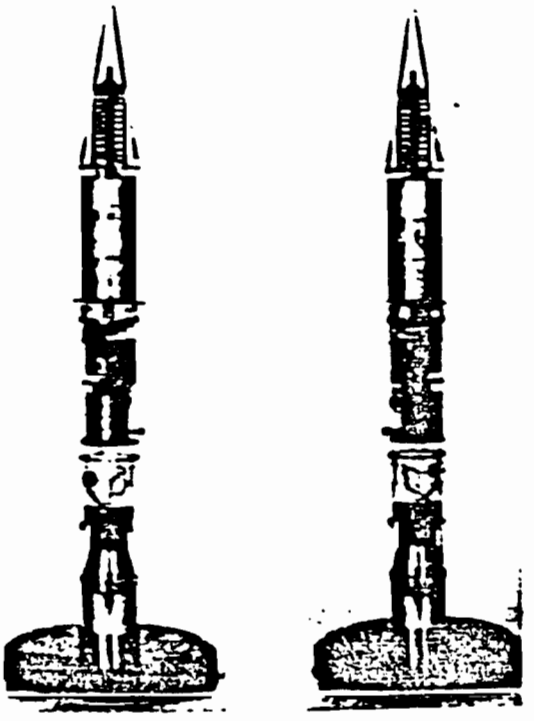

Fig. 5.14--Nose section close-ups.

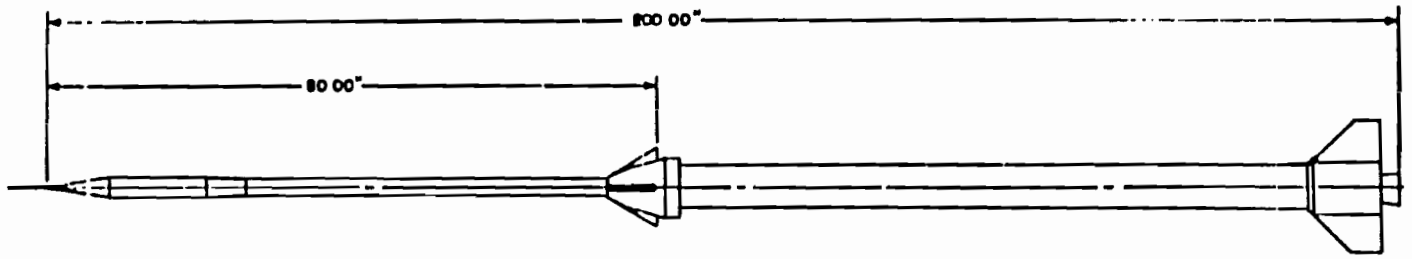

WEIGHTS

LAUNCH	DEACON BOOSTER-	228 LBS
	VIPER BOOSTER-	270 LBS
SECOND STAGE		41 LBS
NOSE ASSEMBLY		18 LBS

MOTOR SPECIFICATIONS

	A-8 DEACON	VIPER II	ARROW II
THRUST, LBS	8000	8270	8000
IMPULSE, LBS-SEC	16,000	31,100	9600
TIME, SEC	3.0	3.8	1.9
DIAMETER, IN	8.0	6.5	3.0
LENGTH, IN	110.2	108.8	80

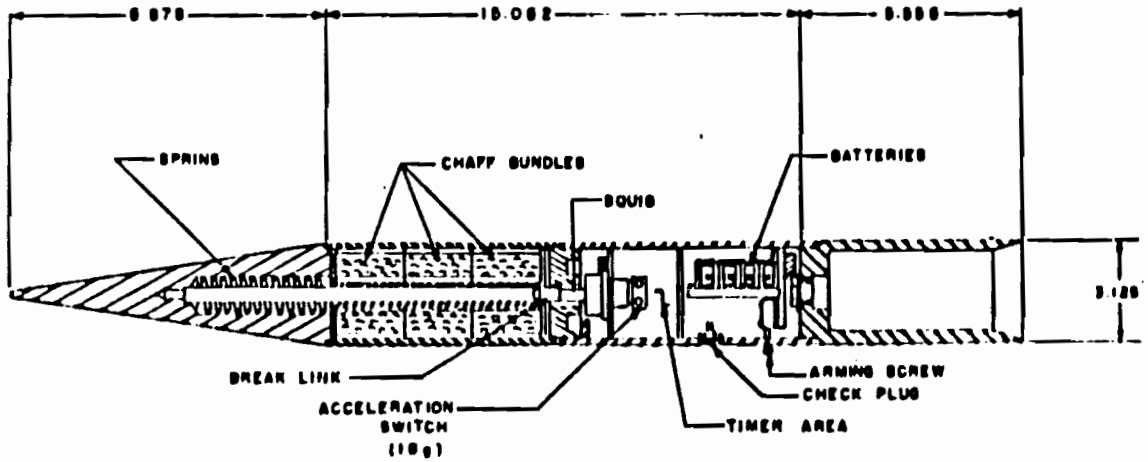

Fig. 5.15--Detail drawing of chaff rocket.

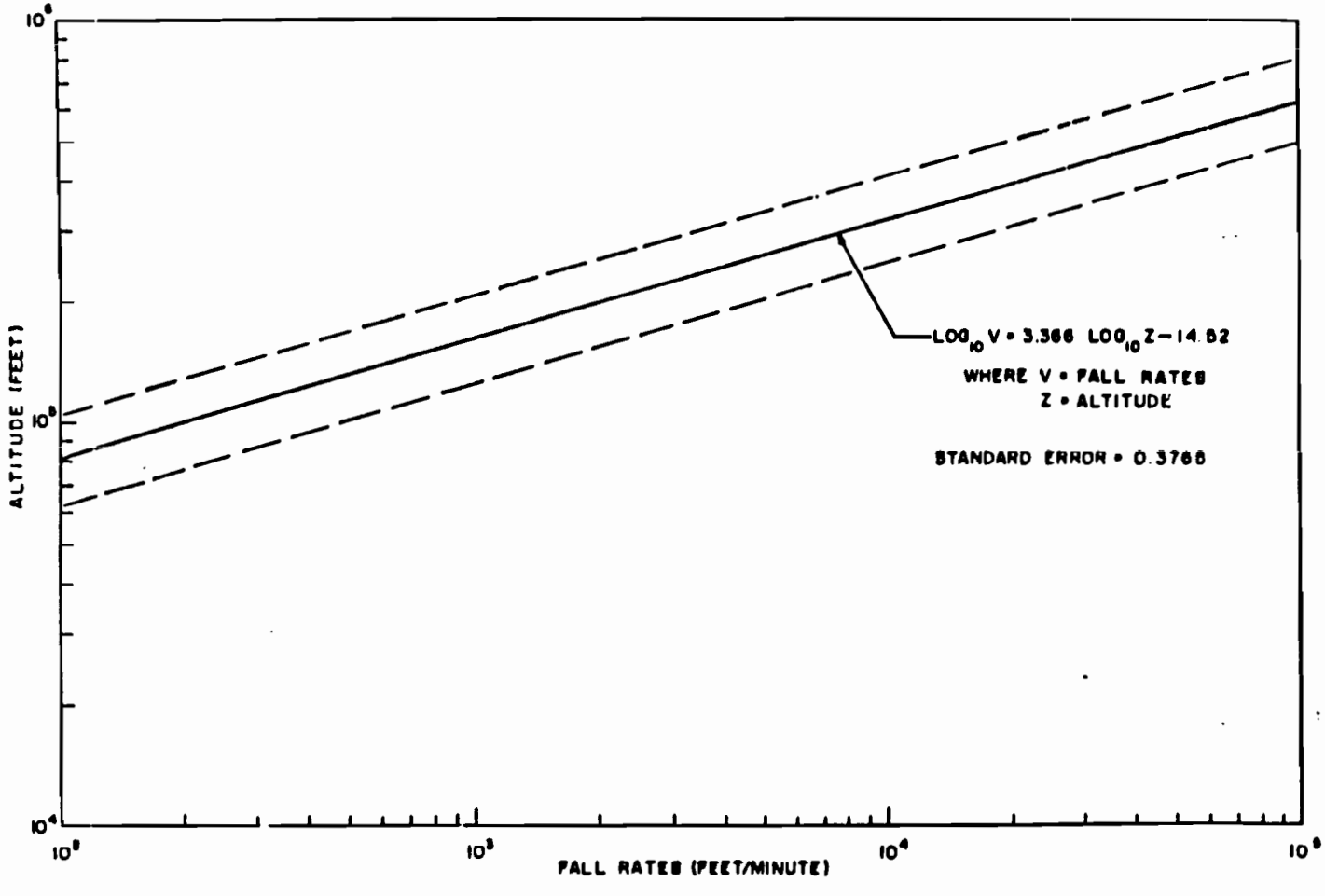

Fig. 5.16--Fall rates of 5-cm chaff particles.

Since trajectory accuracy was not a crucial factor, a zero-length launcher was employed because of its simplicity. With this launcher, elevation-angle settings of 60 to 90 degrees and azimuth changes of 16 degrees were possible without resetting the base plate. Computed dispersion mean error of the 20 firings in the Pacific was 45 mils, with a maximum of 68 mils.

Some system aerodynamical characteristics are shown by Fig. 5.17, providing plots of altitude and velocity versus time, and Fig. 5.18 showing variation of maximum altitude as a function of second-stage weight and launch angle. Second stage here is the sum of Arrow and nose section weight. These curves result from calculations on the IBM 704 and are predicated on a sea level launch, a total unit weight of 228 pounds, and a second-stage weight of 41 pounds, including 11 pounds nose assembly plus 5 pounds ballast. Since ballast was added to decrease apogee altitude, target ejection occurred near minimum speed.

Firing of the booster at launch results in an initial 27-g acceleration on the unit. This closes an acceleration switch which requires 18 g to actuate; the latter starts a mechanical timer. After booster burnout, differential drag separates the stages prior to sustainer ignition at 22 seconds. The second stage continues on a ballistic course to altitude, where the dual-purpose timer fires a squib which expells the nose cone and chaff cylinder housing, exposing the chaff for dispersal by air drag and centrifugal forces.

Ground instrumentation employed in following the target consisted of two MSQ-1A radars, furnished and manned by the Air Force. These radars operate at frequencies near 2900 megacycles with peak power output near 1 megawatt at sea level. They have a range in excess of 10^6 feet. Raw data from the radar, consisting of slant range and elevation and azimuth angles, were fed through a computer to a plotting board, which provided a horizontal plan plot of the target movement. Altitudes, corresponding to time marks every 30 seconds, were noted manually on this plot.

5.3.3 Wind Prediction

From observations made in tropical and temperate latitudes, limited wind data are available upward to the maximum temperature layer near 164,000 feet. During the summer months the layer extending from 60,000 to at least

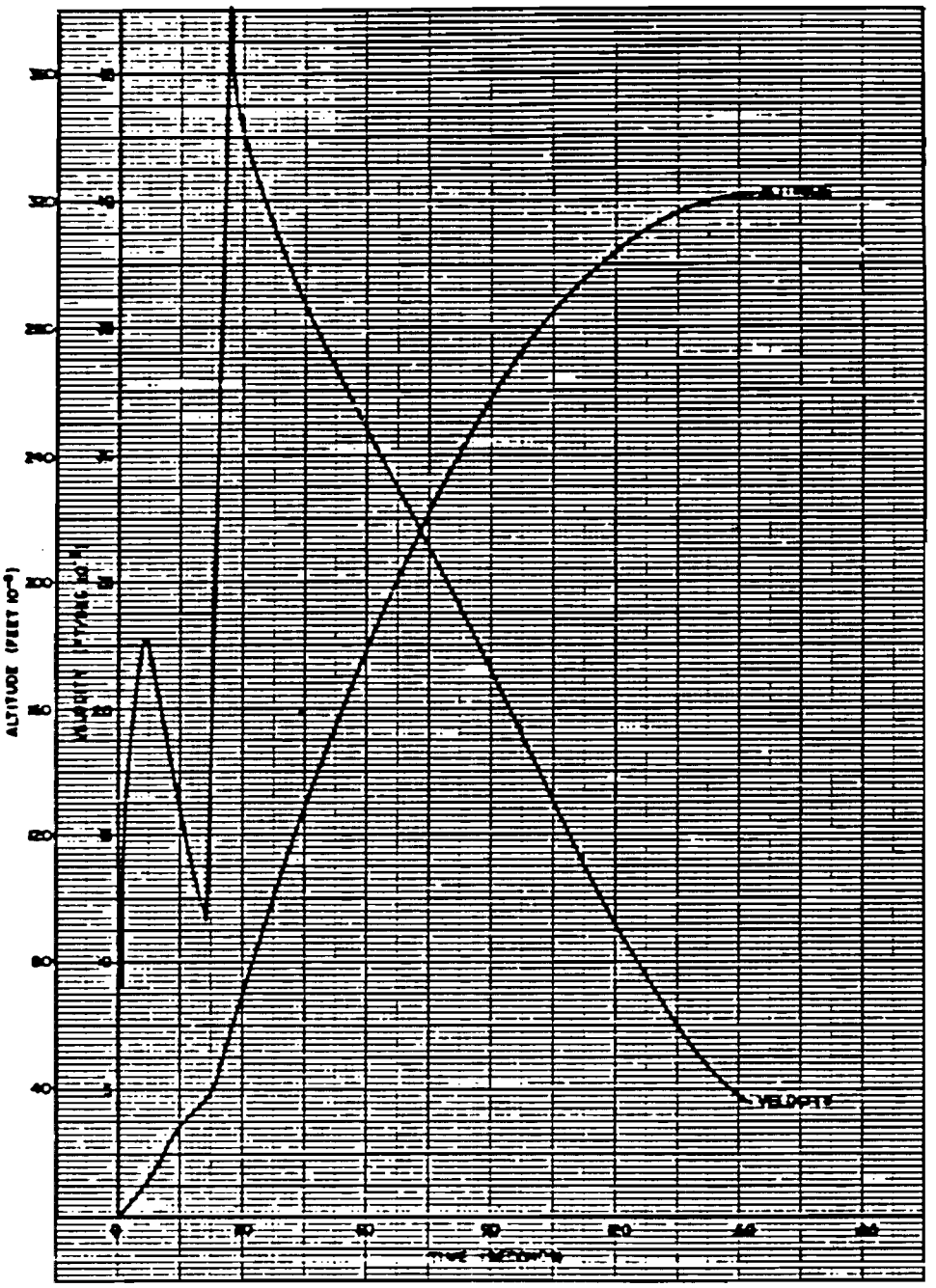

Fig. 5.17--Altitude and velocity versus time of chaff rockets.

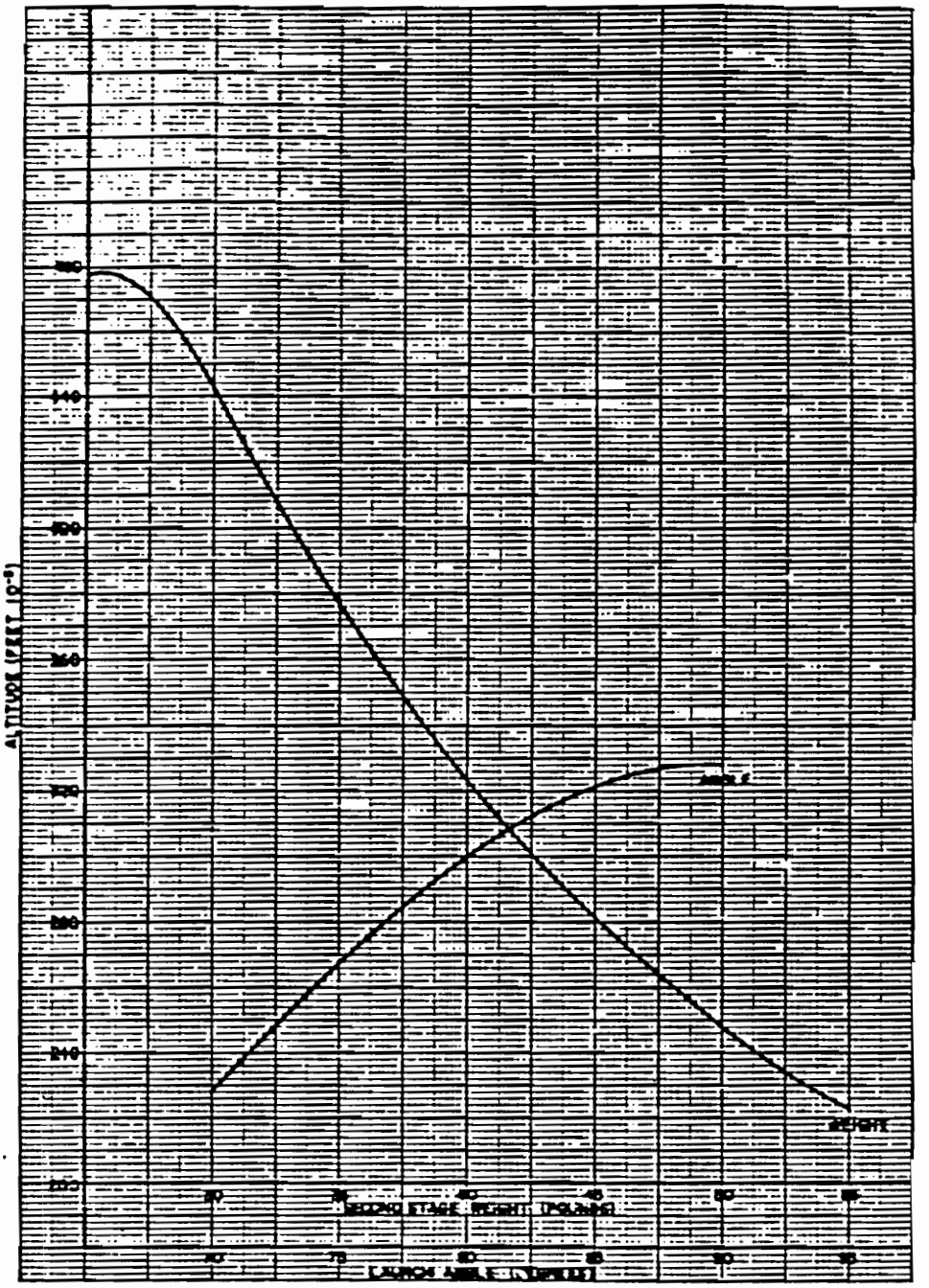

Fig. 5.18--Variation of maximum altitude of chaff carriers with sustainer weight and launch angle.

[redacted]

160,000 feet shows persistent easterly winds. Extrapolation of these data to the Johnston Island region, plus two pre-Orange measurements, provided data for forecast winds. Verification was provided by interpolation between the chaff wind soundings approximately 14 hours before and 12 hours after shot time. The resulting prediction for Orange was a mean wind from 065 degrees at a speed of 60 knots. This represents a mean wind for the layer between 145,000 and 165,000 feet. The actual wind was interpolated to be 065 degrees and 78 knots.

No wind measurements have been made in equatorial regions for the height interval from 200,000 to 300,000 feet. Some limited and inconsistent data have been derived from observation of noctilucent clouds at high latitudes and from reflection of radio waves on meteor trails.[8,9,10] These data did not appear to be suitable for a point location forecast. Some data have been obtained from observations in this altitude range by following chaff, smoke puffs, and sodium as targets. These were taken at White Sands and Tonopah test ranges; the Tonopah data represents three test rounds of the Sandia Deacon-Arrow system described here. These observations were taken in May with easterly winds of 50 to 100 knots observed, although variations from these values were quite apparent. Direct extrapolation of these mid-latitude measurements would be hazardous because of uncertainty as to latitude variation.

Studies of atmospheric radiation balance indicate the peak temperature region near 160,000 feet with a minimum near 260,000 feet (approximate Teak altitude). The area between is thought to be characterized by turbulent motions and large diurnal, seasonal, and geographical variations due to the negative temperature lapse rate with height.[11] These studies indicate that the probable top of the lower altitude easterlies is near 260,000 feet, but for equatorial latitudes this is unverified.[8]

Theoretical explanation of atmospheric tides requires that the forces exerted by these oscillations on the high-altitude circulation increase with altitude, accompanied by decreasing latitude. Resonance between a free period in the earth's atmosphere and the gravitational and thermal influence of the sun result in a strong semidiurnal periodicity. It has been postulated, on the basis of winds derived from radio probing of the ionosphere, that this semidiurnal force at 330,000 feet (100 km) comprises as much as 40 percent of the total wind vector.[12] If this is true, considerable variation would exist between day and night winds in direction and speed, with a clockwise turning during the diurnal period.

[redacted]

Although the above factors were considered, the apparent persistence of the easterlies from approximately 230,000 to 260,000 feet was the main tool used in making the forecast. The actual 24-hour prediction for Teak was a wind from 060 degrees with a 60-knot speed. Interpolation between winds measured 14 hours before and 12 hours after shot time provides a wind for zero time from 106 degrees with a 33-knot speed.

5.3.4 Observed Data

A total of 15 rocket-wind soundings were made before the Teak event; one observation was made at 1000 hours on D + 1 for postanalysis. Table 5.1 lists these observations covering the period July 11 to August 1, in addition to winds computed from four observations made between August 5 and August 12 in connection with predictions for the Orange event. Most observations were made at 1000 and 2200 local time to obtain 12- and 24-hour variations from scheduled Teak zero time of 2200 LST. Altitudes (HHH) are expressed in thousands of feet, speeds (VVV) are in knots, and directions (DDD) are those from which the wind was blowing on a 360-degree compass scale, with North at 360 degrees. Local time at Johnston Island can be obtained by subtracting 11 hours from indicated Greenwich (Z) time. Winds are computed only on that portion of the plot which reflects automatic tracking of the target. When it was necessary to track manually, data were taken on the size of the chaff cloud, but no winds were computed.

5.3.5 Summary of Results

On the basis of these data only, several prominent features can be noted in the wind structure between 210,000 and 280,000 feet. Heights given as dividing one zone from another are only approximate.

(1) A typical profile of wind versus altitude through the layer between 230,000 and 255,000 feet shows persistent easterly winds. Some winds with important north-south components are observed, but no appreciable westerly flow is apparent in this layer. In the mean, a speed maximum appears to be centered near 240,000 feet.

(2) The layers above 255,000 feet and below 230,000 feet, the vertical extents of which are unknown, are characterized by considerable variability. Westerly winds of appreciable magnitude are observed in these zones. Chaff

[redacted]

TABLE 5.1-- WIND OBSERVATIONS PRIOR TO TEAK

Observation: RW-43
Time-Date: 2100 Z - 11 July 1958

HHH	DDD	VVV
264	140	143
260	128	122
256	135	80
253	146	45
250	167	47
248	178	62
246	177	66
244	178	78
242	179	70
241	201	60
238	208	60
237	203	49
228	243	98
226	218	95
226	240	80
225	209	55

Observation: RW-44
Time-Date: 2056 Z - 18 July 1958

HHH	DDD	VVV
262	143	112
258	110	157
254	103	125
250	106	133
248	088	137
242	080	132
240	092	101
238	089	61
238	093	57
235	100	85
235	100	85
234	094	62
232	262	132
227	254	226
223	235	197
219	240	99
217	123	52
216	170	43

Observation: RW-47
Time-Date: 2135 Z - 23 July 1958

HHH	DDD	VVV
251	072	103
249	067	117
246	069	109
244	073	102
242	082	109
240	081	100
238	066	90
236	066	85
236	053	60
233	046	58
232	051	55
231	330	48

Observation: RW-48
Time-Date: 0300 Z - 24 July 1958

HHH	DDD	VVV
261	058	108
258	058	122
254	068	110

[redacted]

[redacted]

TABLE 5.1 (cont:)

Observation: RW-91
Time-Date: 2100 Z - 5 Aug. 1958

HH :	DDD	VVV
182	077	82
179	085	85
177	037	62
176	101	60
174	089	74
173	089	76

Observation: RW-93
Time-Date: 0900 Z - 10 Aug. 1958

HHH	DDD	VVV
151	087	64
149	071	61
146	013	61
143	136	46
140	102	50
139	062	80
137	132	62
136	109	55
134	061	46
131	090	70

Observation: RW-94
Time-Date: 2100 Z - 12 Aug. 1958

HHH	DDD	VVV
157	083	94
155	083	65
153	173	41
151	134	64
149	092	73
147	080	65
145	082	74
142	085	48
140	084	58

Observation: RW-103
Time-Date: 2300 A - 12 Aug. 1958

HHH	DDD	VVV
156	082	70
154	085	83
152	083	90
150	098	80
148	094	73
146	092	75
144	090	69

[redacted]

[redacted]

TABLE 5.1 (cont)

Observation: RW-49
Time-Date: 2137 Z - 27 July 1958

HHH	DDD	VVV
282	031	56
253	084	123
250	084	120
248	083	114
242	087	80
240	063	75
239	061	68
236	061	62

Observation: RW-50
Time-Date: 0830 Z - 28 July 1958

HHH	DDD	VVV
269	046	08
262	139	24
258	060	25
255	019	53
252	013	70
250	358	80
248	348	105
245	352	85
243	013	70
241	025	82
238	017	55
236	320	25
235	106	60

Observation: RW-51
Time-Date: 2100 Z - 28 July 1958

HHH	DDD	VVV
272	204	95
266	190	107
262	168	80
255	146	75
249	103	108
239	094	93
238	095	78
237	097	58
235	063	55
234	042	70
232	021	70
231	011	68
230	017	53
229	023	34
228	082	59

Observation: RW-52
Time-Date: 0830 Z - 29 July 1958

HHH	DDD	VVV
270	013	64
265	004	74
262	345	53
258	274	27
254	188	47
251	128	72
248	095	73
247	095	95
244	099	97
242	094	74
240	091	88
239	084	82
238	082	72
236	089	64
234	081	61
233	090	48

[redacted]

[redacted]

TABLE 5.1 (cont)

Observation: RW-58
Time-Date: 1500 Z - 31 July 1958

HHH	DDD	VVV
261	341	64
255	023	34
252	023	73
249	032	82
246	061	86
244	065	95
242	061	91
241	054	87
239	054	87
236	045	73
235	058	62
233	062	55
232	079	64
228	089	95
228	069	95
228	061	82
227	068	84
226	063	78
224	067	60

Observation: RW-80
Time-Date: 1915 Z - 31 July 1958

HHH	DDD	VVV
263	220	68
259	212	24
256	189	2
253	032	31
250	034	74
248	028	95
246	024	106
244	030	100
242	043	93
240	044	95
239	043	82
237	044	81
236	047	94
234	062	77
232	071	72

Observation: RW-89
Time-Date: 2100 Z - 31 July 1958

HHH	DDD	VVV
269	343	93
264	337	69
260	336	34
256	032	61
254	050	72
251	057	65
250	063	81
243	076	90
241	090	80
240	092	58
233	081	48
231	098	91
228	106	65
226	088	65
226	071	65
224	068	68
221	089	73
219	090	77
215	081	72
213	065	56
212	046	58

Observation: RW-90
Time-Date: 2330 Z - 1 Aug. 1958

HHH	DDD	VVV
284	078	43
274	143	40
267	248	40
262	280	60
259	300	70
254	291	67
252	184	29
248	135	82
246	126	121
244	129	122
242	124	107
240	116	110
239	111	115
237	100	112
235	088	112

[redacted]

TABLE 5.1 (cont)

Observation: RW-54
Time-Date: 2100 Z - 29 July 1958

HHH	DDD	VVV
265	144	12
260	099	47
249	084	75
248	070	92
245	069	102
243	070	103
241	069	106
239	071	107
236	072	94
235	076	61
233	071	60
227	004	70
224	357	67
219	104	79

Observation: RW-55
Time-Date: 0830 - 30 July 1958

HHH	DDD	VVV
282	174	13
272	267	47
266	278	31
261	187	32
258	177	33
255	169	25
252	106	32
249	067	45
247	056	54
245	055	60
243	053	47
242	058	36
241	072	33
240	089	26
239	107	24
237	090	22
235	058	17
234	023	25
233	027	23
230	067	25
229	085	13
228	066	25
228	082	20

Observation: RW-56
Time-Date: 2100 Z - 30 July 1958

HHH	DDD	VVV
266	012	92
261	350	43
256	222	3
252	103	37
249	116	72
247	118	58
246	108	82
244	107	121
242	106	90
241	107	133
238	106	139
[illegible]	[illegible]	[illegible]
236	094	142
234	119	110
225	111	112
224	112	96

Observation: RW-57
Time-Date: 0900 Z - 31 July 1958

HHH	DDD	VVV
259	061	26
257	055	66
253	058	95
250	061	105
247	061	89
244	077	77
242	090	82
240	078	86
239	069	87
237	083	132
235	081	125
[illegible]	[illegible]	[illegible]

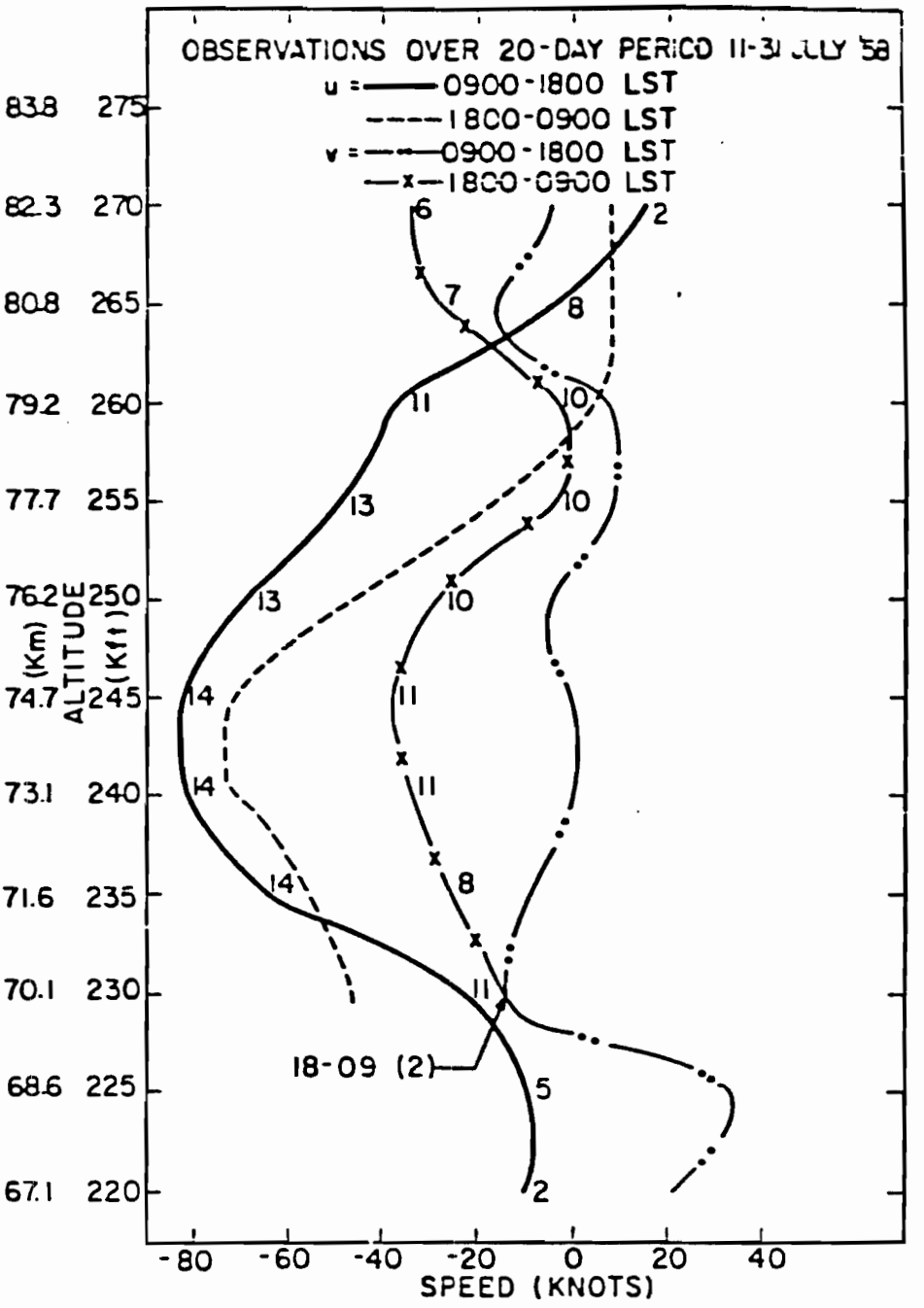

Fig. 5.19—Mean east-west (u) and north-south (v) wind component for daytime and nighttime periods. Number of data points used to compute mean values shown at 5-kft intervals along curves.

[redacted]

was expelled at 290,000 feet and had large fall rates in the first several thousand feet, with the result that horizontal speeds can be shown to be less reliable in this zone than in others. Direction should be accurate except in cases of extreme fall rates.

(3) Most observations were terminated between 220,000 and 230,000 feet; the longest fell to 211,000 feet. Below 230,000 feet, radar operators noted an apparent rapid dispersion of the chaff target. This accelerated dispersion may result from strong turbulence and vertical shears in this zone, or it is conceivable that it is a relatively constant function of time after release.

(4) Although it is possible to prove the existence of 12- and 24-hour periodicities in these measurements, their correlation with atmospheric tides was difficult to substantiate because of data scarcity. This lack of observations precluded use of harmonic analysis which would have allowed a direct determination of phase and amplitude of possible oscillations. Instead, a sine function of two harmonics was fitted to these data; its significance was proven by the F test, and these computed periodicities were then compared with semidiurnal theoretical tidal motions as provided by Stolov.[13] The west-to-east components (u) and the south-to-north components (v) of the winds were thus fitted at 240,000, 250,000, and 260,000 feet. Comparison with theoretical computations indicated an average phase difference near 30 degrees and an amplitude ratio of approximately two to one, with the fitted curves larger. Since theory is not well verified at lower latitudes, this agreement is considered good. Also, theory omits lunar influence, which tends to decrease the difference in phase by an unknown amount. Justification for belief that theoretical amplitudes should be greater is found in recent observations in equatorial regions which show larger tidal effects than anticipated in the E and F layer virtual height variations.[14]

(5) A plot of altitude versus average u and v components for the 12-hour periods beginning and ending at 0900, local standard time, is given in Fig. 5.19. Here all observations within either 12-hour period were summed to obtain the average. This plot indicates a small but apparently definite decrease nocturnally in speeds and the meagerness of the cross-latitudional flow v. Finally, short period variations of less than 6 hours appear to be small on the basis of the three observations of July 31.

[redacted]

[redacted]

(6) The greatest observed vertical shear was 260 knots in 3000 feet. The same observation and altitude of 227,000 feet indicated a maximum wind of 226 knots from 264 degrees.

In the zone from 130,000 to 180,000 feet, winds were relatively stable easterlies with moderate speeds, generally 50 to 100 knots. Turbulence appears to be at a minimum and vertical shears are very small. Both of these variables are less than those usually recorded in the troposphere (below 40,000 to 60,000 feet). These data seem to substantiate the usual concept of this layer; i.e., it is of great stability where temperature increases with height. Based on these data, extrapolation upward from winds determined from balloon observations at their maximum altitude (120,000 to 140,000 feet) would provide an accurate wind estimate to approximately 180,000 feet.

REFERENCES

1. Banister, J. R., A Computation of the Sampler Performance for Shots Teak and Orange of Operation Hardtack, SC-4172(TP), Sandia Corporation, December 1, 1958.
2. Bethe, H. A., Some Phenomena in High-Altitude Explosions, LA-2164, Los Alamos Scientific Laboratory, December 1957.
3. Mayer, H. L., Early History of High Altitude Nuclear Explosions, AFSWC-TR-57-16, Aeronutronic Systems, Inc., May 1957.
4. Capabilities of Atomic Weapons, TM 23-200, Samuel Glasstone, Editor, Department of the Army, Navy, and Air Force, June 1, 1955.
5. Kennard, E. H., Kinetic Theory of Gases, The McGraw-Hill Book Company, New York, 1938.
6. Notes and Tables for Use in the Analysis of Supersonic Flow, NACA-TN-1428.
7. Force, C. T., Characteristics and Performance of a Deacon-Arrow Rocket System, SCTM 79-58(51), Sandia Corporation, July 1958.
8. Murgatroyd, R. J., Winds and Temperatures Between 20 km and 100 km - A Review, Quart. J. Roy. Meteorol. Soc., 83, October 1957, p. 417.
9. Ludlam, F. H., Noctilucent Clouds, Tellus, Vol. 9, No. 3, August 1957.
10. Stormer, C., Height and Velocity of Luminous Night Clouds Observed in Norway, 1932; Publ. 6, Univ. Obs. Oslo, 1933.
11. Mitra, S. K., The Upper Atmosphere, Monograph Series, Vol. 5, The Asiatic Society, Calcutta, 1952.
12. Goody, R. M., The Physics of the Stratosphere, Cambridge Monographs on Physics, Cambridge University Press (American Branch, New York), 1954.
13. Stolov, H. L., Tidal Wind Fields in the Atmosphere, J. Meteorol., 12, No. 2, April 1955.
14. Chapman, S., Atmospheric Tides and Oscillations, Compendium of Meteorol., Am. Met. Soc., Boston, 1951, pp. 510-530.

[redacted]

[redacted]

Chapter 6

MICROBAROGRAPH

6.1 THEORY AND ANALYSIS

6.1.1 Introduction

One primary purpose in conducting the Teak test at the 250,000-foot altitude level was to establish detectability of acoustic or other signals at large distances from high-altitude tests.[1] Research by Shelton[2] on bursts to 100,000-foot altitudes indicated a vast decrease in energy contained in the blast wave with increased burst altitude above 60,000 feet. Blast from 125,000 feet altitude was expected by Shelton's second approximation to contain 18 percent of the sea level burst blast energy. Extrapolation of this reasoning showed that nearly all ultrahigh-level burst energy would be radiated thermally, and the pressure wave generated by Teak would be negligible and impossible to detect by acoustic observation.

Subsequent calculations by Hudson[3] gave an alternative mechanism for blast-wave generation in the ozonosphere from Teak from which could come pressure amplitudes that could be easily detected within a few miles of ground zero (GZ) but not at any large distance. A later study by Bethe[4] indicated in addition that about one-fourth of bomb yield would remain in the form of kinetic energy of the warhead materials. The result would be a blast, in the ordinary sense of the word, that could be scaled in the normal manner.

Sound-ray calculations for a point-source blast wave beginning at the mesopause* level (250,000 feet) showed that nearly two-thirds of the initial point source acoustic-wave energy could be ducted between the mesodecline and the low ionosphere (ducted between 150,000 and 300,000 feet). Blast energy emitted at declination angles below -35 or -40 degrees strikes the ground at ranges out to possibly 100 miles. This wave is reflected from the ground and, as it passes through the ionosphere, a portion of its surface could be refracted

*High-atmosphere terminology from Goody[5] is used throughout this chapter.

[redacted]

[redacted]

back again toward the ground at ranges from 200 to 300 miles. Repetitions of this ionospheric ducting process could lead to detectability at great ranges. Past experience has shown, however, that attenuation is very great for sound propagated in the extremely low-density ionosphere, and no identifiable signals have been recorded beyond the second or third cycle strike.

A possibility existed that strong sound signals ducted near the Teak source level would scatter or diffract detectable signals to the ground. There is no adequate theory nor any previous observation to check this phenomenon; quantitative predictions of long-range noise from this source were not attempted.

Pressure-wave recordings were planned in the microbarography of Operation Hardtack at various ranges to measure and observe detectability and to prove or qualify the inconclusive theories which existed for ultrahigh-altitude bursts. Sandia microbarographs were located on Johnston Island* and at stations 500 and 800 miles away. Some airborne pressure measurements were made by other projects. AFTAC attempted pressure recordings at many points around the world.

Since each station consisted of two or more sensing units planned to be about a mile apart along a line from GZ, the incidence angle of each sound-wave front could be established. With measured temperature and winds along sound-ray paths to various stations, it was anticipated that some definition of a source size, shape, and location could be calculated by acoustic-ray tracing to blast-wave source.

With equipment in place for the Teak event, microbarograph measurements were also made on the Orange event. It was hoped that results would give an intermediate point for interpreting Teak data and checking the Shelton theory. Long-range detectability estimates could also be verified.

6.1.2 Predictions

[redacted] Obviously,

*Johnston Island stations were planned at 7 miles from intended GZ, but burst-position error placed close stations only one-half mile from actual GZ.

†It is realized that application of this theory to Teak is a gross over-extension of the theory and, as pointed out by Shelton, the theory must be suspect by the time ambient density at burst altitude is one-one hundredth of that at sea level. Teak density was less than one ten-thousandth of sea level density.

[redacted]

[redacted]

under this line of reasoning no detectable blast wave would result from this shot.

Hudson[3] developed a model for a shock generated in the ionosphere where ultraviolet radiation is completely absorbed in the ozone layer. He reasoned that this mechanism could generate a plane-wave shock which would travel to the ground with little divergence [redacted] It was speculated further that low concentrations of ozone at these higher altitudes could be burned out by high radiation intensities and made ineffective as a blast source, thereby lowering the overpressure predicted by some indefinite factor. Arrival time at GZ for sound generated in the ozone layer would be between 70 and 160 seconds, as compared with over 200 seconds for sound generated near the burst.

Hydrodynamic shock generation in the vicinity of the ultrahigh-altitude bomb was estimated by Bethe[4] to give pressures which would be the same as those from one-fourth the yield of a similar detonation at sea level and at the same distance. [redacted]

Consideration was given to a possible third wave, different from that formed in the ozone layer and from that produced by hydrodynamic motions at the burst point. The mechanism was that of absorption of X-rays in air at some distance from the burst. If a pressure gradient could be produced in this way, a wave might start at something like 2 or 3 kilometers from the burst and outrun the main hydrodynamic blast to the earth. Although no effort was made to predict its probable strength, because of the possibility of detection, it was noted that such a wave should precede the wave produced by bomb material motion by about 2 to 4 seconds. No such wave could be produced by a shot at sea level density, since the X-ray mean free path is less than one meter, and any disturbance would coalesce with the hydrodynamic shock.

Signal predictions for French Frigate Shoals and Honolulu were made only to the extent necessary for establishing microbarograph set ranges. Only very small amplitude sounds were expected because of the ionospheric duct, but set ranges were fixed to contain signal amplitudes following the one-fourth-yield hypothesis of Bethe[4] with $P = R^{-1.4}$ scaling, found empirically from measured maximum amplitude, ionosphere-ducted signals beyond 10^5 feet.[7]

[redacted]

Page 182 is deleted.

[redacted]

Orange shot at 141,000 feet was expected to give blast results more in accordance with normal scaling predictions. However, a reduction in initial blast yield by the mechanism of early radiation proposed by Shelton was expected. Using Shelton's theory, only 9 percent of radiochemical yield should be manifest as a blast wave. Modified Sachs scaling yielded a prediction of 0.22 psi. No separate bomb material, ultraviolet or X-ray, absorption shocks were expected from this event.

6.1.3 Recorded Results

Teak. [redacted] Peak positive and negative phase pressure amplitudes, together with pertinent wave time characteristics observed on Johnston Island, are shown in Table 6.1 and are plotted in Fig. 6.1. Preliminary data points from BRL very-low-pressure gages at Johnston Island and on the USS Boxer and USS Lansing[8] are also shown in Fig. 6.1.

Arrival times from the synchronized recordings at Johnston Island show no detectable (± 0.01 second) difference in shock-arrival time, since the burst was only half a mile from directly overhead from the sensing array. Figure 6.2 depicts the blast wave pressure-time history as recorded by the CH-1 gage. Included in this illustration are marks showing the average and ± 1 σ fiducial limits of the main blast parameters.

[redacted]

Page 184 is deleted.

[redacted]

Results from recordings made at French Frigate Shoals (FFS) and at Lualualei, Oahu, are shown in Table 6.2. Good records were obtained at FFS. The Hawaii observations are of questionable accuracy; the radio blackout interfered with planned range-setting procedure, ambient noise was recorded which may have obscured the blast records, and the microbarograph equipment did not perform properly in all respects. However, the important points were adequately covered by FFS records.

[redacted]

entry of characteristic velocity, sometimes called apparent velocity, is the speed of the wave-front intersection traveling along the ground. It is invariant under refraction and so represents horizontal sound velocity at the altitude level where the blast wave was turned by refraction back toward the ground.

Orange. Pressure recordings made at Johnston Island from Orange shot are summarized in Table 6.3. Data points of overpressure distance are also shown in Fig. 6.1. An average pressure-time history is plotted in Fig. 6.3.

[redacted]

Pages 186 through 191 are deleted.

[redacted]

TABLE 6.7--AEDC MODEL ATMOSPHERE, 1959

Altitude (kft, MSL)	Pressure (millibars)	Sound speed (ft/sec)
60	72.3	968
80	27.8	966
100	11.1	1003
120	4.71	1042
140	2.13	1078
141	2.05	1080
160	1.02	1106
180	0.492	1093
200	0.226	1039
220	9.50×10^{-2}	981
240	3.58×10^{-2}	920
250.2	2.07×10^{-2}	887
260	1.17×10^{-2}	855
280	3.44×10^{-3}	846
300	1.01×10^{-3}	846
350	7.54×10^{-5}	986
400	1.80×10^{-5}	1493
500	4.96×10^{-6}	2180
600	2.35×10^{-6}	2512
800	6.89×10^{-7}	2706
1000	2.37×10^{-7}	2861
1200	9.21×10^{-8}	3000
1400	3.95×10^{-8}	3135
1600	1.84×10^{-8}	3258

[redacted]

Page 193 is deleted.

[redacted]

Off-site records from Orange in Table 6.4 are quite similar to recordings made at comparable distances from other large shots. Arrival times are what would be expected for blasts ducted by the ozonosphere. Incidence angles are not shown, since they are very close to zero degrees. Some of the apparent velocities were calculated to be less than local sound speed, and have therefore probably been affected by prevailing strong northeasterly trade winds at that location. There may also be errors from the survey of the sensor locations. There are no detailed wind observations available, so this peculiarity is being ignored. Experience has shown that this condition does not arise when precise survey, wind, and temperature data are available.

6.1.4 Explanation of Results

With the viewpoint conditioned by Shelton[2] and Bethe[4] and quantities of data from low-altitude tests, blast propagations from Teak and, to a lesser degree from Orange, were astonishing. Everything appeared to be anomalous, but a relatively straightforward application of modified Sachs scaling[16] brings nearly everything observed into agreement. The main unknown was the strength of the equivalent initial point-source blast wave as a function of burst height.

Modified Sachs scaling shows that, independent of burst height, a scaled overpressure,

$$\Delta P = (P/P_o)\Delta P_o ,$$

is observed in an ambient atmospheric pressure P at a scaled range

$$R = (W/W_o)^{1/3} (P_o/P)^{1/3} R_o$$

from a yield W. Zero subscripts refer to values in a referenced standard

condition. Several standard relations for P_o, ΔP_o, R_o, and W_o have been published; the EM Problem M[17] for theoretical blast-wave calculations, as summarized by Broyles[18] has been used here as a convenient reference standard out to 9000 feet from a 1-kiloton free-air burst. At this range, incident overpressure is 0.37 psi. Beyond this range, it is assumed that overpressure decays in proportion to range, $R^{-1.2}$. This nonacoustic decay exponent was found by experiment at Sandia with 1-pound high explosives in June 1961 and verified by preliminary analysis of Project Banshee data. The latter experiment was with 500-pound pentolite spheres, exploded near 60,000 feet MSL over White Sands Missile Range, New Mexico, in the summer of 1961. Reports and references for these test results are not yet published.

Ambient atmospheric conditions at various altitudes observed by the JTF-7 weather service radiosonde balloons are shown in Tables 6.5 and 6.6. Early calculations were made with an upper atmosphere model suggested by analysis of sounds refracted back to ground from the ozonosphere from several atomic test operations.[9] This model now seems to be inaccurate and is no longer used. However, differences between the atmospheric model and standards presented by the Rocket Panel[12] or by the ARDC,[19] as shown in Table 6.7 and used here, do not greatly influence the calculations in this report.

The ground-reflected overpressure recorded on Johnston Island from Teak and Orange would be observed from a 1-mt surface burst at ranges shown by the scaled curve in Fig. 6.1. Since Johnston Island air pressure was 1013 mb, $(P_o/P)^{1/3} = 1$, $W = (1\ \text{mt})(R/R_o)^3$; for Teak, R = 250,230 feet, and for Orange, R = 197,713 feet. Three significant overpressure values from each shot have been used to infer the apparent yields shown in Table 6.8.

Calculated arrival times at Johnston Island in Table 6.8 were obtained by modified Sachs scaling to pressures and shock speeds at approximate 10,000-foot intervals along the line from burst to recorder. Calculated times are close to observed values shown previously in Tables 6.1 and 6.3. Time of arrival at Ie GZ is 190.14 seconds, $\pm$ 0.02 second, nearly the same as at the recorder. Oran however, was at an appreciable horizontal range, and GZ time of arrival may be estimated from the 166.71 seconds observed at gage CH-1, to give the best estimate as 108.1 seconds. In view of the many assumptions made in this calculati this GZ time of arrival may easily be in error by seconds.

If finite-amplitude propagation of small amplitude waves is assumed, in accordance with the derivation of DuMond et al.[20] rather than the acoustic assumption, a much larger source yield is indicated.

DNA (b)(3)

[redacted]

Since ordinary Sachs scaling,[22] based on ambient conditions at burst altitude, gives much lower than observed pressures, results would imply much more than true yield; therefore, this scaling will not be considered further. It appears that random errors of observation and the small data sample obtained by BRL for Plumbbob John[23] may have been responsible for their conclusion that ordinary Sachs scaling worked best, in contrast to the modified Sachs scaling superiority shown by Sandia measurements of Teapot HA.[24]

Apparent-yield-to-true-yield ratios have been plotted versus ambient pressure at burst altitude in Fig. 6.4. Ratios predicted by Shelton[2] and Bethe[4] are also shown. Measurements near ground zero from Teapot HA[24] and Plumbbob John[23] have been used in the same way to calculate apparent yield. This ratio is so nearly proportional to the 0.177 power of burst-level ambient pressure that no regression was derived. The line indicates that a curve necessary to arrive at a unit ratio at sea level burst altitude is primarily dependent on data from shots at less than 20,000 feet MSL. This appears to conflict with previous observations[25] that the energy partition does not vary with burst altitudes to 10,000 feet MSL.

A review of air-burst data collected in the past, using modified Sachs scaling, should be made for comparison with LRM Problem M. It is possible that the lower P-D curve recommended after Upshot/Knothole[25] may also have resulted from use, for the most part, of air-burst data.

The early Teak signals recorded at French Frigate Shoals, shown in Table 6.2, arrived at high incidence angles. This implies that sound speed at turnover altitude is high and in turn must be at extremely high altitude. A simple approximation for calculating turnover altitude was found previously[1] for

Page 197 is deleted.

surface bursts to be

$$h = R\left[0.865 - 0.789\,\frac{R}{tV_p}\right],$$

where h is turnover altitude in feet, R is distance in feet from shot to recorder, t is recorded arrival time in seconds, and V_p is the ray characteristic velocity in feet per second. By assuming a straight-line 72-degree ray below Teak height of burst, a virtual ground source has been estimated in Fig. 6.5 for use in the equation at R = 2,827,000 + 250,200 cos 72° = 2,904,000 feet. As noted in Section 6.1.3, the acoustic vertical arrival would have been 234 seconds near Teak ground zero. Thus, along the 72-degree ray, travel time would be 234/sin 72° = 246 seconds, so an arrival at FFS from the virtual source would be (see Table 6.2) approximately t_a = 925 + 246 = 1171 seconds. Further,

$$h = (2{,}904{,}000)\left[0.865 - 0.789\,\frac{2{,}904{,}000}{(1171)(3618)}\right] = 944{,}000 \text{ feet MSL.}$$

That this characteristic velocity is higher than sound speed (Table 6.7) for this turnover level is not surprising, considering the many approximations made.

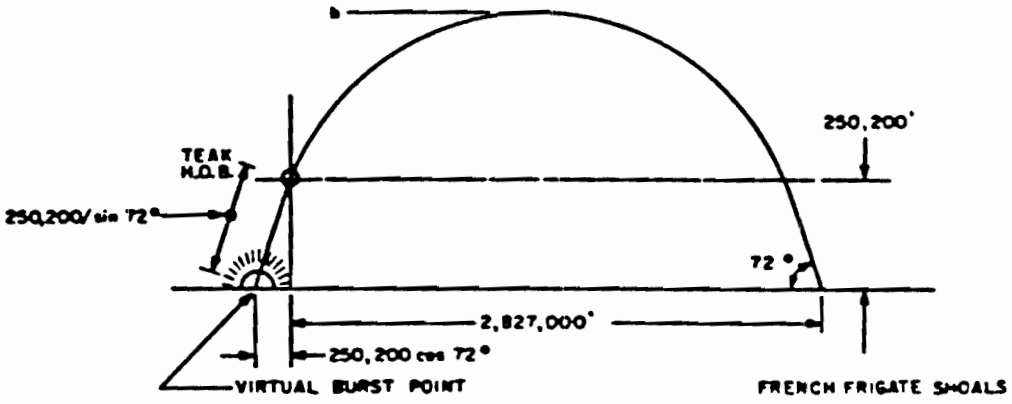

Fig. 6.5--Teak shock ray geometry.

As a further projection, with the concept of rays traveling to 10^6 foot altitudes, acoustic ray calculations shown in Fig. 6.6 have been made through

[redacted]

the assumed atmosphere model. The acoustic ray emanating originally at 58.5 degrees from Teak burst point lands very close to French Frigate Shoals and is in fair agreement with the 72-degree incidence angle observed.

[redacted] But application of modified Sachs scaling for shock strength, using the [redacted] source estimated from Johnston Island GZ blast data, together with ambient pressure altitudes, gives shock speeds along the ray path. Integration of shock speed along this path gives an arrival tim[redacted] for comparison with [redacted] observed. Arrival times calculated for the ± 1 σ yield range in Table 6.8 are 752 and 827 seconds. These calculated arrival times are all smaller than those observed, but the error is not nearly as great as acoustic travel time would produce. Observed arrival would require [redacted] apparent source strength. Two factors could cause smaller shock strengths along a path to FFS. First, a portion of the shock energy was lost by radiation since it was observed to be of still glowing intensity as it passed over FFS. Additionally, refractive convergence which ducted rays into FFS, as shown in Fig. 6.6, is accompanied by a relatively silent region above the turnover point, and a considerable upward diffraction of energy could have taken place. In summary, calculated arrival times [redacted]

DNA (5)(3)

The Teak shock wave was photographed from Hawaii at irregular intervals up to 2 minutes after zero time.[26] From these pictures approximate positions and shock speeds have been calculated as shown in Fig. 6.7. In addition, the field of shock speeds calculated by modified Sachs scaling for a [redacted] yield, together with ambient atmospheric pressures and temperatures, are shown.

[redacted]

Pages 200 and 201 are deleted.

[redacted]

[redacted] timing for each photo was possibly inaccurate and the scale factors may have been erroneous, since these were not taken in a carefully planned manner and the persistent spectacle had not been predicted. Further, and possibly more important, is the geometric error in assuming the glowing blast wave pictured was in a vertical plane through the burst point. A successive approximation solution for the correct geometry does not appear to be justified in view of the other uncertainties in the measurements. Finally, if shock speeds were actually only half the scaled values, as the photos indicate, the rough agreement between shock arrival-time calculations and observations and incidence angles at French Frigate Shoals could be negated.

On the USS Boxer, many faint pops and bangs were audible from Orange about 10 to 15 minutes after zero time. These are believed to be similar to noises recorded at Eniwetok from Bikini megaton-class shots. Shock rays from the burst originating at high elevation angles above the horizon suffer energy reduction by spherical expansion at first and become nearly acoustic. Then, as they travel to extreme altitudes (60 to 80 miles), they again become shock rays in the very-low ambient atmospheric pressure, travel supersonically (to Mach 2 to 3), and are thus turned back to ground by refraction, where they strike at high incidence angles.[10]

6.2 INSTRUMENTATION

6.2.1 Instrument Description

The microbarograph instrumentation system was first used during Operation Upshot/Knothole. Since this system, designated 3-PEM-2, has been described in detail in SC-2990(TR)[27] and WT-9003,[10] it is described only briefly in this report.

The change of pressure resulting from nuclear detonation is sensed, together with undesirable high- and low-frequency noise, in a cross-shaped hose array leading into a Wiancko sensing head. The general theory of operation of the system is diagrammed in Fig. 6.8. The hose array has an upper

[redacted]

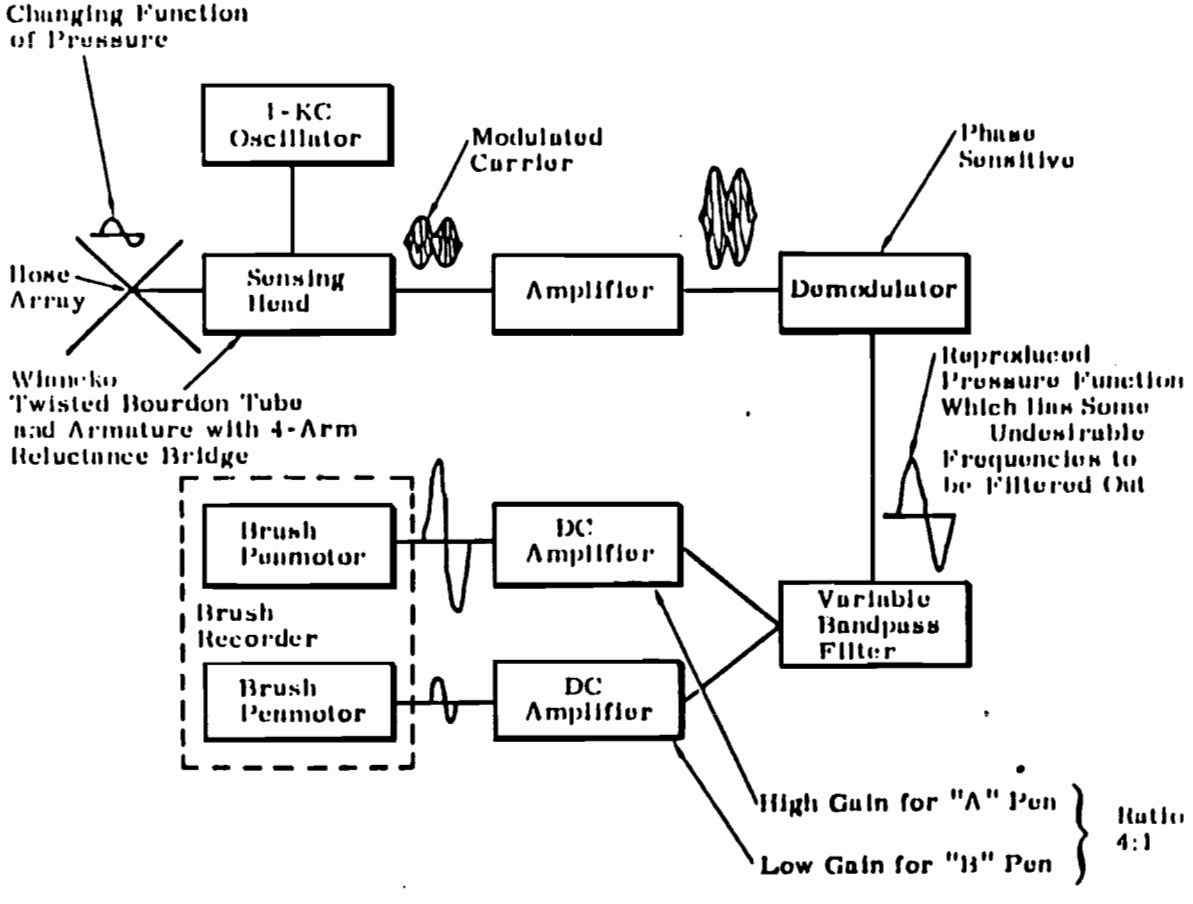

Fig. 6.8--General theory of operation of microbarograph system.

[redacted]

half-amplitude cutoff frequency of 45 cps. A filter volume with a bleeder provides a low-frequency cutoff (half power) of 0.0073 cps on the sensing head. Sensing is done by a twisted Bourdon tube carrying an armature in the field of a reluctance bridge having four active arms. Changes in the armature modulate a 975-cps carrier which is transmitted through a four-conductor cable to the receiver up to a mile away. At the receiver, the modulated signal is impressed across a sensitivity-range attenuator with eight full-scale settings from 4 to 12,000 microbars. After range attenuation, the signal is amplified to about 50 volts by a conventional four-stage, resistance-coupled amplifier. A phase-sensitive demodulator demodulates the signal and sends it to an adjustable band-pass filter, which attenuates most of the noise while maintaining most of the signal at nearly full amplitude. The filtered signal is next amplified by two DC amplifiers in parallel, one of which has four times the gain of the other. These amplifiers drive the pens of two Brush recorders. A side pen on the recorders marks 1-, 10-, and 100-second intervals on signal from a time-mark generator. Since the range setting of the attenuator and the timing on the record are known, the record can be interpreted for amplitude and period.

This time-mark generator has been added to the system since the reports referred to above[10,27] were written and is therefore described in some detail. The time-mark generator drives the marker pens on both Brush recorders at a 1-second rate and identifies by length every tenth and hundredth 1-second pulse. The equipment making up the time-mark generator consists of a Type 2001-2D frequency-standard time box manufactured by American Time Products, Inc., four Type 700A Berkeley decade scalers, phase-inverting amplifiers, monostable multivibrators, and a power supply.

The output of the 2001-2D time box is taken from the grid circuit of the cathode follower output tube in the form of negative-going, 90-volt pulses at 100 cps. This output drives a Type 700A decade scaler, the 10-cps output of which drives a second decade scaler. The 1-cps output from the second 700A drives both a third 700A and a phase-inverting amplifier stage which triggers a monostable multivibrator. The output of this multivibrator is a positive-going voltage, 0.1 second wide, that energizes a relay coil for 0.1 second. The relay contacts connect a 6-volt DC power supply to the side-marking pens on both Brush recorders which are, in turn, deflected for 0.1 second to record

[redacted]

[redacted]

the 1-second timing mark. The 0.1 cycle-per-second output from the third 7001 decade scaler drives a fourth 7001 decade scaler and an amplifying phase-inverting stage that triggers a monostable multivibrator set to give a 0.4-second, positive-going voltage output. This output deflects the side-marker pens for 0.4 second every tenth time mark. Similarly, the 0.01-cps output of the fourth decade scaler drives a phase-inverting amplifier stage that triggers a multivibrator, the output from which deflects the side-marker pens for 0.8 second every one hundred 1-second time mark.

The electronically regulated power supply is capable of supplying -275 volts at 180 milliamperes with ± 1 percent regulation for AC line variations of 105 to 130 volts.

6.2.2 Operations

Microbarograph stations were located on Johnston Island, French Frigate Shoals, and Oahu, Hawaii, at positions shown in Table 6.9. The notation used is explained in Fig. 6.9. The sensing heads at each microbarograph station were placed about 1 mile apart in order to separate signals, since difference in arrival times at the two heads was necessary for complete data reduction and signal comparison. The relative positions of these stations and Teak GZ are shown on the map in Fig. 6.10.

Since no experience existed on which to base predictions or pressure from the very-high-altitude burst of Teak, the sensitivity range at each station could not be predicted accurately, and thus ranges could not be fixed before the shot. However, since it was known that the signal would be received at Johnston Island well before it would be received at the other stations, a procedure was established for resetting ranges on advice from Johnston. In order to avoid rebalancing more than one amplifier, the two amplifiers at each outlying station began operations on different range settings established by predictions as accurate as could be made. One or the other of the settings was to be changed, as described in the procedure below, in accordance with radio instructions from Johnston Island.

All microbarograph recorders operated at a paper speed of 2.5 mm/sec (medium speed setting). With this paper speed and the maximum necessary recording periods (H - 5 minutes to between H - 10 and H - 120 minutes), each

[redacted]

TABLE 6.9--HARDTACK MICROBAROGRAPH STATION LOCATIONS

Station	Sensing head	Latitude (degrees north)	Longitude (degrees west)	D-Teak (feet)	θ-Teak	d-Teak (feet)	D-Orange (feet)	θ-Orange	d-Orange (feet)
Johnston Island	Close 1	16°44'17.38"	169°31'36.03"	3,095	N48°03'35"W	1628.2	138,597	901°17'54"W	188.9
	Close 2	16°44'17.38"	169°31'35.92"	3,103	N48°11'31"W	1625.0	138,598	901°18'10"W	188.9
	Far 1	16°43'58.80"	169°31'36.03"	4,573	N30°13'27"W	--	136,714	901°19'00"W	--
	Far 2	16°43'58.80"	169°31'35.92"	4,578	N30°20'27"W	--	136,715	901°19'16"W	--
French Frigate Shoals	Close	23°51'56.84"	166°17'28.93"	2,826,014	S22°34'38"W	2170.6	2,892,856	S21°32'13"W	2130.1
	Far	23°52'09.10"	166°16'58.30"	2,828,240	S22°37'16"W	--	2,895,056	S21°34'47"W	--
Oahu, T. H.	Close	21°26'40.03"	158°08'06.85"	4,291,524	S64°39'40"W	5266.4	4,323,715	S63°00'13"W	5234.4
	Far	21°26'59.23"	158°07'14.84"	4,296,800	S64°39'50"W	--	4,328,968	S63°00'29"W	--

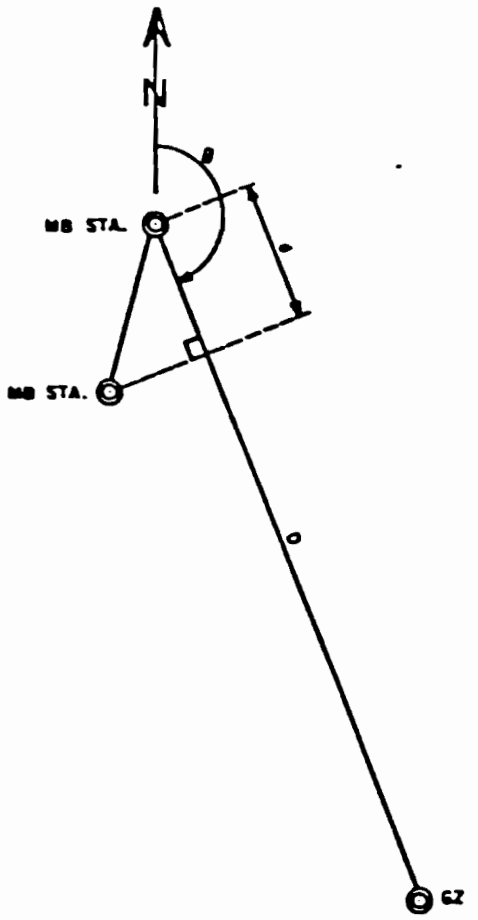

Fig. 6.9--Microbarograph dual station arrangement.

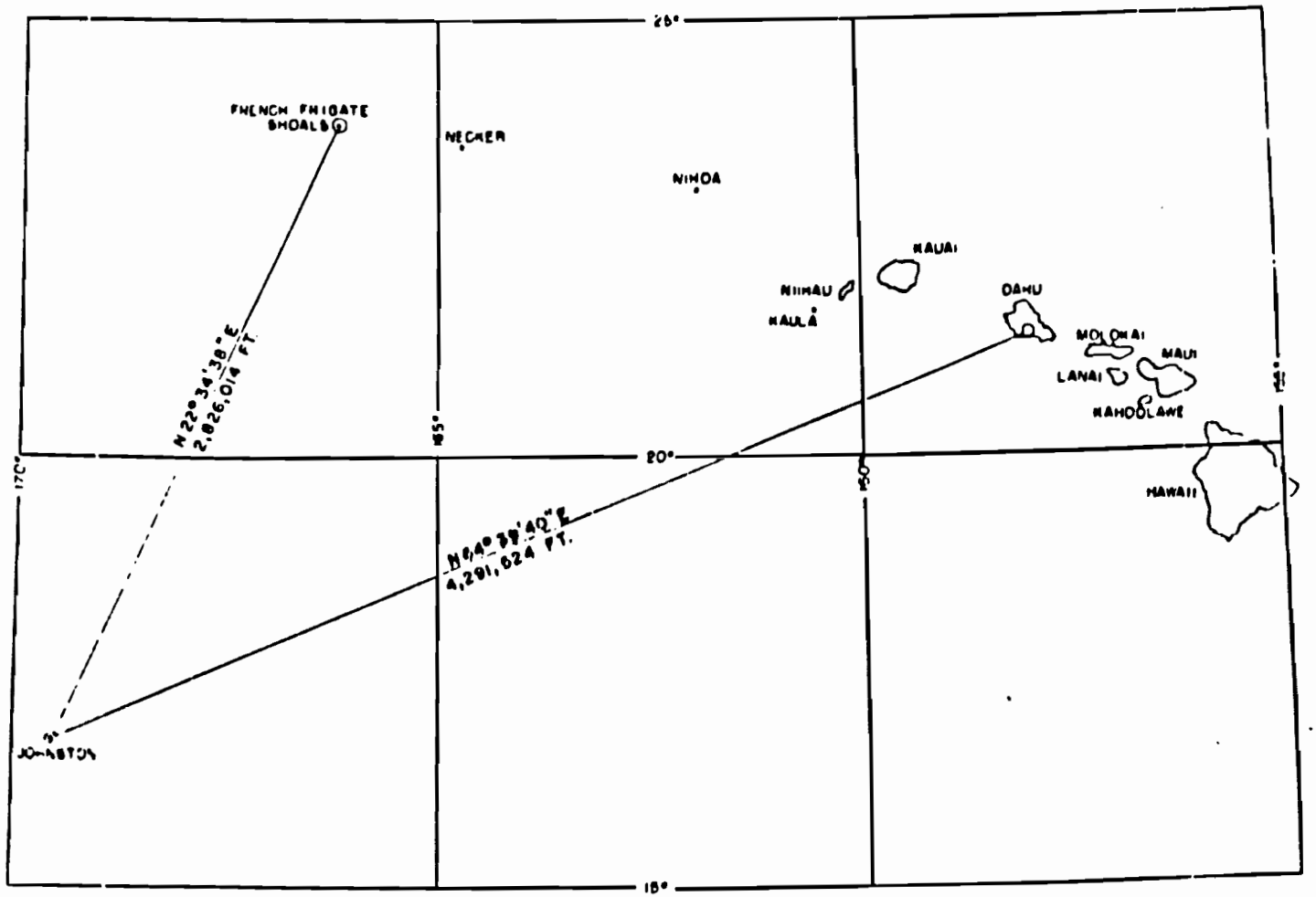

Fig. 6.10--Map of Johnston Island area.

[redacted]

operator determined paper-roll size on the basis of a table designating signal arrival times for each shot. These arrival times were computed from approximate shot-to-station distances. Each paper roll had WWV time ticks every 5 minutes, except during recording of shot signals. Since analysis requires synchronization of station pairs to 0.01 second, a single button was provided on the time-mark generator which marks calibrations (three-fourths of full deflection) at tick times simultaneously on the four channels of the two recorders.

The top channel (Fig. 6.11) on one recorder (time-marker pen at the bottom) records the high-sensitivity trace from the near head, i.e., the head closest to the shot; the lower channel records the low-sensitivity trace from the far head. The other recorder shows the far-head, high-sensitivity trace in the top channel and the near-head, low-sensitivity trace in the lower channel. This recorder arrangement provides accurate differences in arrival times from which the incidence angles can be computed. It was adopted to enable the operator to observe approximate travel-time differences on one recorder.

The Johnston Island station maintained one pair of sets (one near, one far head) on the 12,000-set range, and the other pair (one near, one far head) on the 4000-set range. According to instructions, if the recorded signal from Teak exceeded 6 millibars, the operator was to transmit the instruction UP ONE, and the other stations would immediately change their lower range microbarographs to the higher range already on the other set. If the recorded signal at Johnston Island was less than a 6-millibar amplitude, the operator was to transmit the instruction DOWN ONE, and the other stations would immediately step down the range settings of their higher sets to agree with the range on the lower range set.

In the event that Johnston pressures exceeded 34 millibars, an UP TWO instruction was to be sent. Stations set on 120 and 400 initially were instructed to put both sets on 1200 range. Finally, if the Johnston recording showed less than 2 millibars of pressure amplitude, a DOWN TWO instruction was to be transmitted. The operators were instructed to change first the setting farthest from set range, then the setting nearest set range.

[redacted]

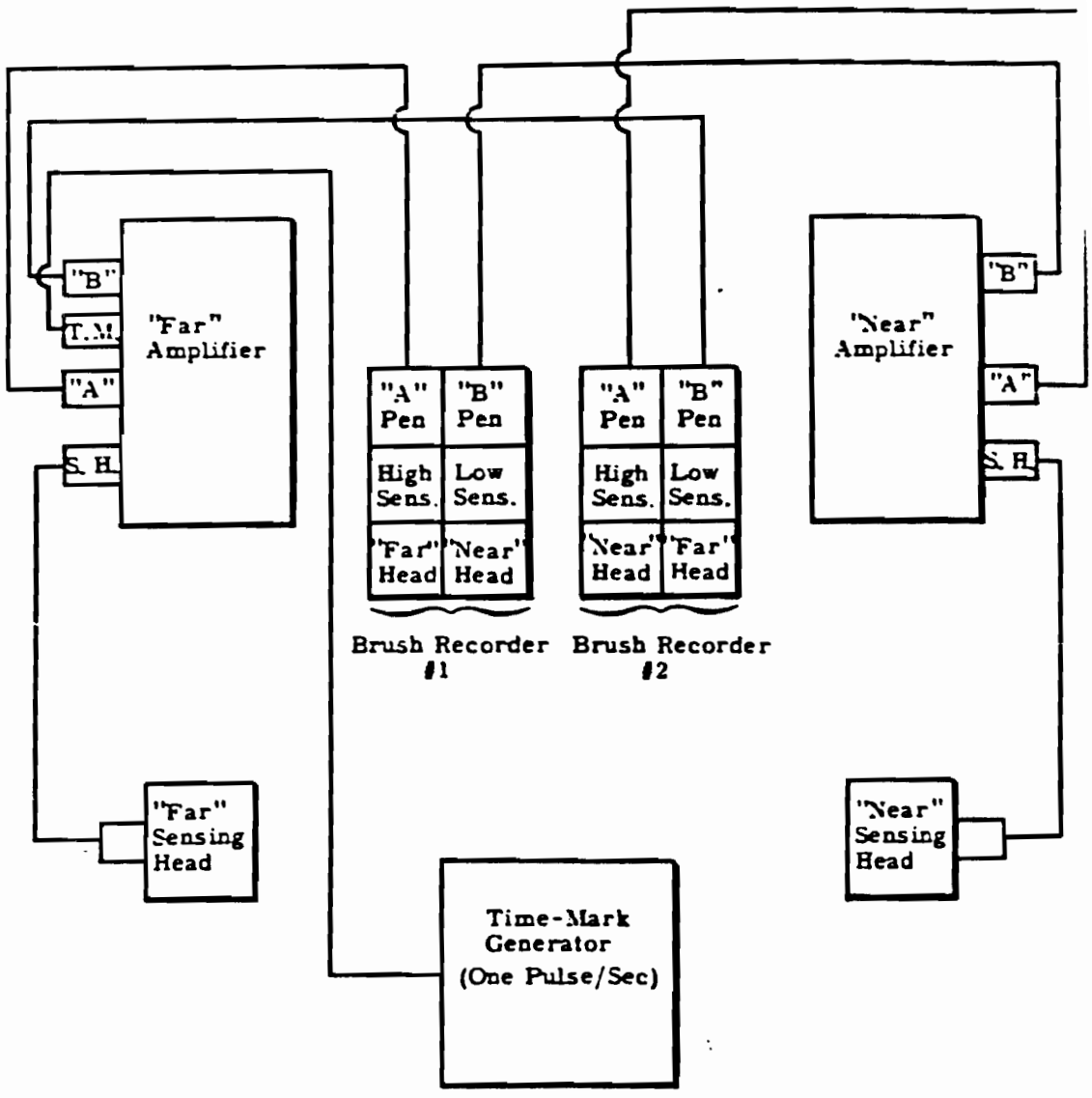

Note: Recorded Data Should be Read from Recorder #2

Fig. 6.11--Cabling diagram.

[redacted]

6.2.3 Instrument Performance

The microbarographs located at Johnston Island did not experience any technical difficulty. The French Frigate Shoals station incurred a defective time-mark-generator output but maintained 10-second time marks. This established sufficient reference for determining travel time of the blast wave. The Oahu recordings did not furnish internally consistent pressure amplitudes or arrival times, but observations by other agencies gave enough information so that a reasonable interpretation could be made.

The sensing heads were all calibrated prior to their being positioned at their respective survey points, and they possessed balance-down capability throughout the tests.

At H + 5 minutes during the Teak event, an UP ONE instruction was transmitted from Johnston Island to French Frigate Shoals and Oahu. This meant that operators at these stations were to change from their 120 microbarograph sets on the 400-microbar range. The French Frigate Shoals station received the instruction UP ONE, but instead of changing the 140 range to 400, the operator changed the 400 range to 1200. This decision was based on the blast intensity as he saw it, which resulted in a wider range of blast wave-recording capability but made analysis somewhat more difficult. The Oahu station did not receive the instruction because of communications blackout.

French Frigate Shoals and Oahu were given 400 set ranges for the Orange event with no provision for changes.

[redacted]

207

REFERENCES

1. Report of SAB Nuclear Panel on High-Altitude Weapons Effects, Scientific Advisory Board to the Chief of Staff, Headquarters, U. S. Air Force, November 19, 1956.
2. Shelton, F. B., High-Altitude Effects on Blast-Thermal Partition of Energy from Nuclear Explosions, and Associated Scaling, SC-2969(TR), Sandia Corporation, September 15, 1953.
3. Hudson, C. C., A Note on Radiation-Produced Shock, SCTM 75-57(51), Sandia Corporation, February 5, 1957.
4. Bethe, H. A., Some Phenomena in High-Altitude Explosions, LA-2164, Los Alamos Scientific Laboratory, November 7, 1957.
5. Goody, R. M., The Physics of the Stratosphere, Cambridge University Press, 1954.
6. Capabilities of Atomic Weapons, TM 23-200, Armed Forces Special Weapons Project, Washington, D. C., Rev. Ed., November 1957.
7. Reed, J. W., Additional Notes for Hardtack Microbarograph Operators, SCTM 74-58(51), Sandia Corporation, February 1958.
8. Meszaros, J. J., et al., Air Blast Phenomena and Instrumentation of Structures, Operation Hardtack, Project 1.7 Preliminary Supplement, ITR-1612-2, Field Command, Armed Forces Special Weapons Project, October 24, 1958.
9. Reed, J. W., A Recommended Upper Atmosphere Model (16 - 400 kilometers), SCTM 66-59(51), Sandia Corporation, April 2, 1959.
10. Cox, E. F., and Reed, J. W., Long Distance Blast Predictions, etc., General Report on Weapons Tests, WT-9003, AEC/TID, Oak Ridge, Tennessee, September 20, 1957.
11. Manual of the ICAO Standard Atmosphere, NACA-TN-3182, Calculations by the National Advisory Committee for Aeronautics, May 1954.
12. The Rocket Panel, Pressures, Densities, and Temperatures in the Upper Atmosphere, Phys. Rev. 88 (5), December 1952.
13. Bethe, H. A., and Fuchs, K., Asymptotic Theory for Small Blast Pressure, LA-1021, Los Alamos Scientific Laboratory, August 13, 1947.
14. Cowan, M., Negative-Phase Duration as a Measure of Blast Yield, SC-3170(TR), Sandia Corporation, September 1, 1953.
15. Cowan, M., Sander, H. H., and Munro, D. N., Test Results from Automatic Yield Indicators, Operation Hardtack, WT-1737, Sandia Corporation, August 1961.
16. Bond, J. W., Scaling of Peak Overpressures in a Nonuniform Atmosphere, SC-1939(TR), Sandia Corporation, July 1951.
17. IBM Problem M, (Performed at Los Alamos Scientific Laboratory) original data tabulations.

[redacted]

REFERENCES (Continued)

18. Broyles, C. D., IBM Problem M Curves, SCTM 266-56(51), Sandia Corporation, December 1, 1956.

19. Minzner, R. A., Champion, K. S. W., and Pond, H. L., The ARDC Model Atmosphere, Air Force Cambridge Research Laboratory, 1959.

20. DuMond, J. W. M., The Determination of the Wave Forms and Laws of Propagation and Dissipation of Ballistic Shock Waves, J. Acoust. Soc. Am., Vol. 18, No. 1, July 1946.

21. Willett, J. E., and Lehto, D. L., Computed Shock Overpressure Distance Curves for Atomic Explosions at Detonation Altitudes from Sea Level to 150,000 Feet, NavOrd Report 6152, U. S. Naval Ordnance Laboratory, September 1, 1958.

22. Sachs, R. G., Dependence of Blast on Ambient Pressure and Temperature, BRL-466, Ballistic Research Laboratories, May 15, 1944.

23. Bryant, E. J., and Keefer, J. H., Basic Air-Blast Phenomena, Part 2, Operation Plumbbob Project 1.1, ITR-1481, BRL, FC/AFSWP, December 13, 1957.

24. Reed, J. W., Banister, J. R., and Shelton, F. H., Ground-Level Microbarographic Pressure Measurements from a High-Altitude Shot, Operation Teapot, WT-1103, Sandia Corporation, July 1956.

25. Summary Report of the Technical Director, Programs 1-9, Operation Upshot/Knothole, WT-782, FC, Armed Forces Special Weapons Project, March 1955.

26. Champeny, J. C., Very-Long-Range Light Measurements, Report B-1866, Edgerton, Germeshausen, and Grier, Inc., December 1958.

27. Microbarograph Evaluation Report, SC-2990(TR), Sandia Corporation, September 18, 1953.

[redacted]

Chapter 7

RADIO-FREQUENCY ATTENUATION

7.1 EXPERIMENTAL PLANNING AND INSTRUMENTATION

Several missile and antimissile systems depend wholly upon radio-frequency transmission for guidance. Considerable concern has therefore been expressed on the effects that very high-altitude nuclear detonations might have on such transmission. Radio-frequency signals undoubtedly suffer severe attenuation in the highly ionized atmosphere containing a nuclear explosion. Apparent shifts in phase of the transmitted signal because of refraction could conceivably result. Radio-frequency effects studies were undertaken by Sandia Corporation in an attempt to measure these effects as a function of distance, frequency, and time. The Sandia effort was begun at the request of the DOD in December 1957, only four months before the scheduled Teak firing date.

7.1.1 Method of Measurement

Several methods for making the measurement had been considered. The technique used was based on establishment of four transmitting stations so spaced at altitude to enable receiving stations to look through the center of the burst as well as through the fringe areas. Each station in space consisted of two missiles each of which carried a transmitter, one operating at a frequency of about 225 mc, the other at a frequency of about 1500 mc. Two receiving stations were used. Each housed eight receivers, four of which were high-frequency and four low-frequency. The output of each receiver, proportional to signal strength of the received signal, was recorded on both paper and magnetic tape. The 80-kc I-F of the low-frequency receivers was directly recorded on magnetic tape to permit detection of large variations in phase. An attempt to measure phase shifts of less than 100 cycles per second was made by first mixing the 80-kc I-F with a stable and manually adjustable local oscillator before recording on the paper oscillograph. The range of attenuation measurable by the telemetry system was calculated to be approximately 35 db at 225 mc and 40 db at 1500 mc.

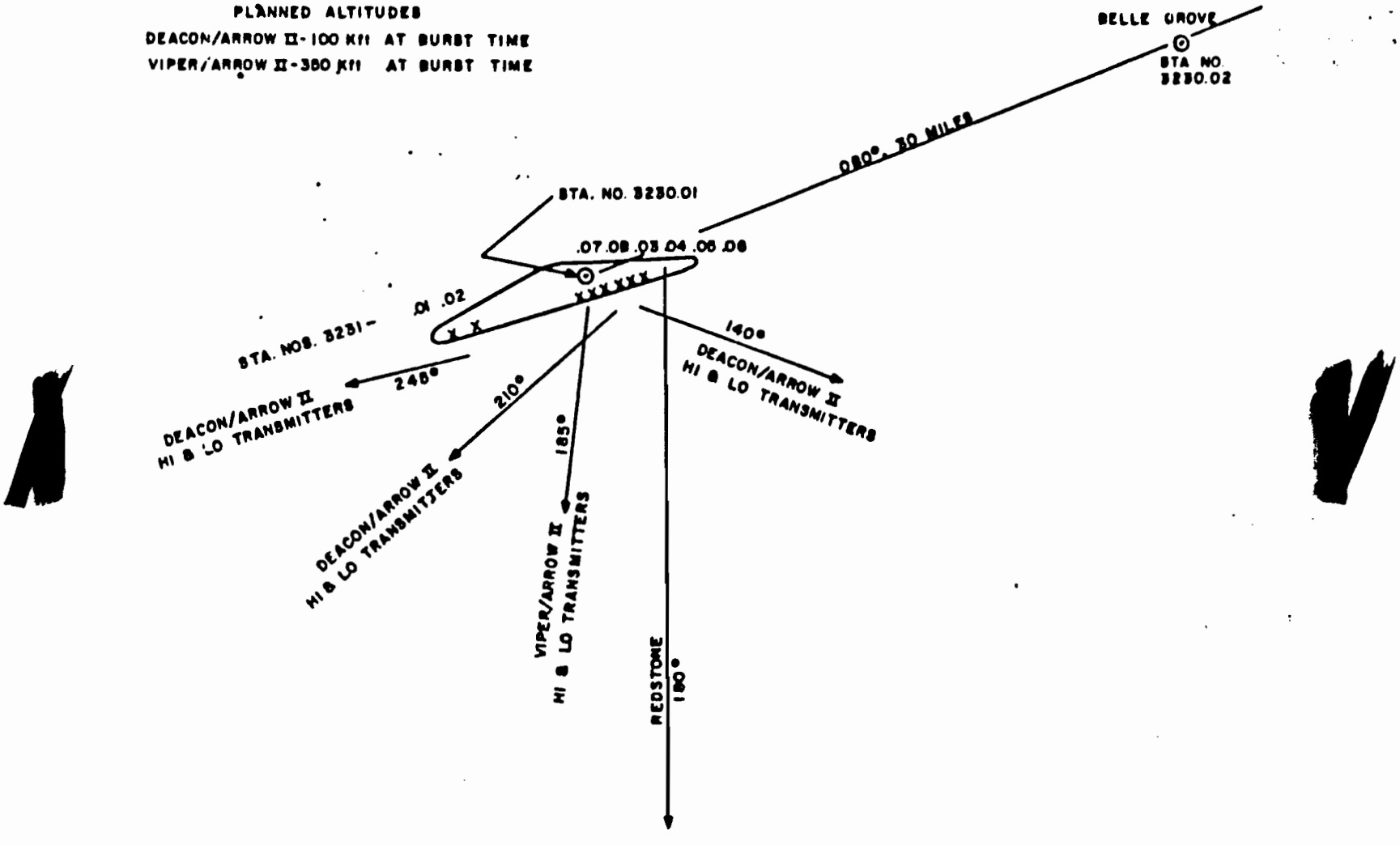

Fig. 7.1--Planned transmitter missile array, Teak shot.

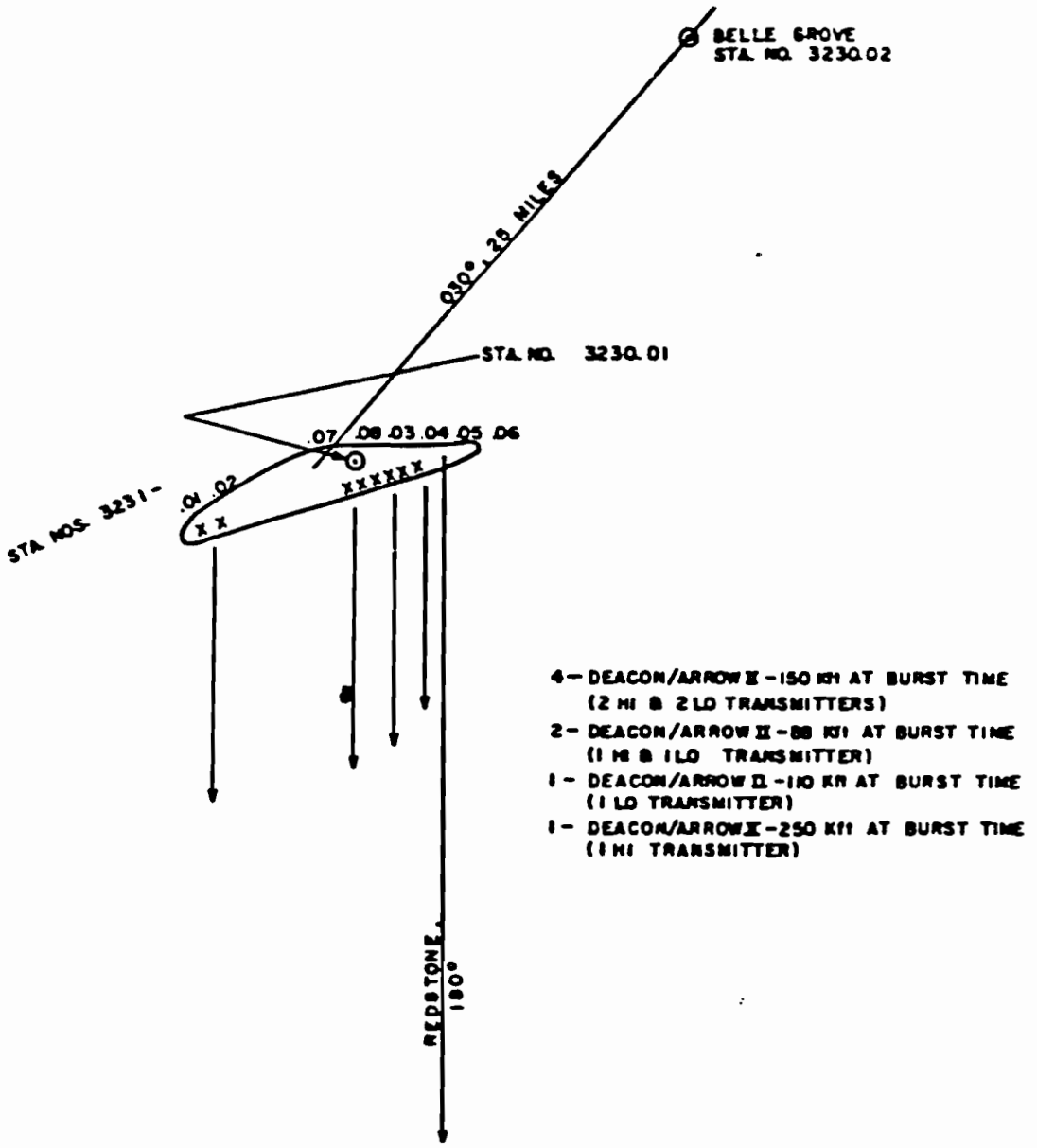

Fig. 7.2--Planned transmitter missile array, Orange shot.

TABLE 7.1--RADIO-FREQUENCY ATTENUATION DATA, TEAK SHOT

Station number	Launch azimuth	Missile system	Altitude at burst	Apogee altitude	Flight time	Transmitter frequency	Results
3231.01	245°	Deacon-Arrow	96 K	243 K	274s (284)	[redacted]	[redacted]
3231.02	245°	Deacon-Arrow	96 K		(284)	[redacted]	[redacted]
3231.03	210°	Deacon-Arrow	96 K	243 K	276s (284)	[redacted]	[redacted]
3231.04	210°	Deacon-Arrow	96 K		(284)	[redacted]	[redacted]
3231.05	140°	Deacon-Arrow	96 K	243 K	278s (284)	[redacted]	[redacted]
3231.06	140°	Deacon-Arrow	96 K		(284)	[redacted]	[redacted]
3231.07	185°	Viper-Arrow	350 K	(390 K)	(380)	[redacted]	[redacted]
3231.08	185°	Viper-Arrow	350 K	(420 K)	(380)	[redacted]	[redacted]

*These transmitters were tracked by the MIDOT system.
Planned values are shown in parentheses.
Deacon-Arrow: Launched -40s Viper-Arrow: Launched -131.6s
Belle Grove position: Heading 064° T, Lat. 16°49'40" N, Long. 169°01'00" W

[redacted]

DNR

(b)(3)

TABLE 7.2--RADIO-FREQUENCY ATTENUATION DATA, ORANGE SHOT

Station number	Launch azimuth	Missile system	Altitude at burst	Apogee altitude	Flight time	Transmitter frequency	Results
3231.01	180°	Deacon-Arrow	(150 K)	155 K	230s (240)		
3231.02	180°	Deacon-Arrow	88 K	155 K	232s (240)		
3231.03	180°	Deacon-Arrow	(150 K)	155 K	(240)		
3231.04	180°	Deacon-Arrow	(150 K)	155 K	(240)		
3231.05	180°	Deacon-Arrow	(250 K)	250 K	(286)		
3231.06	180°	Deacon-Arrow	110 K	258 K	284s (284)		
3231.07	180°	Deacon-Arrow	152 K	152 K	228s (240)		
3231.08	180°	Deacon-Arrow	(88 K)	155 K	(240)		

*These transmitters were tracked by the MIDOT system.
Planned values are shown in parentheses.
Bulle Grove position: Heading 016° T, Lat. 17°05'55" N, Long. 169°18'30" W

[redacted]

[redacted]

DNA (b)(3)

7.1.2 Site Geometry

The transmitter missile array for Teak shot is shown in Fig. 7.1, and for Orange in Fig. 7.2. Eight two-stage missiles, either the Deacon-Arrow or the Viper-Arrow combination, were set for launch on each shot. Their launch times were variously related to Redstone launch as tabulated below and in Tables 7.1 and 7.2. Launch azimuths of the missiles were carefully determined in an attempt to optimize their positions in space consistent with the following boundary conditions:

(1) Line-of-sight transmitter stations to receiver stations must penetrate the center of the burst as well as the anticipated fringe areas of total blackout.

(2) Planned point of detonation:

	Teak	Orange
Range	36,122 feet	125,000 feet
Altitude	250,063 feet	125,000 feet
Azimuth	180° from Johnston	180° from Johnston
Flight Time	170.5 seconds	154 seconds

(3) For Teak, there was a minimum 5-degree separation in azimuth between the nearest transmitter missile trajectory and the Redstone trajectory.

(4) Antenna beam widths to half-power points:

225 mc transmitting	60°
1500 mc transmitting	41°
225 mc receiving	44°
1500 mc receiving	27°

Launcher Pads. Eight concrete launcher pads, 6 feet square and 6 inches thick, were constructed along the southern shore of Johnston Island. A small zero-length launcher mounted on each pad was used to direct the missiles along the calculated trajectories. Identification of launchers, launch azimuths, and frequency of each transmitter missile are tabulated in Tables 7.1 and 7.2.

Receiving Stations. One receiving station was located on Johnston Island (Station No. J-3230.01). The other station was located in a trailer on the USS Belle Grove (Station No. J-3230.02). The ship was positioned approximately on an azimuth 080° TN from Johnston Island, 30 miles away, during Teak, and 030° TN, 25 miles away, during Orange.

Timing Signals. EG&G timing signals indicating seconds before burst are shown below:

7.1.3 Missile Configuration

The transmitter carrier-missile system was selected from available components in an attempt to meet the primary requirement of lifting a 10-pound payload to an altitude of approximately 500,000 feet. The smallest possible rockets were selected in order to reduce problems of handling and procurement of metal parts.

System Description. A combination of Deacon booster and Arrow sustainer was believed capable of satisfying design requirements. Somewhat inconsistent flight test data indicated that this system would reach an altitude of only about 250,000 feet. A typical trajectory of the system is shown in Fig. 7.3. To obtain desired data at higher altitudes, a combination of Viper booster and Arrow sustainer was tested, with initial indications of a maximum altitude of about 500,000 feet. A calculated trajectory of this combination is illustrated in Fig. 7.4. Details of both rockets are given in Fig. 7.5.

An adapter section joins the first stage to the second stage. The transmitter canister is attached to the Arrow II with a second adapter section. The

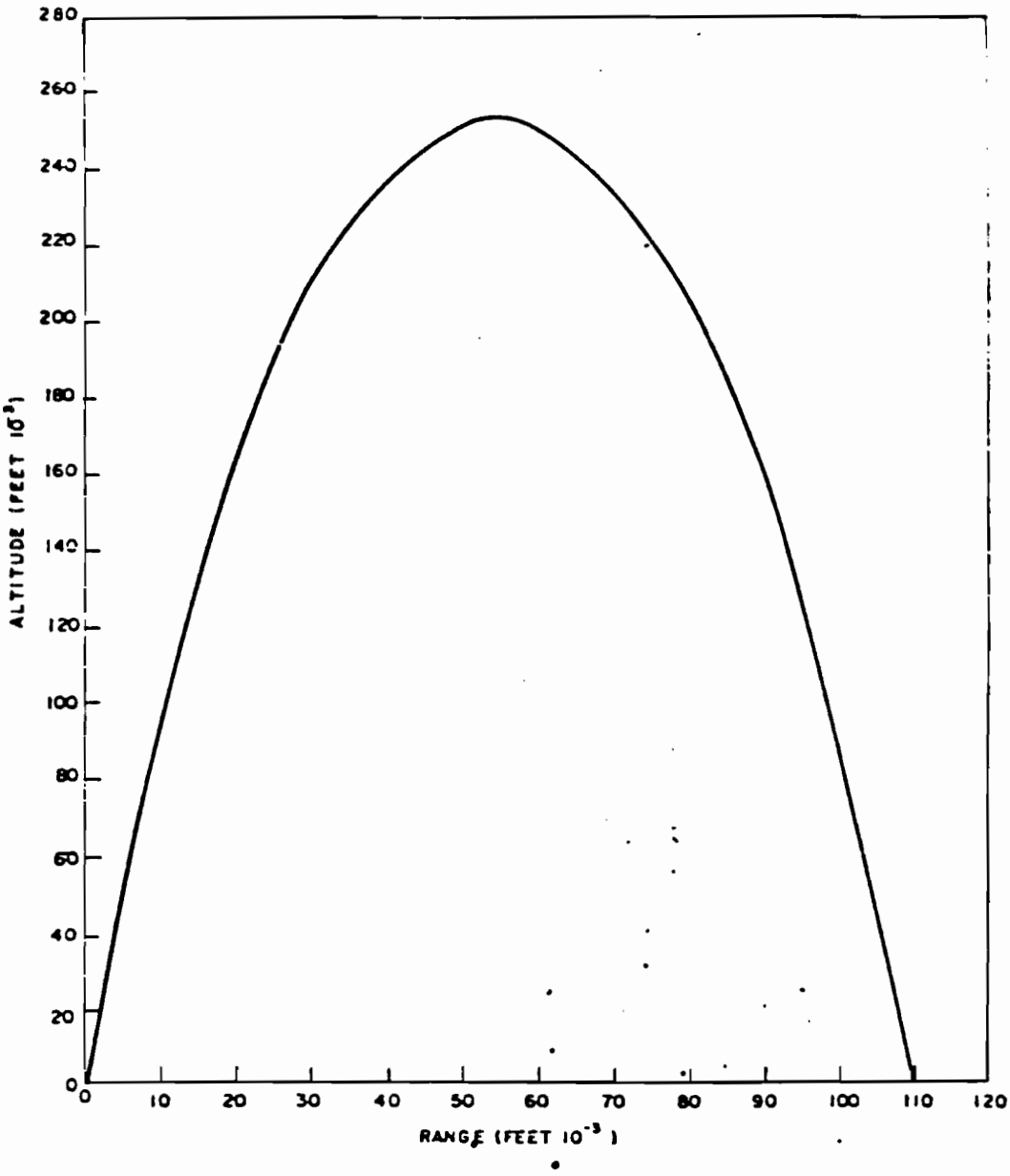

Fig. 7.3--Altitude versus range of Hi-Lo carriers.

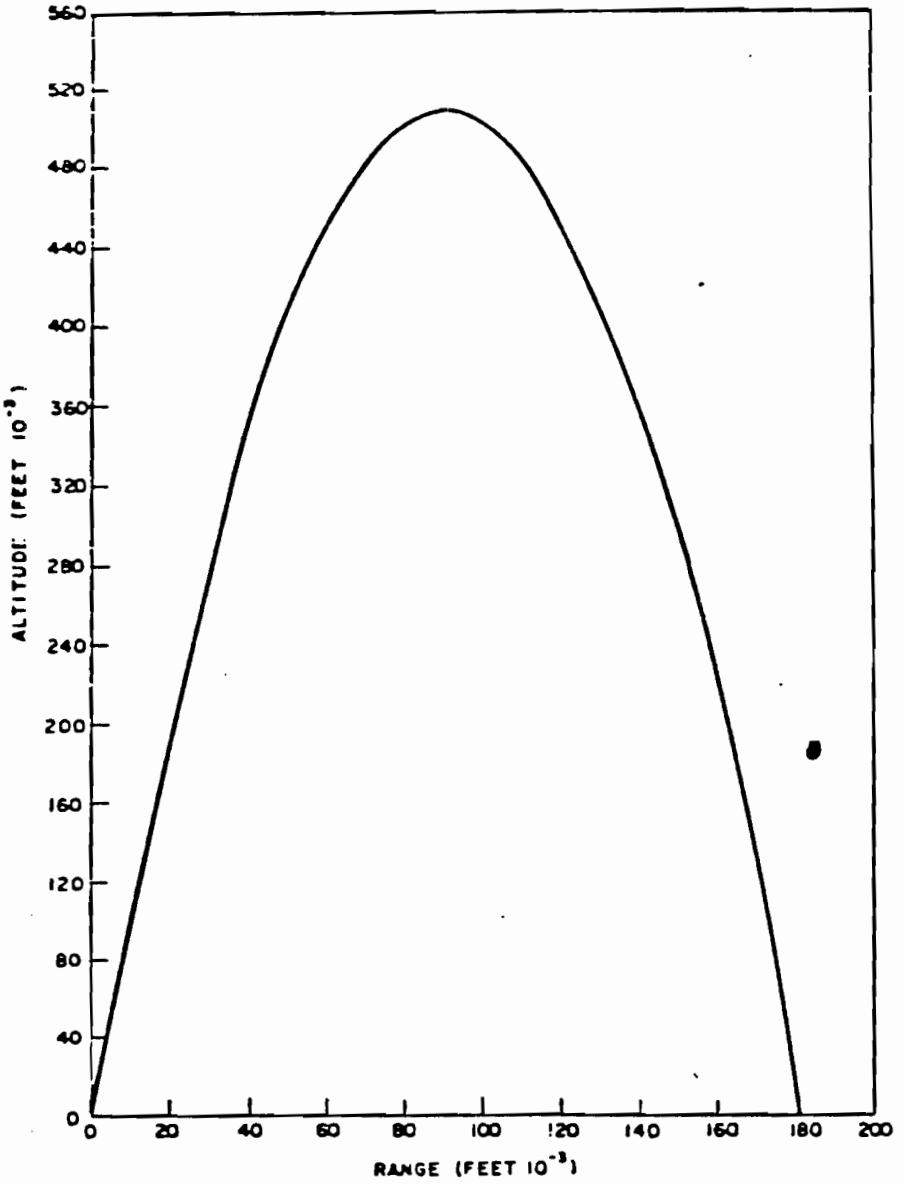

Fig. 7.4--Altitude versus range of Hi-Lo carriers with Viper booster.

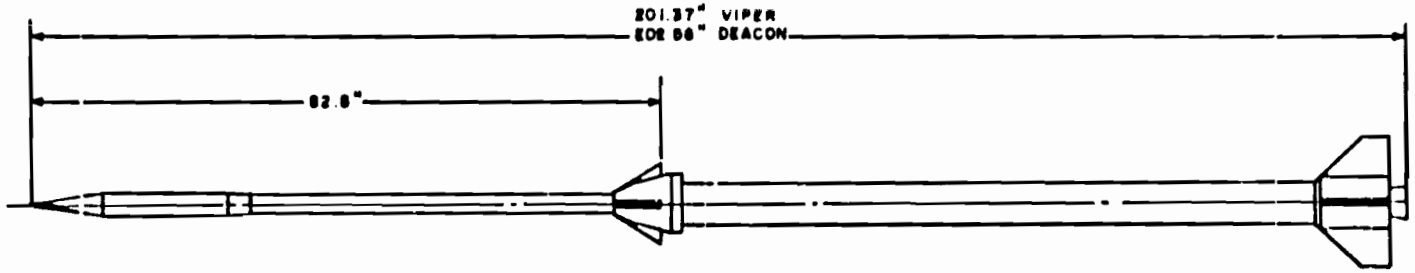

WEIGHTS

LAUNCH	DEACON BOOSTER -	228 LBS
	VIPER BOOSTER -	270 LBS
SECOND STAGE		41 LBS
NOSE ASSEMBLY		18 LBS

MOTOR SPECIFICATIONS

	A-8 DEACON	VIPER II	ARROW II
THRUST, LBS	6(100	8300	3000
IMPULSE, LBS-SEC	18,000	31,100	3800
TIME, SEC	3.0	3.8	1.8
DIAMETER, IN	6.0	6.6	3.0
LENGTH, IN	110.8	106.8	80

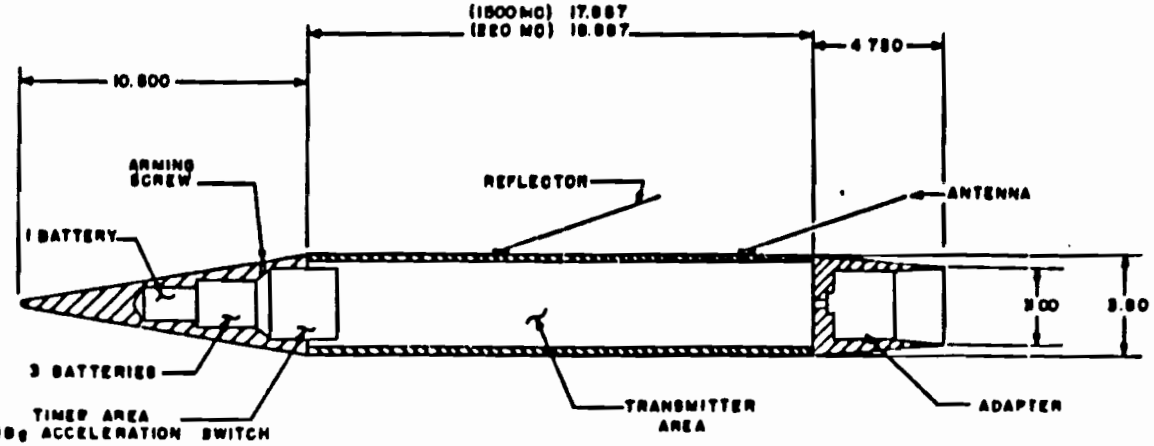

Fig. 7.5--Transmitter rocket.

nose cone fastens directly to the transmitter canister and contains the second-stage firing circuitry.

Firing Circuitry. The first stage of both missile systems is fired by direct connection through a safing plug to the EG&G timing relay and then to a 24-volt battery pack. The Arrow II second stage is fired by the circuit shown in the block diagram of Fig. 7.6. The arm-safe switch is manually actuated before launch. The acceleration switch senses a fraction of missile acceleration and fires the timer squib. The timer runs a preset 22 seconds and fires the second stage which carries the transmitter canister to desired altitude at burst time.

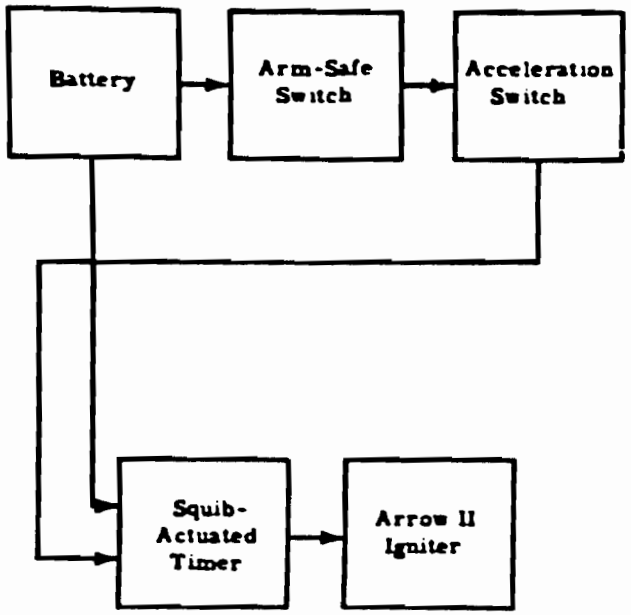

Fig. 7.6--Arrow II firing circuitry.

[redacted]

7.1.4 Description of Transmitters

Both the 223- to 225-mc and the 1450- to 1500-mc transmitters are packaged in a canister 3-1/2 inches in diameter by 15 inches long. The approximate weight of either canister is 9-1/2 pounds. Nickel-cadmium battery power supplies were selected to provide approximately 50 minutes of operation. The transmitter power supply is switched on and off, as required, before launch by a magnetic holding relay controlled by manually actuated signals. Signals are sent to the transmitter canister through an explosively actuated disconnect plug and cable assembly. Antennas for both high- and low-frequency transmitters are trailing dipole whips.

Low-Frequency Transmitter.

Schematic:	Fig. 7.7
Transmitter:	Bendix TXV-13
Frequencies:	222 mc, 223 mc, 224 mc, and 225 mc
Power output:	2 watts cw, nominal
Modulation:	None, grounded grid input
Power requirements:	
Filament:	18 v DC, 400 ma
Plate:	200 v DC, 100 ma
Power source:	
Filament:	18 v, 500 mah capacity
Plate:	200 v, 100 mah capacity
Antenna:	Trailing dipole whips, 1/4-wavelength, 45° to missile longitudinal axis
Beam width to half-power points:	60°
Gain:	4 db

High-Frequency Transmitter.

Schematic:	Fig. 7.8
Transmitter:	Cavity resonator, tube type 2C39
Frequencies:	1450 mc, 1475 mc, 1500 mc, and 1525 mc
Power output:	2 kilowatts peak, nominal
Modulation:	Pulse, 200 cps, 1/2 microsecond pulse width

[redacted]

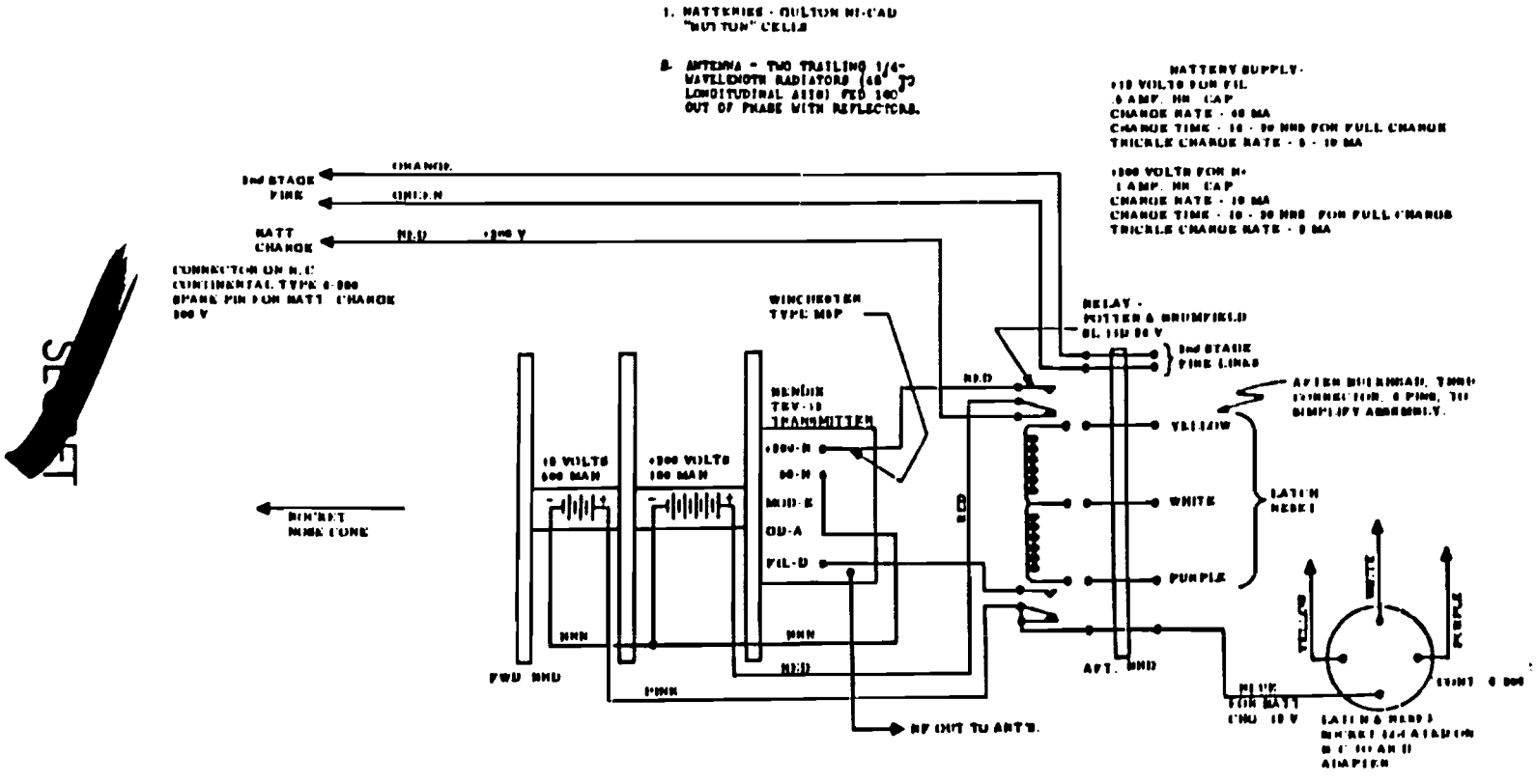

Fig. 7.7--Low-frequency transmitter packages.

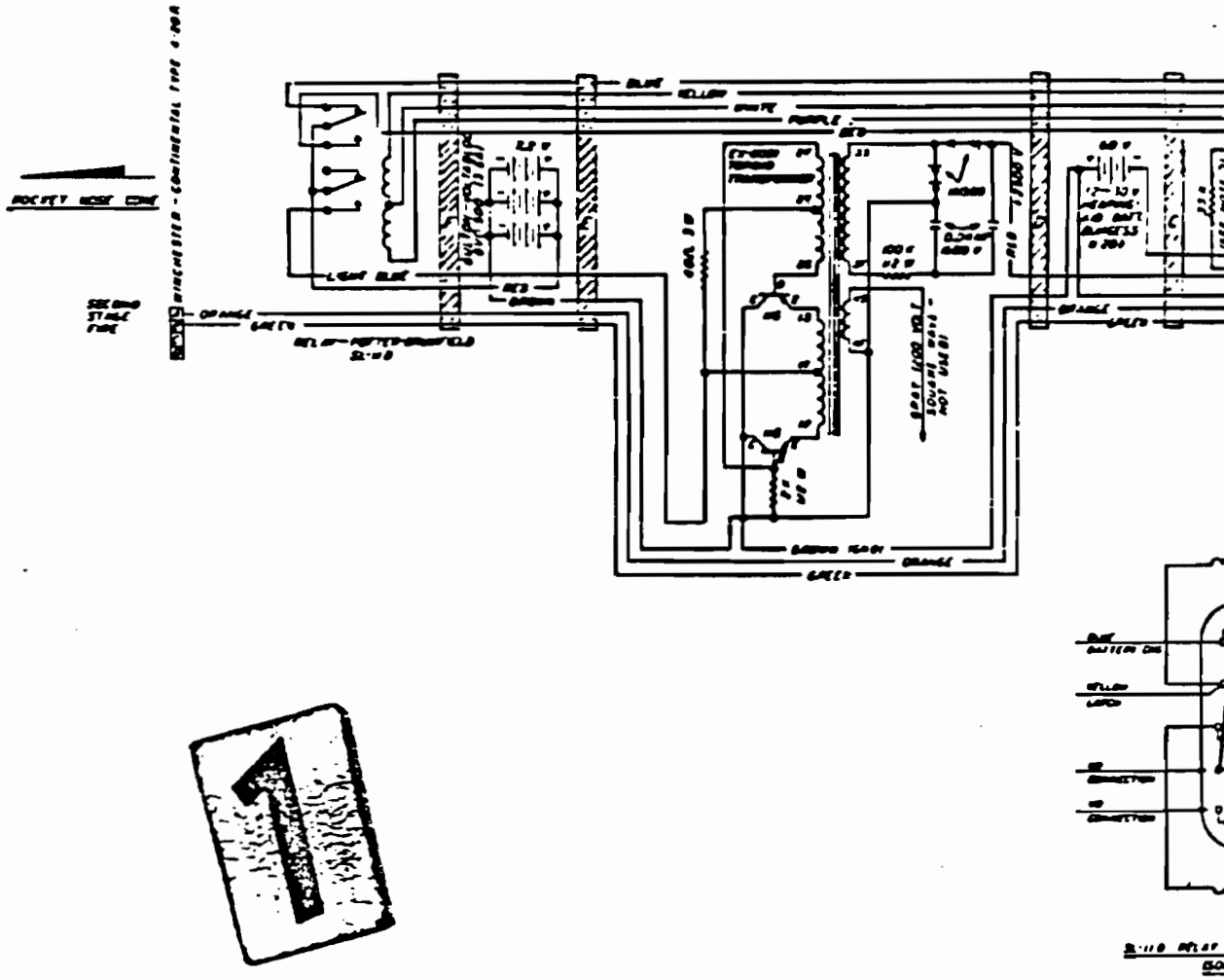

Notes: Cable lengths to Microdot feedthrus are such that the total cable lengths to the antennas will feed the antennas 180° out of phase.

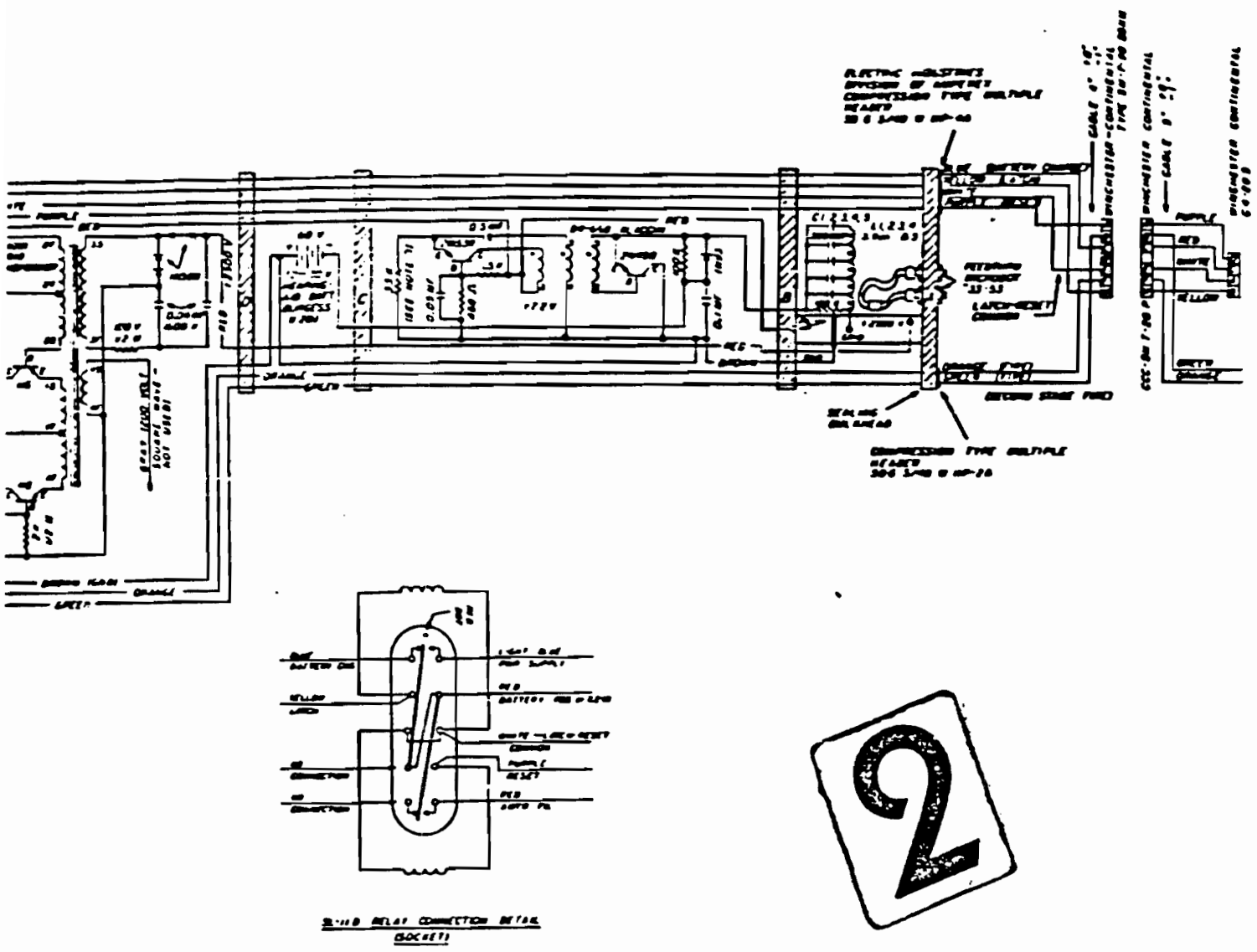

Fig. 7.6--High-frequency transmitter.

[redacted]

High-Frequency Transmitter (cont).

Power requirements:	
Filament:	7.2 v DC, 1.0 amp
Plate:	2.5 kv, 500 microamps
Power source:	
Filament:	7.2 v, 1.5 ah capacity
Plate:	Transistor power supply, 7.2 v to 2.5 kv, 250 ma input
Antenna:	Trailing dipole whips, 3/4 wavelength, 20° to missile longitudinal axis, with reflectors
Beam width to half-power points:	41°
Gain:	4 db

7.1.5 Receiving Station Description

A block diagram of the two receiving stations is shown in Fig. 7.9. Basically, the transmitted signal is received by a high-gain helical antenna, amplified by an RF amplifier, detected in a receiver, and recorded on both paper oscillographs and magnetic tape recorders. An ASCOP preamplifier and multicoupler are used at 225 mc for amplification and coupling; a traveling wave tube amplifier is used at 1500 mc. The signal from the cathode of the S-meter tube of the National 300 low-frequency receiver, through a cathode follower, is recorded on a Miller paper oscillograph in parallel with an Ampex 800 magnetic tape recorder. This recorded signal varies in proportion to the received signal. The 80-kc I-F of the National receiver is recorded directly by the Ampex tape recorder to measure large phase variations in the low-frequency transmitted signal. In measuring phase variation below 100 cps, the 80-kc I-F is also mixed with a local oscillator, which is stable and manually adjustable, and is sent through a cathode follower to the Miller oscillograph for recording. From a differential amplifier at the detector end of the 40-mc I-F in the high-frequency Polarad receivers, a signal proportional to the peak power of the transmitters is fed through a DC amplifier to both the Miller and the Ampex recorders.

Low-Frequency Receiving Equipment:

Antenna:	Helix, 7-turn, 14 db gain, 44° beam width
RF amplifier:	ASCOP multicoupler, Model AMC-2, 9-db gain, 9.5-db noise figure

[redacted]

225

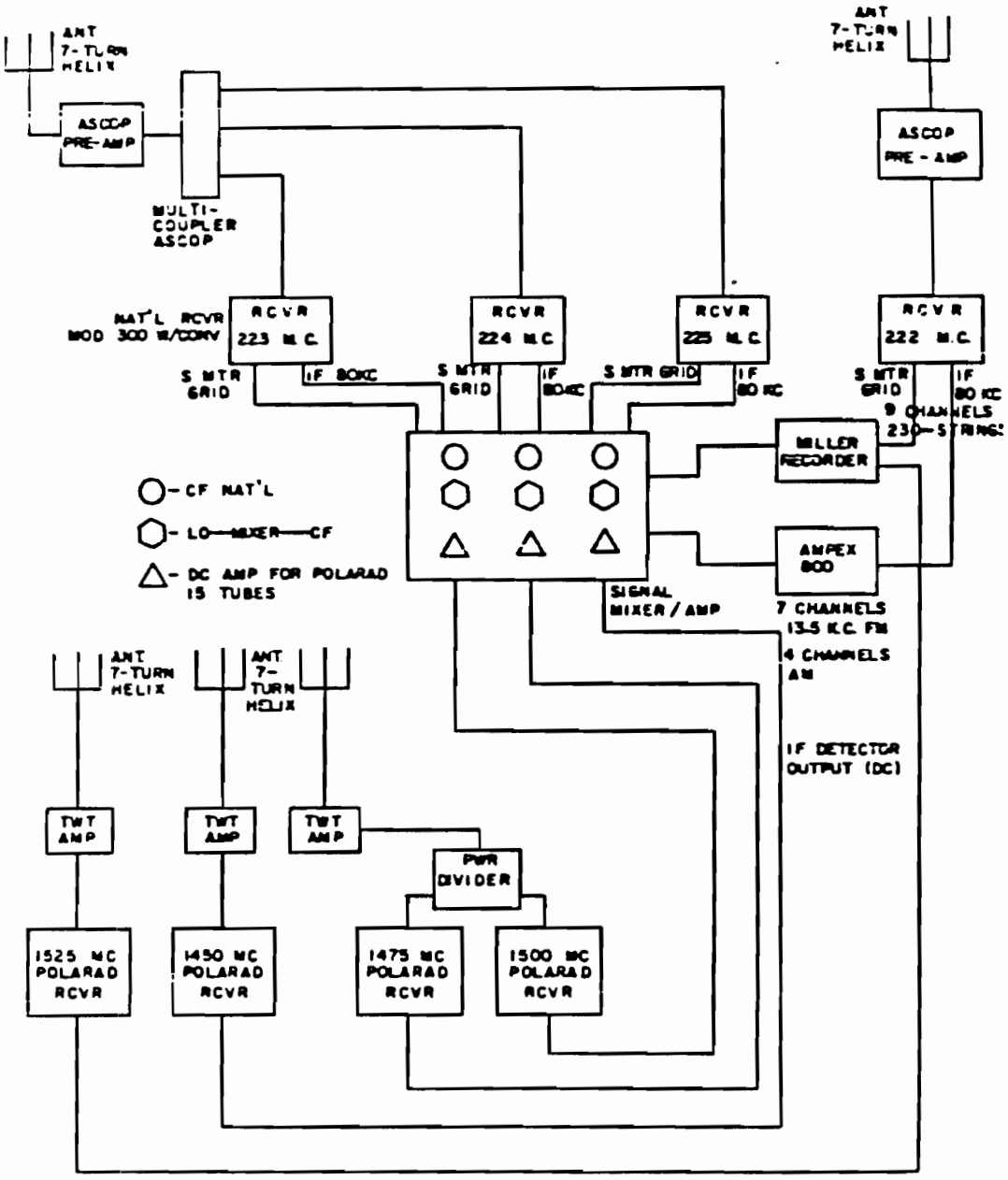

Fig. 7.9--Receiving station diagram.

Low-Frequency Receiving Equipment (cont).

RF preamplifier:	ASCOP, Model APA-2, 15-db gain, 2.5-db noise figure
Receiver:	National 300, with converter; sensitivity 0.1 microvolts at 50 ohms; 10-db noise figure
Recorders:	Miller, paper oscillograph, with 230-cps galvanometers; Ampex 800, with FM recording amplifiers, 13.5-kc center-frequency; direct recorders, 20- to 100-kc response

High-Frequency Receiving Equipment.

Antenna:	Helix, 7-turn, 15-db gain, 27° beam width
RF amplifier:	RCA A-1056 traveling wave tube, 32-db gain, 7-db noise figure
Receiver:	Polarad Model R, sensitivity, minus 80 dbm, 8-db noise figure
Power divider:	Admittance, Namco Corporation Model CB-3, 3-db split
Recorders:	Miller; Ampex 800

Measurable Range of Attenuation. A calculation incorporating antenna gains, path attenuation, preamplification, receiver sensitivity and noise, and transmitter power produced the following results:

Frequency	Range Measurable
225 mc	35 db
1500 mc	40 db

7.1.6 Transmitter Positioning

The Sandia MIDOT system[1] was used to track the 222-mc and 224-mc transmitter missiles on both Teak and Orange.* The MIDOT system functions in a manner similar to the Michelson light interferometer. Two high-gain helical antennas, separated a measured number of wavelengths at the received frequency, are fed into a single summing point (T connector). The single output of the T goes to an ASCOP multicoupler, then to a Nems-Clarke receiver, and thence to a Miller paper oscillograph recorder. A null occurs at the summing

*In addition to the above referenced report[1] which gives a complete description of the MIDOT system, further information appears in Chapter 9 of this report.

point any time a 180-degree phase difference is produced as a result of difference in arrival time of the RF signal at the two antennas. A mathematical relationship can be derived which relates the angle between the line of sight to the transmitter and the antenna base line to the wavelength of the received frequency as follows:

$$\alpha = \cos \frac{-1(K + 1/2)\lambda}{D},$$

where α = angle between line of sight to the transmitter and the antenna base line when a null occurs, K = an interger, λ = wavelength of received frequency, and D = number of wavelengths in the antenna base line. An accuracy of 2 mils in an angle in trajectory determination can normally be expected. With the short base lines used at Johnston Island, the theoretical accuracy is somewhat less than 2 mils in angle. Extremely accurate placement of two receiving stations, each with orthogonal base lines, is a minimum requirement. A common time base, 1000 cps, is recorded on the Miller oscillograph simultaneously with the data.

7.2 EVALUATION OF SYSTEM PERFORMANCE

Six Deacon-Arrow missiles and two Viper-Arrow missiles were fired on Teak. The Deacon-Arrow missiles were placed at 96,000 feet at burst time (see Figs. 8.5 through 8.8, Chapter 8) along various azimuths. It was anticipated that these would bracket the fringe areas of ionization. The Viper-Arrows were dispatched along a 185-degree azimuth with the intention of allowing the transmitters to be viewed through the center of the fireball. Four high- and four low-frequency transmitters were used. Both Viper-Arrows suffered first-stage instabilities and fell to Johnston Island prior to burst time. Some data were recorded on five of the six transmitters functioning at burst time. As a result of jamming of the Miller recorder in the Johnston Island receiving station, no data were recorded from the sixth transmitter. The Deacon-Arrow missiles flew in accordance with a predetermined trajectory. MIDOT trajectory data were obtained on the 224-mc transmitter.

Eight Deacon-Arrow missiles were in place for launch on Orange. Four were launched at a 70-degree angle and were to have been approximately at apogee at burst time to permit viewing through the fireball. Two more were to

have been on the same trajectory, as were the first four, but at about 88,000 feet at burst time. The remaining two were on the Teak 86-degree trajectory, one at apogee at burst time, the other at 110,000 feet on the ascending portion of flight. Four high- and four low-frequency transmitters were used. The 224-mc transmitter was off at burst time as a result of the probable failure of the second stage of the missile to ignite. There are some marginal indications that one high-frequency transmitter was functioning at burst time; two failed before burst; one was not launched because of frequency duplication. Good quality data were obtained on three low-frequency transmitters the trajectories for which are shown in Fig. 7.10. The recorded signal level was too low to be useful on the one high-frequency transmitter working at burst time.

7.3 TABULATION OF DATA

Launching pad identification, launch azimuths, trajectory characteristics, and transmitter frequencies are itemized in Tables 7.1 and 7.2. Coordinates of launching pads and receiver stations are presented in Table 7.3. To enable system gain calculations to be made, antenna arrays used at both receiving stations on both shots are shown in Figs. 7.11 and 7.12. Plots of signal strength versus time of the various received frequencies are reproduced in Figs. 7.13 through 7.24.

Burst time is noted on each curve in the series. Figure 7.13 is a plot of signal strength versus time received at Johnston Island from a 224-mc transmitter missile fired during the Teak rehearsal. Data recorded is typical of the signal expected (with no ionization present) from a Deacon-Arrow missile flying the high-angle trajectory depicted in Fig. 7.10. Superimposed on the actual signal received is a plot of the signal as it would be expected to vary as a result of increasing path attenuation with distance alone.

Variations in phase of the received signals from the low-frequency transmitters are shown in Figs. 7.25 through 7.32. Because of the greater resolution of the phase-measurement circuitry, minute observation of signal variations near receiver noise level can be made.

Low-frequency signal strength records are normalized to the curve of free-space attenuation versus distance and are compared in Figs. 7.33 through 7.36.

TABLE 7.3--STATION LOCATIONS

Station number	Holmes Narver Area Coordinates		Location
	North	East	
3231.01	197,520.78	196,179.85	Launcher Pad
3231.02	197,562.70	196,270.65	Launcher Pad
3231.03	199,072.00	199,492.00	Launcher Pad
3231.04	199,113.91	199,582.79	Launcher Pad
3231.05	199,155.82	199,673.58	Launcher Pad
3231.06	199,197.73	199,764.37	Launcher Pad
3231.07	198,988.18	199,310.42	Launcher Pad
3231.08	199,030.09	199,401.21	Launcher Pad
3230.01	199,715.00	199,670.00	Bldg. T. 249, Rcvr. Sta.
3230.02	231,281.00	374,744.00	Belle Grove Rcvr. Sta., Teak
3230.02	329,429.00	272,650.00	Belle Grove Rcvr. Sta., Orange

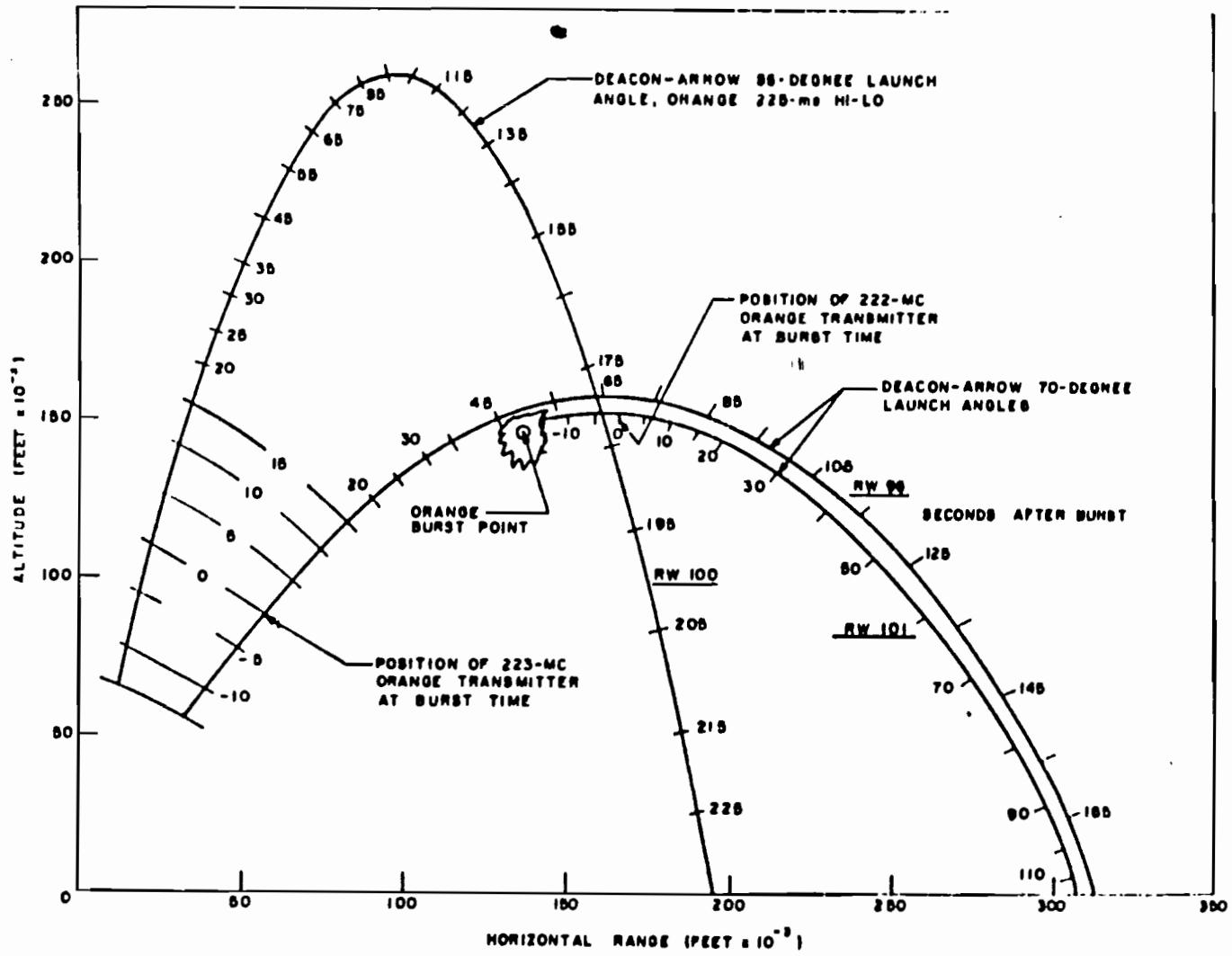

Fig. 7.10--Deacon-Arrow trajectories for Orange Hi-Lo rockets.

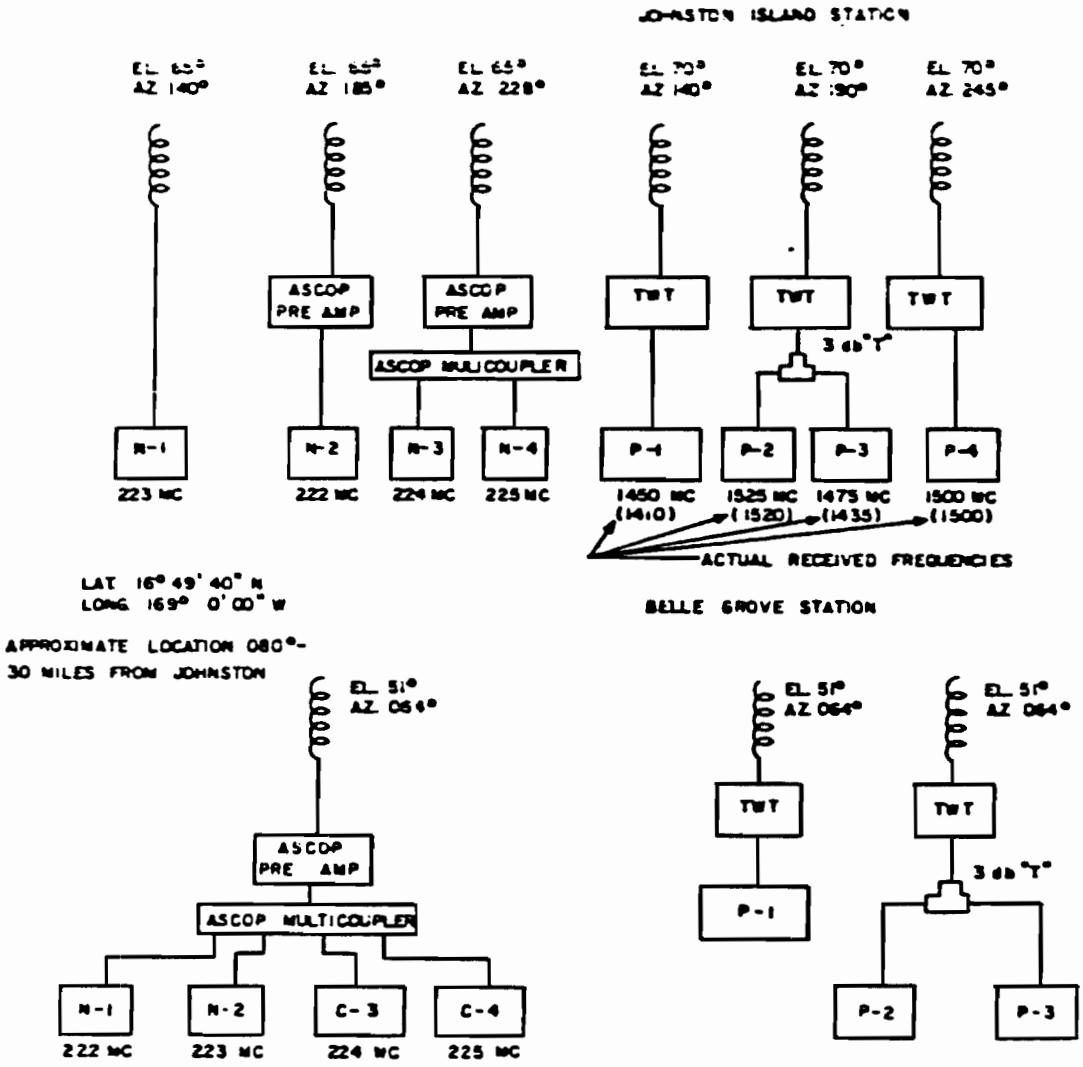

NOTE:
N - NATIONAL 300 RCVR W/CONVERTER
P - POLARAD RCVR
C - NEMS - CLARKE RCVR

Fig. 7.11--Teak antenna array.

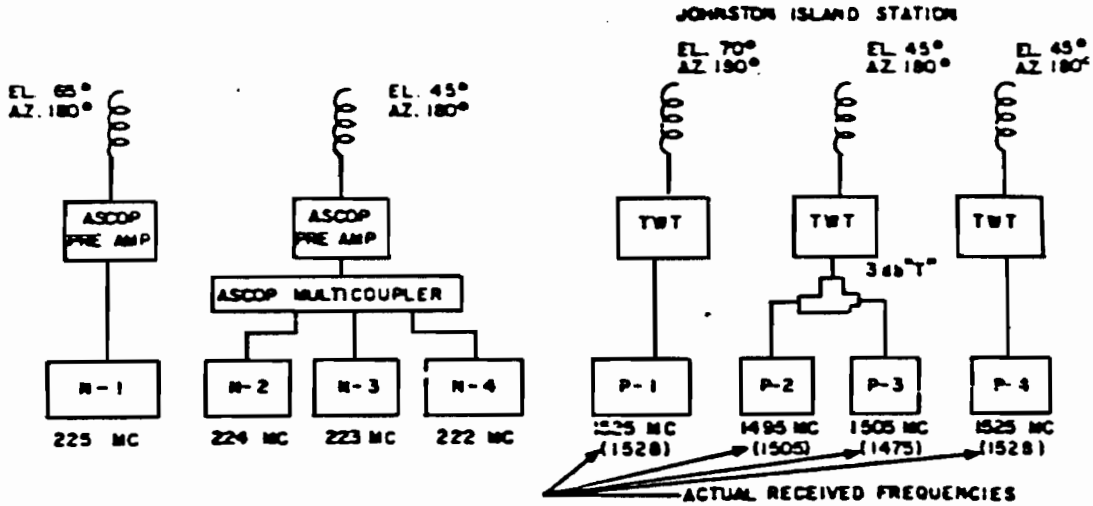

[LAT. 17°05'55" N
LONG. 169° 18' 30" W]

BELLE GROVE STATION

APPROXIMATE LOCATION 030° 25 MILES FROM JOHNSTON

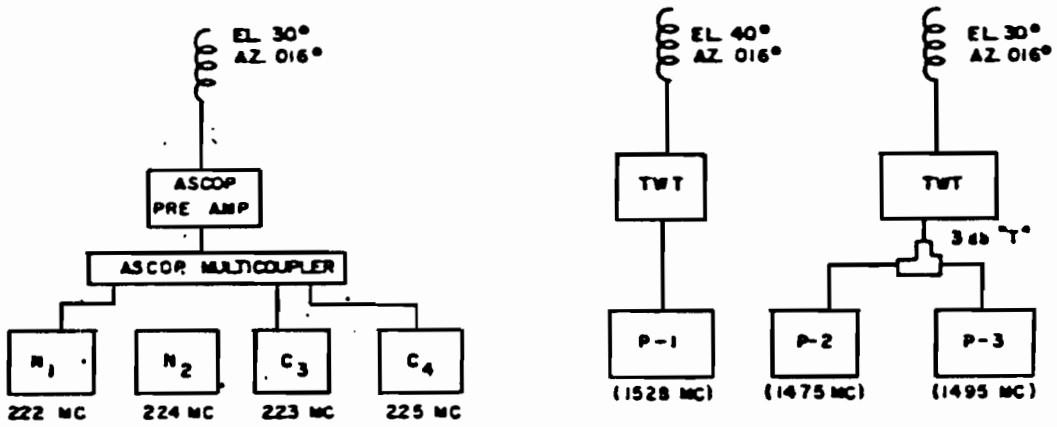

Fig. 7.12--Orange antenna array.

Fig. 7.13--Received signal versus time, pre-Task rehearsal, Johnston Island station, 224 mc, 185-degree azimuth, 86-degree launch elevation.

[redacted]

[redacted]

Pages 239 through 261 are deleted.

[redacted]

Signal strength records of stations TK-209 and TK-252 of Project 32.4 are presented in Figs. 7.37 and 7.38, since the similar frequencies, 233.5 mc and 235.0 mc, and zero-time positions contribute significantly to interpretation of the attenuation data.

Figure 7.39 is a composite plot of horizontal range from ground zero, altitude, and RF signal attenuation versus time of TK-209, TK-252, and the Teak Hi-Lo rockets. Figure 7.40 is a representation of these same data with attenuation at given times tabulated on the flight trajectories. Figure 7.41 is a plot of Orange trajectories with attenuation at given times plotted on the curves.

7.4 CONCLUSIONS

The difficulty of reducing the MIDOT tracking data for the Hi-Lo rockets required that additional test rounds be fired in order to give better theoretical estimates of the trajectories. A series of Deacon-Arrow rockets were fired at Point Arguello, California, early in 1961. These sea level launchings resulted in the trajectories used in Figs. 7.39 and 7.40 and agree well with the attenuation data.

The systems used for this project have accuracies of about 3 db, and data variations within these limits should not be interpreted as significant.

Attenuation due to ionization as a function of time must be determined with regard to rocket position. To arrive at generalizations without entering the physics of ion recombination is somewhat difficult. It appears that the following statements can be made:

[redacted]

*Blackout is defined as receiver noise level, approximately 50 db down from receiver saturation.

[redacted]

Pages 263 through 267 are deleted.

[redacted]

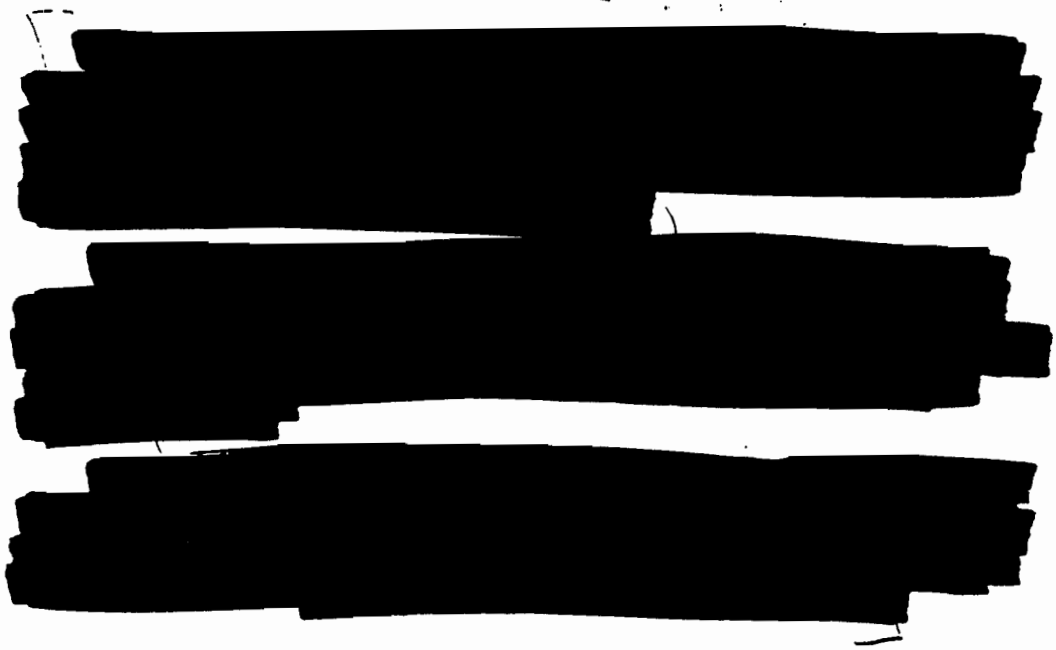

7.5 RECOMMENDATIONS

Recommendations which may be helpful in event future attempts are made at measurements of this kind are as follows:

(1) A carrier-rocket system having an altitude capability sufficient to permit a view through the center of the burst at time of detonation should be used.

(2) A transmitting antenna should be designed and used which radiates uniformly in all directions; extraneous modulation of the carrier would thereby be considerably reduced.

(3) If measurements at frequencies higher than 225 mc are desired, more emphasis should be placed on design of an adequate high-frequency transmitting and receiving system.

(4) Positions of transmitters at burst time, rocket firing sequences, radiating frequencies, receiving antenna patterns--the measurement system as a collective whole--should be optimized to yield maximum usable data versus cost and effort involved.

[redacted]

REFERENCE

1. Pace, T. L., Crawley, T. V., and Hansen, J. W., The MIDOT System, SCDM 76-56(52), Sandia Corporation, December 12, 1956.

Chapter 8

INSTRUMENT CARRIERS

8.1 SAMPLER AND INSTRUMENTATION ROCKETS

8.1.1 Introduction

Instrument carriers for the Teak and Orange events[1] were fin-stabilized, ballistic-type rockets. These vehicles are propelled by solid-fuel rockets from a 24-foot rail launcher. Each diagnostic rocket was launched so as to be in position at its apogee point at time zero. Of the two rad-chem samplers launched for Teak, one was launched so as to be at apogee at zero time, while the second sampler was programmed to pass through air zero 20 seconds after zero time. For Orange, three samplers were programmed to pass through an altitude of 160,000 feet above the burst point at 40, 80, and 90 seconds, respectively, after zero time. A fourth was to pass through 170,000 feet 120 seconds after zero. Trajectory control was achieved by ballasting the carriers and varying launcher elevation and azimuth angles. A total of six instrument carriers and two rad-chem sampler rockets were launched for the Teak event. Four rad-chem samplers and three diagnostic rockets were launched for the Orange event. Teak and Orange instrument locations are shown in Figs. 1.1 and 1.2 and more accurate locations are tabulated in Table 1.1.

8.1.2 Aerodynamics and Design

The aerodynamic configuration (Fig. 8.1) of the vehicles is of two types: a single-stage design which is essentially the same for all carriers used below 80,000 feet, and a two-stage configuration for the high-altitude carriers and rad-chem samplers. The second stage of the latter is identical to the single stage except for a reduction in length of the midsection and the absence of launcher shoes on the second stage. The nose, which houses the instrumentation, is a 3.0-caliber, ogive shape. Geometry of the fins is the same for all stages and is the result of a compromise for simplicity, stability, and aeroelastic requirements.

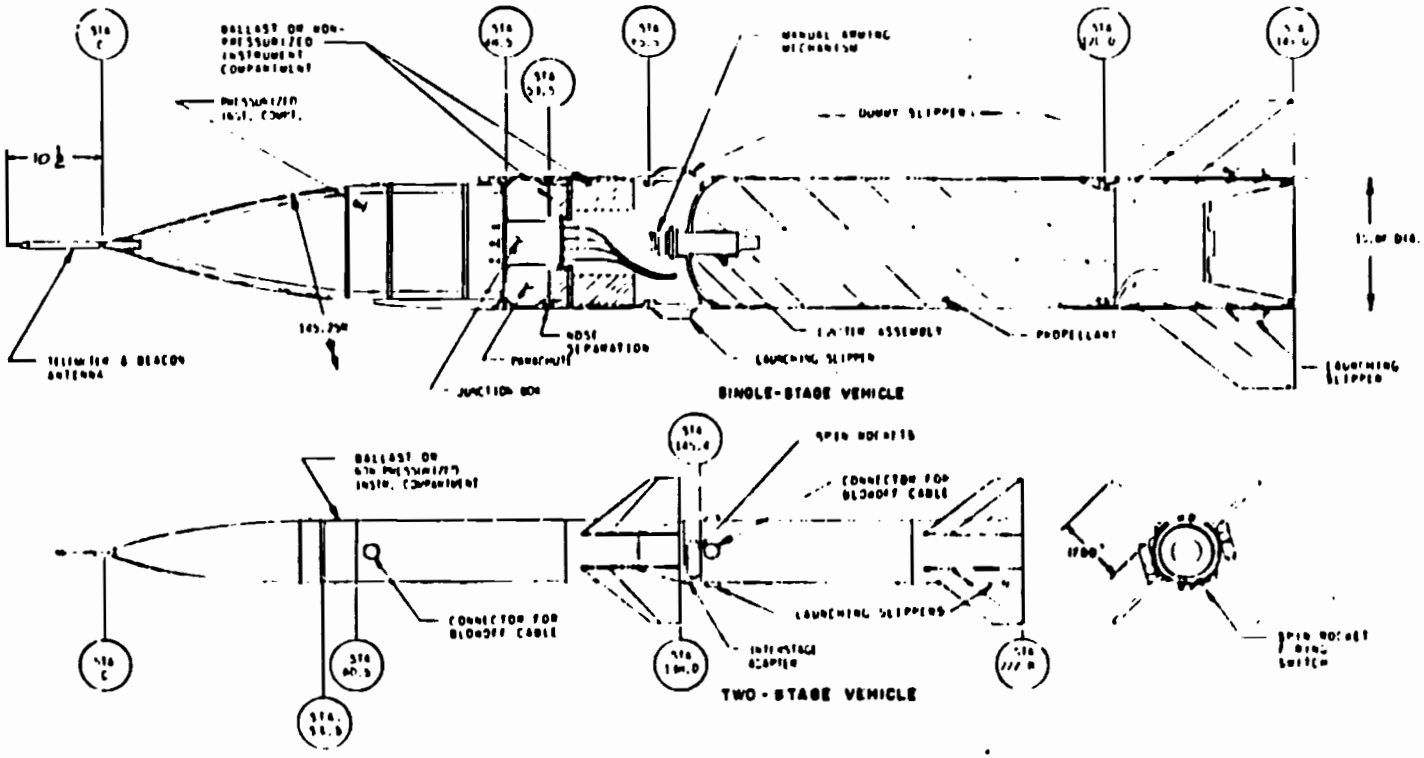

Fig. 8.1--Teak instrument vehicle.

For reasons of design simplicity and logistics, the same engine was used for all stages of the vehicle. A modified LaCrosse engine, TX-52, manufactured by the Thiokol Chemical Corporation, was found to best suit requirements. This engine delivers a total of approximately 50,000 lb/sec impulse and has a burning time of 2.6 seconds. The second-stage units of the two-stage carriers for Orange were fired 15 seconds after launch; those for Tenk were fired 19 seconds after launch. The latter time was selected because it yields a maximum of altitude and minimizes variation of apogee for any deviation in second-stage ignition time. Also, this delay reduces the airloads and aerodynamic heating of the second stage.

The carriers are rotated aerodynamically in order to average out thrust malalignment and trim errors. To accomplish this the fins are mounted at an incidence angle of one-half degree. For the single-stage carriers this produces a roll rate of approximately 6-1/2 revolutions per second at burnout. Two spin rockets are attached to the booster of the two-stage carriers and serve to initiate a roll rate of 2-1/2 revolutions per second immediately beyond the end of the launcher. The second stage reaches a maximum roll rate of 4 revolutions per second at burnout.

Since it was necessary to retrieve a portion of the instrumentation for analysis, a system was provided for recovery of the instrumented noses. The nose is joined to the midsection and motor assembly by a split-ring, clamp-type connector. At a specified time, an electrical impulse fires two squibs which separate the two components. A 12-foot, solid-canopy parachute stowed in the nose is then deployed by a 10-foot static line attached to the midsection bulkhead. The same chute design was utilized in recovery of all the carriers; thus, strength requirements were dictated by the 40,000-foot vehicle. For the single-stage carriers, separation occurs approximately 5 to 15 seconds after apogee. For the two-stage carriers, it is necessary to allow the second stage to descend to a lower altitude where the descent rate after deployment is near sonic speeds or less, yet not so low that the parachute could be overstressed. Therefore, altitudes in the region of 160,000 feet seemed to be the best choice. Descent time of the recovery operation ranges from 11 minutes for the 40,000-foot nose unit to 25 minutes for the sampler nose. Impact velocities are 44 feet per second for the instrumented noses and 32 feet per second for the sampler noses.

[redacted]

8.1.3 Ballistics

A program was devised whereby trajectories for the instrumented carriers are calculated on the IBM 704 EDPM.[2] The program was flexible enough to accommodate both the single- and two-stage carriers and to allow also for changes in vehicle parameters such as weight, impulse, and launching conditions. The same program is used for predicting the trajectory for a given wind structure.

Trajectory calculations are based on equations of motion of the vehicle in a rectangular coordinate system on a nonrotating earth. Since all trajectories are nearly vertical or short-ranged, error resulting from use of rectangular coordinates is small. The effects of Coriolis were computed for theoretical, no-drag trajectories and are added as corrections to the IBM 704 results. A monthly average for atmospheric temperature and density above Johnston Island was used. This was sufficiently accurate, in that the difference in the effect of two extreme atmospheres on the altitude is approximately 2 percent. Drag coefficients were determined from wind-tunnel tests and have been corrected with results obtained from several developmental single-stage firings. The earth's gravity potential is assumed to decrease with altitude from the local value at the surface.

For a given rocket engine, nominal total impulse in the IBM program is corrected by a factor dependent on the propellant weight of the rocket as compared to a nominal propellant weight. Loss in impulse during the boost phase of the two-stage rockets caused by early separation is allowed for, as is also the added impulse of the second stage caused by burning under lower ambient pressure conditions. The mass of the rocket is assumed to decrease linearly during burning. Effects of varying the parameters of weight, launch angle, and impulse are given in Table 8.1.

The effect of winds on the trajectory is attributable mainly to the weather-vaning effect and, to a lesser extent, wind drift. For the calculations, consideration is given to the effect of weather vaning during burning, but drift is neglected. Direction and magnitude of wind vectors at various intervals of altitude are inserted in the IBM program. The major portion of the wind effect for the Johnston Island wind structure was expected to take place in the region just above the surface. In addition, consideration is given to the effect of wind drift on the parachute during the recovery phase of the trajectory.

[redacted]

Page 274 is deleted.

Preliminary trajectories for the carriers were calculated for mean seasonal winds in order to establish initial orientation of the launchers and minimize the amount of final launcher adjustment required 15 hours prior to shot time. The preliminary trajectories also served to ascertain carrier gross weights and firing times. Since winds predominantly affect the range and azimuth of the trajectories, gross weights as calculated originally would still hold after the final computations.

Before each of both Teak and Orange shots, final launcher settings (Table 8.2) were determined from a 24-hour wind forecast. Theoretical trajectories based on these forecasts are shown for Teak and Orange (Figs. 8.2 and 8.3). A summary of predicted apogee positions and sampling points of the diagnostic and sampler rockets are given with respect to zero time (Table 8.3). Actual positions are given in Table 9.1.

8.1.4 Postshot Summary of Performance

Of the six diagnostic carriers launched for Teak, all appear to have performed normally and, with the exception of TK-48 and TK-60, all were recovered. Both rad-chem rockets failed in flight, and no cloud sample was obtained. The exact cause of failure has not been determined; however, it is thought that the second stages became unstable at the end of burning, with associated structural failure of the fins immediately thereafter. Both sampler noses were recovered short of the intended impact points under 30 feet of water.

Trajectories of the Teak and Orange diagnostic rockets as determined from MIDOT records are included in Chapter 9.

Although no cloud samples were gathered by the four rad-chem rockets on Orange, all units, including the diagnostic rounds with the exception of Station OR-115R, appear to have followed their intended trajectories. The units recovered were within 2.5 miles of the expected impact points. Because of the short telemeter time (2 minutes) the 115R unit either failed to separate or the parachute failed at deployment, allowing the unit to sink on impact. Parachute failure would indicate a possible low-apogee altitude.

TABLE 8.2--INSTRUMENT CARRIER AND SAMPLER LAUNCHING SUMMARY

*Final unit designation	Predicted unit designation	Launcher station	Weights		Launch angles		Launch time from zero
			Gross wt. at launch	2nd stage	Elevation	Azimuth	
Teak	Teak						
TK-252	N-45-242	3261.02	1955.2	1047.1	85.02	206.7	-137.2
TK-209	N-34-222	3261.01	2028.0	1124.6	87.35	214.3	-131.6
TK-80	N-35-80	3260.01	1140.5		76.12	197.3	-66.6
TK-59	N-36-60	3260.04	1356.5		72.10	196.4	-57.8
TK-48	N-38-50	3260.06	1306.9		68.17	194.9	-51.4
TK-39	N-37-40	3260.02	1460.9		64.20	194.6	-46.8
	RC-2-APO	3260.03	1799.8	952.4	87.31	215.7	-191.4
	RC-3-251	3260.05	1797.6	946.6	85.90	212.0	-76.2
Orange	Orange						
OR-115R	N-40-125R	3261.02	2404.5	1465.7	78.67	194.3	-98.0
OR-125S	N-46-125S	3261.01	2328.9	1217.2	71.73	208.3	-97.5
OR-72	N-41-80	3260.01	1111.6		77.33	199.5	-66.6
	RC-6-170	3260.03	1919.6	1032.0	73.12	194.6	-39.4
	RC-7-160	3260.02	1907.4	1028.2	72.91	192.7	-19.4
	RC-8-160	3260.06	1915.8	1032.5	72.19	190.4	-40.6
	RC-9-160	3260.04	1911.9	1023.7	71.86	192.2	-1.0

*Final unit designations are used throughout the report with the exception of Chapter 8. These designations are defined as altitude in thousands of feet at burst time as measured by MIDOT.

TABLE 8.3--PREDICTED TRAJECTORY SUMMARY

Predicted unit designation	Time from burst zero	Altitude (feet)	Range (foot)	Bearing from launcher	Scientific grid position North	East
Teak						
Redstone	0	250,616	33,501	187.8	166,840	195,736
N-45-242	+0.3	243,240	61,700	187.9	137,990	191,510
N-34-222	+0.9	222,990	24,720	187.8	164,760	196,740
N-35-80	+0.2	80,170	33,190	187.9	166,500	195,650
N-36-60	+0.2	60,110	33,280	188.1	166,490	195,670
N-38-50	0	49,870	33,350	188.3	166,490	195,690
N-37-40	0	40,100	33,430	188.4	166,490	195,700
RC-2-APG	+0.1	298,680	34,760	193.4	165,790	195,650
RC-3-251	+20.3	250,290	34,730	191.4	165,510	193,970
Orange						
Redstone	0	126,105	122,866	181.3	77,210	197,687
N-40-125R	+0.5	125,930	83,760	180.9	116,550	198,700
N-46-125S	+1.5	128,910	137,750	200.2	79,480	152,540
N-41-80	+0.2	80,820	33,340	188.7	166,450	195,190
RC-6-170	+123.4	171,580	118,820	186.9	81,600	186,360
RC-7-160	+87.4	162,550	110,240	185.2	89,790	190,550
RC-8-160	+37.4	159,570	114,480	183.3	85,220	193,980
RC-9-160	+77.0	160,190	116,710	185.1	83,200	190,050

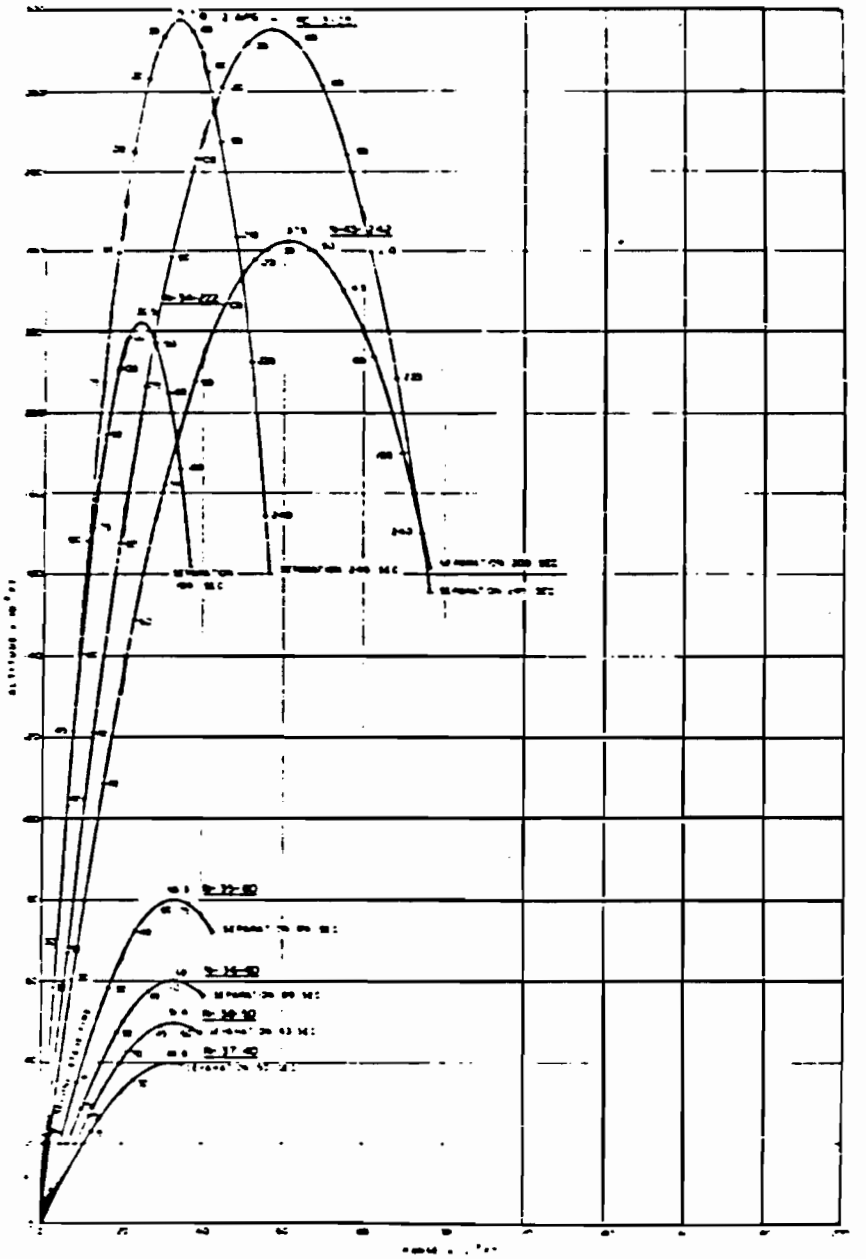

Fig. 8.2--Teak predicted trajectories. See Section 9.3.4 for measured trajectories.

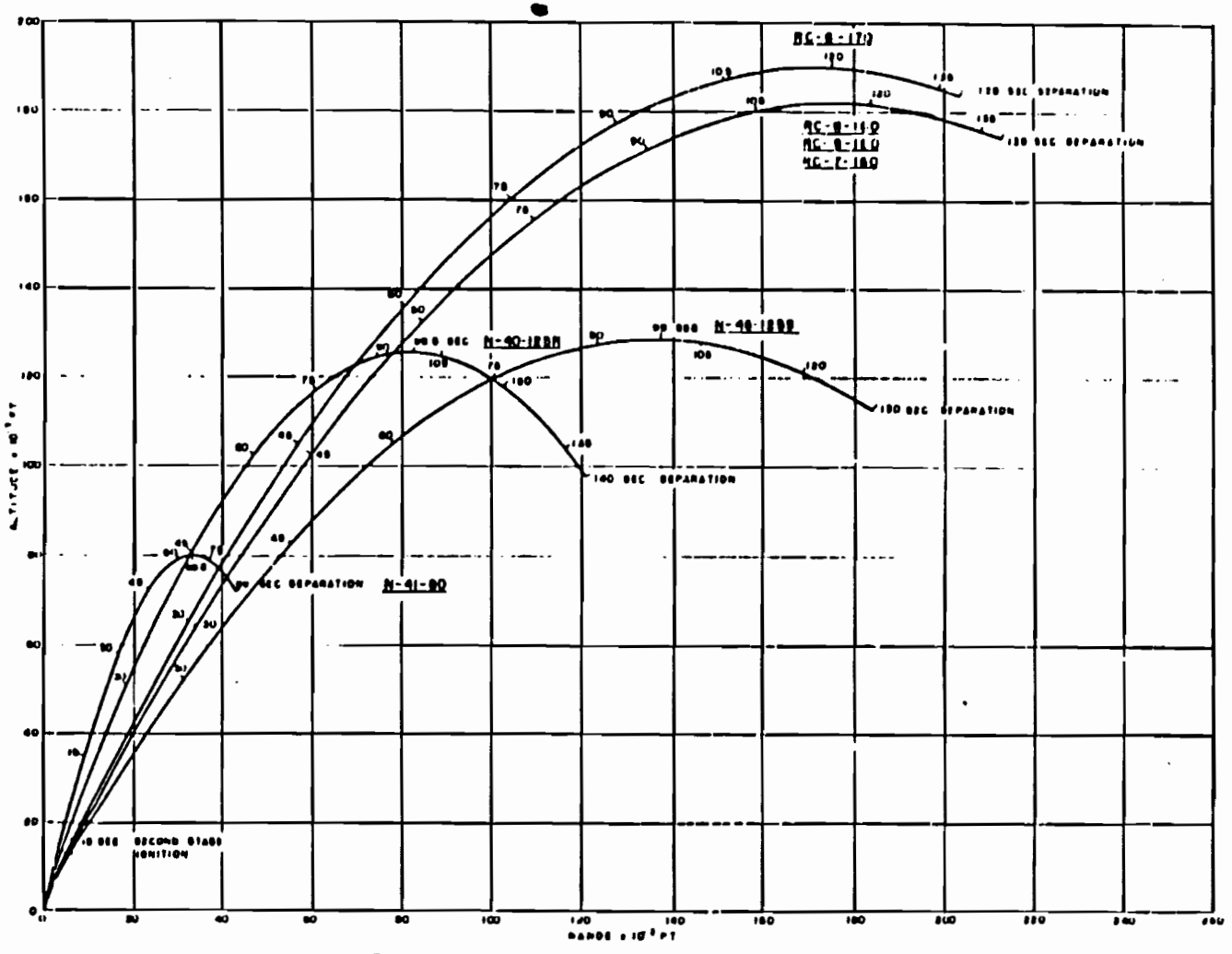

Fig. 8.3--Orange predicted trajectories. See Section 9.3.4 for measured trajectories.

8.2 ENGINEERING AND OPERATION OF SAMPLER AND INSTRUMENTATION ROCKETS

8.2.1 Vehicle Description

Figure 8.1 shows the principal features of both the single- and the two-stage instrument carriers. Both vehicles are 16 inches in diameter. The single-stage vehicle is approximately 153.5 inches long overall. Of this length, payload space is available aft as far as Station 65.5 The two-stage vehicle is approximately 233.3 inches long overall. Payload space is available aft as far as Station 60.5. The single-stage vehicle and the second stage of the two-stage vehicle are each made up of four major assemblies: (1) nose assembly, (2) midsection compartment, (3) rocket engine, and (4) tail assembly.

The recoverable nose assembly, which is identical on both instrumentation vehicles, extends aft as far as Station 53.5 A bulkhead at Station 48.5 makes the instrument compartment ahead of that station pressure tight. The compartment between the pressure bulkhead and Station 53.5 houses parachute, dye-marker containers, and electrical junction box.

The midsection extends from Station 53.5 to Station 65.5 on the single-stage vehicle. On the two-stage carrier it extends only to Station 60.5. This compartment is used for carrying instrumentation, ballast for altitude control, or both. It is not pressurized and is not recoverable. On the single-stage vehicles the midsection compartment is used for carrying ballast only. The rockets with predicted apogees of 222,000 and 242,000 feet (see Fig. 8.2) have X-ray and thermal instrumentation as well as a small amount of ballast mounted in this compartment.

The recoverable nose assembly is held to the midsection by a ring which engages a circumferential groove around each of the two parts. The ring is held together at two diametrically opposite locations by pins which, at the separation signal, are driven out of the ring by pressure squibs. This leaves the ring free to fall away. The ring parts are thrown clear by centrifugal force resulting from the spin of the vehicle, leaving the nose free to fall. Nose separation occurs as a result of aerodynamic and inertial loads. The parachute is deployed by means of a static line which is of sufficient length to assure that the nose is clear of the remainder of the vehicle.

With the exception of modifications made to the case and nozzle to reduce weight and adapt it to this particular application, the TX-52 (see Section 8.1.2)

is identical to the XM10 engine developed for the Army by Thiokol. As a result of this similarity, no development test program was required on the engine itself. The engine unit is 16 inches in diameter, 77.5 inches in length, and weighs approximately 730 pounds. It develops approximately 35,000 pounds of thrust for 2.6 seconds.

A manually operated arm-safe device provides a means of shorting out the electrically operated squibs in the igniter. When in the "safe" position, the ignition unit is also physically blocked off from the main propellant charge so that, even if the igniter were fired, the main propellant charge would not be ignited. The TX-52 engine has a high resistance to all types of adverse environment and, aside from standard procedures for solid fuel propellants, no special precautions are necessary in handling or storage. This, together with the inherent simplicity of the solid fuel engine, made it ideal for this application.

The skirt-fin assembly fits over the engine nozzle and is bolted to a boss on the engine at the aft end of the fuel chamber. The four fins are bolted to the skirt in a manner which permits adjustment of the fin angle anywhere between approximately 1/2 and 1-1/2 degrees to provide the desired roll rate. Fin angle is accurately set by use of a specially designed aligning jig. Since altitude is controlled largely by control of vehicle weight, fins, midsection, and launching slippers may be made of either steel or aluminum, as weight of the configuration requires.

Engine and tail assembly for the booster on the two-stage vehicle are identical to those on both the single-stage vehicle and the second stage. A cone-shaped interstage adapter which fits into the nozzle of the second-stage unit is bolted to the front end of the booster engine. At the high angles of firing necessary to this program, the second stage needed only to be set on the cone-shaped adapter on the booster; no further physical connections between the two stages were required. At burnout of the booster, normal drag separates the two stages. Spin rockets are used on the two-stage vehicles. These rockets are attached to the interstage adapter on the booster and are fired by a switch on the aft end of the booster as it clears the launcher.

8.2.2 Electrical System

The internal electrical system for all carriers consists of two timers, a timer junction box, and three cables. A fourth cable is required in the booster. The external electrical system consists of a jettisonable control cable to each stage of the vehicle, launcher junction box, and remote arming box.

The timers are motor-driven and provide three separate times, adjustable from zero to 220 seconds for the instrument vehicles and from zero to 440 seconds for the sampler vehicles. Normally closed contacts are used in conjunction with a relay in the timer junction box to provide the required fourth time. The timers are mounted on the bulkhead inside the pressurized nose cone on the instrument carriers and in the midsection on the sampler. The timer junction box provides all the circuits between the pressurized nose compartment and the aft sections of the carrier, with facilities for disconnecting these electrical connections at nose separation. Relays and fuses required for timer operation are also enclosed in the box. Connections from the timer junction box to the control cable connector, motor igniter squibs, and aft instrument compartments, when used, are provided by three cables. A fourth cable provides a control cable connector to the booster igniter on all two-stage vehicles.

The control cable providing circuitry from the launcher junction box to the rocket are furnished with a spring-loaded breakaway connector. A small steel cable between the connector and the launcher trips the latch on the connector at first movement of the carrier, allowing the spring to eject the cable. The launcher junction box routes all circuits from the telemetering control box, the EG&G timing relay used to fire the rocket motor, and the 30 VDC external power source to the vehicle via the control cable. The launcher contains the firing relay which provides a firing or safing signal for the motor-igniter and timer-start circuits and a key interlock switch which prevents closing of the firing circuit except from the remote arming box. Also provided are two lights to monitor the timers in the carrier, one light to monitor position of the key interlock switch, and one lamp to indicate safe condition of the EG&G timing relay.

The remote arming box is located a minimum of 800 feet from the nearest vehicle and is connected to the launcher junction box by a four-conductor shielded cable. The key from the key switch in the launcher junction box is

installed in the key switch on the remote arming box. It is operated to close the circuit to the fire relay after it is determined that the safe lamp on the remote arming box indicates that the EG&G timing relay is open. A ready lamp indicates that the key switch is operating. Closure of the EG&G timing relay will fire the carriers.

8.2.3 Handling Equipment

The following six items of specialized handling equipment are required:

(1) A castered assembly dolly which holds the engine while the nose and tail assemblies on the interstage adapter are attached.

(2) A strongback for lifting the engine unit from its shipping container onto the assembly dolly.

(3) A nose-assembly stand to facilitate assembly and checkout of the nose.

(4) A strongback assembly for lifting the nose assembly and holding it in position for attachment to the rest of the vehicle.

(5) A strongback for handling the midsection. (Although this section is relatively small and is normally handled by hand, when fully ballasted for the 40,000-foot station, it weighs several hundred pounds.)

(6) A strongback for loading the assembled vehicles on the launcher. This equipment has the capability of picking up the vehicle from a horizontal position and rotating it to a near-vertical position for loading onto the launcher.

The handling equipment is used in conjunction with any commercial crane with a boom of approximate 30-foot length and 5000-pound capacity. All assembly, with the exception of installation of the spin rockets, is done on the ground before installation on the launcher. In the assembly of the two-stage vehicles, the assembled booster is loaded onto the launcher, and the assembled second stage is then placed on top of the booster. For safety reasons, the spin rockets are not installed until both stages have been loaded onto the launcher.

8.2.4 Test Equipment

A PT-80 tester is used in the laboratory to hi-pot and check continuity of all circuits in the timer junction box and all cables. In the field a timer tester is used to check timer setting, reset timers, and simultaneously

check all timing circuits in the timer junction box. A firing-set tester, which simulates the vehicle, and an EG&G telemetering simulator are used to check operation and circuitry of the external electrical system.

8.2.5 Launcher

Figure 8.4 shows a launcher with a two-stage vehicle, loaded and ready for firing. The launcher has a single rail to provide 24 feet of guided travel. Two launching slippers are used. Figure 8.1 shows location of the launching slippers on the vehicles. Depending on the altitude desired, the slippers either remain on the vehicle or are jettisoned at the end of the launcher. If they are left on the vehicle, identical slippers are attached diametrically opposite to provide aerodynamic and static balance. Track and slippers are so designed that the front slipper leaves the rail at the same time as the rear one. The same launcher may be used for either vehicle.

The guidance rail is supported, for rigidity, on a structural member. The rail assembly is supported at the lower end of the triangular base of the launcher, at the center, and at the upper end by two sets of legs. Elevation adjustment is made by changing the length of the support legs and by the addition of a fine-adjustment screw built into the base. Azimuth adjustment is made by pivoting the launcher base from left ro right. The structure is mounted on and is tied down to concrete pads at the corners of the base. A modification of this launcher uses steel tubing in place of fabricated legs and rail support.

Aiming of the launcher with respect to a known base line is accomplished by use of an inclinometer to set the elevation angle and by an engineering transit used in conjunction with a mirror system mounted on the rail to set the azimuth. Once the launcher has been aimed at a certain point, last minute changes to correct for winds can be quickly and easily made.

8.2.6 Operational Aspects

Preparation for firing the instrument carriers consists of three separate phases: (1) preparation of the launching sites, (2) erection of the launchers, and (3) preparation of the vehicles for firing.

Preparation of the launching site included the laying of electrical cable and the pouring of concrete pads on which the launchers are set. Pouring of

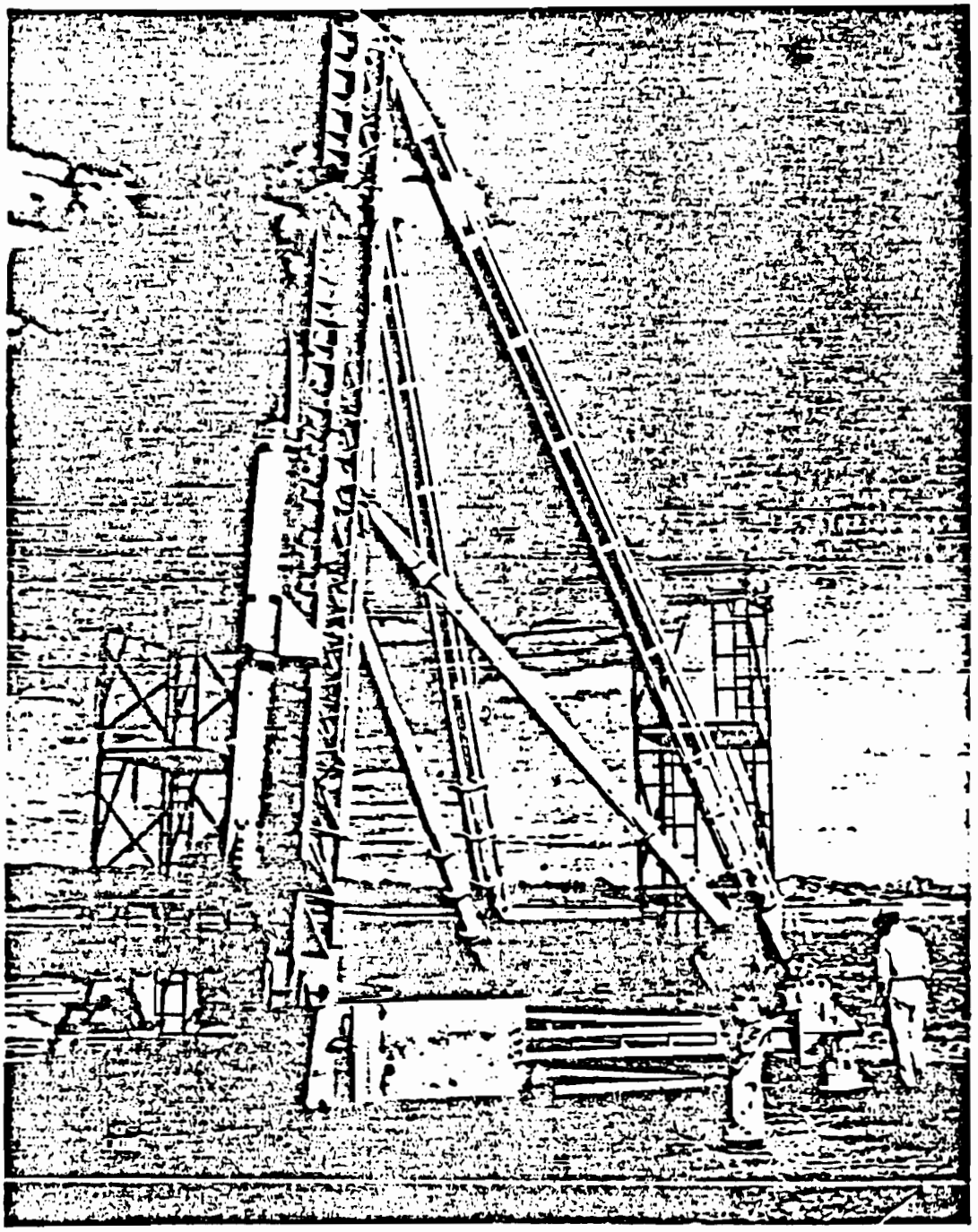

Fig. 3.---Two-stage rocket and launcher.

the pads was done several weeks in advance of launcher erection to permit the concrete to obtain sufficient strength. Locations of launcher stations are given in Table 8.4.

Preparation of the launchers included necessary preassembly, erection, and preliminary alignment. For preassembly and erection purposes, a crew of five men took approximately two days per launcher. In addition to standard hand tools, a crane of approximately 40-foot boom length and 10,000-pound capacity, and a second, smaller crane or boom truck were required. After erection was completed, several hours were required to set azimuth and elevation angles.

Preparation of the vehicles for firing, after instrumentation has been checked out, consists of assemblying major subassemblies, described in Section 8.2.1, into the ready vehicle, loading onto the launcher, final checkout, and final launcher alignment. A four-man crew requires one to two days to prepare a vehicle for firing. During the assembly period, suitable protection from rain and blowing sand and dust is required. After the vehicles are assembled and loaded on the launchers, they must remain for extended periods at temperatures up to 120 degrees Fahrenheit with no protection other than waterproof tape over open joints and ports. Tape must be removed before firing. Launchers and vehicles are painted white to minimize radiation temperature effects and as a protection against environment.

Final preparation for firing consists of removal of protective tape, manual arming of the rocket engines, and electrical arming of launching circuits. This requires only minutes, and final preparation time may be extended to several hours, provided elevation and/or azimuth adjustments are required.

8.3 PERFORMANCE OF RF ATTENUATION AND CHAFF ROCKETS

A rocket system capable of carrying either chaff or a transmitter to high altitudes was developed for use in conjunction with the Teak shot. The purpose of the chaff system was to measure winds at burst altitude. The transmitter configuration, designated as Hi-Lo, was designed to measure attenuation of radiofrequency waves caused by ionization accompanying the burst. A complete series of rounds was available for use as a backup on Teak. When these were not required for the intended purpose, a decision was made in the field to expend them on Orange. The system was flexible enough to adapt to Orange

[redacted]

TABLE 6.4--LAUNCHING LOCATIONS

Station	Scientific Grid Position	
	North	East
(Redstone Pad)6001	200,040	200,500
3261.02	199,290	199,964
3261.01	199,347	200,108
3260.01	199,404	200,231
3260.04	199,461	200,355
3260.06	199,518	200,478
3260.02	199,575	200,602
3260.03	199,632	200,725
3260.05	199,689	200,849

[redacted]

burst, and the participation there was similar to that on Teak. Two different rocket vehicles were actually used: the Deacon-Arrow was the primary system, and the higher performance but relatively unproven Viper-Arrow was the second vehicle. These rocket systems have been described in detail in other reports.[3,4,5] Since design information is of secondary importance to the information presented here, it will not be repeated. Discussion of performance will be oriented toward (1) the performance as it influences analysis of the data, and (2) a brief comparison of predicted and actual performances.

8.3.1 Chaff Rocket Performance

Chaff was ejected at the desired altitude and required wind data were obtained from each of the twenty rounds launched at Johnston Island. One point may be noted in retrospect: while the apogee altitude and, consequently, the upper or ballistic portion of the trajectory was estimated correctly, parameters which were used to obtain the trajectory were in error. First-stage burnout velocity, although underestimated, had been compensated by underestimation of second-stage drag coefficient. Wind data which were obtained are presented and discussed in Section 5.3.

8.3.2 Hi-Lo Rocket Performance

Estimating performance of the Hi-Lo rockets proved to be the most difficult problem encountered on this phase of the program. Because of late entry of the Hi-Lo project into the program, the MIDOT tracking system was not equipped to track these additional units. Enough equipment was added to MIDOT, however, to permit tracking of two of the eight Hi-Lo rounds. It was then anticipated that the two known trajectories would be combined with the theoretical performance parameters and used to estimate probable trajectories of the untracked units. For reasons which will be discussed later, MIDOT trajectories were obtained on only one round each for both the Teak and Orange shots. Estimates were then made as planned of trajectories of the untracked vehicles.

8.3.3 Trajectory Analysis

During the year and a half following the bursts, as attempts were made to analyze the radio-frequency attenuation data, it became apparent that some

rather serious discrepancies existed between the trajectories, both theoretical and measured (MIDOT), and the observed attenuation. In addition, neither the Teak trajectory (maximum altitude) nor the Orange trajectory (maximum range), as determined from MIDOT, agreed with their respective theoretical nominal trajectories. In the intervening time interval, the rocket system had been adopted by other programs, and thus considerable information and experience, including three wind tunnel tests, with the system had subsequently been acquired. Consequently, in early 1960, this information was used to re-estimate the most probable trajectories of the untracked units. However, in terms of application in the attenuation analysis, results were qualitatively similar to those of previous estimates. Also, discrepancies still existed between theory and the two measured trajectories.

By March, 1960, it was decided that a larger effort should be directed toward resolution of these discrepancies. A program was initiated for this purpose.* The program was essentially a two-pronged attack on the problem; specifically, both analytical and experimental approaches were planned. The analytical approach was an analysis of the various factors which determine a trajectory. It attempted to evaluate both the relative influences of the various parameters and the accuracy with which each was known. Work done prior to the Teak shot had verified that the trajectory computational technique yielded sufficiently accurate results. The experimental approach has been outlined.[4] It involved fabrication of eight rounds which were as identical as possible to the original Hi-Lo vehicles. They were to be tracked as they flew over trajectories similar to the Teak and Orange flights. These vehicles were launched at Point Arguello, California, in early July, 1960. It should be noted here that, although a considerable number of Deacon-Arrow rounds had been flown by this time, the configurations had differed from that of the Hi-Lo and the shots had been fired from Tonopah, Nevada, which has an elevation of 5300 feet MSL. Thus, to use information obtained from the Tonopah rounds, it was necessary to normalize the data. Such normalization required use of parameters which were themselves being questioned. It was in order to eliminate this normalization that the eight rounds duplicated the original Hi-Lo rounds and were flown from sea level.

*Funding for the trajectory analysis program was made available by DASA through interagency cost reimbursement, Order Number ET Hi-Lo Nr. 1, dated July 12, 1960.

The program to resolve the discrepancies is nearly complete. The accuracy and degree of confidence which can be attached to the final estimates of the Texas and Orange Hi-Lo trajectories is considerably better than was anticipated at the time of the high-altitude shots. Results of this trajectory analysis program will be reported separately[6] and will therefore only be summarized here. Final trajectory estimates are included at the end of this section.

6.3.4 Time of Flight and Maximum Altitude

One extremely significant and basic fact was brought out by the trajectory analysis which greatly improves confidence in the altitude-versus-time history of the rockets. This is the most critical trajectory parameter for attenuation studies. Specifically, it was noted that the total time of flight of a vehicle was related to the maximum altitude reached by that vehicle. The relationship was of the form $h = A e^{Bt}$, where h is maximum altitude, A and B are constants, and t is total time of flight. Thus, once A and B were determined, only t was required to evaluate h. Fortunately, the recorded Hi-Lo attenuation data were in the form of received signal strength versus time and, consequently, total time of flight could be determined from the signal cutoff. The importance of this relationship cannot be overemphasized. For example, two vehicles will have nearly identical total times of flight even though one vehicle is launched vertically but attains only a relatively low altitude because of poor rocket motor performance, while the second vehicle is launched over a low, flat trajectory to the same maximum altitude with normal rocket motor performance.

Another way to present this relationship is to state that vertical motion is independent of horizontal motion. Although this statement is valid for flight in a vacuum, that it might also be true in the presence of an atmosphere is far from obvious. To the contrary, it can be shown that, with the action of drag as a factor, horizontal and vertical motions are actually interdependent. If a coasting portion of the trajectory is considered, during which drag is significant, the equation for the vertical motion is:

$$\frac{dV_Z}{dt} = -\frac{\rho C_D S V^2 S}{2W} \sin \theta - g ,$$

where V_Z is the vertical velocity component, dV_Z/dt is vertical acceleration, g is the acceleration of gravity, C_D is the drag coefficient, ρ is atmospheric density, S is the drag reference area, V is total velocity magnitude, W is vehicle weight, and θ is the angle between the vehicle longitudinal axis and the horizontal plane. For a rocket vehicle such as the one under consideration which has adequate static stability, it is reasonable to assume that if aerodynamic forces are large enough that the drag is significant, they are also large enough to hold the vehicle at zero angle of attack. Thus drag will be the only aerodynamic force acting. This implies than $\sin\theta = V_Z/V$. By substituting this in the above equation, the relation becomes:

$$-\frac{dV_Z}{dt} = (g\rho)\left(\frac{S}{2W}\right) C_D V_Z V + g .$$

Note that g and ρ are functions of altitude, or Z, only; $\left(\frac{S}{2W}\right)$ is constant during coasting flight; C_D is a function of Mach number which is, in turn, a function of ambient temperature (again a function of Z) and velocity; velocity is obviously a function of both the horizontal and vertical velocity components. From this, it appears that vertical motion is coupled to horizontal motion by C_D and V.

Both theoretical and actual trajectories indicate that these motions are approximately independent. Obviously the product $(C_D V)$ is either constant or a function of Z only. A typical drag coefficient curve is shown at the right. In the region above Mach 1, the drag coefficient is proportional to 1/M. The Mach number is defined by the following expression:

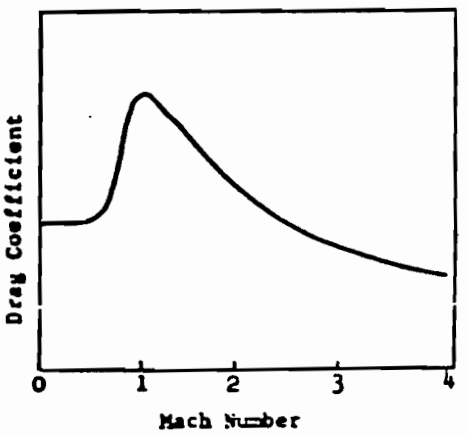

$$M = \frac{V}{49.02\sqrt{T}} ,$$

where T is ambient temperature in degrees Rankine and V is velocity in feet per second. This temperature is again a function only of altitude. Thus the drag coefficient may be approximated as the product of a function of altitude and the reciprocal of the velocity between Mach numbers

of 1 and 5. Another significant point is that most of the flight in the sensible atmosphere occurs at Mach numbers between 1 and 5. It is primarily the accuracy of this approximation which determines the accuracy of the time-of-flight technique. However, because of the number and nonlinearity of the variables which determine trajectory, no simple step exists for going from the known accuracy of the above approximation to an estimation of the accuracy of the technique in terms of effect on the trajectory. The major effort of the trajectory analysis was devoted to estimating this over-all accuracy.

The thrust phases of a trajectory are included by considering only that they change the horizontal and vertical velocity components, and that the magnitude of these changes is independent of the value of the velocity components. Although not in reality correct, this statement may conveniently be assumed to be valid by neglecting drag during thrusting and using a pseudo thrust that will yield desired velocity changes. This approach is used for analysis only, not for trajectory computations.

6.3.5 Trajectory Computation

Until this time, the effort had been devoted only to the untracked vehicles, since trajectories of the two tracked vehicles were assumed to be known. However, application of the time-of-flight technique to the two tracked vehicles indicated that these trajectories were seriously in error. At the time of the move to Johnston Island, it was realized that local geography did not permit installation of a satisfactory MIDOT system. Although some doubts were raised at the time about the performance of MIDOT under the restricted geometry, there was little choice but to use it. The system was used to track the main carrier so that it could be correlated with DOVAP (Doppler determination of velocity and position), which was the primary tracking system for the main carrier. In this correlation, MIDOT compared very favorably with DOVAP. The MIDOT trajectories obtained on fifteen of the Doorknob vehicles also looked very good when compared with theoretical trajectories. (There was a discrepancy on the sixteenth round which has subsequently been resolved.) It was primarily for these reasons that MIDOT had never been questioned on Hi-Lo. However, there was a basic difference between the Hi-Lo vehicles and the other rockets: the other units had a much better antenna pattern than did the Hi-Lo units. The poor antenna pattern combined

with the relatively high roll rate of the Hi-Lo's resulted in a roll modulation on the MIDOT records; false nulls caused by this roll modulation were often difficult to distinguish from true nulls. The altitude-time-of-flight relationship on the two MIDOT trajectories is so far out of line with both the theoretical and the experimental relationships that it appears impossible that they are correct.

The approach which was used to obtain final trajectories presented here was to compute trajectories using known Teak and Orange meteorological conditions and launcher settings, together with the present best estimate of drag coefficient and nominal rocket impulse values. Teak and Orange Hi-Lo trajectory estimates are shown in Figs. 8.5 through 8.8. Impact times were then adjusted to the observed value by varying second-stage impulse. Analysis has indicated that only minor altitude differences result from the various possible techniques for controlling impact time. Horizontal motion (Figs. 8.6 and 8.8) resulting from this approach is that which would result for no dispersion, since no data are available on actual horizontal positions. Dispersion is essentially a cone, centered about the nominal trajectory; consequently, horizontal motion limits can be determined by adding the sigma or 2-sigma dispersion angle (dispersion cone half-angle) to the launch angle in the desired direction and readjusting the impact time. Dispersion limits for this vehicle are approximately 3 degrees at the 1-sigma level and 5 degrees at the 2-sigma level. These trajectories have not been run, since the total number of runs involved would be rather large. Limits on horizontal motion can be determined easily if the sigma level and direction are specified. The trajectory analysis, to be published, will describe the technique in detail.[6]

Accuracy limits on the vertical motion have not been completely estimated. However, they are expected to be very close to ± 5000 feet for a 50-percent confidence and ± 10,000 feet for a 90-percent confidence. (These numbers refer to variation in apogee altitude.) Three techniques were finally available for computing the apogee altitude of the series at Point Arguello: (1) experimental (MIDOT was again employed, although the geometry of the setup was very good this time), (2) time of flight, and (3) theoretical. The theoretical technique is basically independent of the experimental approach. Point Arguello results essentially verified the input parameters and were not used to derive them. From the scatter of the altitude points obtained from each

[redacted]

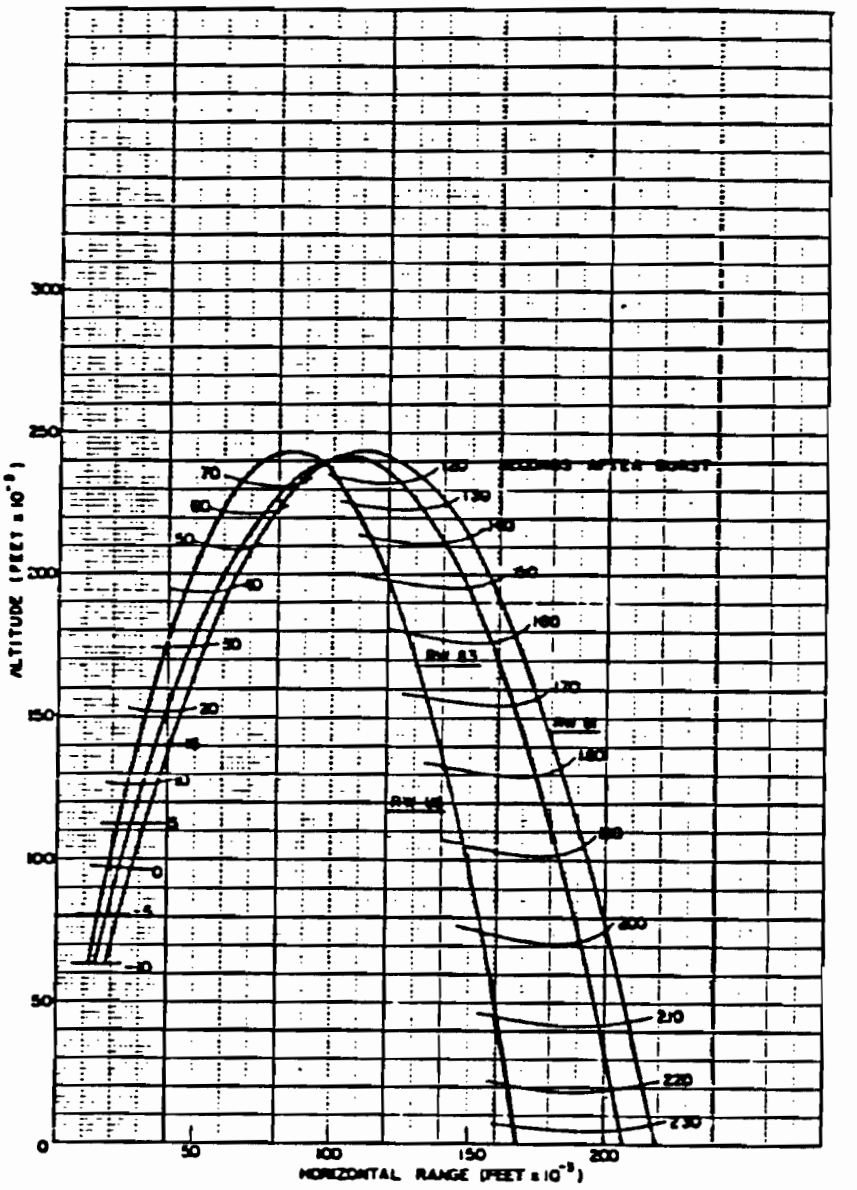

Fig. 6.5--Teak Hi-Lo trajectories. It should be noted that horizontal range is from the main launch pad. Launch time was programmed for +40 seconds from burst. RW01 impact time was 276.99 seconds after Hi-Lo launch; RW03 and RW05 impact times were 276.00 and 276.76 seconds, respectively, after Hi-Lo launch.

[redacted]

Fig. 8.6--Tusk III-Lo trajectories. Origin is at the main launch pad. Launch time was programmed for -40 seconds from burst.

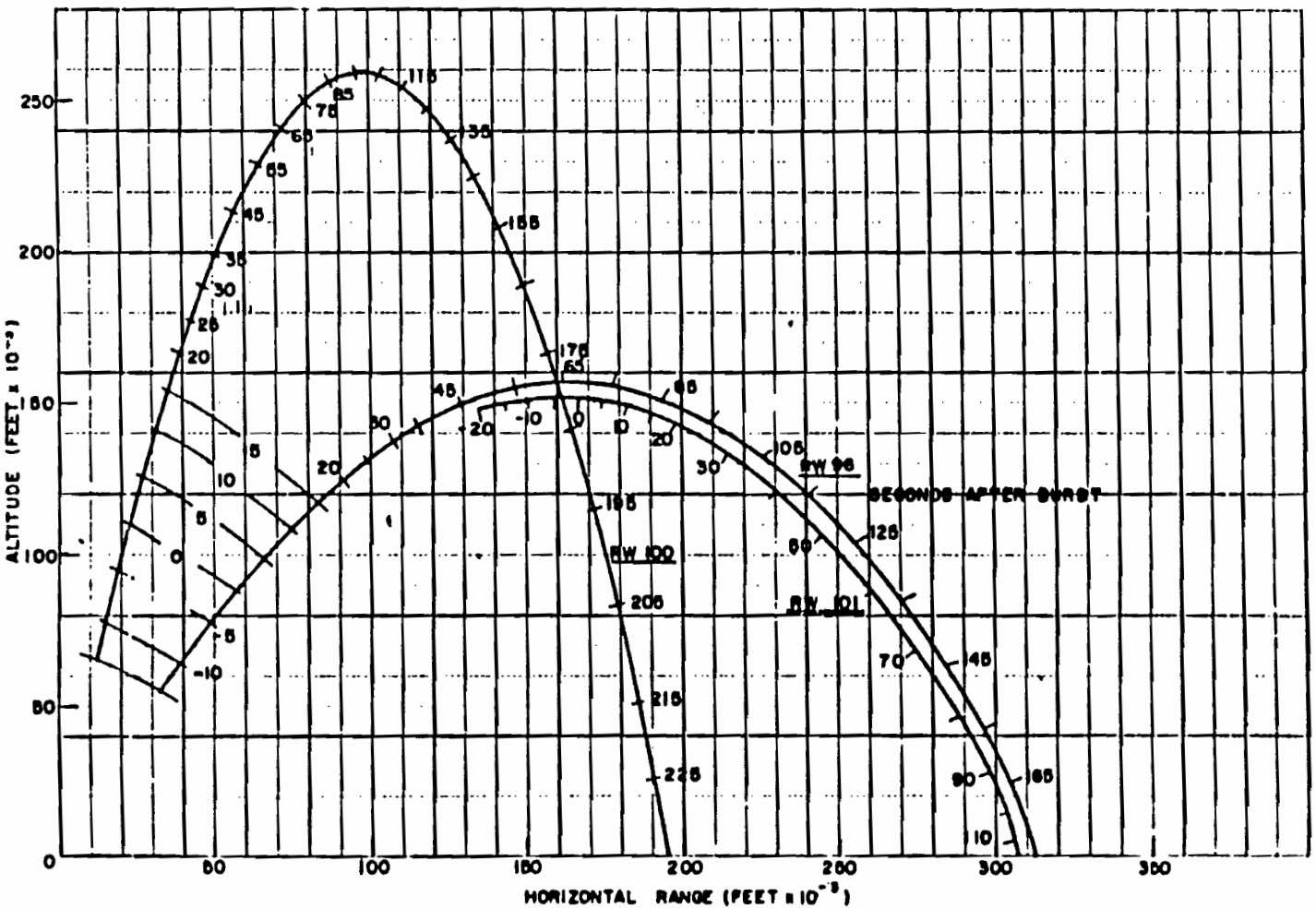

Fig. 8.7--Orange III-to trajectories. Horizontal range is from the main launch pad. RW 98 impact time was 330.99 seconds after III-to launch; RW 100 and RW 101 impact times were 330.16 and 328.01 seconds, respectively, after III-to launch. Also, it should be noted that launch time for both RW 98 and RW 100 was 63 seconds before burst; launch time for RW 101 was 110 seconds before burst.

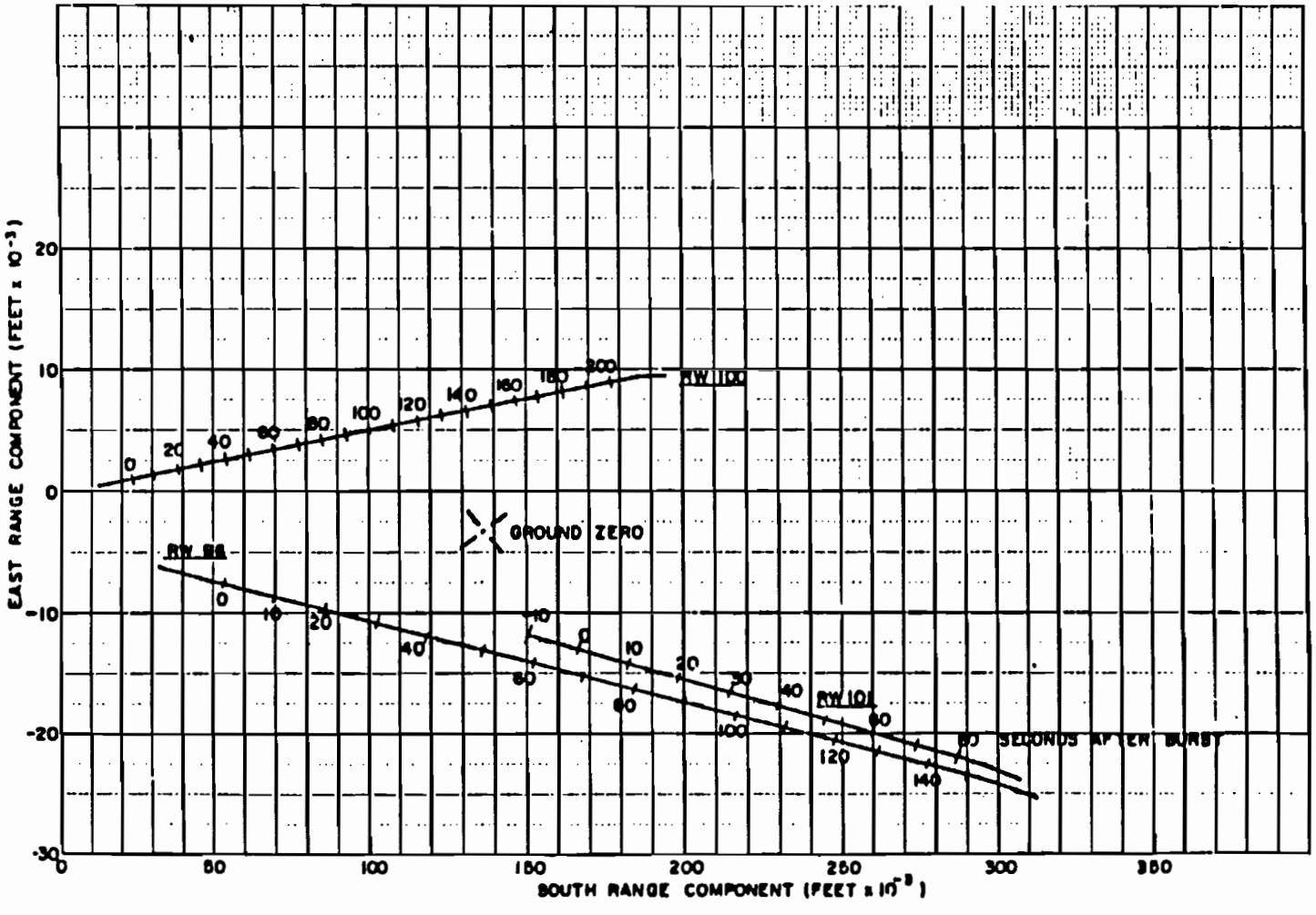

Fig. 8.8--Orange III-Lo trajectories. Origin is at the main launch pad. Note that the east component scale is greatly expanded relative to the south component scale.

of the three techniques, it appeared that the error of each was comparable to the errors of the other two methods. Errors in the theoretical technique are not errors in computation, but rather, uncertainties in input data. In other words, it now appears that the time-of-flight technique will yield as accurate a vertical position-time history as will MDOT for this rocket configuration. Apogee altitudes of the six Johnston Island Hi-Lo rounds of major interest, as determined by the three methods, are compared in Table 8.5.

TABLE 8.5--APOGEE ALTITUDES*

RW	Empirical (feet)	Theoretical (feet)	MDOT (feet)
81	242,300	243,680	--
83	240,100	241,700	215,000
85	242,300	243,460	--
96	158,700	156,720	--
100	258,400	258,950	--
101	154,400	151,780	196,000

*Johnston Island Hi-Lo rounds.

8.3.6 Rocket System Evaluation

The performance of the rocket system was lower than that originally estimated. The primary reason was underestimation of the second-stage drag coefficient. Specifically, the apogee altitude for a nominal vehicle flown on a Teak-type trajectory dropped from a preshot estimate of 272,000 feet to a final value of 250,000 feet. However, the concept of a nominal trajectory, which had been heavily relied on in the first postshot analysis, lost its significance with the discovery of the time-of-flight relationship. Six Deacon-Arrows were launched on Teak and all flew normally. Two Viper-Arrows were also flown in an attempt to attain more altitude; however, these units both failed aeroelastically shortly after launch. An earlier Viper-Arrow flown on a Teak dry run at Johnston had been successful, and it was subsequently determined that the Viper-Arrow was marginal aeroelastically and that the probable success rate was only 50 percent. One of these Viper units was one of the two vehicles tracked by MDOT, which accounts for the fact

that only one Hi-Lo trajectory was obtained on Teak. Seven Deacon-Arrows were flown on Orange; an eighth unit was ready but could not be launched because of drift in the transmitter frequency. Six of these Deacon-Arrows flew normally; the second stage failed to ignite on the seventh round. Unfortunately, this round, which was the only failure among the 35 Deacon-Arrows flown from Johnston, was one of the two rounds being tracked by MIDOT for Orange. In summary, it appears that (1) the Deacon-Arrow units flew normally, but the nominal altitude performance was about 6 percent below presbot estimates, (2) the Viper-Arrow system was unsatisfactory because of an aeroelastic weakness in the design, and (3) it is possible to make a satisfactory postshot estimate of a given trajectory by using only the total time of flight and the launch conditions.

REFERENCES

1. Design and Planning Status of Program Doorknob, SC-4103(M), Sandia Corporation, Albuquerque, New Mexico, June 15, 1957.
2. Ortega, J. M., An IBM-704 Program for Calculating Theoretical Rocket Trajectories, SCTM 117-58(51), Sandia Corporation, Albuquerque, New Mexico, May 6, 1958.
3. Force, C. T., and Walker, W. E., Design Characteristics and Performance of Sandia's Deacon-Arrow Chaff-Rocket System, SC-4229(TR), Sandia Corporation, Albuquerque, New Mexico, November 1958.
4. Force, C. T., Range Safety Considerations of the Deacon-Arrow Sounding Rocket, SC-4513(RR), Sandia Corporation, January 1961.
5. Force, C. T., Sandia's D-A and V-A Sounding Rockets, Astronautics, July 1961.
6. Force, C. T., The Final Trajectory Analysis of the Hi-Lo Rocket Program, SC-4677(TR), Sandia Corporation, to be published.

[redacted]

Chapter 9

RADIO-FREQUENCY SYSTEMS

9.1 INTRODUCTION

Principal aims of the radio-frequency (RF) measurements program were threefold: (1) to prove the feasibility of a modification of the Sandia-developed, 4000-mc high-resolution telemetering system to obtain diagnostic information on tests at very high altitude; (2) to determine relative positions of the Redstone missile and the Sandia instrumentation rockets at burst time; (3) to transmit data gathered in the Redstone and in the instrumentation rockets to ground recording stations; and (4) to record RF signal strength from the instrument carriers to supplement Project 32.3 RF attenuation data.

To accomplish these objectives the following three separate subprojects were organized: (1) high-resolution telemetry, (2) positioning system, and (3) FM-FM telemetry. Equipment, operations, and results of the systems evolved are discussed.

9.2 HIGH-RESOLUTION TELEMETRY SYSTEM

9.2.1 Design Criteria

In order to proof-test the 4000-mc system for rocket-borne nuclear shots, it was proposed to make quantitative measurements of early alpha (number of e-fold increases in fission reactions per unit time in the primary of the warhead) and transit time (time between fire signal and start of the chain reaction) of the warhead used in the Teak and Orange events. Conditions affecting choice and design of equipment were determined as follows:

[redacted]

(3) Line-of-sight range from the test vehicle to the ground receiving station was expected to be approximately 50 miles.

[redacted]

[redacted]

(4) Position accuracies of the Redstone delivery system were predicted to be:

(a) Burst point range error = ± 1300 feet

(b) Burst point altitude error = ± 1000 feet

(c) Burst point azimuth error = ± 350 feet

(d) Pitch and yaw error of Redstone = ± 1 degree

(e) Roll error of Redstone = ± 5 degrees

(5) Permissible size of the transmission equipment was limited to a volume of about 8000 cubic inches in the Redstone.

(6) System weight should be less than 350 pounds.

(7) Time from initiation of design of transmission equipment to final use was approximately one year.

Other less well-defined and less tangible requirements affected design of the RF equipment for Hardtack. Development costs had of course to be held to a minimum. To avoid loss of control of the development schedule, development of any major portion of the equipment could not be contracted to a supplier. The desire to use a minimum number of people in development and operations tended to restrict development work to equipment with which available personnel were familiar.

9.2.2 Description of System

In the following description a signal is traced from its origin in the detector through the system to the transmitting antenna as outlined in the block diagram of Fig. 9.1. A complete technical description of the system has been given by Brumley and Schultheis.[1]

Gamma radiation generated by the exploding bomb enters the detector case [redacted] causes fluorescence of the plastic fluor inside. This fluorescense is detected by two photomultipliers and one photodiode mounted within the fluor. The threshold levels of these tubes are so adjusted that the ratio of light input necessary for initiation of conduction of the successive stages is 1000 to 1. The outputs of these tubes are sent to the modulating circuitry where they are differentiated and sent to the minimagnetron. [redacted]

[redacted]

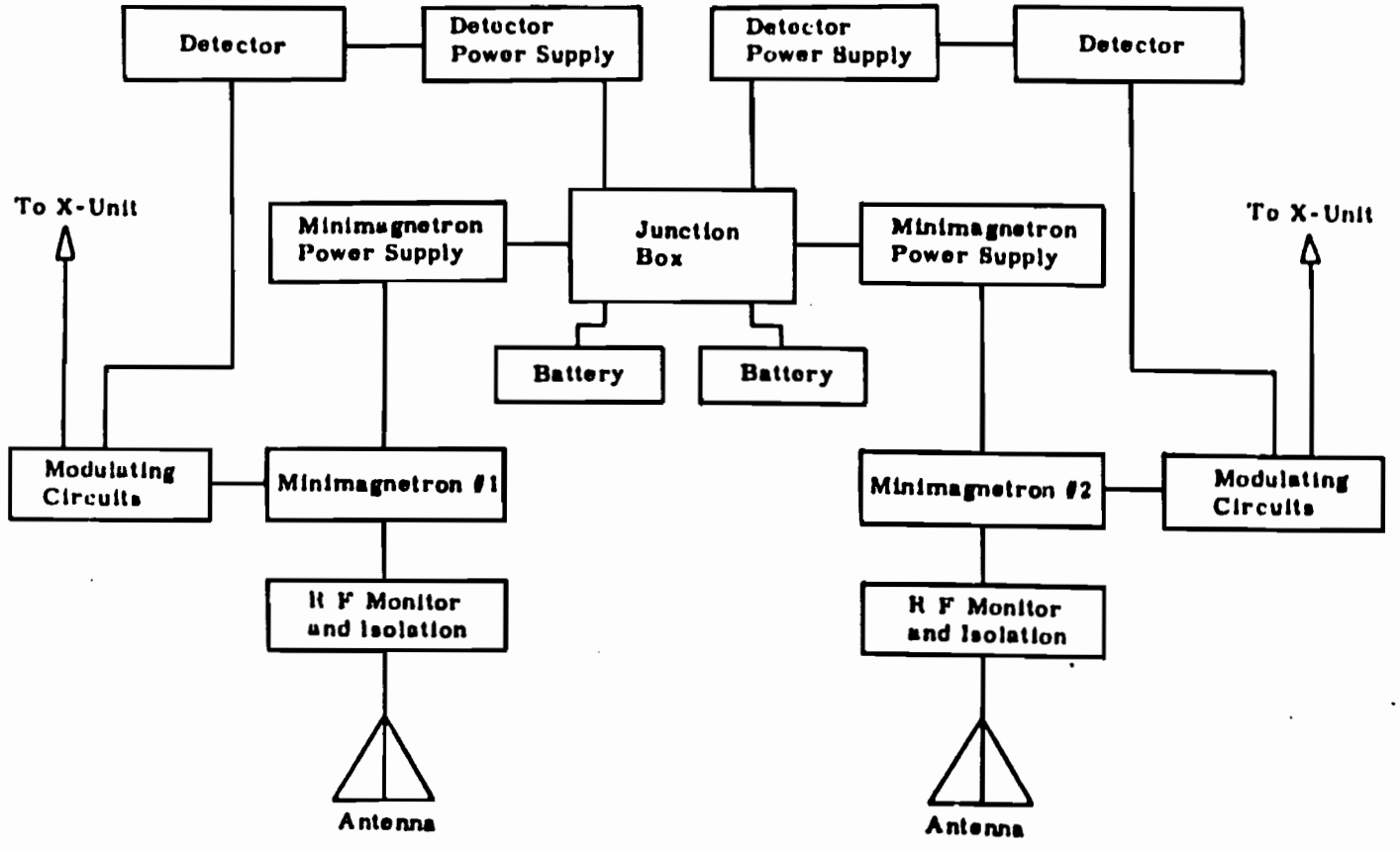

Fig. 9.1--Dual-channel, high-resolution telemeter block diagram.

[redacted]

The pulses developed by the differentiating circuitry (approximately 20 volts) are applied to the minimagnetron and cause a frequency from the pre-selected quiescent frequency (nominally 9000 mc) [redacted]

[redacted]

From the minimagnetron oscillator, the signal goes to the RF monitoring and isolation network which is composed of standard waveguide components. The signal enters this system through a coaxial waveguide transition and hence to a directional coupler. The low-power side of the coupler goes to an absorption frequency meter and terminates in a crystal detector. This portion of the system is intended to monitor frequency and power output of the minimagnetron during preoperational set-up procedures. The high-power side of the coupler feeds into a ferrite isolator which in turn feeds a waveguide-to-coaxial transition. From this transition the RF is conducted by RG-9 coaxial cable through the missile pressure bulkhead to the horn antennas at the rear of the Redstone guidance section.

The signal is next transmitted to the ground receiving station where it is amplified, demodulated, and displayed on a high-speed oscilloscope. The information is permanently recorded by photographing the oscilloscope trace with a moving-film camera.

A complete description of the receiving and recording equipment is given by Brumley and Schultheis[1] and Glass.[2]

9.2.3 Hardtack Operational Plan

Equipment and personnel were transferred from Bikini to Johnston Island to begin set-up and check-out about 35 days before the Teak event. The receiving station was installed on Johnston Island, and parabolic receiving antennas of 1-1/2 and 3-1/2 beam widths were placed on top of the station. Assembly and check-out of the first airborne transmitting system was started after ground installations were completed. Planning called for this equipment to be installed in the Redstone missile July 19 on Johnston Island. Following installation of telemetry equipment, the missile was assembled and erected. Several system checks were made before the system was judged ready for flight.

[redacted]

[redacted]

A brief description of the configurations of equipment aboard the Redstone follows. These are illustrated by Figs. 9.2 and 9.3. With the exception of antennas and antenna feed cables, all components were mounted on a large aluminum plate which was attached to the Chrysler Corporation R&D plate located between the guidance section and the warhead. The detectors were thus within a few inches of the rear dust cover of the warhead. In order to guard against radiation-produced failure of electronic components before the detector signals had been transmitted, none of the high-resolution telemetry equipment was placed closer to the warhead than were the detectors. From the R&D plate, antenna cables went to feedthroughs in the missile pressure bulkhead and then to two 18-db-gain horn antennas mounted in the skirt section of the top unit. These antennas were mounted in such a manner that their radiation would be directed toward the receiving stations, provided the missile was in the prescribed position and attitude at burst time. Before separation of the thrust unit and the top unit, the RF power sent to the antennas was absorbed by material inserted in the antennas. A line attached to the thrust unit pulled this material from the antennas at separation time. Total weight of this installation was about 246 pounds. Power was supplied by two 5-ampere-hour, 28-volt nickle-cadmium batteries connected in parallel. Average power consumption of the system was about 11 amperes. The FM system aboard the Redstone was equipped with one 5-ampere-hour battery, drew about 6 amperes, and weighed 66 pounds.

A similar procedure was followed for Orange shot.

9.2.4 Data

Teak. Teak detonation did not occur at the proper point (see Fig. 1.1) and no information was obtained, since antenna beam widths were such that the burst occurred outside the region in which sufficient signal could have been received.

Orange. The system operated well on Orange, and a good record of transit time was obtained on the low-resolution raster scopes. From these records a [redacted]

The high-time resolution scopes either failed to trigger, or the cameras failed to record the trigger. Therefore, no high-speed alpha record was obtained.

[redacted]

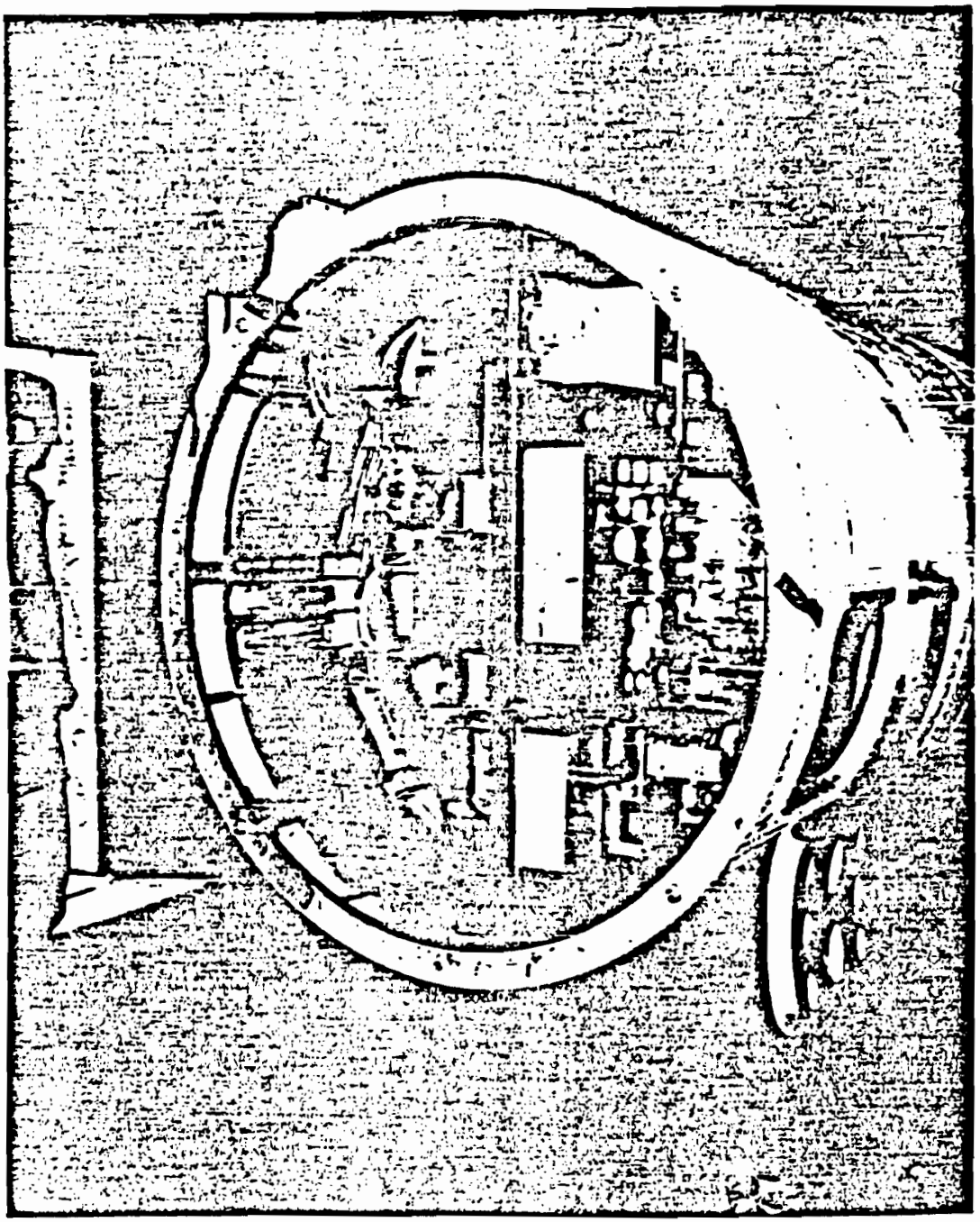

Fig. 9.2--Equipment aboard Redstone.

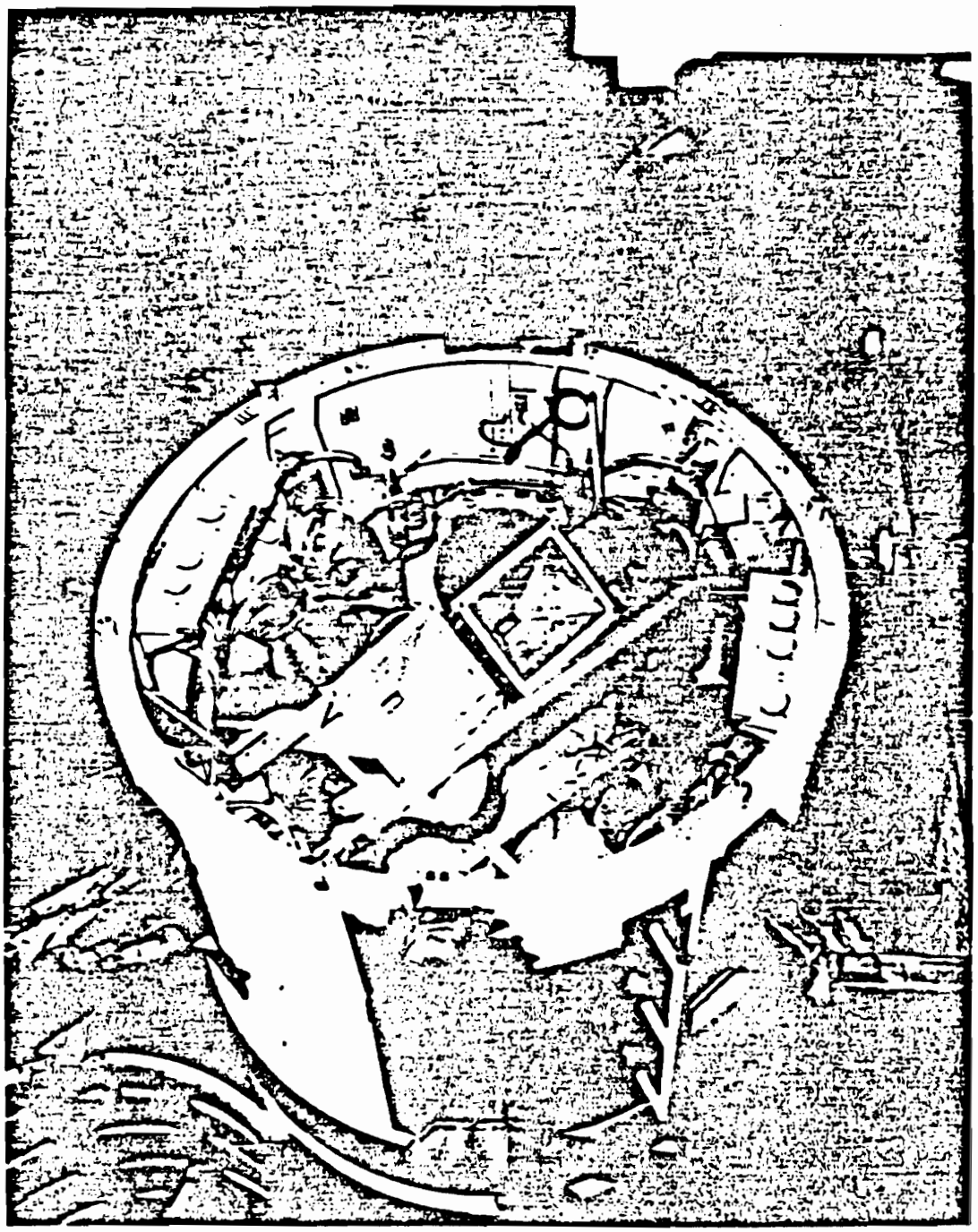

Fig. 9.3--Equipment aboard Redstone.

[redacted]

9.2.5 Summary of System Performance

Teak. Telemetered information indicates that the airborne system functioned properly. The receiving station was manned and operated normally. Immediately following launch of the Redstone, a signal level was observed and recorded at the receiving station, but as the missile moved farther from its prescribed trajectory, this signal faded so that at zero time no signal strength was present. [redacted] ad the missile performed properly, a record of transit time and alpha would almost certainly have been obtained.

Orange. With the exception of failure to record a high-resolution alpha display, the system operated satisfactorily. This failure can be rectified in the future by adjustment of scope trigger levels or use of more sensitive film in the recording cameras. [redacted]

9.3 POSITIONING SYSTEM

9.3.1 Design Criteria

Adequate analysis of data obtained by the instrumentation rockets required that positions of the rockets with respect to burst point be known more accurately than could be ascertained by ballistic prediction. To meet this need, design of a positioning system was undertaken by Sandia Laboratory. The principal conditions governing this design effort were that (a) total system cost, including design, development, and procurement, was not to exceed $200,000; (b) up to a range of about 250,000 feet, position of seven airborne vehicles had to be determined to an accuracy of ± 2000 feet; (c) in considerably less than one year from initiation of design, the system had to be operational to the extent of being capable of tracking one test rocket at a time at the Tonopah Test Range; and (d) the system had to be capable of operating remotely by closure of a few relays.

9.3.2 Description of System

Following is a brief description of the system; for complete details refer to Pace, Crowley, and Hansen.[3]

[redacted]

After consideration of several system types (radar, Cotar, and phase comparison devices such as Minitrack Mk I and Microlock), it was determined that the system most likely to meet all design criteria was a modification of the Minitrack Mk II.

MIDOT (Multiple Interferometer Determination of Trajectory), the system that was evolved, is a passive, null-recording, angle-measuring device. A radio interferometer using two crossed base lines, MIDOT operates from the telemetering signal. A typical MIDOT installation consists of two antennas mounted on each of two orthogonal base lines. The base-line length chosen was approximately 100 wavelengths at the telemetering frequencies.

Signals from antennas at each end of a single base line are added together at an RF tee located midway between the antennas. From this tee the signal is sent to a standard telemetering receiver when a record of signal strength is made. When arrival time of the transmitted signal is 180 degrees out of phase at the two antennas, a null results at the tee. Through application of relatively simple geometric relationships it can be demonstrated that, for the null to occur, the transmitter must be located on a cone the apex of which is at the center of the base line. When double base lines are used, the transmitter location is determined to be on a line formed by the intersection of two cones. Therefore, given two or more double base-line stations, the position of the transmitter may be determined as the intersection of lines from the stations. The system is ambiguous, but the ambiguity can be resolved when the initial condition geometry is known. Experimental data indicate that the system in the field will yield data accurate to about 4 mils, or approximately ± 1000 feet at a range of 250,000 feet with a baseline between stations of 10,000 ± 1000 feet.

Figure 9.4 is a block diagram of a single base-line, seven-channel recording station. The helical antennas feed Andrews Company Heliax cable to the tee at the middle. From the tee the signal is fed to ASCOP multicouplers and then to Sems-Clarke crystal-controlled receivers. Signal strength at each receiver is recorded by a Miller paper oscillograph. Data reduction is complex and time-consuming and requires use of analog and digital computers.

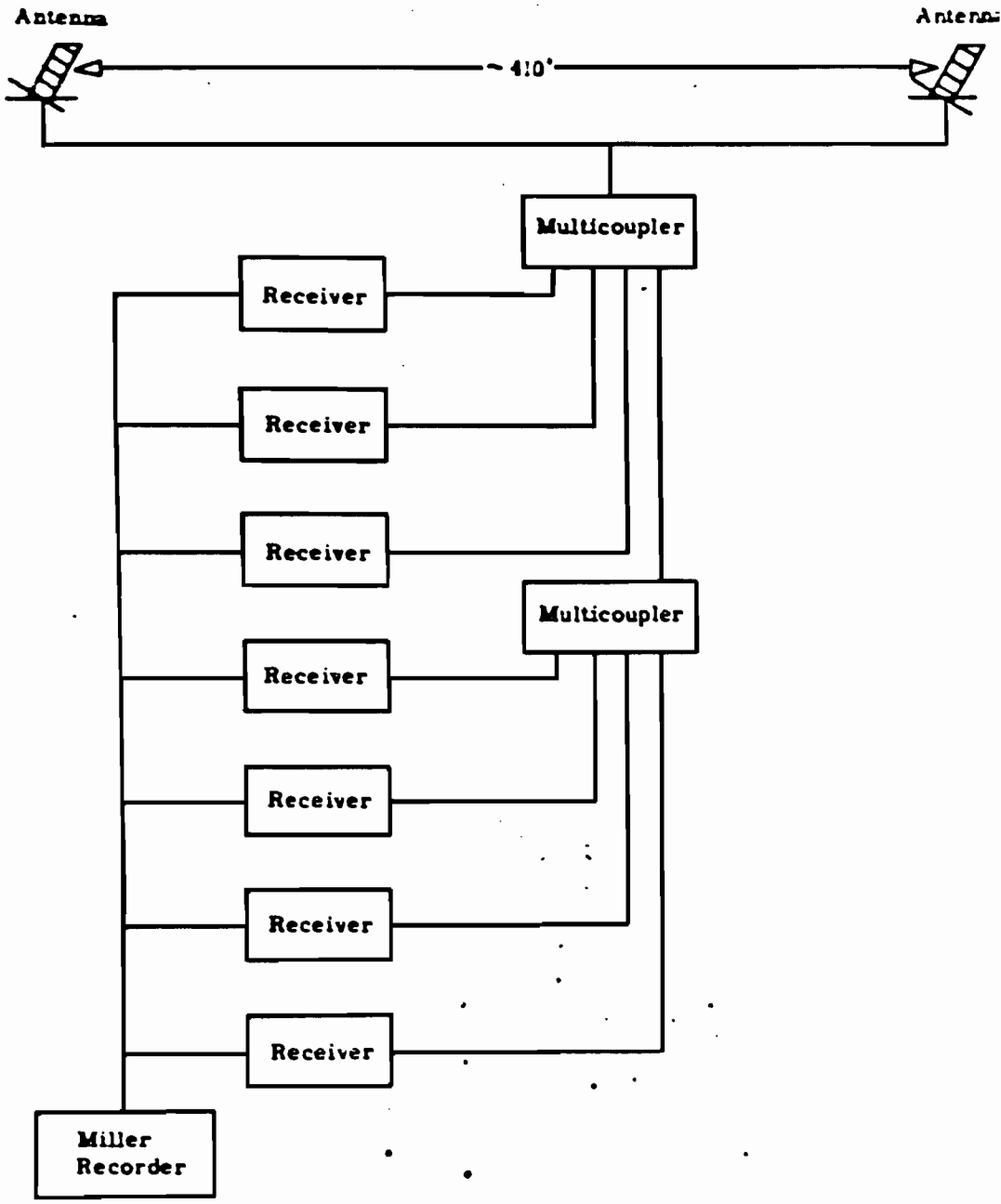

Fig. 9.4--MDOT seven-channel recording station.

[redacted]

9.3.3 Eardtack Operational Plan

Equipment and personnel were transferred to the proving ground in time to begin assembly and check-out about 35 days before the Teak event. Four MIDOT stations (two on each island) were established for the Teak and Orange events on Johnston and Sand Islands (Figs. 9.5 and 9.6). Electronic equipment at each station was contained in a 9-foot instrumentation trailer. Each antenna was mounted on a pedestal, erected, and positioned by the field contractor according to specifications.

At the request of the Army Ballistic Missile Agency (ABMA), equipment was obtained to enable the MIDOT system to track NRL pods used on Orange shot; however, the equipment was not used because of changed plans in the field.

9.3.4 Data

Position data from MIDOT measurements are estimated to be better than design limits by approximately a factor of 2, giving an accuracy of ± 1000 feet in any dimension. A comparison of the Orange burst position given by MIDOT to the ABMA location determination, as specified in WT-1657,[4] agrees within 1000 feet. It is therefore believed that instrumentation locations quoted are within a 2000-foot-diameter sphere. Figures 9.7a through 9.7b are plots of range, altitude, and lateral displacement in feet versus time. Ordinates are referenced to Redstone launch coordinates and abscissas are referenced to Redstone lift-off. The Teak and Orange bursts were 170.6 and 154.1 seconds after lift-off, respectively. Table 9.1 is a tabulation of burst time coordinates and slant range to the bursts. Burst positions are taken from WT-1657,[4] other locations from Sandia MIDOT data. Trajectories for RF attenuation measuring rockets are presented in Chapter 7.

9.3.5 Summary of System Performance

Teak. Nine missiles were tracked during the Teak shot, and satisfactory records were obtained on seven. The two records not reducible are those from the 80,000-foot instrumentation rocket and one of the RF attenuation Viper-Arrow II rockets (see Chapter 7). Transmission from the 80,000-foot rocket ceased 4.2 seconds after launch. No cause for this failure has been determined.

[redacted]

Fig. 3.3--WIDOT electronic equipment located in instrument trailer.

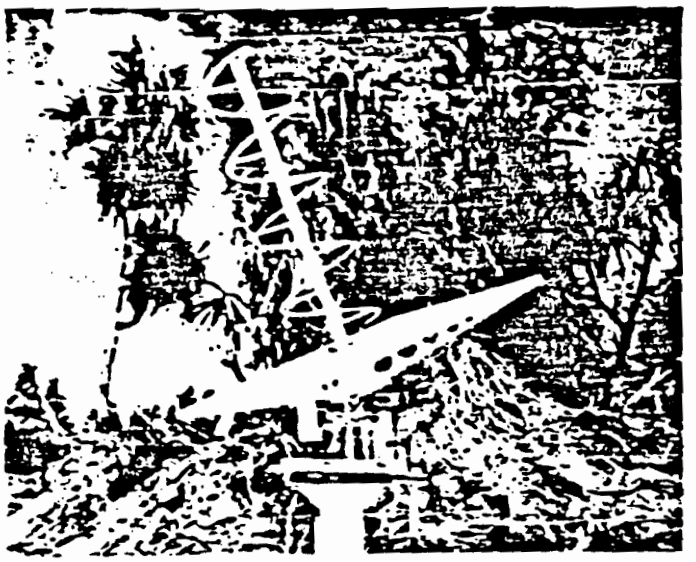

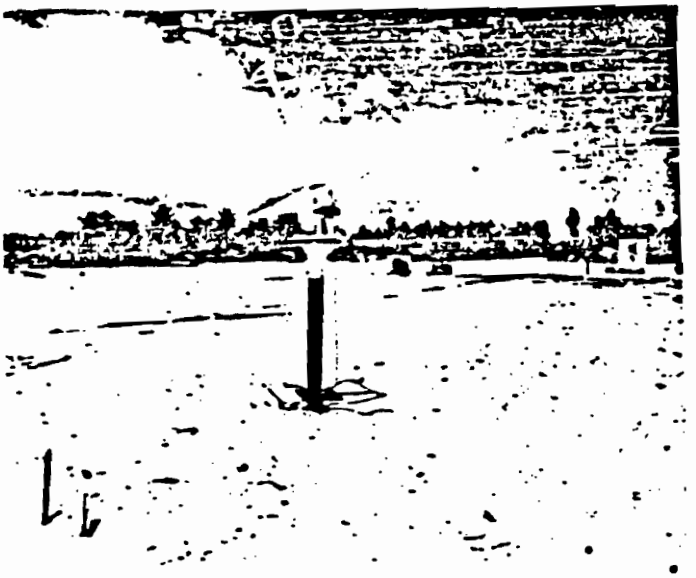

Fig. 9.6--MDOT antenna installations.

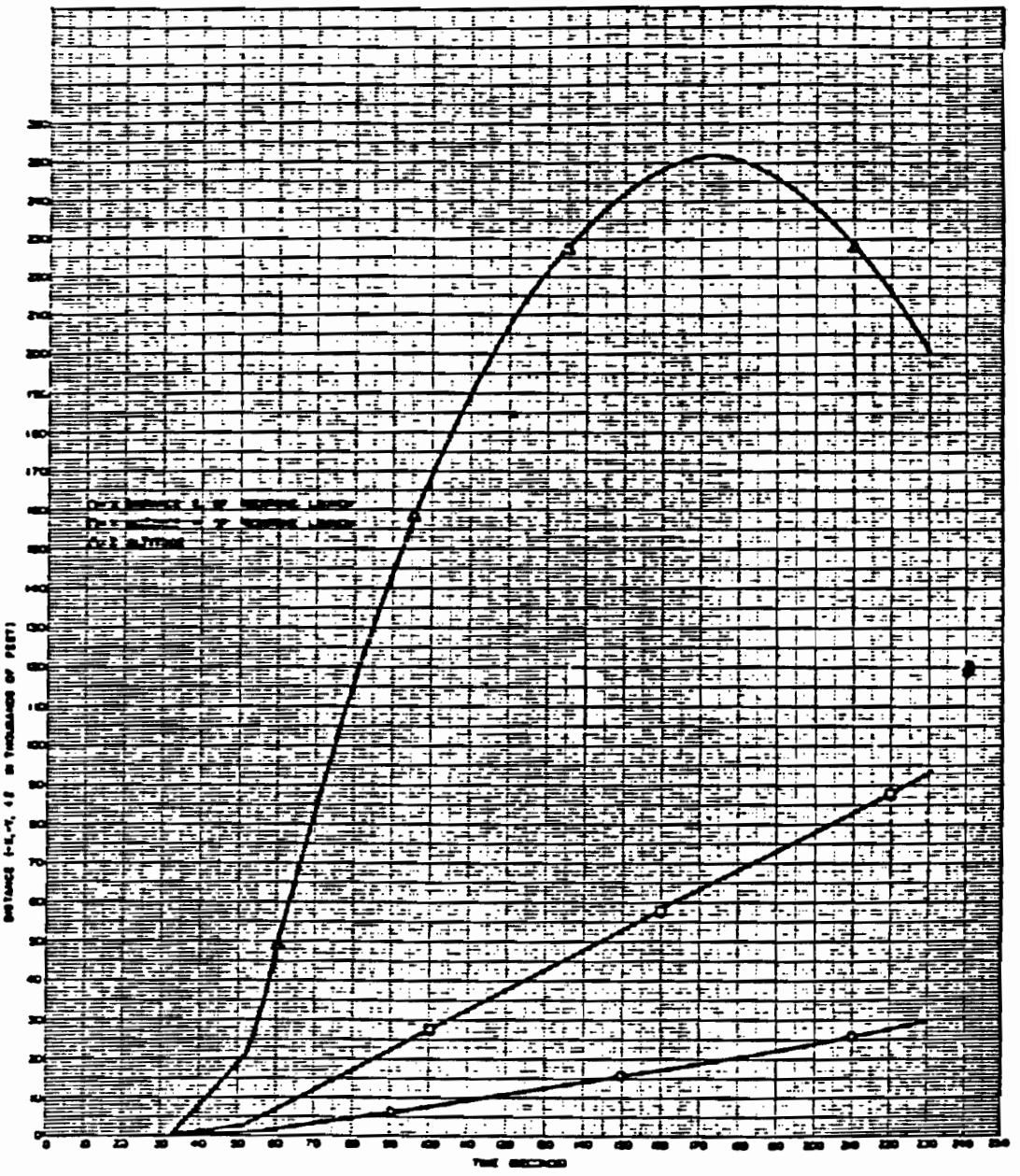

Fig. 9.7a--Station TX-252: x, y, z versus time after Redstone liftoff. Teak burst was 170.6 seconds after liftoff.

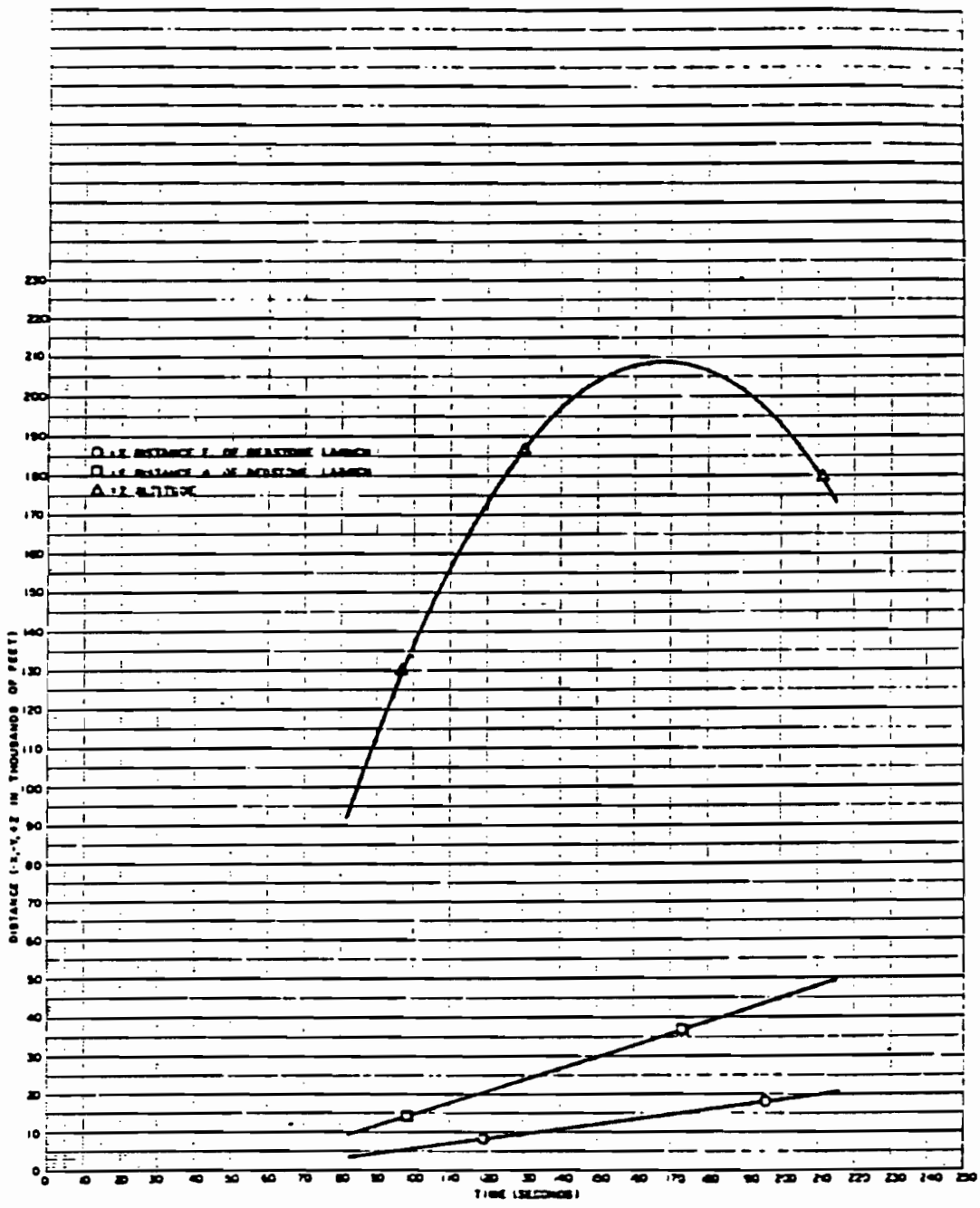

Fig. 9.7b--Station TK-209: x, y, z versus time after Redstone liftoff. Teak burst was 170.6 seconds after liftoff.

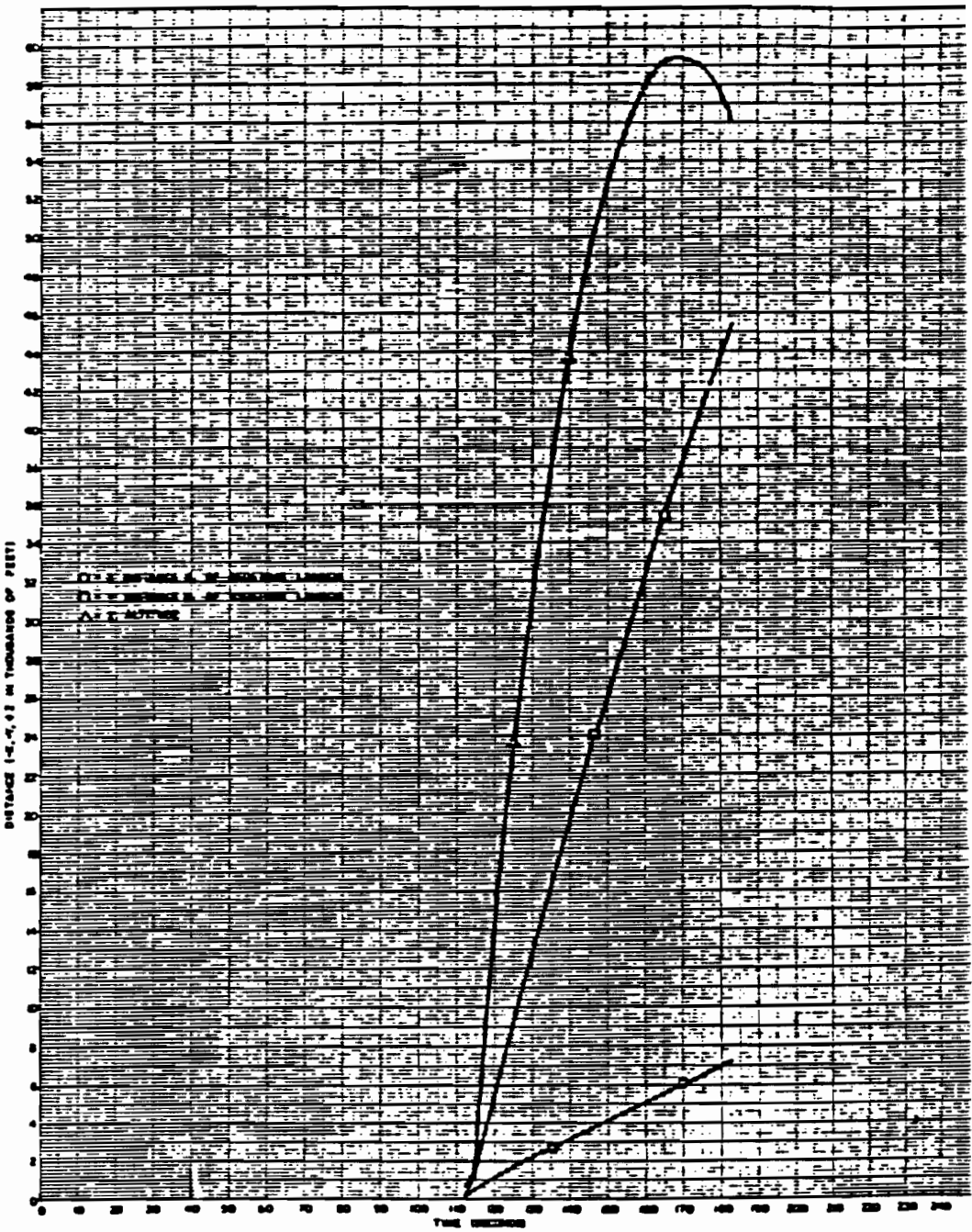

Fig. 9.7c--Station IX-59: x, y, z versus time after Redstone liftoff. Teak burst was 170.6 seconds after liftoff.

[redacted]

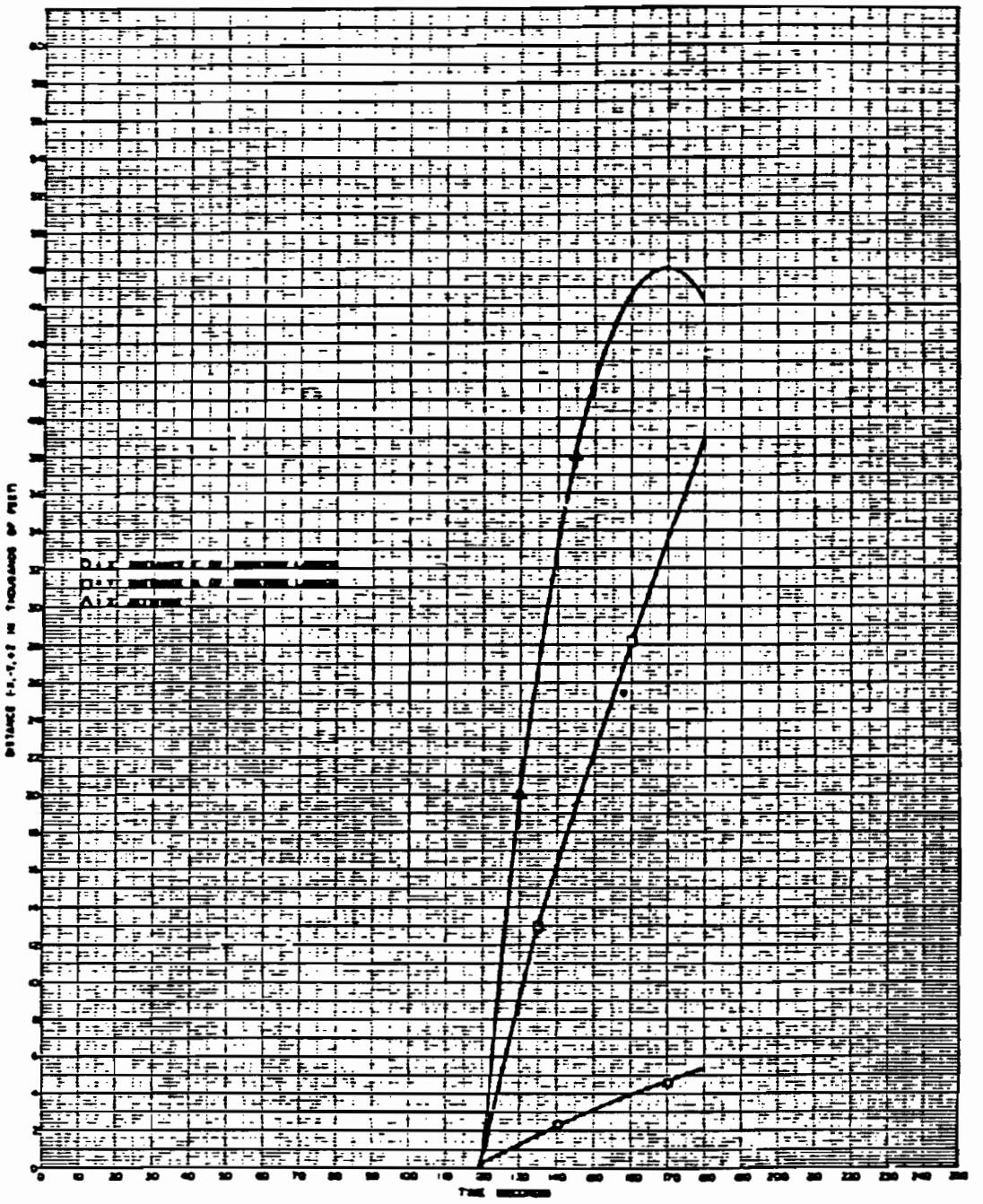

Fig. 9.7d--Station IX-18: x, y, z versus time after Redstone liftoff. Peak burst was 170.6 seconds after liftoff.

[redacted]

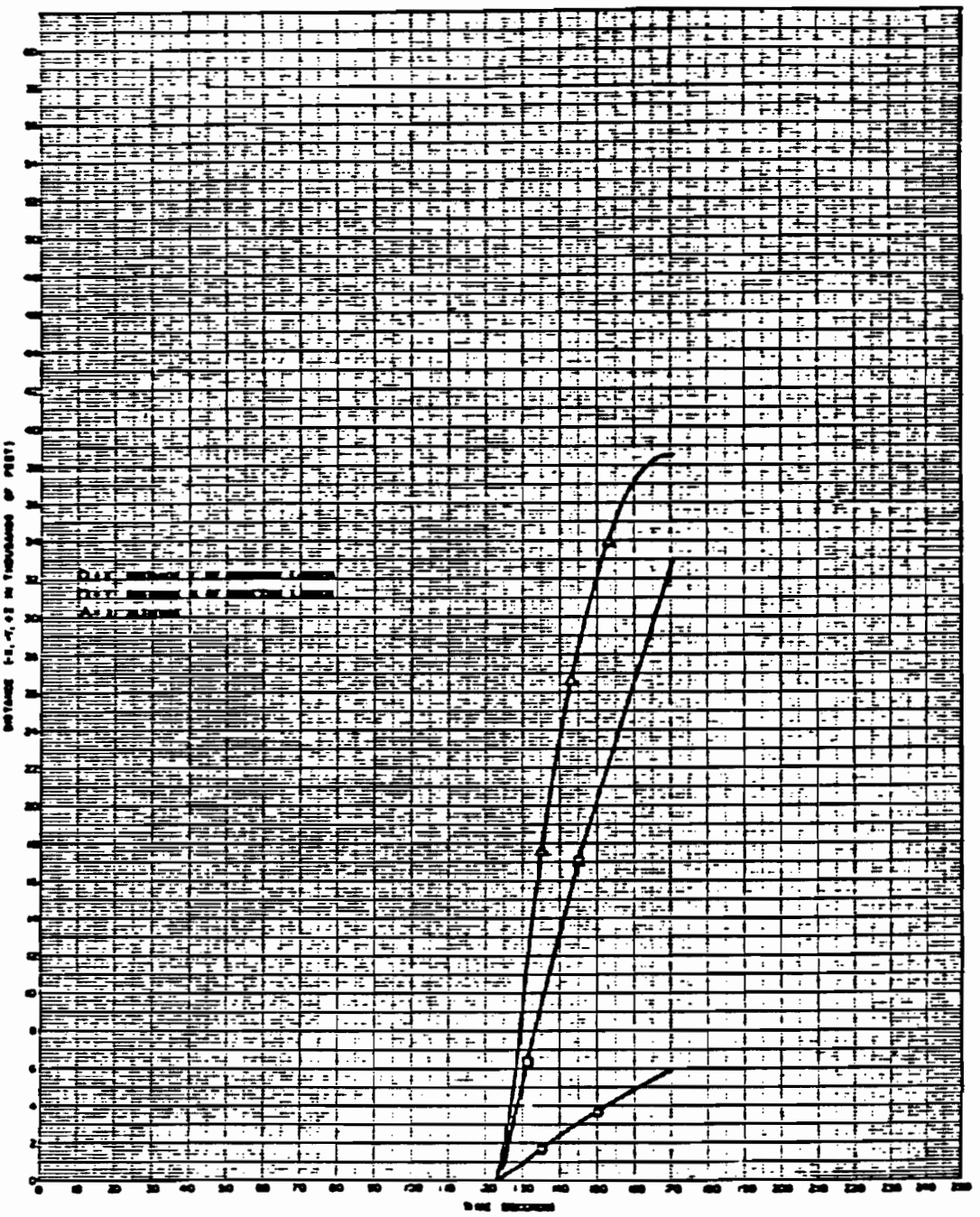

Fig. 9.7e—Station IX-39: x, y, z versus time after Redstone liftoff. Teak burst was 170.6 seconds after liftoff.

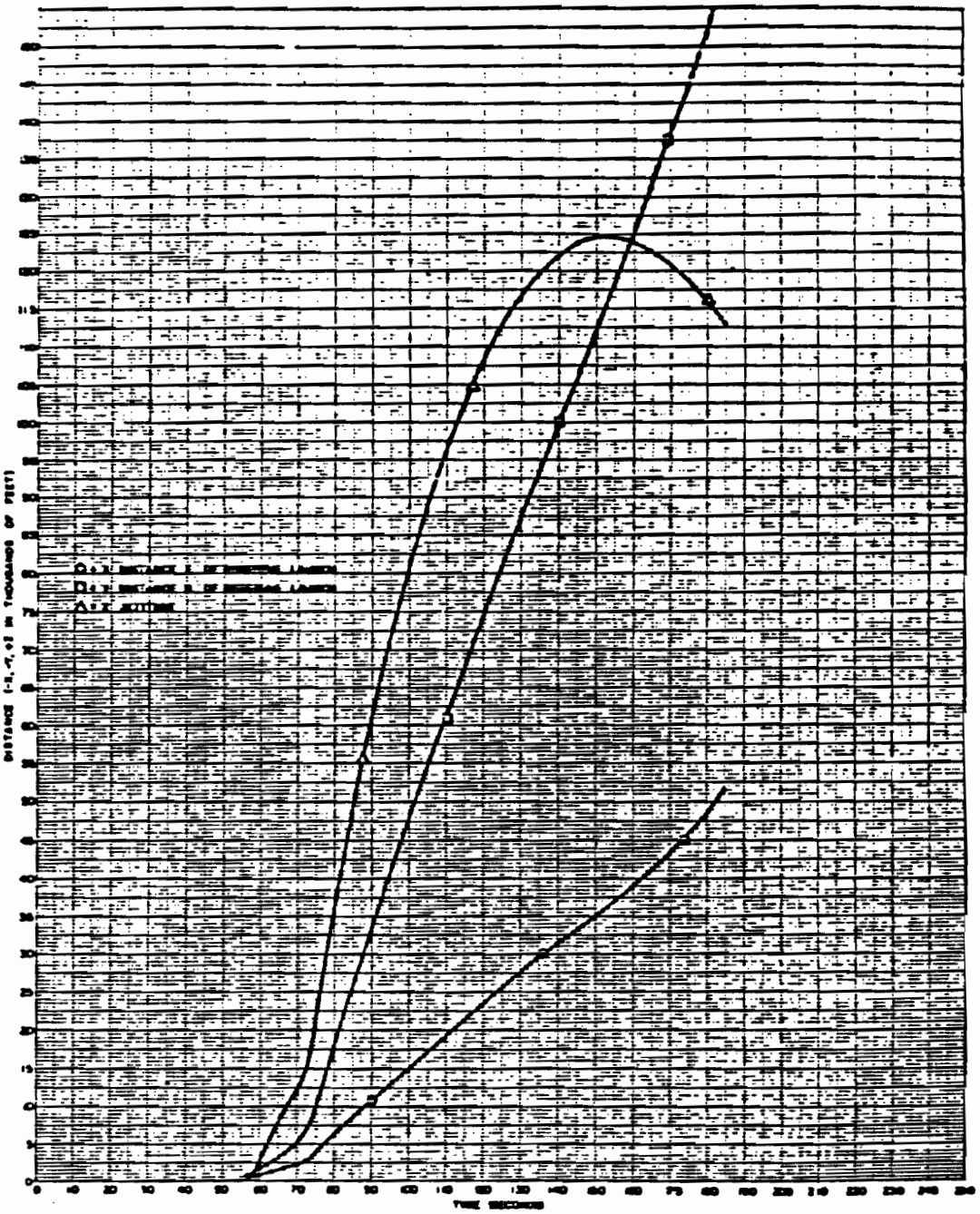

Fig. 9.7f--Station OR-125S: x, y, z versus time after Redstone liftoff. Orange burst was 154.1 seconds after liftoff.

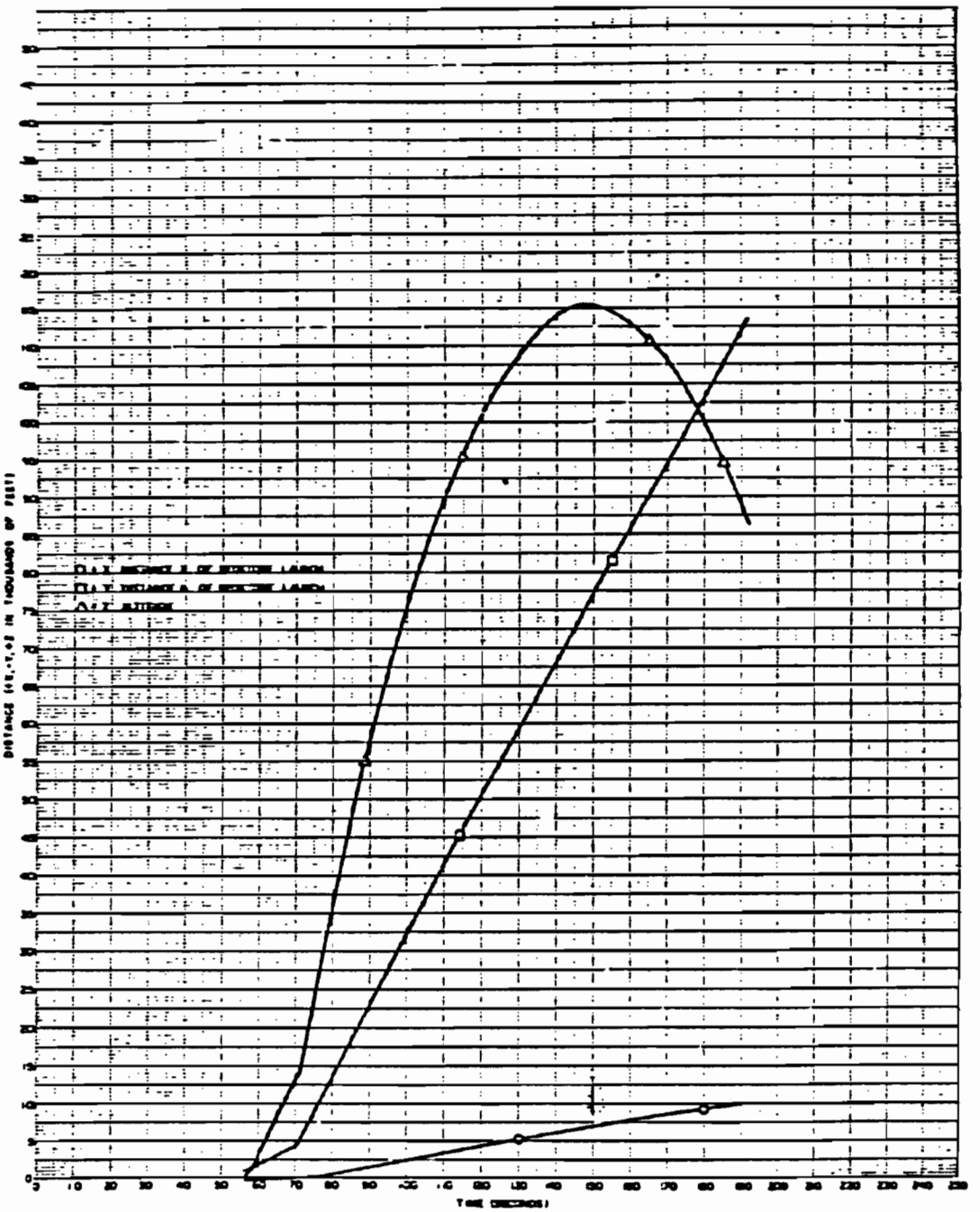

Fig. 9.7g--Station 08-115R: x, y, z versus time after Redstone liftoff. Orange burst was 154.1 seconds after liftoff.

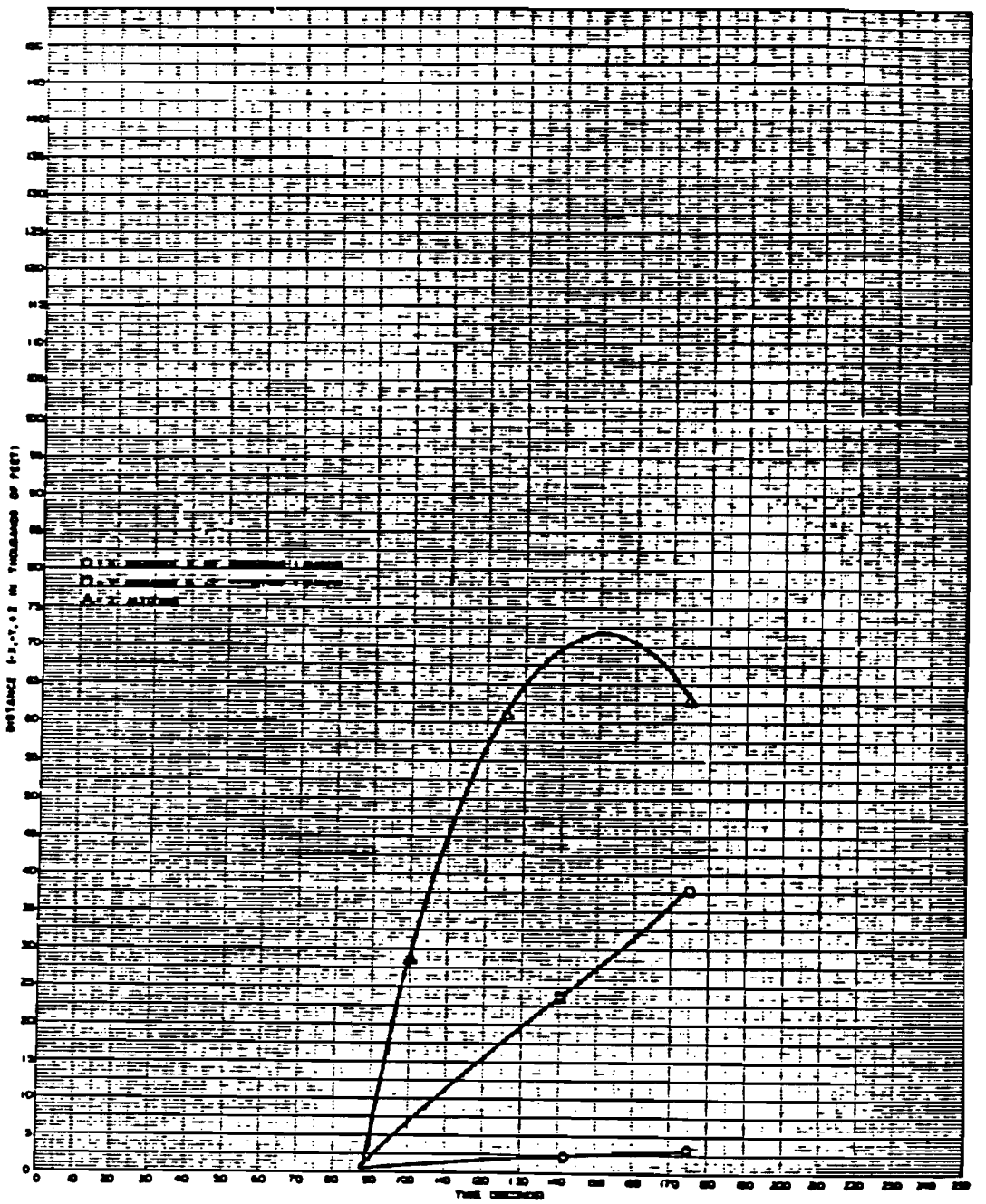

Fig. 9.7h--Station OR-72: x, y, z versus time after Redstone liftoff. Orange burst was 154.1 seconds after liftoff.

TABLE 9.1--BURST TIME POSITIONS RELATIVE TO REDSTONE LAUNCH*

Station	Altitude (feet)	South (feet)	West (feet)	Slant Range (feet)
		Teak		
Burst	250,360	-3,170	2,260	
M-37-39	38,600	32,900	6,000	214,800
M-38-48	48,000	33,900	4,700	205,700
M-36-59	59,400	38,500	6,100	195,500
M-35-80	RF failed	No data		
M-34-209	206,700	36,300	15,000	58,700
M-45-252	252,000	63,300	19,200	68,600
		Orange		
Burst	140,985	136,775	3,060	
M-41-72	71,600	29,200	2,500	128,100
M-40-115R	115,000	80,600	-7,200	62,700
M-46-125S	124,700	117,200	36,600	42,100

*For predicted positions, see Table 8.3.

The Viper-Arrow II missile was destroyed shortly after launch and no data were obtained.

Orange. Of six missiles for which tracking was attempted, five were successfully tracked. The six were the Redstone, OR-115R, OR-125S, and OR-72, in addition to two Deacon-Arrow combinations. The second stage of one of the Deacon-Arrows failed to fire and no trajectory was computed from the MIDOT data (224-mc Hi-Lo, see Chapter 7).

9.4 FM-FM TELEMETRY SYSTEM

9.4.1 Design Criteria

The FM-FM telemetering system was the most important endeavor of Project 32.4 but, since very little development was necessary, it was probably the

simplest to accomplish. The system is intended to accept data from neutron, gamma-ray, thermal, and X-ray transducers and transform such data to a form suitable for transmission and recording. It also is to provide monitoring of warhead command functions and the high-resolution telemetry system.

With the exception of radiation effects, conditions surrounding the Hardtack tests were not greatly different from standard light-missile tests. Accelerations experienced did not exceed 65 g's, and space was sufficient to utilize standard components. The effects of radiation were not well understood, but tests during Operation Plumbbob indicated that no great difficulties should be anticipated at the ranges from burst which were planned for the Program 32 instrument carriers.

9.4.2 Description of System

The system will not be described in great detail, since the techniques are well known and components are commercially available. Figure 9.8 is a block diagram of a typical instrumentation rocket installation. The principal components in the system are as follows:

(1) Bendix TOE-31 subcarrier oscillators
(2) Bendix TXV-13 transmitter
(3) Rheem REL-09 power amplifier
(4) Carter Magnotor 250 w-250 ma
(5) Ni-Cad 2H10 batteries
(6) Sandia-designed, nose-probe antenna
(7) ASCOP commutation switch

Accuracy of the system was expected to be better than 5 percent from data input to reduced data.

The receiving station was mounted in a 34-foot trailer van and consisted of standard commercial equipment. Figure 9.9 is a block diagram of the FM-FM receiving station. Its principal items are:

(1) ASCOP preamplifiers
(2) ASCOP multicouplers
(3) Nems-Clarke Model 1400, crystal-controlled receivers
(4) Ampex FR 114 tape recorders
(5) Miller Model J, 30-channel oscillograph

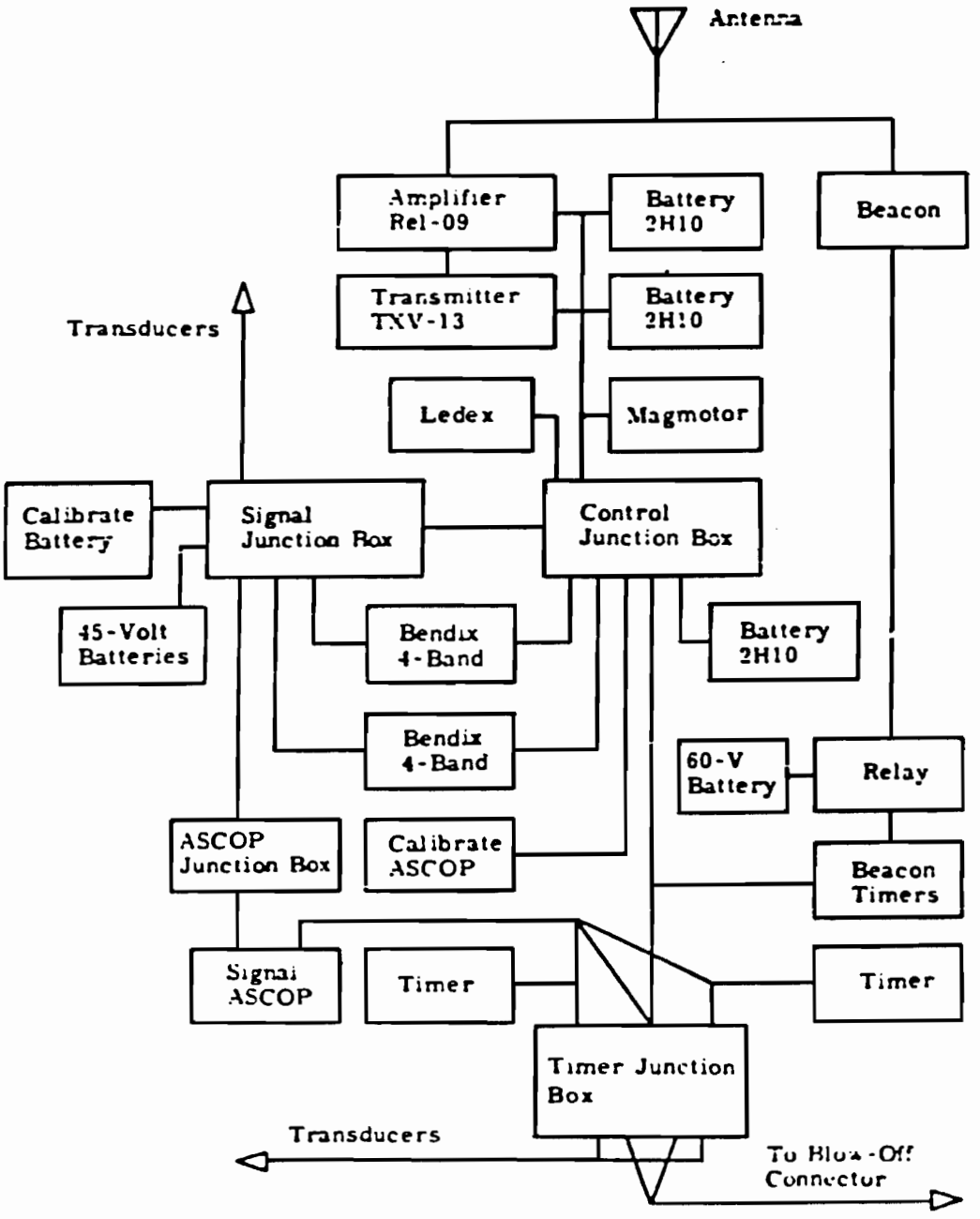

Fig. 9.6--Block diagram of typical instrumentation rocket installation.

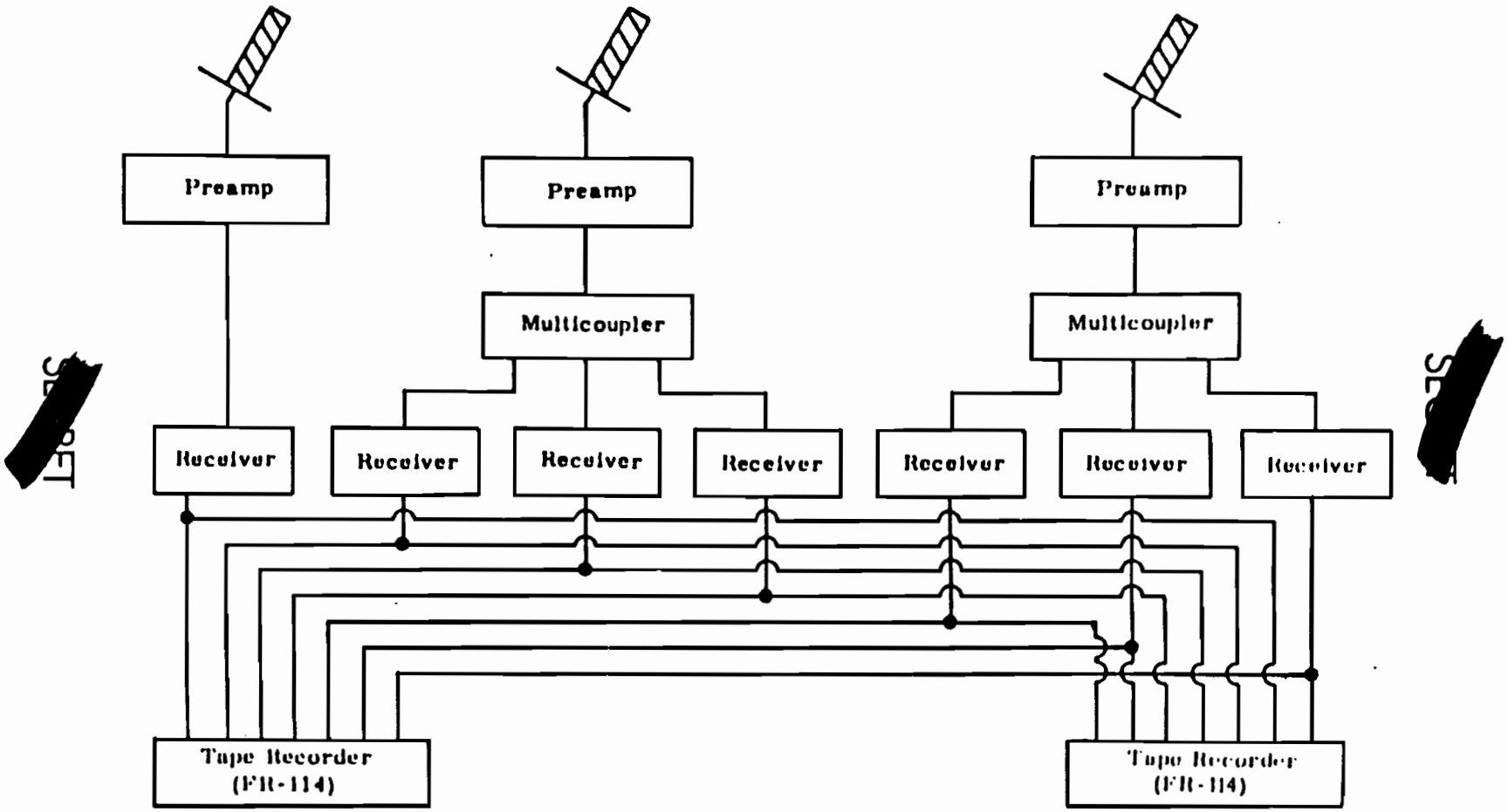

Fig. 9.9--Block diagram of FM-FM receiving station.

[redacted]

9.4.3 Hardtack Operation Plan

Personnel and equipment were transferred to the proving ground in time to begin assembly and check-out about 35 days before the Teak shot. The receiving trailer was moved from Bikini to Johnston Island, and all its electronic equipment was checked out. Immediately following check-out of the trailer, instrumentation rocket telemeters were brought into the trailer for setup and calibration. As nose cones were completed, they were assembled in the missiles and the latter were erected on their launchers. Several signal dry runs were conducted before shot day to assure proper operation of the systems. Sufficient equipment was taken into the field to support two Teak shots.

REFERENCES

1. Brumley, F. B., and Schultheis, T. M., The Doorknob Wideband Telemetering System, SCTM 348-61(72), Sandia Corporation, to be published.
2. Glass, R. E., A Wideband Microwave Link for Telemetering, SCTM 182-57(52), Sandia Corporation, March 25, 1957.
3. Pace, T. L., Crawley, T. V., and Hansen, V. W., The MIDOT System, SCTM 76-58(52), Sandia Corporation, December 12, 1958.
4. Elliott, G. P., Kennedy, B., Grau, D., Operation of Missile Carrier for Very-High-Altitude Nuclear Detonation, WT-1657, Army Ballistic Missile Agency, May 20, 1959.

[redacted]

Chapter 10

TEAK AND ORANGE WARHEADS

10.1 WARHEAD SYSTEM

10.1.1 Introduction

Sandia's responsibility was to provide [redacted] warheads to be carried by the Redstone missile for the Teak and Orange events, and additionally to insure mechanical compatibility between the warhead and the missile as well as electrical compatibility between the warhead and the fuzing system provided by Picatinny Arsenal. Special equipment was installed on each warhead to provide for maximum prelaunch safety and to provide special firing-signal circuits to the diagnostic telemetering system which was installed in the Redstone missile. Final assembly of the warheads was accomplished at an AEC production facility under the guidance of personnel from this project. No difficulties were encountered in assembly or final preparation of the units of the forward area.

Installation of the warhead in the missile-warhead compartment was accomplished on Parry Island, Eniwetok Atoll, for the original Teak operation which was to have been carried out from Bikini Atoll. Following postponement and relocation of the event from Bikini to Johnston Island the missile was returned to Parry Island from Bikini and the warhead was removed. The Teak and Orange warheads were later sent to the Waikele Branch, Naval Ammunition Depot-Oahu, Oahu, Hawaii. This site was used, since no suitable facility existed at Johnston Island. In addition, trained personnel were available at Waikele to maintain the warheads. Warheads in the missiles for Teak and Orange were installed at Waikele with the aid of the AFMA mechanical group and Navy personnel at the site.

Following assembly at Waikele, the units were airlifted by MATS from the Naval Air Station, Barbers Point, to Johnston Island. The units actually used were stored on Johnston Island until they were expended, while the spare warheads remained at Waikele.

[redacted] Page 327 is deleted.

[redacted]

10.1.2 Warhead Description

[redacted]

(Fig. 10.1). The warhead and instrument compartment were sealed before launch, and thus the warhead was exposed to pressure during flight equal to or slightly greater than ambient pressure of the launch site. Details of warhead description and operation are contained in Sandia Corporation document SC-3897(TR).[1]

10.1.3 Warhead Preparation and Test

[redacted]

used. This equipment operated satisfactorily in all respects.

10.1.4 Fuzing System

The fuzing system is described in a joint DMA/DCD/DASA publication.[2] The system consisted of two paralleled T-107 safing and arming devices, a 28-volt thermal battery power supply, and a timing device. As a result of changes incorporated following flight tests at AFMTC, the system was changed so that the primary fire signal was applied directly to the warhead trigger-circuit thyratron grids, and the backup fire signal was applied to the trigger-circuit pulse transformers.

The fuzing system was designed by Picatinny Arsenal and was based, where possible, on use of already developed components. The T-107 devices were similar to those used in the tactical Redstone missile, with modifications as necessary to fit the trajectories. The timing device utilized mechanical escapement timers which had been used by the Ordnance Corps in other weapon applications.

[redacted]

[redacted]

The T-107 devices allowed arming and firing signals to pass the warhead only if the trajectory was correct; the timing device generated arming and firing signals in proper sequence for warhead operation.

The firing signal was delivered by the missile programmer in series with contacts closed by the fuze timing device. This was done in order to provide more accurate control of the burst point. A backup firing signal was provided for additional reliability. One of the warhead arming signals was required to be continuous; if detonation did not occur on either firing signal, this signal would have been interrupted by the fuze timers, causing the X-unit to discharge, and thus to "dud" the warhead.

10.1.5 Safety

A study was made of safety considerations involved in the Teak and Orange tests.[2,3] The conclusion reached by this study was that probability of a nuclear detonation at an altitude of less than about 90,000 feet was less than 10^{-7}.

Safety against a nuclear detonation was dependent primarily upon the T-107 safing and arming devices and upon a missile-generated signal indicating that the missile trajectory is normal before warhead arming is allowed. The T-107 devices sense missile accelerations and require that a predetermined sequence of missile accelerations be experienced at proper times, and that certain signals be received from the missile guidance and control system. These signals include the guidance-check signal, which indicates that the trajectory is such that the missile will be at a safe altitude at burst time.

The warhead electrical system was slightly modified to allow direct control of arming by the Task Force arming coordinator prior to missile launch. The circuit between the high-voltage battery and the X-unit was interrupted and connected to two receptacles mounted on the external skin of the warhead. A nuclear detonation could not occur under any circumstances unless the circuit between these receptacles had been completed. This was accomplished at approximately H - 55 minutes by means of a jumper cable installed by the arming party.

The warheads were monitored as necessary for personnel protection against exposure to tritium gas in the event of a leak. A T-289/336 installation was used in the assembly buildings and was operated continuously wherever a unit was in the bay. At other times during warhead handling operations, T-290 portable air samplers were used.

[redacted]

10.2 SYSTEM MONITORING AND RESULTS

10.2.1 Preflight Safety Checks and Final Warhead Arming

Sandia was given the responsibility of performing final arming of the warhead prior to missile launch. This work was initiated at H minus 65 minutes, after assurance from the ARMA firing coordinator that radio-frequency silence was in effect on the missile and in the area east of the Johnston Island aircraft-control tower.

The first operation performed was a voltage-safety check of the fuzing-system output lines. This step was incorporated to assure that no voltage was being supplied on any of the lines to the warhead. A special test device connected a multimeter through a selector switch to the fuze-output connector. Each wire in the output circuit was monitored individually by means of the selector switch. The multimeter was set on the 2.5-volt range and the meter switched to the AC and DC mode for each circuit. No voltage was detected on any of the input lines.

The second step was a warhead-continuity test performed with the T-304 multiple-purpose test set. This test confirmed that the high-voltage thermal battery had not been activated and that certain critical internal warhead connections were complete.

Following these steps, permission was requested and received from the Commander, Task Group 7.1, to arm the warhead. The cables between the warhead and the fuze were connected, and continuity checks of the warhead and fuze were performed by means of the Picatinny prelaunch control and monitoring panel in the firing bunker. All connectors on the warhead-fuze cables were then safety-wired, and the diagnostic telemetering system was connected to the warhead.

The last step to be performed was insertion of the high-voltage jumper cable which was also safety-wired. Following this operation each member of the arming party performed a visual check of the installation, after which the missile-access doors were closed and sealed.

The final step was a report to the Task Group Commander by the Project Officer that arming was complete and a statement to the ARMA firing coordinator that radio-frequency silence could be lifted.

[redacted]

10.2.2 Inflight Monitoring of Warhead System

Four subcarrier channels of an FM/FM telemetering system were used to monitor performance of the warhead and fuze electrical system. Three channels were used to monitor the three 28-volt signals which the fuzing system supplies to the warhead. The fourth channel was provided by Picatinny Arsenal. A commutated signal from the adaption kit was imposed on this channel and was used to indicate operation of the various AK components. The monitoring system performed properly, and all functions occurred as expected.

10.2.3 Test Results

[redacted]

REFERENCES

1. Status of Design Release of the TX-39-X1 and TX-15-X4 Bombs and the XW-39-X1 Warhead, SC-3897(TR), Sandia Corporation, Albuquerque, New Mexico, March 1957.
2. Report on a Study of the Safety Aspects of UHA and VHA Prime for Operation Hardtack, prepared by Safety Working Group, AFSWP-RD/DA-DMA/AEC, published by Field Command, AFSWP, Albuquerque, New Mexico, October 21, 1957.
3. Letter, McKiernan, J. W., to Commander, FC/AFSWP, Attn: Maj. Ray, Subj: Effect on Safety of Teak and Orange Tests Caused by Deletion of S&A Disarm Function, Ref. Sym: 1283(905), January 27, 1958.

[redacted]

Chapter 11

OPTICAL RADIATION AND PHOTOGRAPHIC COVERAGE

11.1 OBJECTIVES

Photographic coverage on the ground for the Teak and Orange events was designed to record the time history of visible radiation. Basically, three types of coverage were attempted: (1) high-speed framing cameras to record absolute surface brightness in three narrow spectral bands, (2) lensless streak cameras to record irradiance on the ground in three narrow spectral bands, and (3) a spectrographic streak camera to record bomb spectrum versus time. In addition to these, conventional framing cameras using color film were employed to provide documentary coverage and supplementary measurement of the various fireball dimensions and phenomena at late time.

Objectives of the photographic coverage were several. As indicated above, the primary purpose was to gather data which are descriptive of the thermal pulse in quantitative detail. The bearing of this information on the problem of detection of high-altitude bursts is clear. In addition, the information is of interest from the standpoint of weapon effects, e.g., the flash blindness problem. It was furthermore intended that coverage of optical phenomena should contribute substantially to the general fund of data pertinent to an understanding of the physics of a high-altitude fireball plasma. Quantitative measurements were needed for this purpose; qualitative information about unexpected phenomena was also sought.

11.2 THEORY

The following discussion of fireball phenomenology at high altitude summarizes, in part, the thinking of others.[1,2,3,4,5] For brevity, details of calculation are omitted here and only salient results are considered.

At sea level, soft X-rays [redacted] are absorbed within a few meters of the bomb, giving rise to a very hot isothermal sphere. The temperature is so high that energy radiated is largely in the spectral

[redacted]

region and is strongly absorbed by the ambient air. The growth of the sea level fireball is principally by hydrodynamics which form very quickly and carry away most of the energy yield of the weapon. Very little energy escapes the fireball before formation of the shock front which absorbs the radiant energy of the inner fireball, thereby decreasing the effective brightness of the X-ray heated air. After breakaway, the expanding shock becomes transparent and a second maximum in the thermal pulse occurs which contains essentially all the energy radiated from the burst. The fraction of the yield contained in the thermal pulse is about one-third of the total yield for a sea level explosion.

Because of lower air density, [redacted] X-rays is deposited in a larger volume at higher altitude. The air temperature of the fireball is then somewhat lower than at sea level, and more of the radiant energy is in the spectral region for which cold air is transparent. Hydrodynamic phenomena do not form as quickly as at sea level, so that more energy is radiated before the thermal minimum. This enhancement of the radiation constitutes a loss of energy which would otherwise be carried away hydrodynamically. The result is that hydrodynamics become less important and thermal radiation is increased with altitude. Depending on yield, there is an altitude at which there is no second maximum in the thermal pulse. This occurs below 200,000 feet for megaton weapons. At still greater altitudes, the portion of the yield that is in thermal radiation begins to decrease again. This is caused by X-ray deposition which is so diluted spatially that the fireball air is not very hot and cannot radiate effectively.

11.2.1 Orange

Shot Orange [redacted] was not expected to be substantially different from sea level shots in many respects. At this altitude, X-rays are still absorbed in a rather small region around the bomb. Hydrodynamic phenomena develop somewhat later than at sea level but still constitute the most important mechanism for transporting energy away from the explosion. As at sea level, a minimum in the thermal pulse occurs, although later than at sea level, and relatively more radiation escapes in the early stages of the explosion before the minimum. Only a slightly larger fraction of the yield is radiated in comparison to that at sea level.

[redacted]

11.2.2 Teak

Shot Teak [redacted] was expected to represent a marked departure from the phenomenology of a sea-level burst. At this altitude, air density ($\rho/\rho_0 \approx 3 \times 10^{-5}$) is such that X-rays are deposited in a sphere of approximately 30,000 feet radius. Hydrodynamics are much less important than at sea level and develop very late compared to the time for radiation cooling of the fireball. As a result, nearly two-thirds of the yield is radiated away in a single thermal pulse of short duration (about 10 msec). Because of low ambient air density and relatively low temperature of the fireball, the heated air is quite transparent, so that direct observation of the inner portions of the fireball can be made.

11.2.3 Teller Light

Teller light is well known in the case of sea-level bursts[6] as the intense early light from the air surrounding the burst before formation of the fireball. It is generated by gamma radiation absorbed in the air by Compton collisions. Fast recoil electrons (a few hundred kev) rapidly transfer gamma energy to excited states of air molecules, giving rise to a characteristic emission spectrum in the visible from N_2 and N_2^+.

At Teak altitude the air can be similarly excited by photoelectrons produced by absorption of soft X-rays at relatively large distances from burst point. Absorption of both gamma rays and X-rays can thus give rise to prompt emission from excited molecules, and both radiations are therefore considered sources of Teller light.

Because of the long collision time of molecules at 250,000 feet (about 1 μsec), the Teller light phase of the explosion is greatly enhanced. Since the lifetime of an excited state is about 10^{-8} sec, virtually all excited molecules radiate before the excitation is transferred to kinetic energy by collisions.

Because of the long mean free path of gamma rays at 250,000 feet, deposition of gamma energy is much less than that from X-radiation at burst altitude. At an altitude of about 100,000 feet, however, air density is such that there is a broad region of substantial gamma-ray absorption. Thus, most of the Teller light generated by gamma radiation arises from this lesser altitude.

Teller light from X-rays is much more intense and occurs much nearer the burst point. Further discussion of the Teller light pulse is presented in a later section.

11.2.4 Thermal Radiation and Peak Fireball Development

At 250,000 feet altitude, it is estimated that about two-thirds of the [redacted] a large volume because of low ambient air density. X-ray energy is rapidly transferred to energetic photoelectrons and auger electrons which deposit their energy locally by further ionization and excitation. The approximate energy deposition in electron volts per air atom is illustrated in Fig. 11.1 versus radius. The number of ion pairs produced per atom by energetic electrons can be read directly from the graph as $\epsilon/32$, since it requires 32 ev to form an ion pair in air. Thus, for example, all air atoms are at least singly ionized within a radius of about 5000 feet. Radiation emitted by excited air depends on the state of the air immediately following initial deposition. Except for prompt Teller emission already mentioned, the most important processe which now occur are those which bring about a statistical equilibrium.[1]

The general characteristic of the air immediately after deposition of the bomb's energy is the presence of an excess of molecules, neutral and ionized, for the energy content of the air. In the closer region there is, in addition an excess of electrons. In the outer region, dissociation of neutral molecule by collisions is slow (approximately 1 to 100 msec). Thus, in the beginning, at least, radiation from the outer fireball is predominantly from molecules. Closer to the bomb, where there is substantial ionization, molecules and electrons disappear together by a combination of two nonradiative reactions: $N_2^+ + e = 2N$ and $N_2 + N^+ = N_2^+ + N$. The first is dissociative recombination; the second is charge exchange.

Both of these are sufficiently fast that equilibrium is attained in about 1 μsec, and as a result dissociation of all molecules occurs, leaving ionized air atoms and electrons. A simple argument shows that this will be the case out to the radius for which $\epsilon = 10$ ev/atom (approximately), which occurs at about 15,000 feet. This volume is referred to as the ionized core region in Fig. 11.1. The principal source of optical radiation from the

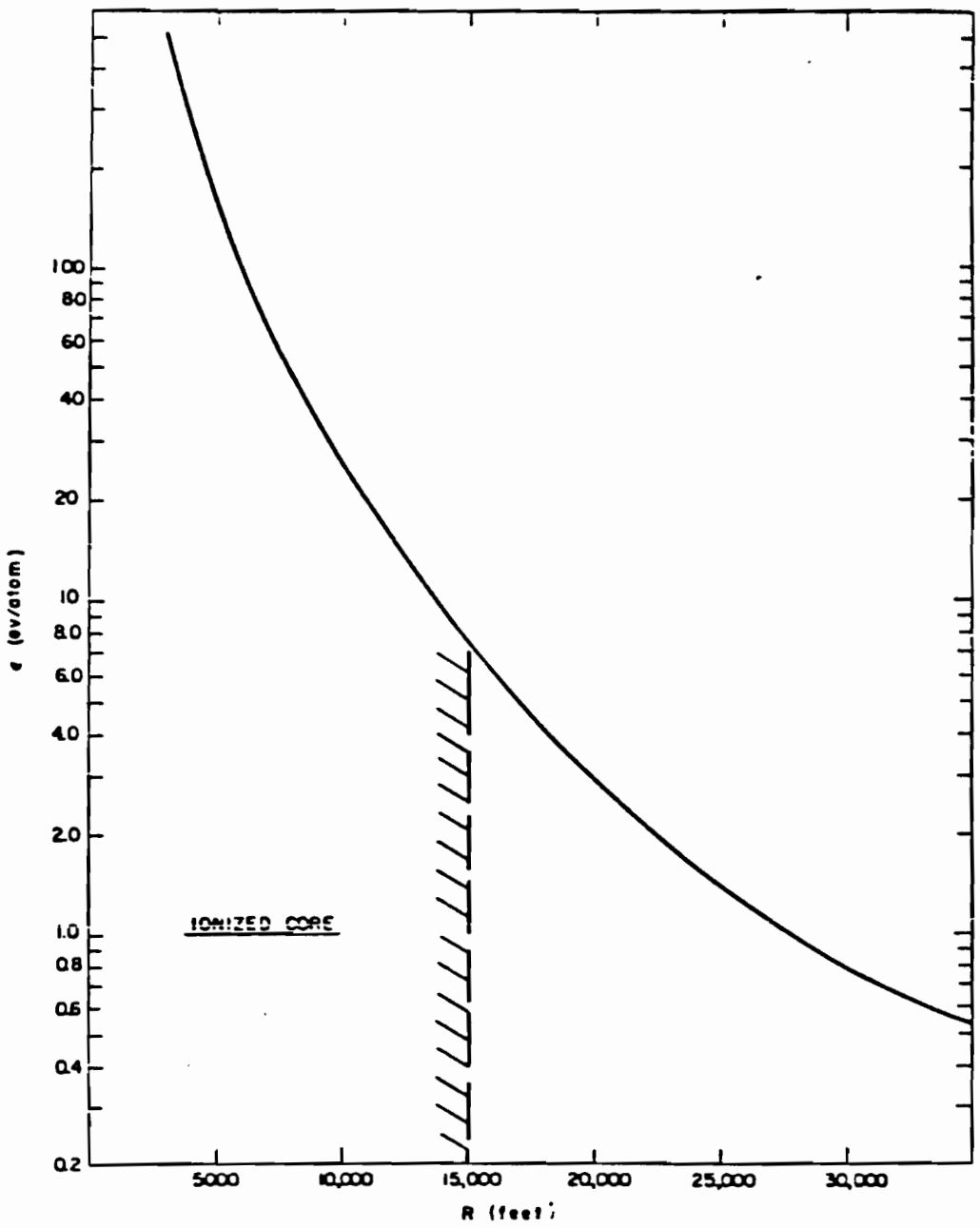

Fig. 11.1--Energy deposition versus radius from air zero.

[redacted]

fireball arises in this region and is caused by the radiative recombination of electrons and atomic ions such as $N^+ + e = N + h\nu$. Recombination time is about 10 msec. Since approximately one-half of the total deposited energy is contained in the core region, cooling time for the fireball is of the order of the recombination time.

In addition to recombination radiation from the core, there is some radiation caused by free-free (Bremsstrahlung) electron interactions in the field of the atoms of the core and some line emission from excited atoms. Hot bomb materials will also contribute in some degree to radiation from this region. Absorption of some of the radiation from the core in the outer "molecular" region gradually isothermalizes the fireball so that at about 5 msec the fireball is an approximate isothermal sphere of about 20,000 feet radius. The temperature at this time is about 10,000 degrees K. Because air at this temperature and pressure is quite transparent,[7] the inner portion of the fireball is observable, and the cooling rate decreases markedly.

[redacted] This energy is absorbed in a large region around the burst by photodissociation of oxygen molecules. Since recombination of neutral atoms to form molecules requires three body collision which are extremely rare at Teak altitude, dissociation of O_2 is essentially permanent, and this energy of the bomb is effectively wasted.

[redacted]

11.3 INSTRUMENTATION

As previously stated, quantities to be measured for the Teak and Orange events were: (1) absolute surface brightness in three narrow spectral bands,

[redacted]

(2) irradiance on the ground in three narrow spectral bands, and (3) bomb spectra versus time. Tables 11.1 and 11.2 give specific camera data.

11.3.1 Framing Cameras

Twelve cameras were centered on expected "air zero." Six 16-mm Fastax cameras at 4000 to 6000 frames per second provided a narrow angle of view. A second group of six 35-mm Fastax cameras at 2000 to 4500 frames per second covered a wider field. The Fastax, a high-speed camera of the rotating prism type, produces discrete frame images. With these cameras, an attempt was made to measure absolute surface brightness in three narrow spectral bands: 4000 A, 5000 A, and 6500 A.

11.3.2 Streak Cameras

Three 35-mm streak cameras were operated. These are essentially normal Fastax cameras except that the prisms have been removed, affording a continuous film transport mechanism with no framing compensation. The cameras were fitted with slits of the desired width to obtain necessary time resolution and exposure. Each slit was divided into four segments. To allow very wide exposure range, three segments accommodated effective neutral density 3, 2, and 1 filters, respectively. The fourth segment remained open, giving exposure at unity. The three cameras were fitted with narrow-band pass filters at 3500 A, 5000 A, and 6500 A, respectively. No lenses were employed with the streak cameras.

11.3.3 Recording Spectrograph

A Hilger 1-meter quartz spectrograph was used to record spectrum versus time during the initial phase of the detonation. A 10-inch focal-length quartz objective was used before the slit.

A film transport mechanism was designed and built to be accommodated by the Hilger instrument. Film width of 9-1/2 inches allowed complete coverage of the spectrum which is available for the spectrograph. The range of the instrument, 2000 A to 10,000 A, exceeds the spectral sensitivity range of the emulsion (Eastman Kodak Tri-X Arecon Panchromatic) used. Time resolution was about 16.7 μsec at 100 ft/sec. A reference marking light was employed to compensate for errors caused by film weave.

TABLE 11.1--TEAK CAMERA DATA

Camera		Lens: Focal length (inches)	Lens: Angular coverage, Vertical	Lens: Angular coverage, Horizontal	Narrow-band pass filter, peak wavelength (Å)	Wratten filter	Neutral density filter (effective density)	Lens setting (f-stop)	Film	Nominal recording rate (frames/sec)	Time of interest after zero (sec)
16-mm Fastax	1A	10	1.6°	2.2°	4000		4.75	8	DuPont 931	6000	0.6
	1B				4000		2.36	11		4000	1.0
	2A				5000	28	4.00	8		6000	0.6
	2B				5000	28	1.95	11		4000	1.0
	3A				6500	25	3.02	8		6000	0.6
	3B				6500	25	1.00	11		4000	1.0
35-mm 1/2-frame Fastax	4A	2	8.1°	25°	4000		3.38	16	DuPont 931	4500	0.6
	4B				4000		2.34	11		3000	1.0
	5A				5000	28	2.92	22		4500	0.6
	5B				5000	28	1.95	11		3000	1.0
	6A				6500	25	1.96	16		4500	0.6
	6B				6500	25	0.97	11		3000	1.0
35-mm Mitchell	7	1	35.9°	47.5°			4.00	8	Anscochrome	64	1 min
	8						2.00	11	931	64	5 min
	9							16		64	5 min
35-mm Fastax streak	10	Slit width, 0.0129 in.			3500		0.00 0.97 2.21 3.02		DuPont 931	150 ft/sec	0.6
	11	Slit width, 0.0139 in.			5000	28	0.00 1.01 2.03 3.12			150 ft/sec	0.6
	12	Slit width, 0.0124 in.*			6500	25	0.00 0.00 1.01 2.06			150 ft/sec	0.6
16-mm Fastax (4th ft)	13	1	10.4°	15°		19	Variable	5.6	DuPont 931	3000	6.0
	14					12		5.6		3000	6.0
Spectrograph	20	10 quartz	4×10^{-5}	2×10^{-3} rad				20	Eastman Tri-X Aerecon	100 ft/sec	1.0

*Except for channel 1 which was 0.110 inch.

TABLE 11.2--ORANGE CAMERA DATA

Camera		Lens: Focal length (inches)	Lens: Angular coverage: Vertical	Lens: Angular coverage: Horizontal	Narrow-band pass filter, peak wavelength (Å)	Kratten filter	Neutral density filter (effective density)	Lens setting (f-stop)	Film	Nominal recording rate (frames/sec)	Time of interest after zero time (sec)
16-mm Fastax	1A	10	1.6°	2.4°	4400		3.65	16	DuPont 931	6400	0.6
	1B				4400		3.65	8		4000	1.0
	2A				5000	98	3.07	16		6000	0.6
	2B				5000	18	3.10	8		4000	1.0
	3A				6500	25	2.10	16		6000	0.6
	3B				6500	25	2.11	8		4000	1.0
35-mm i/c-frame Fastax	4A	8	8.1°	65°	4400		2.65	16	DuPont 931	4500	0.6
	4B				4400		3.55	8		1000	4.0
	5A				5000	98	2.06	16		4500	0.6
	5B				5000	28	2.96	11		1000	4.0
	6A				6500	25	2.06	5.6		4500	0.6
	6B				6500	25	2.07	11		1000	4.0
35-mm Mitchell	7	1	35.5°	47.5°			2.00	11	Anscochrome	24	5 min
	8							16	931	24	5 min
	9							2.5		8	15 min
35-mm Fastax streak	10				3500		0.00 0.97 2.81 3.02		DuPont 931	125 ft/sec	0.8
	11				5000	98	0.00 1.01 2.03 3.12			125 ft/sec	0.8
	12				6500	25	0.00 0.00 1.01 2.06			125 ft/sec	0.8
16-mm Fastax (400 ft)	13	1	16.8°	22°			Variable	5.6	Anscochrome 931	3000	0.8
	14					12		5.6	DuPont 931	3000	0.8
Spectrograph	20	10 quartz	4×10^{-5}	8×10^{-3} rad				20	Eastman Tri-X Aerecon	100 ft/sec	1.0

[redacted]

Two 16-mm Fastax cameras, incorporating automatic exposure control, were used. These cameras, operated at 3000 frames per second, have a film capacity of 400 feet. It is characteristic of this mechanism to orient and follow after approximately 100 μsec. The initial filter setting is made for adequate exposure during the first 100 μsec. Additional to evaluation of the exposure control system, resulting film records were intended to provide early-time radii versus-time data as well as documentary coverage.

11.3.4 Mitchell Cameras

Three Mitchell 35-mm high-speed motion picture cameras were located at the camera station on Johnston Island. Anscochrome color film was used. Generally, emphasis was on radii versus time and later time phenomena, in addition to qualitative or documentary coverage. These cameras afforded a wide field of view (approximately 36 by 48 degrees).

For the Orange event, three off-site Mitchell 35-mm motion picture cameras were added. Two cameras were located at French Frigate Shoals and one was placed aboard the USS Boxer. Prime interest was in very late-time, large-scale phenomena. Here also, Anscochrome color film was used. These cameras were intended to provide qualitative data only.

11.3.5 Ballistic Plate Cameras

Two ballistic plate cameras, especially designed for obtaining positioning data on 10- by 12-inch sensitized glass plates were used. Four sets of fiducial marks were exposed on the plate for accurate and repeatable reference. Lens focal length on these cameras is 12 inches. To assure precise positioning, the ballistic camera incorporates a mount for location of a theodolite directly over the nodal point of the lens. One camera was located at the west end of Johnston Island and the second was established on Sand Island to obtain as long a base leg as possible.

An explosive capping shutter was designed to close while the mechanical shutter was still in its much slower process of closing. Exploding the charge was accomplished by a photocell-controlled circuit triggered by the first light of the test detonation. Effective closing time was approximately 250 μsec.

[redacted]

[redacted]

11.3.6 Timing Reference

One-hundred-cycle time marks were placed on film records in the Mitchell cameras and one-thousand-cycle timing was supplied to all other high-speed cameras and the spectrograph in the Johnston Island camera station. A simple time mark generator was used with the Mitchell camera (slow-speed) aboard the USS Boxer. It provided one time mark approximately every 7 seconds. This camera was used during the Orange event only.

Sync marks were placed on all film records in the Fastax cameras during the Teak and Orange events. These were supplied through two sync mark generators, each triggered by a photocell which was actuated by the first light of the detonation. During calibration of these generators, a delay of approximately 60 μsec was experienced between the first visible light from an electronic flash lamp and actual lighting of the neon flow lamp.

11.3.7 Filters

Metal interference filters were used for the narrow-band pass filters. These were generally second-order filters characterized by a width of half-peak of 100 A and a base width of 1000 A. With the 5000 A and 6500 A filters it was necessary to use Wratten gelatin filters to suppress unwanted bands. Figure 11.2 shows transmission curves of the narrow-band pass filters combined with the Wratten filters where the combination was used. These curves are measured with approximately the same angular spread (5 degrees) in the light as was present in the field. The so-called neutral density filters (Wratten No. 96) were calibrated at the wavelength used. Tables 11.1 and 11.2 give this effective neutral density for the filters used.

11.3.8 Film Recording

The quantitative measurement of light intensity using photographic emulsion requires establishment of known relationships between exposure and resulting density produced in the developed emulsion. The reader is referred to accepted sources such as Mees[10] or Jones[11] for a more complete discussion of the general problem. A thorough discussion of film and camera calibration techniques and data reduction methods for this project is given in a report by Palmer.[12]

[redacted]

Light transmission, T, of a developed film generally decreases with increased exposure. Density, D, of a film is defined as $D = \log_{10}(1/T)$. Figure 11.3 shows a typical relationship between D and the exposure, E. Evident are the toe, a more-or-less straight-line portion, and the shoulder of the curve where the density reaches a limiting value. The relationship between D and E is somewhat sensitive to the wavelength of light used. The reciprocity law (which states that density depends only on total exposure, $E = It$, and not intensity, I, or time, t) holds fairly well for exposure times of interest, 7 to 200 μsec. Film calibration procedures accounted for the wavelength and reciprocity variations. D-log E calibration curves were obtained by exposing the film in modified Fastax streak cameras using the various narrow-band pass filters and several slit widths. The sun was used as a source. Its intensity, after passing through the filter, was measured with a black-body receiver (Eppley thermopile). All film was from the same emulsion number; new calibration films were made at the test site and received the same handling, storage, and developing as the record films. As a relative processing control, sensitometer step wedges were included at the beginning and end of each roll of film. These were exposed on an EG&G MK VI sensitometer at 10^{-4} sec. Figure 11.4 shows typical D-log E curves for the four wavelength regions passed by the filters.

11.4 RESULTS

Curves plotted from control wedge densities indicated that processing was reasonably constant for any one roll of film (Fig. 11.5), but was not as consistent as would be desired from film to film. These differences made direct comparison of test records and calibration records inadvisable. In addition, the step wedge densities do not extend to as high densities as the actual records. To make the data meaningful, a method for obtaining a density-versus-relative-exposure curve was developed which used only the control step wedge densities, the known exposure difference between the four separate channels on each streak record, and the density versus time of these records. The absolute scale was obtained from calibration records. This method is described in detail in Palmer's report.[12] In brief, for the calibration film, the average gradient over an exposure interval of 1.5 log E units is taken so that the line through the end points is tangent to the D-log E curve at the toe end (Fig. 11.2). The intersection of the extension of this line with the exposure

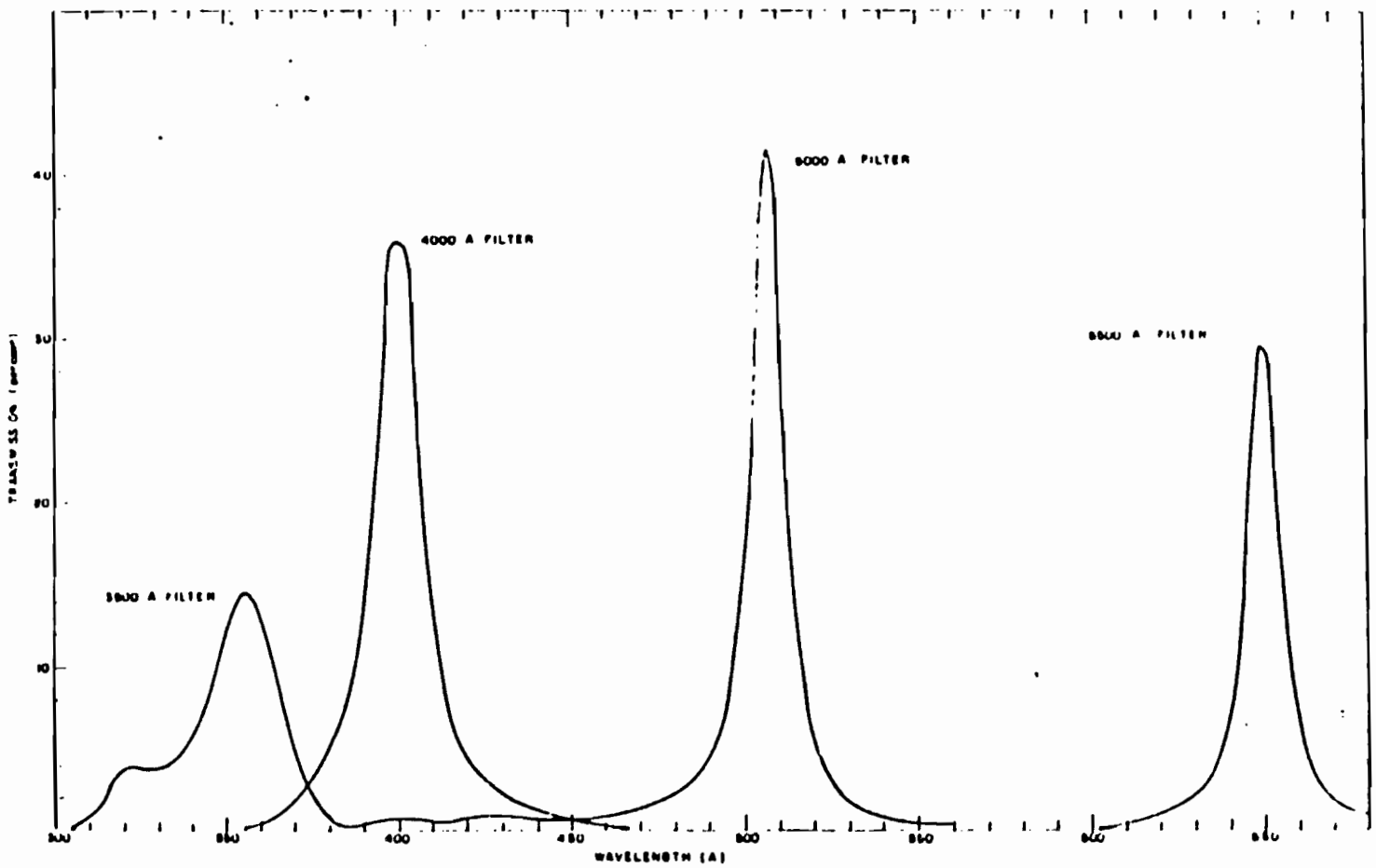

Fig. 11.2--Filter transmissions, typical λ.

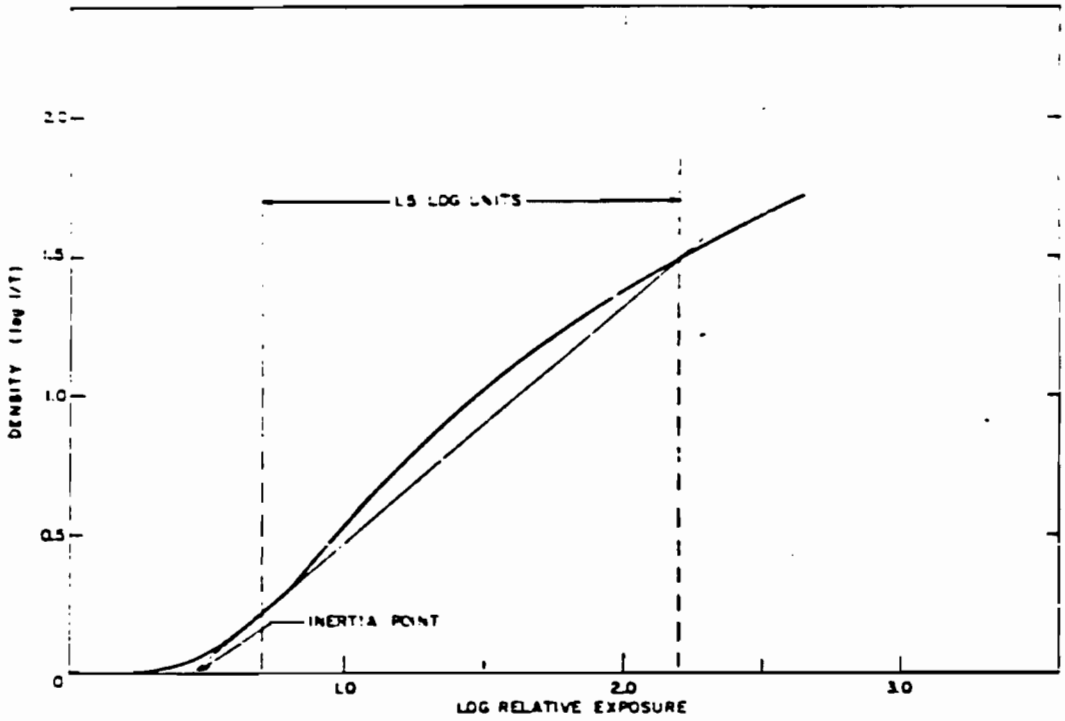

Fig. 11.3--Typical density-exposure curve showing position of inertia point.

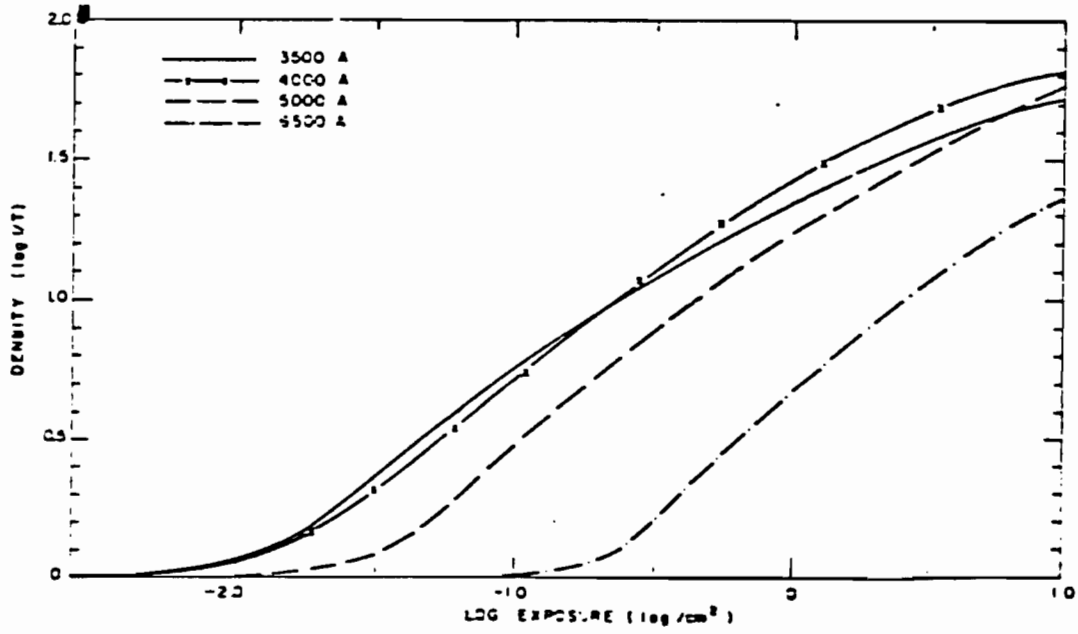

Fig. 11.4--Density-log exposure versus wavelength.

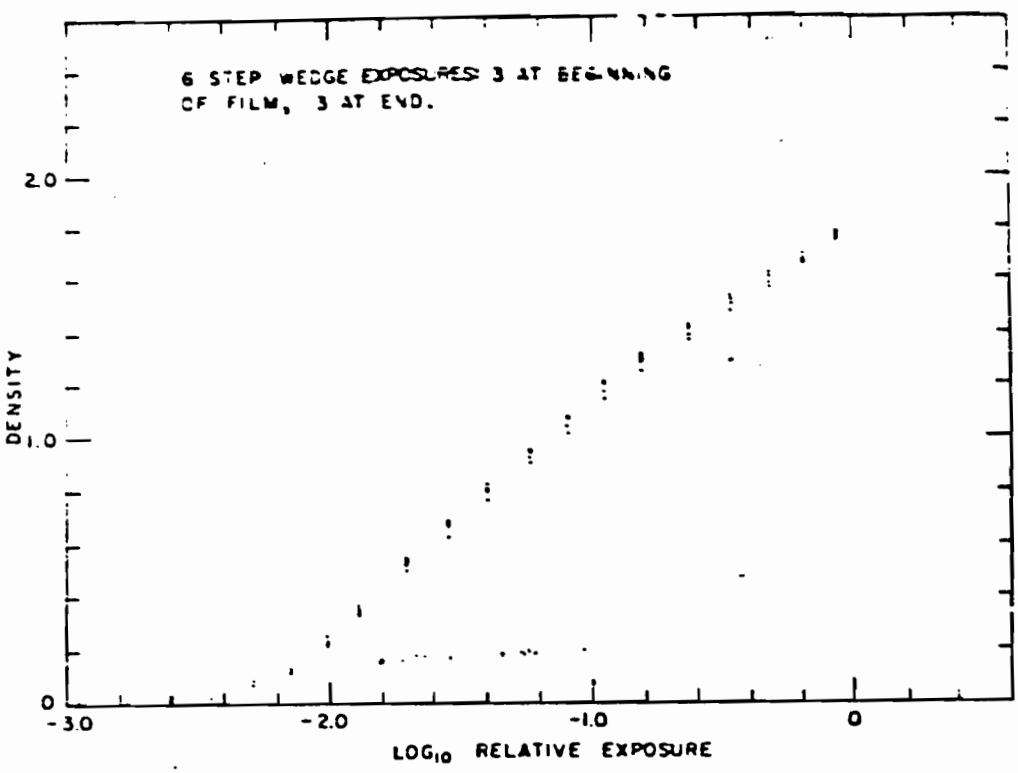

Fig. 11.5--Control step wedges, film T-11.

axis is called the inertia point. It is found that the inertia point position is quite insensitive to variation in development processing. The inertia point from the calibration film was therefore used to place an absolute energy scale on the D-log E curves obtained as follows. The exposure ratio between any two channels of a streak camera is known from the relative filter transmissions. Thus at any fixed time, four points on a density-versus-relative-exposure curve are obtained. By going to other times, other groups of points can be obtained, and thus a complete curve can be built up. It was found that data from channels with minimum exposure (and to a much smaller extent the one with the next greater exposure) did not fit well with the higher density channels. Subsequent laboratory tests have shown that there is sufficient scattering in the film and camera to cause a distortion of the channels which have been attenuated factors of 100 to 1000 as were the two least dense channels. Therefore, only data from the two most dense channels on each film were considered reliable and used in subsequent analysis. The autocalibrated curves

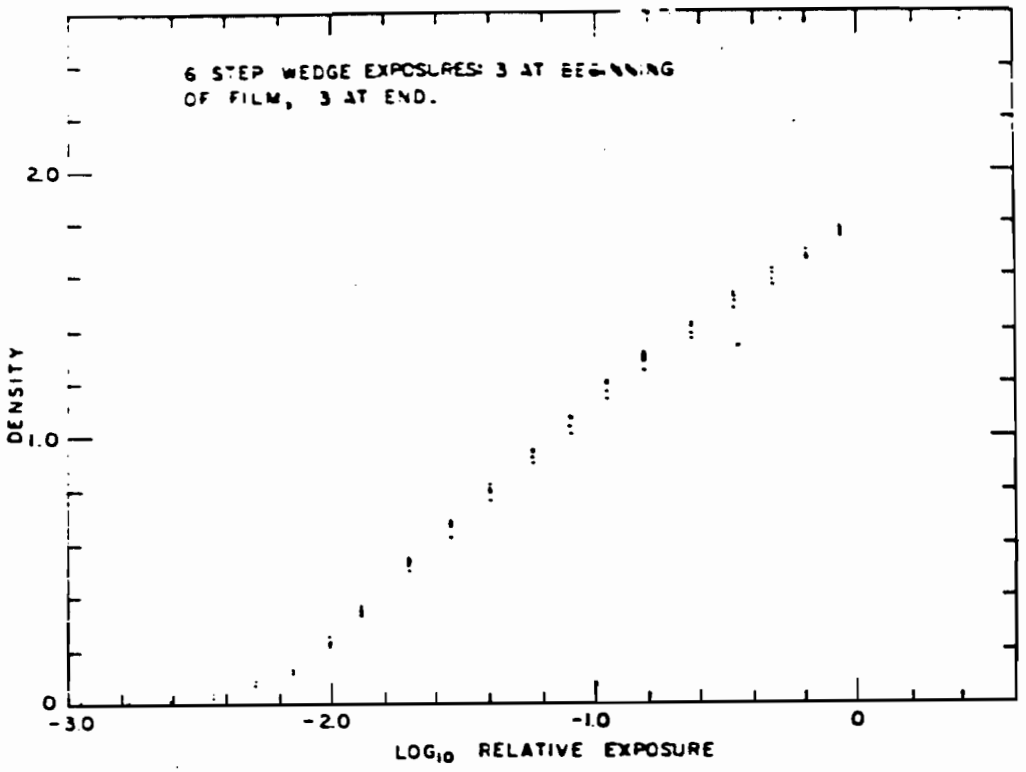

Fig. 11.5--Control step wedges, film T-11.

axis is called the inertia point. It is found that the inertia point position is quite insensitive to variation in development processing. The inertia point from the calibration film was therefore used to place an absolute energy scale on the D-log E curves obtained as follows. The exposure ratio between any two channels of a streak camera is known from the relative filter transmissions. Thus at any fixed time, four points on a density-versus-relative-exposure curve are obtained. By going to other times, other groups of points can be obtained, and thus a complete curve can be built up. It was found that data from channels with minimum exposure (and to a much smaller extent the one with the next greater exposure) did not fit well with the higher density channels. Subsequent laboratory tests have shown that there is sufficient scattering in the film and camera to cause a distortion of the channels which have been attenuated factors of 100 to 1000 as were the two least dense channels. Therefore, only data from the two most dense channels on each film were considered reliable and used in subsequent analysis. The autocalibrated curves

[redacted]

matched well with the control-step wedge curves in the region of overlap, and together give a density-versus-exposure curve over the entire range of interest.

Table 11.3 summarizes results obtained from photographic instrumentation.

11.4.1 Framing Camera Data

Good quality high-speed framing camera data are lacking for both shots. The loss in the case of Orange is due to cloud cover at shot time which obscured the burst from the ground. Burst position error caused the loss in the case of Teak. Although exposures were obtained on the narrow field records, the fireball is not included in the frame. Exposures obtained presumably represent light from the fireball which was scattered into the field of view by atmospheric haze. While the scattered light is, in fact, data, an attempt to carry out an analysis has not been made. This same consideration applies to exposures from the wider angle framing cameras. These include a small portion of the fireball near the edge of the frame. The Fastax shutter action is such that this is the portion for which the exposure is uncertain. Radius-time data from these cameras add very little to data obtained from the wide-angle color records. Because of loss of the 3500 A record on Teak it was believed useful to attempt to secure relative exposure for the 4000, 5000, and 6500 A bands for the first 10 msec from these records. This requires only the assumption that exposure reduction caused by shutter action is the same for all wavelengths.

The color framing cameras provided excellent qualitative and quantitative data about the fireball structure up to about 3 seconds for Teak (Figs. 11.6 and 11.7). In addition, a few frames demonstrate the aurora emanating northward from the bomb debris as a source. Of course, because of the cloud cover, no data of this kind were obtained for Orange. A Mitchell camera aboard the USS Boxer provided excellent coverage to several minutes after detonation for the Orange event (Fig. 11.8). Two additional Mitchells located at French Frigate Shoals produced no significant data. This was at least partly attributable to cloud cover.

11.4.2 Streak Camera Records

Except for the loss of one (film breakage, 3500 A, Teak), the streak camera records are the most reliable quantitative data obtained on both Teak and Orange. The data obtained are of good quality out to about 700 msec.

[redacted]

Pages 348, 349, and 350 are deleted.

TABLE 11.3--DATA SUMMARY

Instrument	Type data	Success of data obtained: Tesh	Success of data obtained: Yucca
Recording spectrograph	Bomb spectra versus time	Saw Teller light only because of burst position and narrow angle of view. Record seriously damaged by light leak in film transport system	Exposure reduced because of cloud cover. Data not significantly useful. Record seriously damaged by light leak in film transport system.
Narrow-angle Fastax	Absolute surface brightness of fireball versus time	No data due to erroneous shot position. Three most heavily exposed records show overall density, frame by frame, which decreases versus time. This is very probably light scattered into field of view by lower atmosphere. Narrow angle of view completely missed fireball.	No data because of cloud cover. One camera jammed and failed to complete its run.
Wide-angle Fastax	Absolute surface brightness of fireball versus time	Cameras recorded only a small portion of fireball because of erroneous shot position. Image lies near frame edge where its density is affected by Fastax prism "shutter action."	No data because of cloud cover.
Streak Fastax	Irradiance (on ground) versus time	Good data obtained at 5000 A and 6500 A peak wavelengths. Camera at 3500 A peak wavelength broke film at initiation of run and did not record.	Records obtained at 3500 A, 5000 A, and 6500 A peak wavelengths. Data of lessened value because of cloud cover.
Variable-filter Fastax	1. Radii versus time 2. Qualitative data (documentary)	No data after approximately first 20 frames. Filter mechanism lagged seriously. Just over one-half of fireball in frame because of erroneous position of burst.	No fireball data because of cloud cover. Because of difference in light decay time for Orange, filters followed more correctly.
Mitchell cameras (Sta. 3-62)	1. Radii versus time 2. Qualitative data (documentary), late time	Excellent data for radii and shock velocities from approximately 15 msec to late time, as well as good documentary coverage in color.	No fireball data because of cloud cover. Cameras recorded brightness in clouds and a few rocket trails
Off-site Mitchell cameras	Qualitative data (documentary), late time	(Used on Orange shot only.)	(a) Two cameras at French Frigate shoals gave no significant data. Only a few frames were recorded by each camera. Failure was at least partly attributable to cloud cover. (b) Camera aboard USS Sumner provided excellent late time data, which were recorded and time-correlated.
Ballistic rate cameras	Shot position	(a) One camera recorded excellent data (Sand Island). (b) One camera shutter failed (Johnston Island). No data.	Image recorded by both cameras. Because of cloud cover and resultant diffuse images, accuracy of data seriously limited.

Because of uncertain transmission through the cloud layer, absolute irradiances measured for Orange are probably of lessened interest; relative spectral irradiances are also degraded by uncertainties in the spectral dependence of cloud transmission.

11.4.3 Spectrography

The spectrograph was, for both shots, directed toward air zero. Because of the Teak burst error, the very narrow field of the spectrograph did not include the fireball proper. The spectrographic record does show a distinct Teller spectrum as outlined below. For Orange, the cloud layer seriously reduced exposure, so that little data are discernible. A light leak in the film transport mechanism seriously fogged film records for both shots, making an estimate of continuum radiation, for example, very difficult.

11.4.4 Automatic Exposure Camera Results

Teak films from the automatic exposure control cameras show a few good early frames. Because a greater part of the luminescence was over in so short a time, the filter mechanism followed late, resulting in gross underexposure. Due to erroneous shot position, only a portion of the fireball was within the field of view. Because of cloud cover during the Orange event, initial phases of the detonation were underexposed. At later time, the images are diffuse, again because of clouds, but exposure is more nearly correct. This would seem to indicate that the filter mechanisms functioned properly. However, minimal data recorded during both Teak and Orange is not considered significant.

11.4.5 Ballistic Plate Camera Results

During Teak, one ballistic plate camera recorded excellent data. A shutter failure occurred with the second camera and no data were obtained. Both cameras functioned during Orange, but because of the cloud cover and resultant diffuse images, accuracy of the data is seriously limited.

11.5 IRRADIANCE MEASUREMENTS

11.5.1 Teak Measurements

Figure 11.9 shows data from the narrow band-pass filter streak cameras. The irradiance is that incident on the camera, having had no atmospheric

Page 353 is deleted.

attenuation correction applied. At the measured wavelengths this would be a small correction and nearly the same for both channels. Transmissions of the narrow band-pass filter were calculated for a 1-ev black-body source; however, temperature is not an important factor here. The fraction of the black-body radiation in the band pass that is transmitted by the filter varies only 3 percent while the temperature varies from 0.3 to 20 ev. Figure 11.10 shows surface brightness versus time taken from the framing camera records that saw only the edge of the fireball. The brightness is taken at a point about 1 km from the edge. Again no correction has been made for atmospheric transmission, and the absolute scale is uncertain because of the approximate nature of the correction for camera transmission near the frame edge.

Fig. 11.10--Surface brightness of Teak fireball near edge.

[redacted]

Several gross features are immediately obvious. [redacted]

As an indication of decay rate at different times, streak records may be analyzed as a sum of exponential decays. Although this type of analysis is admittedly arbitrary and somewhat ambiguous because of experimental uncertainties, it may nevertheless be instructive, pointing up similarities and differences at the two wavelengths. [redacted] Table 11.4 gives decay constants found in this manner as well as extrapolated intensities at burst time. Intensities at small times, of course, do not actually approach extrapolated values for very short decay times. The decay of intensity versus time is qualitatively consistent with predictions, although details do not give quantitative agreement. A curve calculated from LAMS-2453[9] monochromatic contours is shown on an arbitrary scale for comparison. [redacted]

TABLE 11.4--EXPONENTIAL ANALYSIS OF TEAK

[redacted]

[redacted]

[redacted]

Filter transmissions were calculated for a 1-ev black-body spectrum for the wavelength intervals 4450 to 5470 A and 6130 to 6650 A. The integral of energy incident on the cameras was then calculated and is shown in Fig. 11.11.

[redacted]

Fig. 11.11 Energy versus time, Teak shot.

Figure 11.12 shows the calculated ratio of the irradiances of 6500 A and 5000 A versus temperature of the fireball based on a black body and on the calculations given in LAMS-2453.[9] This latter calculation neglects line emission.

[redacted]

Pages 357 + 358 omitted.

[redacted]

From Fig. 11.15 it can be seen that the light is emitted from an effective sphere [redacted] This radius and a height of burst of 250,000 feet are used to calculate the irradiance on the ground (1) for black-body emission, and (2) for emissivities from LAMS-2453.[9] These are shown in Figs. 11.16 and 11.17 for 5000 A and 6500 A, respectively. Experimental curves shown in these graphs are obtained from measured irradiances (Fig. 11.9) and inferred temperatures (Fig. 11.14). [redacted]

11.5.2 Orange Measurements

Results of streak records at 3500 A, 5000 A, and 6500 A are shown in Fig. 11.18. As before, I represents irradiance of the film plane in watts/cm^2 A. [redacted]

[redacted]

Pages 360 through 365 are deleted.

[redacted]

11.6 FIREBALL RADII

Various radii observed as a function of time from color camera records are shown in Fig. 11.15. The bright fireball proper, observed as a distinct bright disc from the ground, is referred to in the illustration as the X-ray sphere. [redacted]

11.7 SPECTROGRAPHIC DATA

11.7.1 Teak Data

As described previously, the spectrograph was aligned toward the planned burst point. Because of error in the point of detonation, the actual line of sight passed through a point 28,000 feet south of air zero at 250,000 feet. Although light leakage present seriously exposed the film, the film record indicated [redacted]

[redacted]

[redacted]

The record was analyzed by means of a JACO recording microphotometer. A typical trace over a portion of the spectrum is shown in Fig. 11.20. It is seen readily that the spectrum is made up of molecular band emission. The observed wavelengths of several prominent bands have been noted. The poor quality of the trace is due in part to the light leak on the film.

Results of a complete identification are summarized in Table 11.5. The

[redacted]

3

Time histories of several prominent bands were found by obtaining microphotometer traces along the film time axis. Results are shown in Fig. 11.21. The time origin in each case was arbitrarily selected as the time (on the film record) at which detectable density was recorded. Because of the limited time resolution (17 μsec) of the spectrograph, this time does not correspond necessarily to actual zero time for light reaching the ground along the line of sight. The ordinate is the approximate film exposure as obtained from the characteristic curve and an estimate of the film sensitivity. Because of uncertainty in the film spectral sensitivity, relative exposures of the various bands are accurate to only about 50 percent. The absolute exposure at any one wavelength is certain within less than an order of magnitude.

A more complete discussion of this time dependence is given by Proud,[16] where it is shown that the time dependence is approximately accounted for by the light transit times from various positions along the line of sight.

11.7.2 Orange Data

Because of combined effects of light leakage and cloud cover, spectrographic data for shot Orange was not very useful. A continuum was apparent, however, in which were seen some of the O_3 absorption bands. The quality of the record does not warrant an analysis of the type carried out in the case of Teak.

[redacted]

Pages 368 through 370 are deleted.

[redacted]

11.8 RECOMMENDATIONS

For instrumentation of future high-altitude detonations, these several recommendations are offered with the intention of procuring more complete data.

11.8.1 Photoelectric Recording

The possibility of using photomultipliers for absolute measurements of radiant energy as described in this report warrants consideration. The certainty of calibration, relative simplicity of data reduction, immediacy of data, and the ease of handling this type of equipment in the field are inviting qualities, indeed.

11.8.2 Diameter versus Time

The use of high-speed streak cameras with lenses is recommended to record high-resolution diameter versus time. A writing speed of 150 ft/sec to 200 ft/sec, in combination with a narrow slit (0.002 inch), could obtain time resolution of the order of 1 μsec.

11.8.3 Motion Picture Coverage

The use of several high-speed 35-mm motion picture cameras in the range of 1000 to 2000 frames/sec is suggested for more adequate early-time color photographs. Instrumentation should continue through a range of cameras to equipment of the "pulse" type which could record extreme late-time phenomena.

REFERENCES

1. Bethe, H. A., Some Phenomena in High Altitude Explosions, LA-2164, Los Alamos Scientific Laboratory, December 11, 1957.
2. Mayer, H. L., Early History of High Altitude Nuclear Explosions, AFSWC-TR-57-16, Air Force Special Weapons Center, May 31, 1957.
3. Brode, H. L., and Gilmore, F. R., Estimates of the Thermal Radiation from Nuclear Weapons Burst at High Altitudes, RM-1963, RAND Corporation, September 1957.
4. Brode, H. L., and Meyerott, H. E., Thermal Radiation from Atomic Detonations at Times Near Breakaway, RM-1651, RAND Corporation, August 1956.
5. Proceedings of the High Altitude Symposium, January 27-28, 1958, ORO-SP-3, Operations Research Office, Johns Hopkins University, May 1958.

[redacted]

6. Diesz, G. H., The Spectroscopy of Some Explosives, LA-1[illegible], Los Alamos Scientific Laboratory, August [illegible], 1[illegible].

7. Sivel, B., and Bailey, K., Tables of Radiation from High Temperature Air, AVCO-RR-21, AVCO Research Laboratory, December 1957.

8. Oberlin, H., et al., Teak Phenomenology, LAMS-2417, Los Alamos Scientific Laboratory, May [illegible], 1960.

9. Simmonich, A., Teak Fireball Formation, Radiative Growth and Brightness History, LAMS-2453, Los Alamos Scientific Laboratory, June [illegible], 1961.

10. Mees, C. E. K., The Theory of the Photographic Process, Revised Edition, The MacMillan Co., New York, 1954.

11. Jones, L. A., Measurements of Radiant Energy with Photographic Materials, Chapter VIII, Measurement of Radiant Energy (Forsythe, W. E.), pp. 246-[illegible], McGraw-Hill Book Co., New York, 1937.

12. Palmer, M. A., Photographic Instrumentation for Teak and Orange Events, SCTM 130-61(51), Sandia Corporation, April 1961.

13. Hansen, D. F., Perry, J. E., and Rockman, A. G., Power-Time and Total-Thermal Measurements, Operation Hardtack, WT-1650, Naval Research Laboratory, August 1960.

14. Parker, W. J., Jenkins, R. J., and Ian, E. C. Y., Early-Time Spectra of Very-High-Altitude Nuclear Detonations, Operation Hardtack, WT-1650, Defense Atomic Support Agency, June 1960.

15. Pearse, R. W. B., and Gaydon, A. G., The Identification of Molecular Spectra, John Wiley and Sons, Inc., New York, 1950.

16. Proud, J. M., Jr., Teak Teller Light, SCTM 50-59(51), Sandia Corporation, Albuquerque, New Mexico, March 6, 1959.

Chapter 12

CONCLUSIONS AND RECOMMENDATIONS

Teak and Orange shots are only the opening rounds of many which will be required before adequate understanding is achieved of nuclear burst outputs and of their interaction with the ambient environment above 100,000 feet.

Recommendations and conclusions are included in each of the separate chapters and represent the views of the individual authors. Many of the particularly puzzling items which remain unsolved are gathered together in Chapter 1 and will not be restated here.

There are broad regimes of potentially important phenomena which are yet almost completely undocumented experimentally and which require bursts at altitudes above 100 kilometers. As a general recommendation, any well-instrumented and well-planned burst at an altitude of 100 kilometers (350,000 feet) or higher would be extremely valuable in providing facts and understanding of the physical phenomena produced by burst outputs and of the potential application of these outputs.

Many engineering, scientific, and operational problems were met during the tests covered by this report which had never been encountered before in nuclear testing. If the United States plans to develop a capability to do rocket-borne delivery and diagnostics on nuclear device tests, a continuous, long-term effort must be established in order to efficiently meet the challenge of these unique test requirements.

[redacted]

Appendix A

EYE-WITNESS ACCOUNTS OF TEAK AND ORANGE BURSTS

A.1 TEAK OBSERVATIONS by T. B. Cook, Jr.

This is a narrative description of Teak burst as transcribed on August 19 from rough notes made the morning after Teak burst.

Teak was detonated July 31 at 23:30 Johnston Island Time. The original schedule called for detonation at 22:00 Johnston time. The first delay of about one hour was because of trouble in telemetry from two of the Redstone pods assigned to neutron measurements. There was another slight delay to adjust the telemetering on the pods.

The view which we had as observers was from the USS Boxer, an aircraft carrier located 50 miles to the north of Johnston Island. For three or so minutes before burst time Johnston Island looked as though the natives were celebrating the Fourth of July. The Redstone rocket stood out from all others by its long steady glow, similar to a cool meteor moving slowly but surely upward. We were instructed not to look at the burst and to have long clothing covering all of the skin area. After burst we turned toward the burst and took off our dark glasses. Within three seconds after detonation our glasses were removed and the most obvious thing in the sky was a dazzling, large, yellow core. Surrounding the yellow core was a bright, intense bluish glow. Overhead, and slightly to our right, were long purplish-red streaks--auroral streamers--extending on over us to the north. One could not observe any auroral streamers going to the south. One of the first things that impressed you when you took off your glasses was the faint, red glow which was all around and extended down to the horizon for a full 360 degrees around our observation point.

The moon was full and well above the horizon about 35 degrees and, in spite of the full moon and rather light background which we had before the burst, the intensity of the illumination for many seconds, even minutes, after the burst was very pronounced. Even 10 minutes after Teak one could

[redacted]

have read a description with [illegible] Part [illegible] this was [illegible] to the fact that the moonlight was rather distinct. However, [illegible] rate one would say at 10 minutes the glow from Teak was still equal to the glow from the full moon. Teak was burst only one day after full moon. The large reddish-purple streamers which extended to the northeast had a distinct terminus. There were finger-like projections on the northern end of the aurora and these finger-like projections continued to grow apparently toward the ground as time went on, and they grew for more than a minute after the Teak detonation. Within a few tens of seconds after burst, the intense blue glow in the area of the burst disappeared and the sky was filled then with the very yellow central core which remained behind and the large aurural streamers running to the northeast.

Immediately after our glasses were taken off, one could see a doughnut-shaped white cloud which mushroomed out from the burst point, grew larger and fainter and by one minute was pretty much invisible. There were no sounds heard which could have originated from the ozone layer and would thereby have taken something like 120 seconds or so to reach the Boxer. At that time no sounds were heard. However, aboard the Boxer and also on Johnston Island there was a sharp crack heard at zero time. On the Boxer we had speculated that there was an electromagnetic signal injected into the [illegible] system; however, since the crack was also heard on Johnston, there was apparently some sound, a sharp, low-intensity crack at zero time. The primary shock wave arrived at the Boxer at about 6 minutes; its amplitude was about 0.06 psi and it indeed startled everyone, since most people had expected no acoustic disturbance from Teak. The auroral phenomena stabilized within a few minutes after burst. The bright yellow core continued to grow whiter as time went on, and it appeared to remain fixed in the sky. The aurora became less distinct and sharp streamers diffused out. It was apparent that the source of the auroral phenomena was the burst point. There had been speculation that auroral phenomena might be produced by neutron decay from neutrons which had gone many thousands of feet into the atmosphere and decayed naturally with 13 minutes half life, into protons and electrons. This was apparently not the source of the auroral phenomena which were observed. At about 11 minutes after burst everyone was in the midst of many wild speculative discussions attempting to explain the aurora and the very long intensity of illumination which had been observed, the intense sound wave, and so forth. At this time everyone was amazed to find, in

[redacted]

looking up to the sky, that there was a circular streak which originated at the burst point in a very sharp luminous front. It was brilliant initially but seemed to turn reddish and fade away as it moved out from above the burst area. Explanation of this phenomenon has not yet been satisfactorily made, although it is quite possible that this was a hydrodynamic shock propagated up into the atmosphere to such a point that the shock strength had increased to that required to produce radiation from the shock front. Between 10 and 15 minutes we began to see some very unusual white clouds form in a northeasterly direction. They were very spotty and patchy, and they grew with time; that is, more patches appeared. They also seemed to glow or luminesce and were far to the north. People were speculating that this was caused by debris from the bomb that had been ejected up into the atmosphere to such an altitude that sunlight, even though it was almost midnight in time, was illuminating the debris. Some observers who happened to wander up to the deck four hours after Teak detonation reported there was still at that time a visible, but very faint, red glow covering the sky, and that the glow had relatively intense streaks running in an east-west direction across the sky. The yellowish, very persistent core which stayed relatively fixed in space has not yet been explained. It looked like it was about 15 moon diameters.

An estimated 10 percent of the birds on Sand Island (a bird refuge) were killed; many others had scorched wings. The morning after burst there were many birds sitting out on the water. Their wings were soggy with water, whereas ordinarily their oily protection keeps them from getting wet. The birds appeared to be blinded; they would not fly when you came up to them. They would even walk right up to you on Johnston Island, not run from you as they usually did.

A.2 ORANGE OBSERVATIONS by T. B. Cook, Jr.

This is a description of the Orange detonation of Operation Hardtack transcribed on August 19 from rough notes made within two hours after observation of the Orange burst. Orange was detonated at 23:30 Johnston Island Time, August 11, 1958. The observation point was from aboard the USS Bover, an aircraft carrier, which was 50 miles north of Johnston Island. The scheduled burst point for Orange was about 25 miles south of Johnston and at an altitude of about 25 miles. There were many delays on Orange and, from early which

[redacted]

[redacted]

have been passed around, the delays were apparently uncalled for. It suffices to say that by the time the burst actually took place, clouds were obscuring the view from the Boxer, and also the view was obscured from Johnston Island. It was almost a minute after detonation before we began to get a distinct view of the Orange phenomena above the cloud cover. At about two minutes we made estimates of the debris diameter which indicated that the doughnut-shaped, white debris cloud must have been 30 miles or so in diameter.

When the fireball first began to appear above the clouds there was a reddish glow all around it, but at that time there were no aurorae. The glow was more or less uniformly distributed around the cloud. Shortly before two minutes after the burst we began to see some auroral streamers start to grow. This was about the time expected for this phenomena after much discussion of Teak aurorae. The streamers were very diffuse compared to those of Teak, but there were about four streamers running toward the north an estimated distance of three to four fireball diameters--not nearly as far as Teak nor as intense nor as well defined. By two minutes one could see through the clear hole in the white doughnut and also see aurorae extending out to the south very clearly. It seemed from the Boxer that the aurorae could not have extended more than about to Boxer distance from the burst, or about 75 nautical miles. At about three minutes after burst there was a large, clear hole inside the whitish doughnut from Orange and a small, red cloud puff appeared, very small and distinct; shortly thereafter, a very transient white cloud appeared. Its nature was somewhat similar to those which we had seen at 10 to 15 minutes after Teak burst. It was very transient in nature and seemed to glow and luminesce just like the Teak clouds, but it disappeared within a minute or so. By five minutes the edge of the doughnut appeared to be about over the Boxer, a tremendous thing, with a large, clear hole in the center. Through this hole at five minutes, we began to see some turbulent, high-velocity motions, apparently very high up in the atmosphere, also somewhat similar to the Teak burst.

A distinct front, probably a shock front, moved out from within the doughnut. At seven minutes after detonation the primary shock wave arrived at the Boxer. It was a muffled shock compared to that of Teak. After the first shock arrived, there continued to be a barrage of muffled sounds, as though one were near a distant battle field. These sounds must have numbered between

[redacted]

[redacted]

50 and 100 and, even at 15 minutes after Orange, there was a very distinct boom.

Some people claim they heard these sounds as late as 20 minutes after detonation. At 10 minutes after burst one could easily read a newspaper from the light from Orange detonation, although the aureal display was almost gone and diffused out to where it was very dim and indistinct. At nine or ten minutes there were also still some rapid motions taking place in the upper atmosphere--very turbulent processes taking place near the center of the large doughnut. By 30 minutes after Orange--and Orange was detonated on a dark night--the lighting produced by the residual glow in the atmosphere would be estimated to be equivalent to that of a half moon. It was still possible to read a newspaper, but you would consider it poor lighting.

Again, within an hour after Orange, a heavy rain set in. There has been a lot of speculation as to whether Orange and Teak had anything to do with the rains which occurred after both bursts.

All in all, the Orange detonation was not as spectacular as Teak. All indications were that the Orange burst point was in the proper place, although in Teak the Redstone apparently went straight above Johnston Island. No birds were injured at the Sand Island refuge. There was a very effective smoke screen over Sand Island, although, in view of the very intense clouds which apparently cut down the amount of light transmitted to about six percent of that which would have gotten there on a clear night, the smoke screen was not needed to protect the birds.

A.3 TEAK OBSERVATIONS FROM FRENCH FRIGATE SHOALS by H. E. Bell

At zero time, of course, I was inside the timer house at the Loran station in order to give a zero-hour time hack, etc.; but at zero, even though the light was on in the room, I could see out of the corner of my eye that the whole room took on an instantaneous bright glow. Then I took a fast glance outside; the whole airfield looked a brilliant white, then quickly died out. This must have taken at least from six to eight seconds.

Then I left the recorders for a couple of minutes, expecting to see possibly a small mushroom, judging from past experience. The first thing I saw

[redacted]

was this white mass bursting through the cloud layer that is normally covering over the sea at about 6000 feet altitude, ... 1000 feet. Right on top of the white stem was this brilliant red, fan-shaped fireball. As it rose above the cloud mass, it, of course, became a ball with the usual white stem. The stem seemed to be more white than usual.

The red glow continued to rise and grow larger, during which time we noticed the aurora at the lower right hand corner, at about five o'clock. It look as a rain cloud does during a heavy summer shower, or as a cloud looks sometimes with the sun shining through the edge (light streaks).

By this time everyone was awe-stricken because the sight was much more than anyone--and particularly, the Coast Guard personnel--had anticipated. The fireball was about two thirds its full size at this point and I expected it to subside as usual. When it kept right on expanding larger and larger, I don't mind admitting we were all beginning to wonder if it was going to stop. By this time about eight to ten minutes had elapsed, and it looked to us as if the fireball--knowing the geography of the Pacific, Honolulu, Johnston, and French Frigate Shoals--we judged the glow to be at least 500 miles across. It gave us the feeling that we should somehow put our hands up to stop it from rolling over us like a huge, pink balloon.

The aurora had stayed about the same condition as before, a little dissipated by this time, of course. It drifted off to the west several degrees and finally faded out. We judged the fireball lasted nearly 20 minutes. I judged that the reason it spread so far and so rapidly is that being up so high, there was nothing to stop it.

Standing here looking at the ball as it grew and grew, I could not help but wonder how Johnston and the people on it, particularly the barracks, could possibly survive such a terrific blast of heat, not to mention the concussion that must have followed.

I had checked the recorders several times already, as you will note on the records. We received your message "up one" and, as we received the message stating that you were sending it "blind," we didn't know for sure what to think at first. But when you didn't elaborate, we doped it out that you could not receive messages, but thought you were able to transmit. We heard you loud and clear "5 x 5," as well as Oahu KOMO, but we, too, were off the

[redacted]

air for at least 12 hours. I believe this condition was due to the cosmic ray disturbances in the air caused by the blast. The Army is here measuring this theory and condition. Immediately after zero, the noise level went down to <u>almost</u> zero and did not come back up to normal again until about H + 30 hours.

Maybe this theory is right; maybe not!! That about covers everything. I am sorry that I didn't know more about what to expect. We would have been prepared at least with some photo coverage and by some crude means of measurements. <u>NEXT TIME</u>!

[redacted]